

DOCTORAL THESIS

Research and Development of Energy Storage Control Strategies for Residential Area Microgrids

Tobias Häring

TALLINN UNIVERSITY OF TECHNOLOGY
DOCTORAL THESIS
21/2022

Research and Development of Energy Storage Control Strategies for Residential Area Microgrids

TOBIAS HÄRING



TALLINN UNIVERSITY OF TECHNOLOGY

School of Engineering

Department of Electrical Power Engineering and Mechatronics

This dissertation was accepted for the defence of the degree 02/05/2022

Supervisor:

Prof. Dr. Argo Rosin
School of Engineering
Tallinn University of Technology
Tallinn, Estonia

Co-supervisor:

Prof. Dr.-Ing. Dr. h.c. Helmuth Biechl
Faculty of Electrical Engineering
University of Applied Sciences Kempten
Kempten, Germany

Opponents:

Prof. Dr. Ilya Galkin
Faculty of Electrical and Environmental Engineering
Riga Technical University
Riga, Latvia

Prof. Dr. Mehdi Savaghebi
SDU Electrical Engineering
Department of Mechanical and Electrical Engineering
University of Southern Denmark
Odense, Denmark

Defence of the thesis: 08/06/2022, Tallinn

Declaration:

Hereby I declare that this doctoral thesis, my original investigation and achievement, submitted for the doctoral degree at Tallinn University of Technology, has not been submitted for doctoral or equivalent academic degree.

Tobias Häring

signature



European Union
European Regional
Development Fund



Investing
in your future

Copyright: Tobias Häring, 2022

ISSN 2585-6898 (publication)

ISBN 978-9949-83-827-1 (publication)

ISSN 2585-6901 (PDF)

ISBN 978-9949-83-828-8 (PDF)

Printed by Auratrükk

TALLINNA TEHNIKAÜLIKOO
DOKTORITÖÖ
21/2022

Energiasalvestite juhtimisstrateegiate uurimine ja arendamine elamupiirkondade mikrovõrkudele

TOBIAS HÄRING



Contents

List of publications	7
Author’s contribution to the publications	8
Abbreviations	9
Symbols	10
1 Introduction	13
1.1 Thesis objectives	15
1.2 Hypotheses.....	15
1.3 Research tasks.....	16
1.4 Contribution and dissemination.....	16
2 State of the art	18
2.1 Microgrids	18
2.1.1 Topologies and design.....	19
2.1.2 Operation modes	23
2.1.3 Technical Challenges	23
2.1.4 Energy markets and advanced metering infrastructure	24
2.2 Typical renewable generation and storage systems in residential microgrids	26
2.2.1 Renewable energy sources	27
2.2.2 Storage systems	29
2.2.3 Home appliances and buildings as TES	33
2.3 Machine learning applications in microgrids	36
2.3.1 Forecasting and prediction with machine learning.....	37
2.3.2 Control and coordination with machine learning	38
2.3.3 Disaggregation with machine learning.....	39
2.4 Power hardware in the loop and real time simulations.....	40
2.5 Conclusions	42
3 Research and development of object models for microgrid components.....	44
3.1 PV-system profile	44
3.2 Thermal and electrical load profiles.....	45
3.3 BESS and FESS model	49
3.3.1 FESS model with basic converter control.....	49
3.3.2 BESS model.....	52
3.4 Freezer, water heater and simplified space heating model.....	53
3.4.1 Freezer model	53
3.4.2 Water heater model.....	54
3.4.3 Simplified space heating model	55
3.5 Neural network-based space heating model	56
3.5.1 Description of used civil engineering models	57
3.5.2 Creation of comprehensive datasets with civil engineering models	59
3.5.3 Development and training of neural network-based models	60
3.6 Conclusions	65
4 Validation of mathematical object models for storage systems.....	67
4.1 Validation of BESS and FESS models	67
4.1.1 Validation of FESS model	67
4.1.2 Validation of BESS model.....	69

4.2 Validation of TES models.....	70
4.2.1 Validation of freezer model	70
4.2.2 Validation of water heater model.....	72
4.2.3 Validation of the simplified space heating model.....	73
4.2.4 Validation of neural network space heating model.....	75
4.3 Conclusions	78
5 Research and development of control strategies for residential microgrids.....	82
5.1 Cyclic lifetime and security of supply improvement with FESS and BESS.....	82
5.1.1 FESS control.....	83
5.1.2 BESS control	87
5.1.3 Results of cyclic lifetime and security of supply improvement control	87
5.2 Energy cost minimization with TESs.....	89
5.2.1 Price-based control algorithm description.....	90
5.2.2 Results of price-based control algorithms	91
5.2.3 Comparison of space heating model complexities	92
5.3 BESS capacity minimization with TESs	95
5.3.1 Islanded control algorithm description.....	95
5.3.2 Results of islanded control algorithms.....	99
5.4 Cost and capacity minimization with different dwelling occupancies	100
5.5 Conclusions	104
6 Analysis of social and financial feasibility	106
6.1 Social acceptance analysis	106
6.1.1 Concerns regarding user comfort interference.....	106
6.1.2 Concerns regarding privacy.....	109
6.2 Financial feasibility analysis	114
6.2.1 Financial investigation for the complete proposed system	114
6.2.2 Financial investigation regarding flywheel and TESs.....	118
6.3 Conclusions	121
7 Conclusions, recommendations and future work	124
7.1 Modelling techniques for space heating.....	125
7.2 Control algorithm selection in different scenarios.....	127
7.3 Recommendations for microgrid designers, building and dwelling owners.....	127
7.4 Future work.....	129
List of figures.....	130
List of tables	133
References	135
Acknowledgements.....	151
Abstract.....	152
Lühikokkuvõte.....	153
Appendix	155
Curriculum vitae.....	246
Elulookirjeldus.....	247

List of publications

The list of author's publications, on the basis of which the thesis has been prepared:

- I T. Häring, T. M. Kull, R. Ahmadiyahangar, A. Rosin, M. Thalfeldt, and H. Biechl, "Microgrid Oriented modeling of space heating system based on neural networks," *Journal of Building Engineering*, vol. 43, p. 103150, Nov. 2021, doi: 10.1016/j.jobbe.2021.103150.
- II A. Antonov, T. Häring, T. Korötko, A. Rosin, T. Kerikmäe and H. Biechl, "Pitfalls of Machine Learning Methods in Smart Grids: A Legal Perspective," 2021 International Symposium on Computer Science and Intelligent Controls (ISCSIC), 2021, pp. 248–256, doi: 10.1109/ISCSIC54682.2021.00053.
- III T. Häring, R. Ahmadiyahangar, A. Rosin and H. Biechl, "Machine Learning Approach for Flexibility Characterisation of Residential Space Heating," IECON 2021 – 47th Annual Conference of the IEEE Industrial Electronics Society, 2021, pp. 1–6, doi: 10.1109/IECON48115.2021.9589216.
- IV N. Cinay, T. Häring, A. Rosin, T. Korötko, R. Ahmadiyahangar and H. Biechl, "Lifetime-Oriented Control Strategies for Hybrid Energy Storage Systems in an Islanded Microgrid," 2021 22nd IEEE International Conference on Industrial Technology (ICIT), 2021, pp. 1267–1272, doi: 10.1109/ICIT46573.2021.9453617.
- V T. Häring, A. Rosin, T. M. Kull, J. Helguero and H. Biechl, "Thermal Modelling of a Control Center for Flexibility Analysis in nZEB Nanogrids," 2020 IEEE 61th International Scientific Conference on Power and Electrical Engineering of Riga Technical University (RTUCON), 2020, pp. 1–6, doi: 10.1109/RTUCON51174.2020.9316568.
- VI F. Plaum, T. Häring, R. Ahmadiyahangar and A. Rosin, "Power Smoothing in Smart Buildings using Flywheel Energy Storage," 2020 IEEE 14th International Conference on Compatibility, Power Electronics and Power Engineering (CPE-POWERENG), 2020, pp. 473–477, doi: 10.1109/CPE-POWERENG48600.2020.9161458.
- VII T. Häring, R. Ahmadiyahangar, A. Rosin and H. Biechl, "Impact of Load Matching Algorithms on the Battery Capacity with different Household Occupancies," IECON 2019 – 45th Annual Conference of the IEEE Industrial Electronics Society, 2019, pp. 2541–2547, doi: 10.1109/IECON.2019.8927495.
- VIII T. Häring, R. Ahmadiyahangar, A. Rosin, H. Biechl and T. Korötko, "Comparison of the Impact of Different Household Occupancies on Load Matching Algorithms," 2019 Electric Power Quality and Supply Reliability Conference (PQ) & 2019 Symposium on Electrical Engineering and Mechatronics (SEEM), 2019, pp. 1–6, doi: 10.1109/PQ.2019.8818270.
- IX T. Häring, A. Rosin, and H. Biechl, "Using common household thermal storages to support the PV- and battery system in nearly zero energy buildings in off-grid mode," *Sustainable Energy Technologies and Assessments*, vol. 35, pp. 12–24, Oct. 2019, doi: 10.1016/j.seta.2019.05.014.

Author's contribution to the publications

Contributions to the papers in this thesis are:

- I Tobias Häring, as the main author of the paper, developed the concept for the publication and researched and developed the methodology for synthesizing neural network-based space heating models from civil engineering models, including a model validation with error and accuracy analysis.
- II Tobias Häring, as a co-author of the paper, developed the concept for the publication, analysed and identified the user concerns in machine learning methods for the advanced metering infrastructure and developed the related mapping for the proposed tool in form of a table.
- III Tobias Häring, as the main author of the paper, developed the concept for the publication and researched and developed the simulations for the flexibility analysis of neural network-based space heating models to investigate related long- and short-term influences on the energy consumption.
- IV Tobias Häring, as a co-author of the paper, developed the idea and concept for the control strategy investigation of a hybrid storage system for a microgrid, including a battery and flywheel storage, and supervised the content development for the main author's master thesis, which was the basis for this publication.
- V Tobias Häring, as the main author of the paper, developed the concept for the publication, coordinated the data acquisition and preparation for the civil engineering model, and finally investigated the influence of space heating models with different modelling complexities on the performance of price-based control algorithms, considering the related user comfort.
- VI Tobias Häring, as a co-author of the paper, developed the idea and concept for the power smoothing control investigation on the existing flywheel storage system and supervised the content development for the main author's master thesis, which was the basis for this publication.
- VII Tobias Häring, as the main author of the paper, developed the concept for the publication and investigated the influence of different household occupancies on the performance of control algorithms for thermostatically controlled common household thermal storages to support the battery storage system during the islanded operation mode.
- VIII Tobias Häring, as the main author of the paper, developed the concept for the publication and investigated the influence of different household occupancies on the performance of price-based control algorithms for thermostatically controlled common household thermal storages.
- IX Tobias Häring, as the main author of the paper, researched and developed the modelling and control algorithms for thermostatically controlled common household thermal storages to support the battery storage system during the islanded operation mode of a household.

Abbreviations

AMI	Advanced metering infrastructure
BESS	Battery energy storage system
BMS	Battery management system
DE	Germany
DG	Distributed generation
DoE	Design of experiment
DSM	Demand side management
DSO	Distribution system operator
DUT	Device under test
EE	Estonia
EMS	Energy management system
EnWG	Energiewirtschaftsgesetz (Energy Industry Act)
ESS	Energy storage system
EU	European Union
FESS	Flywheel energy storage system
GDPR	General data protection regulation
HAN	Home area network
HES	Head-end system
IPCC	Intergovernmental Panel on Climate Change
MDMS	Meter data management system
ML	Machine learning
NILM	Non-intrusive load monitoring
NN	Neural network
nZEB	Nearly zero energy building
PHIL	Power hardware in the loop
RMSE	Root mean square error
SAIDI	System Average Interruption Duration Index
SM	Smart meter
SOC	State of charge
SOH	State of health
SOLI	State of life indicator
TES	Thermal energy storage
TSO	Transmission system operator
WAN	Wide area network

Symbols

A_{Object}	Surface area of object [m ²]
A_{Room}	Room area [m ²]
$C_{Bat,nom}$	Nominal battery capacity [Ah]
COP_x	Coefficient of performance for device x
C_{px}	Specific heat capacity of material x [J kg ⁻¹ K ⁻¹]
C_{user}	User comfort related scaling factor
d_i	Freezer door opened {0;1}
DOD_x	Depth of discharge of device x
dT_{amb}	Temperature change due to ambient losses [°C]
dT_{cold_water}	Temperature change due to water exchange [°C]
dT_{food}	Temperature change due to food exchange [°C]
dT_{freeze}	Temperature change due to freezing [°C]
dT_h	Temperature change due to heating or cooling [°C]
dT_{occ}	Temperature change due to room occupancy [°C]
dT_{rad}	Temperature change due to sun irradiation through windows [°C]
dT_{vent}	Temperature change due to ventilation [°C]
$E1$	Experiment 1
$E2$	Experiment 2
$E3$	Experiment 3
$E4$	Experiment 4
$E_{door-loss}$	Energy loss for each door opening [Wh]
E_{in}	Input energy [Wh]
E_{out}	Output energy [Wh]
E_{rot}	Rotational energy [J]
$Error_{total}$	Total error metric for neural network based model
i	Time step
I_{cd}	Charging (>0) and discharging (<0) current [A]
i_{ds}	Flux forming current [A]
i_{ds_ref}	Flux forming stator current [A]
i_{qs_ref}	Torque forming current [A]
J	Inertia [kg m ²]
k	Coverage factor
k_i	Number of people in the room
L_m	Mutual inductance [H]
L_r	Rotor inductance [H]
m	Mass [kg]
m_i	Food exchange [kg/Δt]
$N_{cycles,24h}$	Number of cycles in 24 hours
$N_{cycles,max}$	Maximum number of cycles according to datasheet

n_p	number of motor poles pairs
\bar{P}	Mean power error [W]
\tilde{P}	Test model heating power [W]
p_0	Regression parameter p_0
p_a	Regression parameter for x_a
p_b	Regression parameter for x_b
p_{ab}	Regression parameter for dependence x_a and x_b
$P_{el,x}$	Electrical power for device x [W]
P_{CE}	Civil engineering model heating power [W]
P_{Person}	Typical heating power of one person [W]
Pr	Current electricity price [€/kWh]
Pr_{avg}	Average electricity price [€/kWh]
Pr_{dev}	Electricity price deviation [€/kWh]
Pr_{max}	Maximum electricity price [€/kWh]
Pr_{min}	Minimum electricity price [€/kWh]
P_{ref}	Active power reference [W]
Pwr	Current power [W]
Pwr_{avg}	Average power [W]
Pwr_{dev}	Power deviation [W]
Pwr_{max}	Maximum power [W]
Pwr_{min}	Minimum power [W]
Q_{ref}	Reactive power reference [VAR]
r	Radius [m]
R_r	Rotor resistance [Ω]
$RMSE_T$	Temperature root mean square error [$^{\circ}\text{C}$]
$RMSE_P$	Heating power root mean square error [W/m^2]
SOC_x	State of charge of device x
SST	Sum of squares total
SSA	Sum of squares for parameter x_a
SSB	Sum of squares for parameter x_b
$SSAB$	Sum of squares for parameter dependence x_a and x_b
T	Temperature [$^{\circ}\text{C}$]
\tilde{T}	Civil engineering model mean air temperature [$^{\circ}\text{C}$]
T_{amb}	Ambient temperature [$^{\circ}\text{C}$]
$t_{Bat,cyclic}$	Cyclic lifetime for BESS [a]
$T_{f_corrected}$	Corrected food temperature [$^{\circ}\text{C}$]
T_{f_actual}	Actual food temperature [$^{\circ}\text{C}$]
T_{goal}	Goal temperature [$^{\circ}\text{C}$]
T_{ref}	Torque reference [Nm]
TSA	Time step accuracy

T_{set}	Chosen set point for thermal storage [°C]
$T_{set,max}$	Maximum set point temperature [°C]
$T_{set,min}$	Minimum set point temperature [°C]
U_{DC}	DC-link voltage [V]
U_{NN}	Uncertainty of neural network based space heating model
U_{Object}	U-value of object [W/m ² K]
U_f	Uncertainty of freezer object model [Wh/day]
U_{MATLAB}	Uncertainty of Matlab calculation [Wh/day]
U_{total}	Total uncertainty of freezer simulation [Wh/day]
V_{Object}	Volume of object [m ³]
V_i	Water/Air exchange [l/Δt]
V_{MG}	Microgrid voltage [V]
$V_{MG,min}$	Minimum desired microgrid voltage [V]
x_a	Design of experiment 1 st parameter
x_b	Design of experiment 2 nd parameter
y_i	Freezing/Heating status {0;1}
ΔP_E	Heating power difference error {0;1}
Δt	Time step duration [h]
α	Coefficient [W/K]
β	Coefficient [K/J]
η_x	Efficiency of device x [%]
ρ_x	Density of material x [kg/m ³]
μ	Mean value
ψ_r	Rotor flux [Wb]
ψ_{r_ref}	Rotor flux reference [Wb]
ω	Rotational speed [rad/s]
ω_m	Measured rotational speed [1/min]
#	Set point algorithm

1 Introduction

The latest report of the Intergovernmental Panel on Climate Change (IPCC) was published recently in summer 2021 regarding the current scientific research related to climate change [1]. The main take-aways from this report are of great concern for the current energy policy of the whole world:

1. “It is unequivocal that human influence has warmed the atmosphere, ocean and land. Widespread and rapid changes in the atmosphere, ocean, cryosphere and biosphere have occurred.” [1]
2. “The scale of recent changes across the climate system as a whole – and the present state of many aspects of the climate system – are unprecedented over many centuries to many thousands of years.” [1]
3. “Human-induced climate change is already affecting many weather and climate extremes in every region across the globe.” [1]

There are no more doubts that the human interference with the world climate due to high amounts of released CO₂ did not cause a multitude of consequences we have to deal with now and in the future. To reduce the CO₂ emissions and slow down this process, the Paris Agreement was already introduced in 2015 [2]. All parties agreed to limit the global warming below 2 °C, preferably 1.5 °C, compared to pre-industrial levels by reducing the greenhouse gas emissions permanently in the long-term. However, the IPCC predicts in their report that the 2 °C limit will barely cope with the progress of climate change and that the goal of 1.5 °C or less should be achieved as some consequences are already irreversible [1]. The facts presented about Europe include [1]:

- Temperatures will rise regardless of future levels of global warming.
- The frequency and intensity of hot extremes has increased and will continue increasing regardless of greenhouse gas emission development.
- The frequency of cold spells and frost days will decrease regardless of greenhouse gas emission development.

To cope with the climate change, the European Union (EU) has communicated “The European Green Deal” [3], which includes short- and long-term objectives. Goals for 2030 are greenhouse gas emission cuts of at least 40%, renewable energy share of at least 32% and increased energy efficiency of at least 32.5%. The goal for 2050 for the EU is to be climate neutral. [3]

To achieve the targets regarding the renewable energy share and energy efficiency, a more specific Directive was released by the EU to describe specific goals for target technologies [4]. In this context, there is a multitude of EU funded projects, e.g., in the Horizon 2020 framework. These projects, such as the NetZeroCities [5], Decarb City Pipes 2050 [6], or FinEst Twins [7], aim to achieve the set goals with research on the future design of technologies, their interoperability and feasibility. An important part of the future design of the electrical grid is the construct of a “Smart City” composed of many smaller Smart Grids working in tandem.

For this multi-microgrid design structure, it is generally agreed to use CO₂ neutral technologies as much as possible. This means that current technologies and policies are researched and advanced to overcome challenges in the context of microgrids. The current standard for new buildings is nearly zero energy buildings (nZEB) [8], including renewable energy source integration and often storage technologies to achieve very high energy

performance. From the greenhouse gas emission point of view, this increase of renewable energy sources is remarkable; from a technical point of view, this poses challenges, especially due to the volatile energy production [9]. To balance the energy demand with the energy supply, load scheduling is a viable option by implementing different demand side management (DSM) [10] or energy flexibility [11] related strategies.

This balancing of many distributed generation (DG) units with many small scheduled loads and storage systems involves a large number of devices with a complex control structure. It is inevitable that some device or control error will happen, leading to mismatches and blackouts. However, the renewable energy sources are not only the root cause for this challenge, but they are the solution as well: with DG units in microgrids, it is possible with a storage system for energy buffering to continue operation of a microgrid in islanded mode during a blackout [12]. So far, most of the research regarding control strategies for DG units, energy storage systems (ESS) and load scheduling with DSM are focussed on grid-connected operation [13], [14], [15], as the microgrid will be connected to the main grid most of the time. Thus, further research regarding the islanded operation mode is necessary.

As it is essential to develop these new control concepts and achieve market readiness as quick as possible to reach the set greenhouse gas emission goals, modern research and development approaches are commonly used. Instead of the traditional process from design to testing to building, modelling and analyses are carried out before prototyping a system [16]. Within this modelling and analysing process, approaches are changing from traditional designs and simulations to machine learning (ML) aided designs [17] with real time [18] and power hardware in the loop (PHIL) simulations [19] due to increasing availability and cheaper computational resources.

As it is not enough for a system to be adopted by the wide public if it works only from a technical point of view, social and financial feasibility aspects need to be considered as well [20]. These can include user comfort, data privacy issues, or return of investment as examples. [21]

This thesis aims to contribute to the presented research field in the following way: a topology for microgrid systems is proposed and analysed. The microgrid is designed with CO2 reductions in mind, using ESSs and renewables as the only energy source. To control these devices, islanded and grid-connected control strategies are researched and developed, focussing on the islanded operation. ML as well as PHIL real time simulations are used for modelling and validation purposes. This technical analysis is complemented with social and financial feasibility investigations. General content of this PhD research is summarized in Figure 1.1.

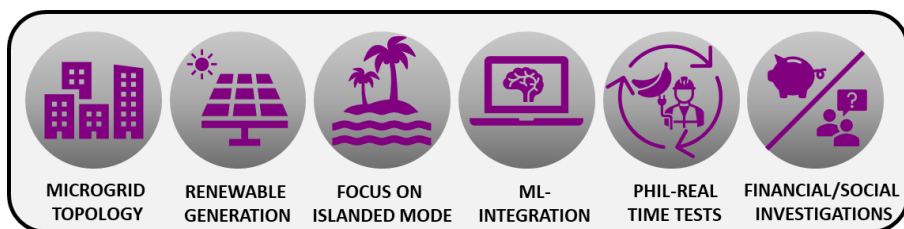


Figure 1.1: General content of this thesis

1.1 Thesis objectives

The main objective of this work is to research and develop object models with improved accuracy and control strategies for hybrid energy storage systems to improve security of supply and financial feasibility of residential microgrids.

The secondary aim is to analyse the investment return time and end user's privacy and comfort requirements with the developed control strategies to increase the users' general acceptance level and provide recommendations for microgrid designers, microgrid and building managers, and homeowners in the development of microgrid systems.

1.2 Hypotheses

The main hypotheses of this thesis are:

- Using PV-systems with hybrid energy (battery, flywheel) storages and home appliances as supporting thermal storages could be a feasible and flexible topology for improving the security of supply and financial feasibility of typical residential microgrids.
- The novel methodology, which synthesizes space heating models by training a neural network with input data from civil engineering thermal building simulations, will create space heating object models more efficiently. This is achieved by reducing the active time and effort for manual modelling and simplifying space heating object models in electrical engineering software with a high level of detail by more than 50%.
- Using space heating models created with the novel methodology based on neural networks will reduce the computational time for microgrid simulations by more than 50% compared to a co-simulation with civil engineering software and will reduce the mean power error by more than 3% compared to a linearized space heating model.
- Using a combination of different (improved and novel) control strategies could increase the battery storage system cyclic lifetime by more than 5% and the islanded operation duration by more than 2%, and simultaneously reduce the energy costs by more than 5% and the necessary battery storage capacity by more than 3%.
- The methodology for evaluation of social acceptance for microgrid developers, which considers the user comfort and privacy concerns, will improve the development and planning quality of residential area microgrids through higher satisfaction of end-users.
- The complex methodology for microgrid development, which will consider security of supply, social acceptance and financially oriented control strategy decisions, could reduce the investment return time of the proposed system to less than 15 years.

1.3 Research tasks

The main research tasks of this thesis are:

- Analysis and classification of common microgrid components and control strategies to develop mathematical object models and design the corresponding simulations
- Research, development, and improvement of mathematical object models for use in microgrid simulations. This includes energy storage systems (ESSs), a renewable energy source and loads.
- Validation of the ESS object models for increased model accuracy and microgrid simulation quality to develop different control strategies
- Research and development of control strategies for security of supply and financial feasibility improvements
- Investigation and analysis of user comfort, privacy concerns, and financial feasibility of the proposed system and control strategies to increase the users' general acceptance level and to give recommendations for the development and design of microgrid systems

1.4 Contribution and dissemination

This thesis presents a comprehensive view with an interdisciplinary research focus on microgrid systems. Contributions were made in the field of electrical engineering with the cooperation of civil engineering, law and social sciences, and information technologies. The work is aimed at microgrid designers, microgrid and building managers, and homeowners for guidance in the development of new and existing microgrid systems.

Scientific novelties:

- A methodology for synthesizing neural network-based space heating object models from simulated data sets of existing thermal building models in civil engineering software was developed, which reduced the simulation computational time by 85% while increasing the model accuracy by 5.7%.
- A combination of improved and novel control strategies was developed, which increased the cyclic lifetime of the battery storage system by 19% and the islanded operation duration by more than 3%, and simultaneously reduced the energy costs by more than 10% and the necessary battery storage capacity by 4%.
- A user comfort definition methodology was developed to specify the comfort requirements of end users regarding the control decisions for a hybrid energy (battery, flywheel, thermal) storage system in islanded and grid-connected operation mode.

Practical novelties:

- A user comfort aspect-based decision tree for selection of the best control strategy to increase user satisfaction was developed to be used by microgrid development and design engineers.
- A mapping of user privacy concerns between technical and legal aspects was developed as an applicable tool for control and data management engineers to develop microgrid systems with increased social acceptance.
- A complex microgrid development methodology and a decision tree for microgrid design engineers considering technical, social and financial control strategy decisions was developed to reduce the investment return rate for microgrid systems.

This thesis comprises results of research published in 9 international publications, including 7 international scientific conferences and 2 international peer-reviewed journals. Additionally, the topic was introduced and presented in 3 doctoral schools. Other researchers' interest in the presentations and results has shown the relevance and importance of the topic.

The knowledge gained in this work supports the research of ZEBE Center of Excellence for zero energy and resource efficient smart buildings and districts (TAR16012), PUT1680 "Power Electronics Based Energy Management Systems for Net Zero Energy Buildings", PSG409 "New generation dynamic sizing methods for heating and cooling systems in intermittently operated buildings", MOBTP88 "Climate impact on the energy balance and cost-optimal design solutions of office buildings in Europe", and the FinEst Centre for Smart Cities (VFP19031 / 856602). Knowledge from this work could additionally be applied in an expertise for Enefit (Eesti Energia AS), the AI4Cities project with Fusebox OÜ, and an expertise for GridIO.

This dissertation is supported by 4 master theses with focus on flywheel and battery storage systems, which were supervised during the doctoral studies.

2 State of the art

The need for balancing demand and supply within the microgrid is increasing due to renewable energy sources that are eco-friendlier than the previously used main energy sources. This creates challenges for grid planners and designers because the existing grid cannot be completely changed immediately to serve as a perfect infrastructure for renewables.

One promising solution to gradually adjust the electricity grid to the new needs is so-called microgrids. These microgrids can be designed and operated in various ways and need to be integrated into the existing energy markets. Within these microgrids, the current regulations and technology regarding buildings are nearly zero energy buildings (nZEB). These buildings try to minimize their electrical energy needs by integrating renewable energy sources, demand side management (DSM) strategies and storage systems within the building energy management. One relevant kind of schedulable load for DSM applications is common household thermal energy storages (TES), such as freezers, water heaters and space heating, as they can store a certain amount of energy for limited time in the form of heat. To gain knowledge about microgrid systems, there is a need for simulations and tests with accurate models and control strategies. This can be achieved with ML, which gained popularity lately, and PHIL setups. These structures, devices and methodologies are presented in the following sections.

2.1 Microgrids

As mentioned, the need for electricity is increasing while the CO₂ emissions must be reduced to fulfil the goal of the Paris Agreement [2]. To cope with these challenges, more and more renewable energy sources must be integrated into the existing electricity grid. The volatile nature of many of those renewable technologies creates a greater need for balancing the demand and supply than before, as recent events already show that the existing grid is quite fragile [22], [23], [24]. One solution to this challenge is splitting up the existing grid into microgrids, which can be managed independently [25].

No unanimous agreement upon the definition of a microgrid has been reached. However, it is often defined as “a group of interconnected loads and distributed energy resources within clearly defined electrical boundaries, which act as a single controllable entity with respect to the grid. A microgrid can connect and disconnect from the grid to enable it to operate in both grid-connected and islanded-modes” [26]. This means:

- that different small power plants, energy storages and controllable demand are connected and controlled as a unit.
- that microgrids are interlinked to each other and share power, if necessary (grid-connected operation), but if a disturbance occurs, they can separate themselves (islanded operation).

Thus, microgrids will play an essential role in the future design of the electric power and energy systems. To get a better overview on microgrids, the listed aspects have been analysed in the literature presented in the following subsections in more detail:

- Topologies and design of microgrids
- Operation modes of microgrids
- Technical challenges in microgrids
- Energy markets and advanced metering infrastructure (AMI)

A general topology for a microgrid is depicted in Figure 2.1.

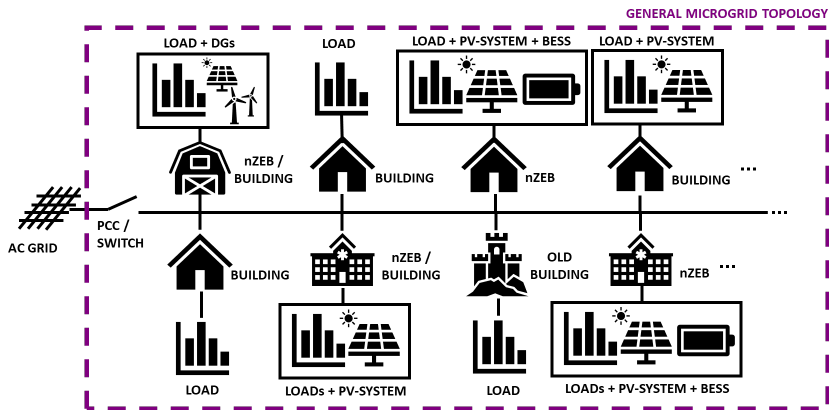


Figure 2.1: General microgrid topology

2.1.1 Topologies and design

Microgrids can generally be categorized into three major topologies: AC-, DC- or hybrid microgrids [27]. AC- and hybrid microgrids can be designed with one single phase or as a three-phase system.

AC microgrids, as the most common topology, typically consist of distributed generation (DG) units (PV, wind turbines, fuel cell etc.), an AC switch, battery energy storage systems (BESS), and (bidirectional) converters. There is an AC connection between the utility grid and AC microgrid. This AC grid is connected to the DG units, which have (bidirectional) converters to connect to their DC buses. The loads are supplied via the AC grid. [28]

A typical AC microgrid is shown in Figure 2.2.

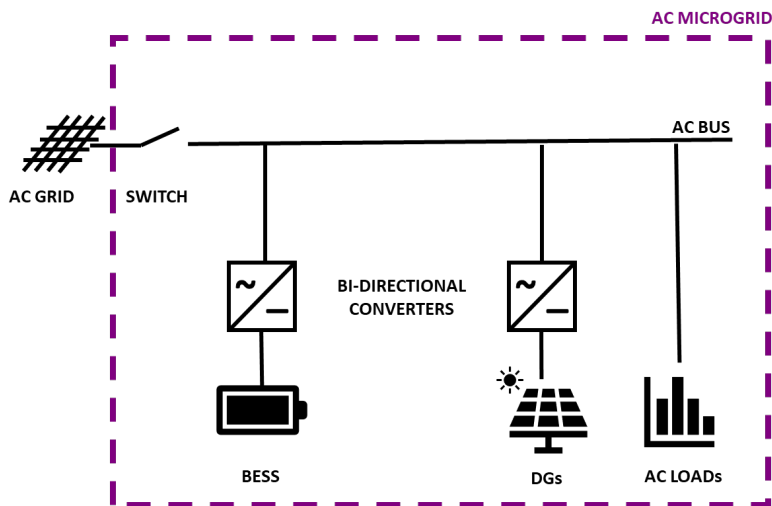


Figure 2.2: AC microgrid topology

DC Microgrids include PV generation systems, DC/DC converters, bidirectional converters, BESSs, DC loads, and AC loads. The PV system is connected through a DC/DC converter to the DC bus as well as to the DC loads, BESSs. The AC loads are supplied by the bidirectional converters. [28]

The Topology for a typical DC microgrid is shown in Figure 2.3.

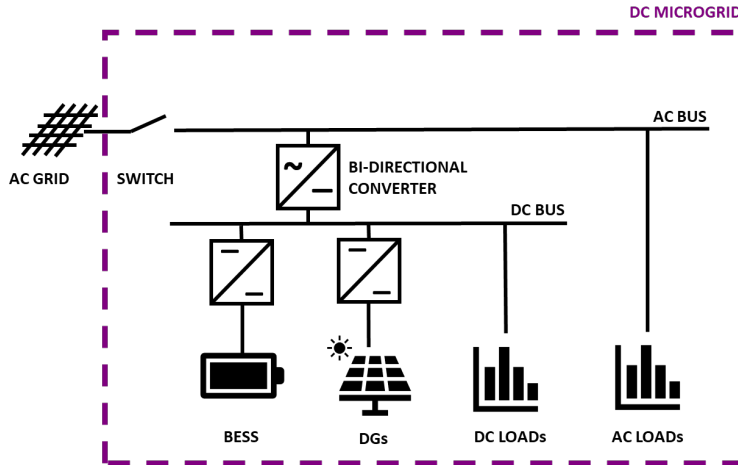


Figure 2.3: DC microgrid topology

Comparison of AC and DC microgrid topologies shows that the number of AC/DC converter can be reduced in a DC microgrid. The AC loads are supplied by the bidirectional converter, which can lead to improvements in power distribution reliability and power quality. [28]

Hybrid Microgrids combine the advantages of both AC and DC architectures, as two networks are combined in the same distribution grid [29]. With this, it is possible to integrate both AC and DC based DGs, energy storage systems (ESS) and loads. [30]. An example topology of a hybrid microgrid is shown in Figure 2.4. The hybrid inverter can be designed like the energy router presented in [29].

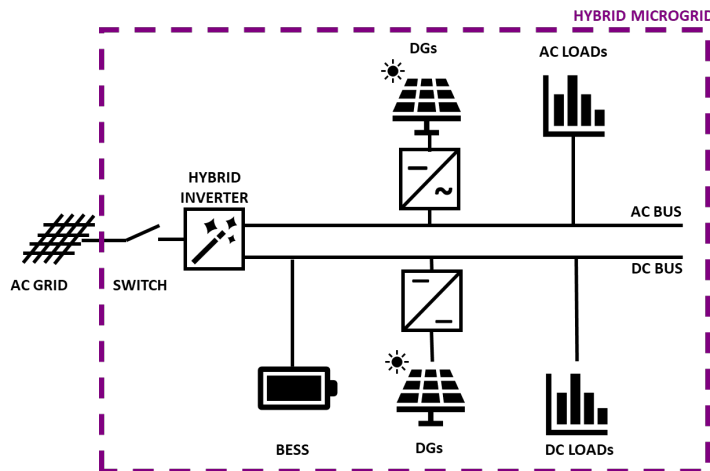


Figure 2.4: Hybrid microgrid topology

As the presented topologies already show, a microgrid contains several components for different purposes:

- DG units
- ESS
- (Controllable) loads

Electricity is produced with DG units [31], including, for example, wind-, PV-, or hydropower, which can be integrated depending on the environmental and geological circumstances. These renewable energy sources will be analysed in more detail in section 2.2.1.

In the design of a microgrid, the supply reliability and controllability of the selected power sources must be considered: PV- and wind power are volatile power sources, for example, while diesel generators are reliable with constant power output, if needed. Wind turbines [22] or hydropower plants [32] are only controllable in the direction of low power supply, while a diesel generator on the other hand can be controlled in both directions. Unfortunately, most of the reliable and fully controllable power sources are not renewable and should therefore be avoided in the design of new microgrids according to the Paris Agreement [2]. An overview of the typical microgrid power sources is given in Figure 2.5.

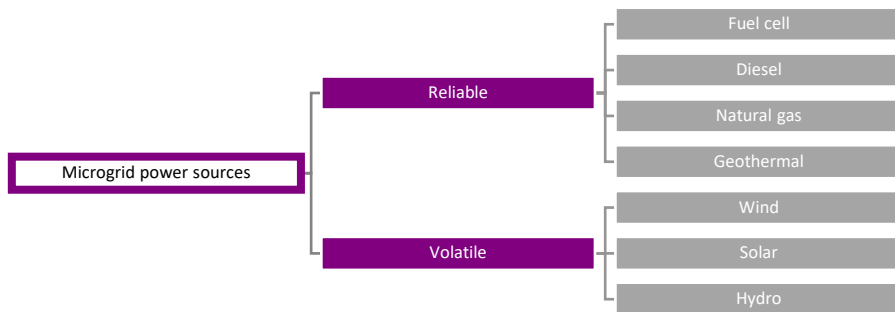


Figure 2.5: Microgrid power sources [33]

As shown in [31], ESS is typically a part of a microgrid. It is preferable over backup power plants with fuels from renewable sources, as its efficiency is higher. There are two operation modes for ESS:

- Charging – if the demand for energy is smaller than the produced energy
- Discharging – if the demand is higher than the supply

More details about the possible storage systems are presented in section 2.2.2.

The loads are evidently important in the microgrid context as well, as they have been subject to extensive research recently in terms of flexibility and demand side management (DSM) [10] [14]. These concepts work as follows:

- DSM: If a lot of energy is available, the demand is increased. If less energy is available, the demand is reduced.
- Flexibility: Demand-side flexibility is defined as the capability of consumption modification in response to control (penalty) signals and is recognized officially [34], [11].

More details about controllable loads are presented in section 2.2.3. An overview of the advantages and disadvantages of the different microgrid topologies is given in Table 2.1.

Table 2.1: Advantages and disadvantages of different microgrid topologies [28], [27], [33]

Microgrid	Advantages	Disadvantages
AC	<ul style="list-style-type: none"> • DG units can be integrated in the current utility grid • It is possible to apply conventional operational concepts for power flux control, protection devices, fault detection etc. 	<ul style="list-style-type: none"> • Need for synchronization of DG units • Control and operation more challenging in islanded mode
DC	<ul style="list-style-type: none"> • No need for synchronization of DG units • Absence of frequency and phase dependences among AC generators • Higher overall efficiency due to fewer interface converters and no circulation of reactive current in the network 	<ul style="list-style-type: none"> • Higher initial cost due to general lack of code recognition and efficiency metric recognition • Problems with certification and code compliance
Hybrid	<ul style="list-style-type: none"> • Better integration of DC-based units • No need for synchronization of generation and storage systems depending on the connection bus • Voltage transformation can be performed on AC-side transformers or DC-side 	<ul style="list-style-type: none"> • Protection devices for DC-based networks need more research • Lower reliability than AC microgrids due to the interface power converter • Management of hybrid microgrids can be more complex due to AC- and DC-bus

Microgrids can be designed as single-phase or three-phase systems: single-phase microgrids, on the one hand, operate at 230 V phase-to-ground voltage. They are becoming more popular as BESS and single-phase hybrid inverters are becoming cheaper. Single-phase microgrids are typically used for small households in a remote location. Three-phase microgrids, on the other hand, operate at 400 V phase-to-phase voltage. The advantages for these are: firstly, the ability to integrate larger renewable energy sources and secondly, the possibility to supply three-phase and single-phase consumers. However, the complexity for a three-phase control system is higher.

2.1.2 Operation modes

As previously mentioned, microgrids can operate in two different modes: grid-connected mode and islanded mode. Some microgrids can operate in both modes constantly or temporarily and depending on the installed devices even switch between the modes seamlessly. In the following, these operation modes are explained for AC-, DC- and hybrid microgrids.

In the islanded mode, an AC microgrid operates without being connected to the utility grid, only using its energy storage systems and DGs [28]. In the grid-connected mode, it is connected to the utility grid: The photovoltaic system generates electricity, which is fed to the public grid. Alternatively, the microgrid can be connected to the utility grid but instead of feeding the produced electricity into the power grid, it is stored in an energy storage. This is often used as a backup system in weaker supply networks or in off-grid mode to ensure greater security of supply. The connected systems are more common in industrialized countries, while the backup systems are used more in emerging or developing countries. [35]

For DC microgrids, DC loads are supplied by the PVs and AC loads by the bidirectional converter in the islanded mode. In case of lower energy demand than generation, surpluses will be used to charge the storage devices. Vice versa, if the energy consumption of the loads is higher than the generation, the ESS will be supplying power to balance the shortage. If the ESS is completely discharged, the system will switch to the on-grid mode to charge the batteries. [28]

An overview of the operation mode schematics is presented in Figure 2.6.

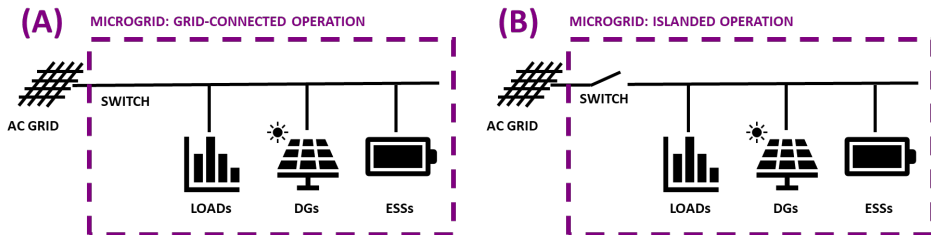


Figure 2.6: Schematic of the grid-connected (A) and the islanded (B) operation mode for a microgrid

2.1.3 Technical Challenges

There are many challenges to be faced when designing or implementing a microgrid. These include a lack of scalable prototype installations, a lack of unified general microgrid metrics, regional regulations, cyber-security concerns etc. The most relevant technical challenges include [36], [37]:

- Power quality
- Control strategies
- Energy management
- Stability and reliability
- Protection

Power quality is extremely important due to the volatile power supply of many renewable energy sources, transition between microgrid operation modes, high reactive power, and nonlinear loads. It is possible to utilize BESS, a flywheel energy storage system (FESS), or other filters to improve the power quality in microgrids. [36], [37]

Control strategies can influence the power quality or minimize costs with DSM. Multiple control strategies for different devices with multiple objectives can be implemented. [36], [38]

The energy management system (EMS) must coordinate the control strategies for efficient and stable operation of the microgrid. This includes managing power flows of DG units and ESS, often making use of load and generation forecasts. [36], [39]

Stability and reliability concern grid synchronization, transition between operation modes, unpredictable frequency deviations etc. [36], [37]

Protection is of critical importance in all electrical power systems. On the one hand, the microgrid should be able to isolate from the main grid during faults. On the other hand, this creates problems as the short circuit capacity is different in the grid-connected and the islanded mode. Traditional overcurrent protection devices may not react in this case and adaptive protection systems need to be considered. [36], [37]

Important standards regarding these points for planning, designing, and modernizing microgrids are [36]:

- IEEE 1547: Criteria and requirements for interconnection of DERs with the main grid
- EN 50160: Voltage characteristics of electricity supplied by public electricity networks
- IEC 61000: General conditions or rules necessary for achieving electromagnetic compatibility
- IEEE C37.95: Protective relaying of utility-consumer interconnections

2.1.4 Energy markets and advanced metering infrastructure

Large parts of the European transmission system are connected and synchronized. There are five regional groups: Continental Europe, Nordic, United Kingdom, Ireland, and Baltic. Within these groups, the frequency is synchronized. To trade between the regional groups, several DC interconnections have been established. [40]

Within these regional groups, there are one or multiple transmission system operators (TSO) responsible for the transmission system stability and power flow on high voltage level. For the medium and low voltage distribution, different distribution system operators ensure the power quality regionally. A list of TSOs and selected distribution system operators (DSO) for Estonia (EE) [41] and Germany (DE) is shown in Table 2.2.

Table 2.2: TSOs and DSOs in Germany and Estonia

Country	TSOs	DSOs
DE	TransnetBW TenneT Amprion 50Hertz Transmission	Kempton (Allgäu) regional: AllgäuNetz GmbH & Co. KG Kaufbeuren regional: Vereinigte Wertach Elektrizitätswerke GmbH
EE	Elering	95% of Estonia: Elektrilevi OÜ

Grid operators need to control the frequency and voltage stability within the grid. To engage power plant operators and microgrid operators into providing these ancillary services, a special market with incentives has been established. This market includes scheduling and dispatch, reactive and voltage control, operating reserves, and frequency control. Smaller microgrids or customers can be accumulated to a virtual power plant. The structure for the frequency control and voltage control reserve is shown in Figure 2.7. The reaction time and delivery duration determine in which category a power plant or a microgrid can be marketed. [40]

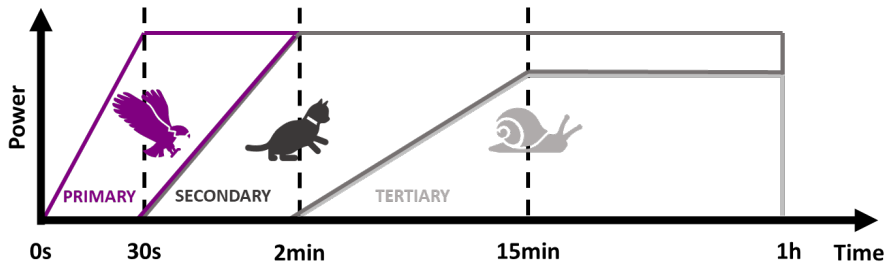


Figure 2.7: Basic schematic of primary, secondary and tertiary control reserve [40]

Participation in the ancillary service market is generally possible even with small plants as they can be included as a virtual power plant. However, there are rules and regulations that need to be fulfilled. For example, in [42], small hydropower plants were investigated for their participation in the ancillary service market for the abovementioned DSO “Vereinigte Wertach Elektrizitätswerke GmbH” in Germany. Due to regional restrictions, the only financially and technically feasible possibility to take part in the market was the installation of a large programmable load. The system would be viable if the heat dissipation of the load is used for district heating. Otherwise §1 EnWG [43] is not met as heat dissipation without further utilization is not eco-friendly. This example shows that regional regulations can create additional challenges.

The general electricity market is structured as follows: quick balancing corrections are made within the ancillary service market. There is the intraday market for hourly corrections within the day and a day-ahead spot market for rough corrections of electricity demand or supply one day in advance. Long-term contracts for electricity dispatch and trade are the cheapest way to buy electricity but the planning must be done days or weeks ahead. [40]

Within this existing market structure, new programmes like demand response and flexibility programmes are established by the TSOs and DSOs to engage prosumers, nZEB communities and microgrid owners more in the electricity market with corresponding incentives to balance the increased amount of volatile renewable energy production. One possibility in this case is, for example, a time of use tariff where the customer pays the real time, hourly or 15-min based electricity market price. The installation of renewable energy sources is often encouraged with governmental funding or similar processes [40].

To establish a bidirectional communication between utilities and prosumers, the AMI was designed [44], [45], [46], [47], [48]. It includes all relevant technologies to provide services for customers, suppliers and DSOs/TSOs, including automated meter reading, billing, information provision, event management, device configuration etc.

Typically, the AMI is composed of smart meters (SM), hierarchically disposed communication networks, meter data management systems (MDMS), and head-end systems (HES). The HES, as the central data system, is responsible for the coordination of the data exchange in its complete service area. The communication network includes home area networks (HAN), wide area networks (WAN), and the utility network with MDMSs as meter data concentrators, respectively as gateways. Compared to traditional energy meters, SMs provide enhanced metering capabilities, data communication and optional auxiliary functions [49], [50], [51]. They are the coupling points of users to the AMI. SMs are essential data sources for analytics as they can be used to report, measure and monitor loading conditions, power quality metrics and power flows.

Considering this structure, the AMI reveals several surfaces for intrusion or other forms of cyber-attacks, as identified in [52], which are presented in Table 2.3.

Table 2.3: Surfaces for intrusion and cyber-attacks of the AMI [53]

Surface	Description
HAN	The consumer side of the AMI. A consumer gateway acts as a bridge between the smart meter and the consumer’s home devices.
SM	The primary point of data collection for power grid energy consumption. Physical access to the meter is considered a vulnerable attack surface.
SM data collector	A hardware computing device aggregating real-time data from multiple smart meters and providing a data collection and management point for the utility; an integral part of the MDMSs
AMI communication interfaces and network	The network along with used communication interfaces linking the smart meter and the SMDCs. The AMI communications network exists alongside the power grid and can be scaled to serve millions of smart meters.
AMI communication protocols and software	The communication links and protocols utilized by the AMI
HES	The AMI management platform at the utility installation providing data warehousing for collected data and centralized management of the AMI

2.2 Typical renewable generation and storage systems in residential microgrids

Nearly zero energy buildings (nZEB) are an important part of microgrids. These buildings aim to accomplish a nearly zero energy balance. Therefore, most nZEBs utilize on-site energy generation and storage systems, which can be integrated into a microgrid as DG units.

To accomplish the energy goal set out by the Paris Agreement [2], the European Union has imposed a directive that requires since the end of 2020 that all new buildings should comply with the nZEB standards [8]. The chosen definition for an nZEB in this directive is “a building that has a very high energy performance. The nearly zero or very low amount

of energy required should be covered to a very significant extent by energy from renewable sources, including energy from renewable sources produced on-site or nearby” [3].

As previously mentioned, the DG units in microgrids and nZEBs must be coordinated effectively to balance the control and demand. Renewable energy sources, such as PV- and wind power, are fluctuating and volatile, while being controllable in one direction only. Therefore, different renewable energy sources are reviewed in subsection 2.2.1.

Microgrids and especially standalone nZEBs tend to have small inertia due to their smaller size compared to conventional large grids, increasing the importance of proper balancing of supply and demand. This can be further aggravated in weaker microgrids and nZEB that have a suboptimal power infrastructure. To effectively balance production and consumption, an ESS is a viable solution. The chosen storage technology should be able to supply or draw power quickly to react to fast changes in the grid parameters, especially in the islanded operation. Different storage technologies are analysed and presented in section 2.2.2. These ESSs can be supported by household appliances, as shown in section 2.2.3.

Another term, which is often being used in the context of nZEBs, is a “prosumer”. Prosumers are members of the energy market which produce energy but are also customers who are consuming energy. Their share increased in the last years noticeably, and it is expected to continue to rise with around 4% per year until 2030 [54]. The preferred DG unit of prosumers is PV-systems and some of them have their own energy storage system, increasing their energy independence from the grid further.

2.2.1 Renewable energy sources

The most common renewable generation sources installed in microgrids are PV-systems, wind turbines or small hydropower plants. These DG units have different requirements and properties. Thus, the selection of the energy production must be tailored to the specific microgrid. The DG units in microgrids can be classified by [36]:

- Availability
- Output characteristics (AC, DC)
- Controllability
- Connection interface
- Power flow control

PV-systems, wind turbines and hydropower plants have common drawbacks, as they are dependent on the geographical location; they are volatile and only uncontrollable in one direction.

PV-systems are a popular installation in nZEBs, as mentioned before. PV-systems have the advantage of easy scalability and lower dependency on the geographical location compared to wind- or hydropower. For example, a solar powered boat travelled around the world from 2010-2012 [55]. However, there are aspects that need to be considered before installing a PV-system in a microgrid:

- Due to easy scalability, PV-systems can usually be installed in residential areas without disturbance of other residents.
- PV-systems are preferably installed in places that have a large amount of clear and sunny days per year, have a high direct normal radiation, are on high altitudes (natural cooling) and have low amounts of shading and dirt collection. [56]

- PV-installations have a lifetime of more than 20 years. Long-term measurements have shown a degradation of 0.11% per year in high altitudes (3450 m a.s.l.) or 0.57% per year on 1270 m a.s.l. However, it must be noted that these old installations are thicker and more durable than newer panels that are available today. [56]
- Dirt on and faults with PV-panels need to be detected and removed to avoid further damage. Thermal imaging can be used for this purpose. [56]
- PV-panels provide a DC voltage that needs to be converted to AC for most installations.

There are basically four different types of wind turbines available: lift- or drag-type turbines. Each of those types can be designed as a vertical or horizontal axis turbine. These types have different efficiencies and applications and can be realized with different numbers of blades. The size of the blades and hub influences the efficiency as well. The type of those turbines generally depicted would be a 3-blade horizontal axis lift-type wind turbine. [57]

However, it can be noticed that the spread of wind power systems is weak in many countries. The problem in many regions is low acceptance due to a “ruined landscape”. That might be true if large wind parks are considered, but carefully planned wind turbines do not harm the landscape. The key to success is the communication with the residents to find a solution that is suitable for everyone. [58]

In general, the following aspects are relevant for the implementation of wind turbines:

- The location needs to be chosen carefully, as the wind profile is to be observed to achieve good efficiency. In complex terrain, this assessment can be complicated. Maintainability should be considered as well if placed at hardly accessible places. [59]
- The residents in the region need to be included in the planning process for a higher chance of acceptance. [58]
- Regional laws and restrictions need to be considered, including flora, fauna, optical disturbances, and noise pollution. [58]

There are different types of hydropower plants: large (>10 MW), small and hidden hydropower plants. Additionally, hydropower can be distinguished into run-of-river plants and plants with a storage reservoir. Traditionally, hydropower plants are extremely dependent on the location, as they can only be placed near a river. Another technology is placing turbines in wastewater systems. The successful placement depends on the wastewater quality. [32]

Generally, the following aspects need to be considered regarding implementation of hydropower plants for microgrids:

- A suitable river or wastewater system is required. [32]
- Placing a hydropower station can interfere with the flora and fauna considerably if a reservoir is created. [32]
- Depending on the size, different turbine types, such as Francis, Kaplan or Pelton turbines are most efficient. [32], [42]
- Region regulations might be established regarding the interference with flora and fauna through water waves or similar matters. This can limit the control possibilities. [42]

- To increase the eco-friendliness, fish or beaver passes may be necessary at additional costs. [32], [42]

Table 2.4 summarizes the comparison of the presented renewable energy sources based on the mentioned classification criteria. The feasibility in urban areas is the biggest advantage of the PV-systems, making them the commonly used technology for nZEBs. As this advantage is highly likely to prevail in future, PV-systems will be used as the object of investigation in this work. However, the knowledge gained about the control strategies will be transferable to microgrids with other renewable sources.

Table 2.4: Comparison of renewable energy source characteristics [36], [60]

Characteristics	PV-System	Wind	Hydro
Availability	Dependent on geographical location		
Output	DC	AC	AC
Controllability	Only output power reduction		
Typical interface	Power electronics converter (DC-DC-AC)	Power electronics converter (AC-DC-AC)	Synchronous or induction generator
Power flow control	MPPT, DC link voltage control	MPPT, pitch and link voltage control	Controllable
Feasibility in urban areas	High	Very low	Low

2.2.2 Storage systems

ESS can collect energy, store the energy, and release the energy again. These three processes are called charging, storing, and discharging [61]. Each of these processes has a certain efficiency η due to heating or friction losses. The output energy is always smaller than or equal to the input energy (2.1):

$$E_{out} = E_{in} * \eta_{ESS,charge} * \eta_{ESS,store} * \eta_{ESS,discharge} \quad (2.1)$$

where: E_{out} : Output energy [Wh]; E_{in} : Input energy [Wh]; η_x : Efficiency of device x [%].

These efficiencies in combination with other properties, like calendric lifetime, cyclic lifetime, capacity, or reaction time, are important characteristics to consider for the choice of an ESS for a certain application. The main function of ESS in the microgrids is balancing of energy demand and supply [62]. In islanded mode, in particular, the generated power from DG units needs to be matched to load demands immediately to ensure stable operation. The ESS capacity must therefore be sufficient to mitigate the volatile renewable generation unbalances on request. Furthermore, the transition between islanded and grid-connected mode should be run seamlessly by the ESS. [63]

An overview of the classification of different ESSs is given in Figure 2.8, and a comparison of different storage systems is shown in Table 2.5.

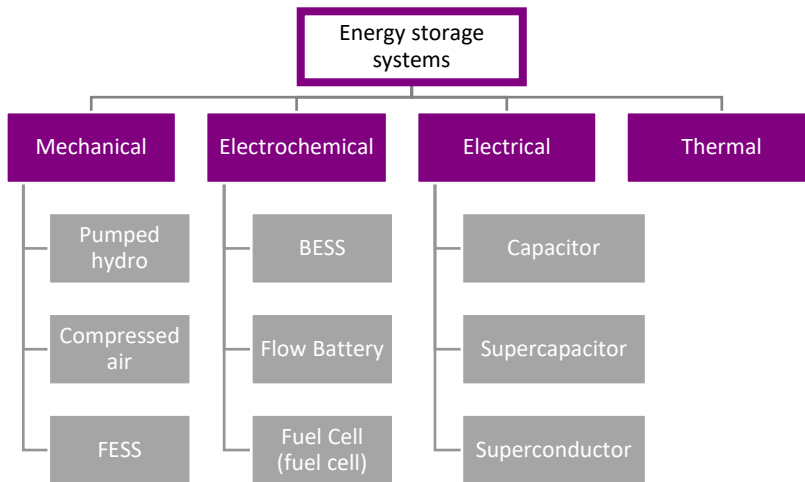


Figure 2.8: Overview of energy storage systems [33]

Table 2.5: Comparison of energy storage technologies [64]

Storage	Li-ion battery	Vanadium redox battery	Fuel cell	Pumped hydro	Compressed air	Supercapacitor	FESS
Efficiency [%]	90-97	70-79	34-51	70-82	70	90-95	83-93
Self-discharge [%/day]	0.008-0.041	0.3	0.03	0-0.5	-	0.004-0.013	72-100
Cycles [n]	400-6000	7000-15000	-	12800-33000	-	1Mio.	>1Mio.
Costs	++	+++	+++	++	++	+++	+

+ low; ++ medium; +++ high; - not available;

As seen in the table, lithium-ion based BESSs have the highest efficiency while showing very low self-discharge rates. Additionally, their costs are lower than for most other technologies. Due to these advantages, BESSs are the best generally feasible technology for nZEBs as a medium-term storage system and will be discussed in more detail in the next chapter. FESSs, on the other hand, have lower efficiency and higher self-discharge rate. But they achieve very high numbers of charging and discharging cycles. The costs for a FESS are much lower compared to supercapacitors with similar strengths. Based on that, FESSs are the most feasible technology for short-term energy adjustments in nZEBs. Therefore, they are investigated in more detail in the following sections as well.

2.2.2.1 Battery energy storage system

BESSs are electrochemical storage systems where the energy is stored as chemical energy. Common battery types are lead acid, nickel, or lithium based. The most widely used battery in smartphones, electric cars, and buildings is the lithium-ion battery [65], [66].

The self-discharge rate during the storing state depends on several parameters, like the electrolyte material, temperature, or the state of charge (SOC). The behaviour of aging for BESSs can be defined by aging over time and aging per cycle. The aging over time, or so-called “calendric lifetime”, is influenced by temperature and SOC. The cyclic lifetime is influenced by the charging and discharging rate, temperature, SOC and discharge depth [61]. A lower number of charging cycles will reduce these aging effects and increase the durability of the BESS. In this regard, battery diagnostics are necessary to observe and maintain reliability, prevent catastrophic failures, and predict the end of battery lifetime. So far there is no quick method to test everything with certainty as a battery can be compared to a living organism. To estimate the state of health (SOH) of a battery, test methods presented in [67] could be used.

For example, the state of life indicator (SOLI) estimates the battery life by counting the total coulombs a battery can deliver in its life. A new battery starts at 100%; delivered coulombs decrease the number until the allotment is spent and a battery replacement is imminent. The full scale is set by calculating the coulomb count of 1 cycle based on the manufacturer’s specifications (V, Ah) and then by multiplying the number with the given cycle count.

According to [68], battery lifetime can be prolonged by:

1. Reducing stress with moderate two- to three-hour-charge rather than an ultra-fast charge within less than one hour
2. Prevent harsh and erratic discharges
3. Rather charge a battery more often than draining a battery fully
4. Prevent unfavourable temperature conditions: extreme cold and high heat
5. Checking small- to mid-sized batteries with a full charge/discharge cycle on a battery analyser
6. Maximizing battery life by slight overdimensioning to cover unknowns and emergencies

2.2.2.2 Flywheel energy storage system

A FESS converts electrical energy into rotational energy and vice versa. For the conversion, an electrical drive is used that is connected to a rotational mass. The energy is stored in the rotating mass. Charging is the acceleration of the rotational mass, rotation at a certain velocity means storing the energy, and decelerating the rotational mass is the discharging process.

A basic schematic of a FESS is depicted in Figure 2.9:

- The electrical drive is connected to an inverter. It can either be a three-phase asynchronous or synchronous induction motor, or a DC motor.
- Additionally, FESSs can have a fan to cool the electric drive.
- The inverter increases, holds, or decreases the rotational speed of the drive.
- The shaft connects the rotational mass and the drive. It must withstand high torques from the drive and rotational mass inertia.
- The mass is fixed with bearings to the chamber to reduce vibrations.
- The chamber itself is completely closed for modern FESS for safety reasons.

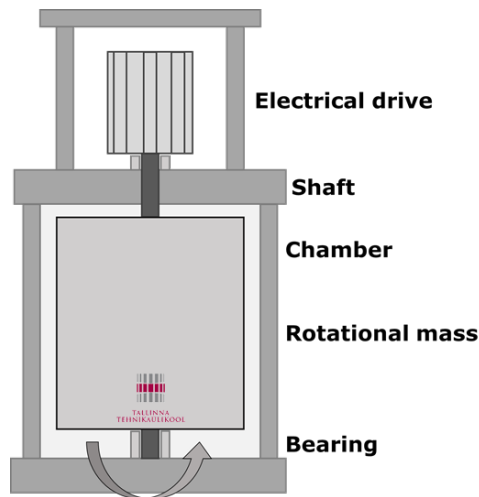


Figure 2.9: Schematic of a FESS [64], [69]

FESSs are scalable for applications from small consumer systems [69] to large grid applications [70]. They are most useful for applications with high power demand for short durations occurring in a cyclic nature. Therefore, FESS can be used for power quality applications [71] as an uninterruptable power supply [71], or for power smoothing [72]. Capacity and maximum power delivery can be scaled by arranging multiple FESS in banks [71], [73]. The advantages of FESSs compared to other storage systems are [74], [75], [76]:

- High power density
- High energy density (high-speed flywheels)
- No capacity degradation over time
- Long lifetime: more than 10^5 charge cycles
- Short recharge time
- Simple SOC estimation
- Low maintenance cost
- Manufactured without rare materials
- Scalable technology

Disadvantages are [74], [75], [76]:

- Low energy capacity
- Low energy density (low-speed flywheels)
- High self-discharge
- High investment cost

The potential of FESS is limited to short-term energy storage applications due to its high self-discharge rate of 3% to 20% per hour [61]. The reason for the self-discharge of FESSs is mainly friction: mechanical friction at the bearings and air friction on the rotational mass. Measures that can be taken are:

1. Using magnetic bearings instead of ball bearings reduces the mechanical friction.
2. Applying a vacuum in the chamber reduces the air friction.

Both of these measures improve the self-discharge of FESS significantly. Based on the basic equations describing a FESS, (2.2) and (2.3), the stored rotational energy, respectively the energy density, can be increased by:

- Increasing the rotational speed
- Design changes at the rotational mass to increase the inertia

$$E_{rot} = \frac{1}{2} * J * \omega^2 \quad (2.2)$$

$$J = \sum_i m_i * r_i^2 \quad (2.3)$$

where: E_{rot} : Rotational energy [J]; J : Inertia [kg m^2]; ω : Rotational speed [rad/s]; m : Mass [kg]; r : Radius [m].

FESS rotational masses can be manufactured from different materials, like steel, titan, or fiber-reinforced plastics. The latter is a relatively new technology for FESS, which increases the potential energy storage compared to steel. Another benefit of reinforced plastics is their behaviour if the rotational mass breaks due to a malfunction: masses out of steel build a dangerous bullet, while the reinforced plastics shatter into lighter, less dangerous pieces [61].

ABB, Amber Kinetics or Beacon POWER produce FESSs. Several grid scale FESSs operate in Asia and the USA. Recently, Siemens Energy announced to install the world's largest FESS for grid stabilization in Ireland [77].

2.2.3 Home appliances and buildings as TES

As mentioned before, one possibility to balance the volatile renewable energy production is to adjust the load side. This process is called DSM or demand response; the total amount or potential for changing the load at a given time is investigated in flexibility analyses.

Grid utilities usually provide lucrative offers for customers to engage in such flexibility or demand response programmes. Within this framework, different devices and loads in a typical dwelling can be scheduled [78]. However, this scheduling needs to be done carefully not to reduce the user comfort [79]. Scheduling a washing machine or a dishwasher needs actively participating users to prepare the device and have a flexible policy for finishing the job, e.g., folding laundry whenever the device is ready.

Another group of schedulable devices available in most households that influences the users' habits much less are freezers, water heaters or space heating systems. These devices cannot just be scheduled but are used as TESs as well. This provides additional energy storage without additional investments into systems like supercapacitors [80] or batteries [81]. The mentioned TESs are even more relevant, considering that such appliances can compose 50% of the electrical energy consumption in buildings [82], as shown in Figure 2.10. A relatively long lifetime of 10-20 years [83] of such devices is convenient for users as well.

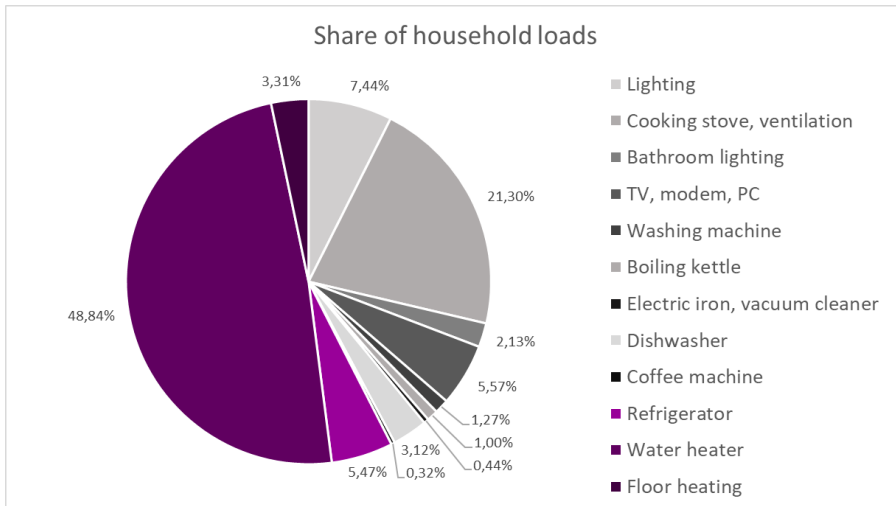


Figure 2.10: Share of household loads; purple: TESs; grey: other [82]

2.2.3.1 Freezers and water heaters

In many publications, freezers and water heaters are studied regarding to scheduling algorithms like in [84], or the performance and feasibility of implementing control as in [85]. Other publications consider a model predictive scheduling method for freezers or water heaters based on the day-ahead or real-time market prices, which leads to cost reductions [86], [87]. Even though the TESs do not influence the user comfort level as much as some other devices, it should still be considered in the control algorithm design. Different boundaries due to user comfort considerations can influence the performance of such algorithms, as shown in [79].

The studies in [10] and [88] addressing the performance and feasibility aspects of DSM algorithms for freezers and water heaters consider the user comfort as well. In their analysis of a grid-connected system, the focus is on price-based control methods. This increases the cost savings of the system, which is important as many microgrids operate most of the time with a grid connection. Few papers consider the possibility to increase the power quality in the off-grid mode with TESs or other scheduled loads [89]. Grid backup or diesel generators are often used in such investigations [90], which is not desirable due to CO₂ emissions, as mentioned earlier. In [91], a simple scheduling algorithm is presented for a water heater and battery storage reductions of about 15-25% for a PV-powered off-grid building including BESS. A power quality control strategy for water heaters investigated in [92] implemented peak load shaving for a grid-connected system.

In summary, freezers and water heaters can be scheduled in a DSM-manner to achieve electricity cost reductions of about 5-30% [86], [10]. Additionally, some publications show power quality and reliability improvements with such devices. In an islanded microgrid scheduling, these loads with a sophisticated algorithm can be used to reduce the battery capacity, ensuring stable operation while providing potential cost reductions for an expensive BESS [93].

2.2.3.2 Space heating of buildings

To develop thermal freezer and water heater models for DSM simulations, knowledge in electrical engineering and thermal engineering is necessary. Modelling a building thermally for electrical microgrid simulations is an even more interdisciplinary approach, where expert knowledge in civil engineering is mandatory to create a detailed model as well. As a result, there are typically three different kinds of models:

1. Complex control strategies with simplified thermal models from the electrical engineering domain
2. Complex thermal models with simple control strategies from the civil engineering domain
3. Co-simulations between different modelling software as a cooperation of both domains

Complex Control Strategies: Several authors present simplified thermal models for heating demand estimation, like [94], where a minimalistic model of space heating is used. Space heating is modelled as a certain percentage of the overall energy consumption, and on that basis, a price-based control strategy is proposed. In [95], a multi-agent system is used for DSM control strategies. The model for space heating is a simple aggregated model in that case. A DSM approach for assessing the flexibility of heat pumps is shown in [96], using simple thermal models for the houses and heat pumps.

Complex Thermal Models: Publications that show accurate thermal models typically do not consider DSM-related electrical control strategies, or only in a limited way. As an example, in [97], a linear time-series model based on historical measurement data is presented. The model shows good results while being computationally light. However, there are no considerations about DSM control methods. Similarly, a detailed thermal model of a building is shown in [98], but DSM strategies are not considered for the control. Other publications, such as [99], [100], present very accurate models of heat pumps or buildings, but the proposed control strategies are quite simple. In this case, the full flexibility potential cannot be achieved and the simple pre-charging for peak shaving does not show the anticipated results.

Based on discussions with civil engineers, the development and modelling of space heating objects will take more than 100 hours, depending on the level of detail and modelling software. In this regard, Matlab and other electrical engineering software is not recommended for fast development of detailed thermal building models and will increase the effort and time for development.

Co-Simulations: If complex DSM control strategies are to be connected with complex thermal models, co-simulations can be a powerful tool. Since civil engineering software often does not provide a good framework for complex DSM control strategies and electrical engineering software has limited tools for thermal models, implementations of both aspects in one software can be very time-consuming in both cases. Co-simulations bring both simulators together [101] and use the complexity and detail of each simulation. To implement a co-simulation, the functional mock-up interface (FMI) or functional mock-up units (FMU) can be used. These are supported by multiple simulators, including Matlab or Python [102]. Another possibility is presented in [103], where the control is modelled in Modelica, while the building is simulated in EnergyPlus. The SimAPI software platform can be used to connect the building model and control, as shown in [104]. A comprehensive overview of co-simulation with fundamental disadvantages,

like slow speed and limited compatibility, is shown in [105]. The following drawbacks apply, for example, to the above-mentioned publications about co-simulations:

- Additional overhead for coordinating and synchronizing
- Initialization of some simulators for each macro time step
- Limited communication and data exchange between simulators
- Complicated implementation in real-time simulations

Thus, existing articles in literature typically cover complex control strategies for DSM with space heating but are lacking complex thermal models by relying on simplified temperature difference based or aggregated models. Vice versa, publications with complex space heating models provide detailed models in the thermal domain, but the control strategies are limited by using fixed set point (FSP) control or other simple methods, given that a DSM related control is considered at all. Co-simulations as an alternative have other limitations, including connection, communication, and compatibility issues with an additional communications overhead that can slow down those simulations. This indicates a need for a new methodology with complex thermal models in combination with DSM related control strategies.

2.2.3.3 User comfort

As mentioned, TESs have a lower influence on the user comfort than some other scheduled household appliances. However, especially for space heating, special attention is to be given to the temperature related user comfort definition and implementation. Comfortable temperature settings are different for every person. In some publications, the researchers use certain preferred or fixed temperature ranges and limits that are typically based on standards, as shown in [106] or [107]. But these limits do not take into account the temperature fluctuations within the limits, which can already disrupt the comfort for some people. Additionally, there are no specific definitions for the user comfort in the temporary islanded operation of a microgrid. Thus, both of these aspects should be considered in this work.

2.3 Machine learning applications in microgrids

In recent years, artificial intelligence has gained increased attention in all fields of research. In particular, machine learning methods have many use-cases in the field of electrical engineering. One reason for this is the increasing number of smart meters and the related availability of recorded data. There are several applications for machine learning, as shown in [17]. The most relevant applications for machine learning regarding microgrids are:

- Forecast of residential loads [108] in connection with flexibility considerations [109] or load modelling [110]
- Forecast of renewable energy sources, like PV- [111] or wind power [13]
- Blackbox modelling of complex objects like [97]
- Control purposes, like general energy management [112], power flow control [113], or bidding strategies [114]
- Disaggregation of SM data to improve recommendations and control of home energy management systems or ambient assisted living [115]

These applications are discussed in more detail in the following sections.

2.3.1 Forecasting and prediction with machine learning

For forecasting loads and renewable energy production, different methods have been researched and developed based on time series analysis methods and more recently on machine learning algorithms. Compared to complex machine learning algorithms, ARIMA or linear regression models [116], [117], [118] are quicker to implement and calculate, thus providing advantages with simple problems.

More complex problems may be solved with a machine learning based regression model, as shown in [109] more efficiently. Additionally, such a method can be used online and in real time. Long short-term memory networks are very well suited for specific forecasts [119], [120], [118] where short- and long-term components are relevant.

A very popular machine learning technique intended not just for predictions of load and renewable production patterns, but also in terms of general approach, is neural networks [121], [118]. This technique can be used for long- and short-term load predictions as well. Figure 2.11 shows an example of the forecast of the hourly energy consumption for Estonia, using linear and NN-based predictions.

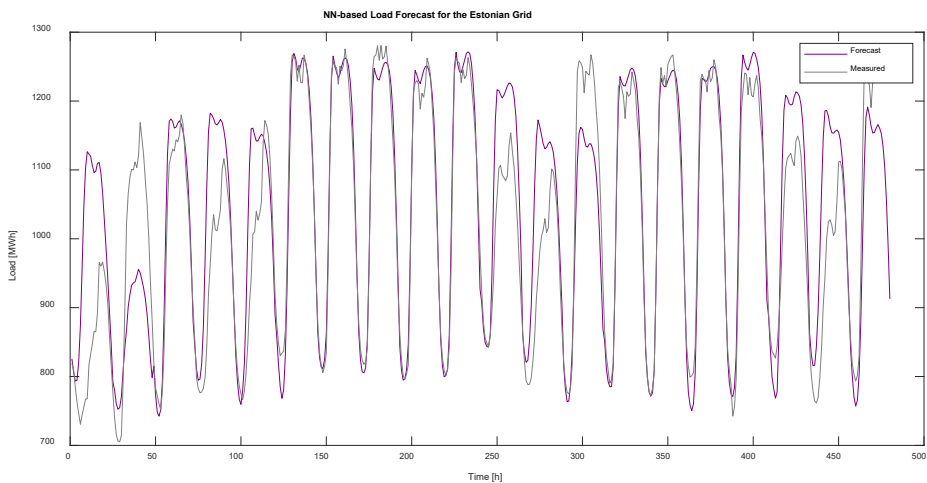


Figure 2.11: Load forecast for the Estonian grid [118]

In this regard, black-box object modelling is a more specific approach of forecasting. In general forecasting tasks, environmental influences, like temperature or weather, are used to estimate a general output, e.g., irradiation or energy consumption, with ML. Additionally, the model is intended for calculations of each time step of a simulation, for example, instead of forecasting the whole load profile at once.

Object modelling does not use just environmental parameters, but also, for example, object internal values or correlations as input data for the ML. This can increase the complexity of the input data set. The output of the ML algorithm is a very specific object variable, like voltage, current or a temperature change, that can be used for calculations in the next time step of a simulation, e.g., as part of an input for the same ML model. The training and use of such an ML-based object model is depicted in Figure 2.12. The model can only be used within the trained limits and has a lower accuracy than the original model or system used for creating the ML input data.

Specifically, to exemplify modelling a space heating system, an approach similar to the one presented in [97] could be used. The authors use a time series algorithm to create a black-box model with measurement data. Instead of using measurement data, it is also possible to create data sets from simulations with accurate models, like [98]. In this case, even more measurement variables are available that can be used for the model training. This results in more complex data sets that can be learnt more accurately by the ML instead of time series methods. The trained algorithm then acts as a black-box model in microgrid simulations with electrical engineering software. Additionally, machine learning based black-box models of microgrid devices, like space heating, can be integrated more easily into real time simulations of microgrids [18] than co-simulations due to the limitation to one simulation environment, as analysed in more detail in Chapter 3.

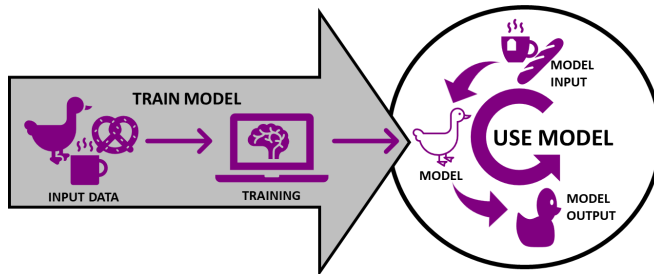


Figure 2.12: Training and use of ML-based object model

2.3.2 Control and coordination with machine learning

Coordination in a microgrid does not only include the specific control task for one object, but multiple control objectives for multiple devices [122]. NNs on the one hand, as well as other supervised and unsupervised machine learning methods, cannot be used directly for control purposes. They can only be included for specific tasks in other control and coordination methods. Reinforcement learning, on the other hand, is a specific machine learning technique for control that can be directly used [123]. A basic reinforcement learning based control system works as shown in Figure 2.13. The reinforcement learning process works as follows:

- The reinforcement learning agent interacts with the environment by taking actions.
- The agent follows a certain policy to take actions.
- The agent observes the environment and gains rewards that are used for learning.

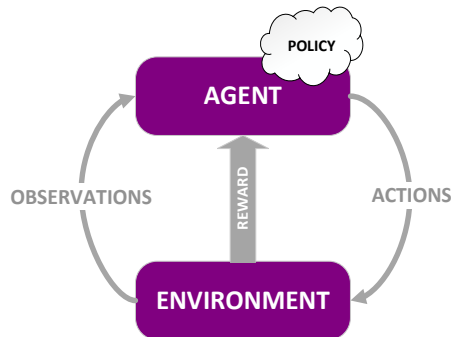


Figure 2.13: Typical reinforcement learning based control

Extending the control capabilities of reinforcement learning to implement machine learning (ML)-based coordination tasks in microgrids results in three main methods, as depicted in Figure 2.14.

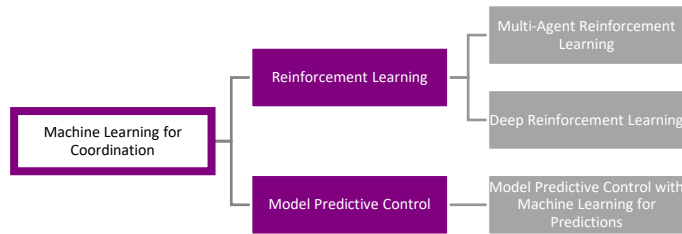


Figure 2.14: Machine learning based coordination methods

Multi-agent reinforcement learning strategies are presented in [124], [125] and [126]. For such coordination approaches, a multi-agent structure is used with reinforcement agents for devices and management.

Deep reinforcement learning is presented in [127], [128] and [129]. This kind of control is using deep artificial neural networks with multiple layers instead of more simple ones inside the reinforcement learning agent to achieve more complex coordination tasks.

Another coordination method is model predictive control including ML-based prediction. Model predictive control itself is not related to machine learning but it is a common control strategy [130]. However, there is a special kind of model predictive control that uses machine learning predictions to determine control decisions. For example, in [131], a recurrent neural network is used for day-ahead predictions that influence the control decisions directly.

Regarding all these ML-based coordination methods, it can be summarized that they are an emerging topic as there are certain limitations to be studied in detail to have a robust and efficient coordination architecture. Advantages of these methods are a decreased need for information about underlying structures, which can be an important reason for deciding the coordination method, considering privacy concerns of users. Thus, this work will focus mainly on the implementation of more robust control strategies and consider ML-based control strategies as a promising option for future developments.

2.3.3 Disaggregation with machine learning

To gain additional information for different applications in microgrids, disaggregation of load profiles can be used. This process is called non-intrusive load monitoring (NILM). Applications of NILM include home energy management systems, ambient assisted living, recommender systems and fault diagnostics [132]. The goals of these applications are different, like power on/off detection, power estimations [133] or predictions for more efficient home energy management [134]. The basic process of NILM is shown in Table 2.6.

The NILM process is quite independent of the used ML methods, like neural networks (NN) or support vector machines. The amount, resolution and details of the collected data, the amount of auxiliary data measurements, and the disaggregation purpose differ between presented methods in the literature. Some publications use different public data sets [135] for their NILM training and tests whereas other publications rely on their

own measurement data, which can complicate performance comparisons. Considering the size of the public data sets, the amount of processed data is large for most of the NILM methods, which can raise privacy concerns of users about the collected data and their use.

Sometimes additional data measurements are used in publications to improve the NILM results. These additional measurements can be voluntary user feedback [136], classifying the user activities [137], or the use of cameras, motion sensors and smartphone apps for tracking [138]. Other additional proposed features for a better user experience are smartphone applications [139], cloud-based monitoring features [115], or novelty detection for new appliances [140]. However, none of those papers consider privacy or cyber-security in any way.

Table 2.6: NILM process stages [132], [53]

Stage	Description
Metering	Data is collected from smart meters and sometimes additional measurement equipment, typically with a low frequency (including current, voltage and power data).
Event detection	Events are detected within the data sets (e.g., an appliance changed its state).
Feature extraction	Every appliance has a certain load signature and features, by which it can be distinguished from others.
Classification	Loads are identified by a classification procedure to determine the times or periods a device was operating.
Analysis of classification	For each specific application, the classification can be analysed to draw conclusions.

2.4 Power hardware in the loop and real time simulations

There are different methodologies to test models and hardware components, like model validation tests etc. The following three types should be distinguished [19]:

1. Software in the loop tests: These are solely run on a virtual device under test (DUT).
2. Classical hardware in the loop tests: A hardware DUT is used and the communication between the simulation environment and the DUT is performed in real time. No high power is running through the DUT, and signals are not measured under real time conditions.
3. Power hardware in the loop (PHIL) tests: A real time test bench is used, where the DUT is analysed under real conditions. During the test, high power is running through the DUT and real physical signals are measured.

In this context, the terms “real time simulation” and “real time simulator” are commonly used. A real time simulator, by definition, is capable of executing a computer simulation or model at the same rate as an actual physical system. For example, if a kettle needs 1 minute to heat the water reservoir, it needs 1 minute in the simulation. This gives the advantage that physical devices can interact with simulated models and vice versa. However, complex systems, including devices with high sample rates, can quickly reach the computational limits regarding the real time requirement. [141], [18]

An example of a PHIL setup is depicted in Figure 2.15. In this example, the load profile and BESS are simulated by the real-time capable PLC. Thus, they are not part of the DUT. The FESS control algorithm runs on the PLC as well and interacts with the simulated models in real-time. The PLC is controlling the inverter, which is connected to the induction motor of the flywheel energy storage and to the grid.

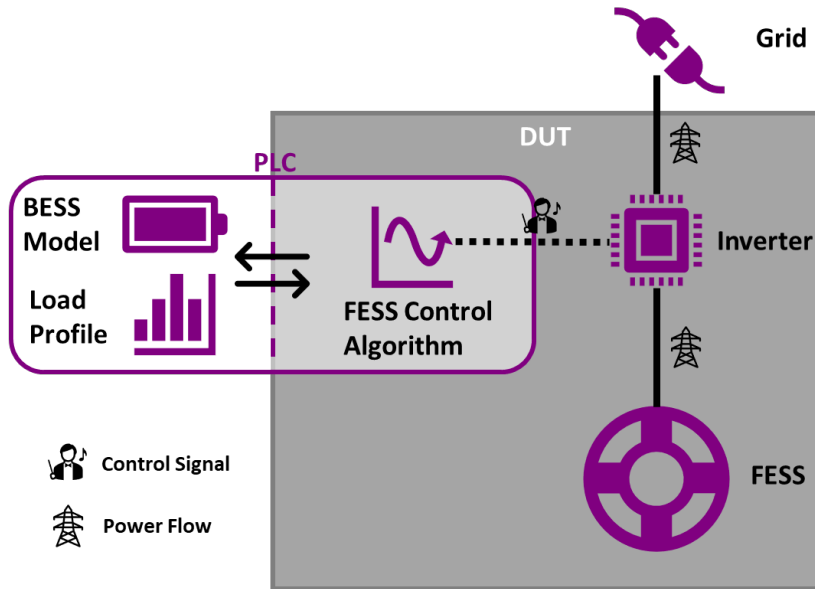


Figure 2.15: PHIL example schematic [64]

There are four main benefits of implementing PHIL technologies [142]:

- Faster and cheaper development due to digital twins
- High fidelity simulation results
- Easy to add or modify simulated devices
- Ability to simulate scenarios that are hard-to-achieve in the real world

The main drawbacks are:

- The inaccuracy of the simulation due to time delays of calculations and signal transmission
- The potential instability of the simulation

The advantages of PHIL setups outweigh their disadvantages, making PHIL systems increasingly popular and better available [143]. Due to differences of DUTs and test scenarios, the PHIL hardware setup is to be chosen carefully to develop a stable setup. The DUT can be any device, like a resistive load, a PV-inverter, an energy storage system (ESS), or even a complete microgrid system [143], [144]. Examples of PHIL setups are:

1. FREA PHIL Setup in Japan [145]: The PHIL components are a diesel generator, PV-system, BESS, load, and measurement devices. The microgrid controller is simulated.
2. AIT PHIL-Setup in Austria [146]: The PHIL components are a programmable load, power amplifier and BESS. A digital twin of the BESS is simulated.

3. Test bench for PHIL simulation of a PowerCorner device [147]: The PHIL components are a power amplifier, A/D and D/A converters, sensors and inverters. PV-system and an energy storage device are simulated.

As microgrid systems can quickly become very complex with multiple different components that have different control needs, the setup of a completely physical testbench for a microgrid may prove a time-consuming and expensive project. A lot of development time and costs for the communication between different controllers of microgrid components can be reduced with a PHIL-setup and expanding such a system with more components is easier as well. Thus, a PHIL-setup for the validation of some models and control strategies of this work will be developed.

2.5 Conclusions

From this comprehensive review of the state of the art, regarding multiple structures, devices and methodologies, the following conclusions can be drawn:

- As DC microgrid systems are not yet standardized, e.g., regarding voltage levels, there could be future-related uncertainties using a DC or hybrid microgrid modelling. Thus, an AC microgrid topology is of higher interest for this investigation.
- Grid-connected operation with participation in energy markets should be considered in the investigation, as the AC microgrid will be operating most of the time with a main grid connection. However, due to the high future penetration of renewables, islanded operation should be the focus for the control strategies in this work to improve security of supply.
- Since the current standard for new buildings and renovations is nZEBs, a typical configuration of such a building should be modelled for the microgrid.
- This includes PV-system for power supply, as it is the most common and most feasible renewable energy source for such applications and storage systems to implement a suitable EMS.
- For the storage system, a BESS is the optimal choice considering capacity, power rating and feasibility.
- The drawback of BESSs is their lifetime, so a FESS should be added for peak shaving and load levelling to reduce stress on the BESS and increase the cyclic lifetime.
- Common household TESs should support the other ESS.
- TESs' impact on the user comfort is to be investigated for the control strategies in different operation modes.
- PHIL real time simulations are used for faster development and validations.
- Machine learning methods can be used for model development.
- Additionally, due to the ML approach, it is relevant to investigate privacy concerns of potential users towards the proposed systems.

On this background, the microgrid topology shown in Figure 2.16 is proposed for the investigation. The PV-system, load, BESS, FESS and TESs need to be modelled first, as presented in the next chapter, in order to validate them and develop control strategies for achieving the aim of security of supply and financial feasibility improvements as a basis for recommendations.

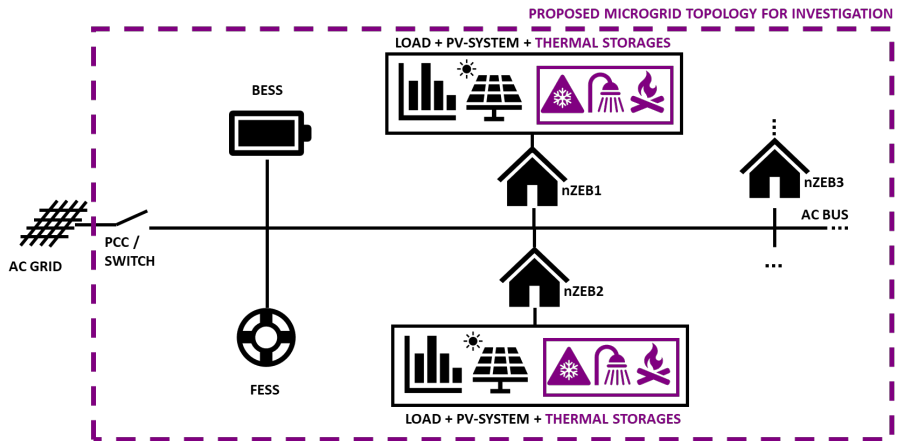


Figure 2.16: Topology of the proposed microgrid system for investigation

3 Research and development of object models for microgrid components

To simulate a microgrid, it is necessary to have object models of all the relevant components and apply control strategies to those models. In this chapter, the relevant object models and used profiles are presented. These include the patterns for PV-systems, thermal and electrical load patterns, FESS, BESS, and common household TESs. The applied control strategies are addressed in Chapter 5.

The FESS and BESS models have several simplifications to ensure a fast calculation speed at reasonable accuracy, as shown in Chapter 4. The TESs, freezer, water heater and space heating are modelled based on linearized equations. A space heating model has a much higher complexity than a freezer or water heater model. This leads to more than 100 hours of manual model development and simplifications if a detailed model is developed in electrical engineering software. Therefore, methodology for a space heating model based on neural networks was created. The error and accuracy analysis to determine the model quality is shown for these models in Chapter 4 as well.

Several profiles were integrated into microgrid simulations to be able to test the implemented scenarios. These profiles can act as object models or as inputs for object models. The following profiles were included:

- PV-system measurements
- Electrical load patterns
- Various consumption resp. thermal load patterns
- Occupancy patterns

These profiles are partly measured data and partly artificially generated data. The following subsections describe the different profiles in detail.

3.1 PV-system profile

Two PV-system measurement profiles with different resolutions and for different locations were used as PV-system models. One profile was measured in Estonia and the other in Southern Germany.

The Laastu Talu OÜ PV-system is a larger installation with 668 PV-panels and an output peak power of 177 kWp. It is located in northern Estonia, south of Tallinn. The available dataset was measured from 17th to 24th September 2019 with a resolution of 1 min [33], [148]. An example day of this profile is shown in Figure 3.1.

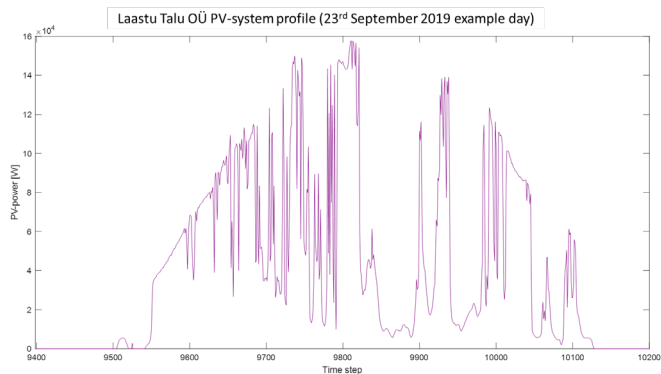


Figure 3.1: Example day from the measured PV-system profile in Estonia

The second PV-profile used was measured in southern Germany by Allgäunetz GmbH & Co. KG. It contains data from 17th to 22nd July 2019 with a resolution of 1 s [64]. As an example, data from 19th July is shown in Figure 3.2.

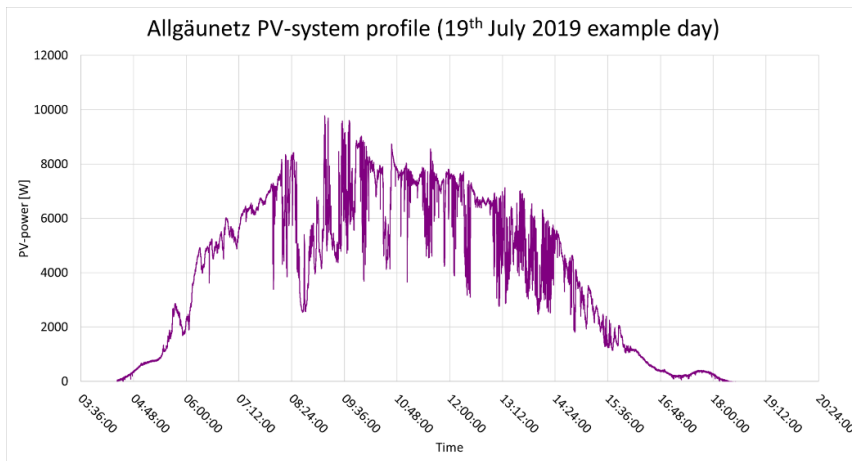


Figure 3.2: Example day from the measured PV-system profile in southern Germany

For different applications and tests, the PV-profiles need to be scaled in size accordingly. This scaling factor [149], [33] can be calculated as shown in (3.1):

$$\text{Scaling Factor} = \frac{P_{\text{Yearly}}}{\frac{Gen_{\text{Typ}}}{P_{\text{Peak}}}} \quad (3.1)$$

where: P_{Yearly} : Yearly power consumption [kWh/a]; Gen_{Typ} : Typical regional solar generation [kWh/kWp]; P_{Peak} : Unscaled peak power of PV-installation [kWp].

For example, Gen_{Typ} can be obtained from PVGIS [150]. The typical regional solar generation values for the locations of the PV-systems are:

- Estonia: 864 kWh/kWp
- Southern Germany: 1000 kWh/kWp

3.2 Thermal and electrical load profiles

There are multiple thermal and electrical load profiles that have been used for different investigations in this work. This was necessary because the modelled laboratory equipment used for verification is dimensioned for different system sizes. Therefore, accordingly sized load profiles should be used for validation tests and simulations. Within reasonable limits, it is possible to transfer the results to larger or smaller sized systems [149].

An overview of the used load profiles with relevant parameters and related applications within this work is presented in Table 3.1.

Table 3.1: Overview of load profiles with relevant parameters [148], [151], [152], [153], [154]

Description	Type	Sizing	Δt	Time	Values	Application
NRG-Building	M	Larger building	1 sec	20 h	El	FESS model and control validation
Measured 3-room apartment	M	Household / Apartment	5 min	1 week	El, W, F	TES control, Water heater validation
Generated single family house	G	Detached single family house	1 min	1 year	El	FESS + BESS control
8 generated households with different occupancies	G	Household / Apartment	5 min	1 week	El, W, F	TES control

M: Measured; G: Generated; El: Electricity Consumption; W: Water Consumption; F: Food Consumption.

The NRG-Building profile was measured on the Tallinn University of Technology campus. The measurement was done for the NRG-Building starting from April 3rd, 2019, 10:00, until April 4th, 2019, 6:00. The measurement resolution was 1 s during that timeframe. This load profile shows the power fluctuations of a university building (c.f. Figure 3.3). Thus, it is suitable for the flywheel model and control validation where such power fluctuations should be balanced.

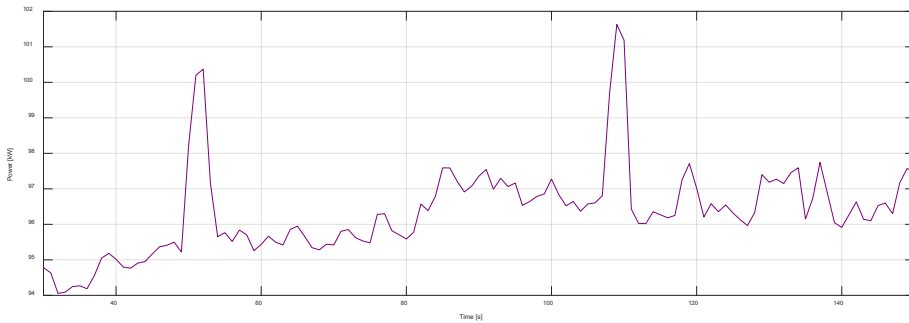


Figure 3.3: Example segment of the measured NRG-Building load profile

The measured apartment profile [151] represents a typical dwelling, as mentioned in section 3.4. It is a 67.4 m², 3-room apartment in the Kristiine district in Tallinn, Estonia. The measurements for different appliances, hot water and food consumption, space heating, and total electrical energy consumption were conducted from 22nd February 2010 until 28th February 2010. It was occupied by 2 adults and 2 children during the measurements. The time resolution for all measurements was 5 minutes. This profile was used in the work for the research of TES control algorithms and in the verification on the water heater model. The total electricity load, and food and hot water consumption profiles as thermal loads are shown in Figure 3.4.

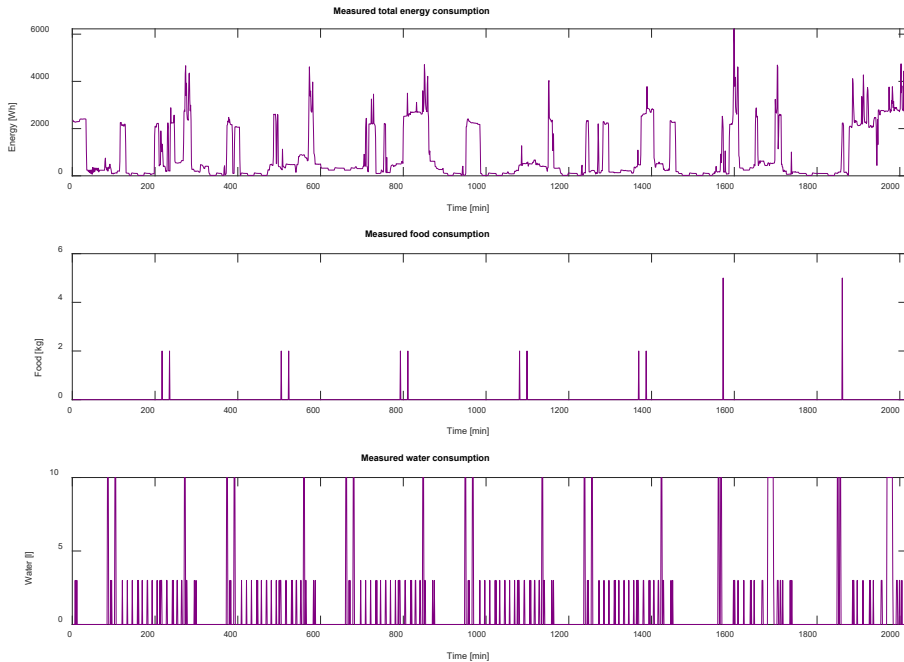


Figure 3.4: Measured total energy, food and hot water consumption

The generated single family house profile [148] and the eight generated household profiles [152], [153] with different occupancies were created using LoadProfileGenerator [155]. This is a software developed for a doctoral thesis at Chemnitz University of Technology in 2016 and is still being maintained and improved by the creator. The quality of the generated profiles has been assessed and validated, showing adequate similarity to measured profiles [156]. The load profile generation is based on an occupant behaviour model. This means that not just the electrical load profile, but also hot water usage, space heating, and cooking (food consumption) patterns are created and can be used. For the correct behaviour of the occupants regarding the weather, an outside temperature profile for Helsinki of the year 2017 from the Finnish Meteorological Institute was applied during the profile creation [157]. Helsinki has similar weather conditions as Tallinn, thus the profile for Helsinki can be used for this purpose.

The generated single family house profile [148] represents a family with 2 children. One adult is working, one is staying at home and the children go to school. The profiles were generated for a whole year with 1 minute time steps. The electricity load profile for one example day is shown in Figure 3.5.

The eight generated households (i-viii) represent the dwelling occupancies as depicted in Table 3.2. These occupancy profiles have been selected to represent typical occupancy scenarios for dwellings. This selection was based on the statistics of the Federal Statistics Office of Germany [158]. The selection criteria and shares according to [158] are shown in Table 3.3. These profiles were used to investigate the influence of different household occupancies on the performance of different control algorithms for TESs.

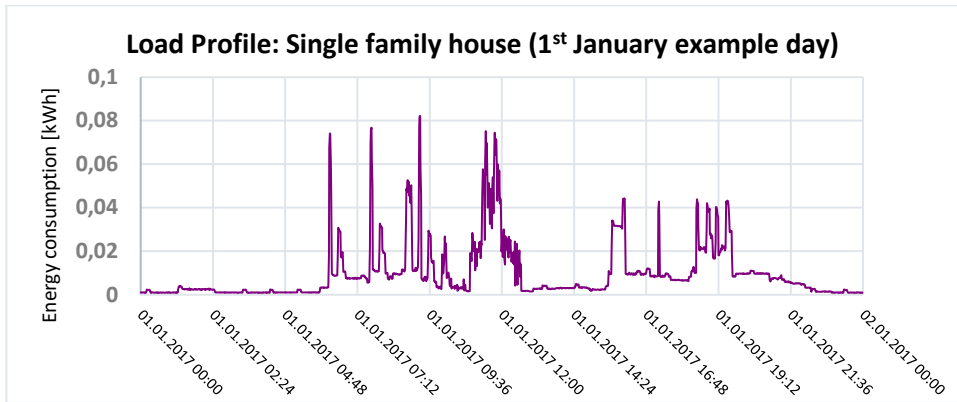


Figure 3.5: Example day from a single family house load profile

Table 3.2: Description of generated occupancy profiles with average electrical energy consumption per day [152], [153]

Household	i	ii	iii	iv	v	vi	vii	viii
Working	2	1	-	-	-	1	-	-
Studying	-	-	1	-	-	-	3	-
Unemployed	-	-	-	2	-	1	-	-
Retired	-	-	-	-	1	-	-	2
Children	-	-	-	2	-	2	-	-
Σ	2	1	1	4	1	4	3	2
El. Consumption [kWh/d]	9.82	4.18	2.15	14.63	2.58	13.10	9.22	5.85

Table 3.3: Occupancy profile selection criteria with typical shares [152], [153]

Number of people per dwelling		
Number of people	Share	Represented in household
1	42%	ii, iii, v
2	33%	i, vii
3	12%	vii
4	9%	iv, vi
Number of children per dwelling		
Number of children	Share	Represented in household
0	72%	i, ii, iii, v, vii, viii
1 or 2	25%	iv, vi
Number of people working per dwelling		
Number of people	Share	Represented in household
0	34%	iii, iv, v, vii, viii
1	36%	ii, vi
2	26%	i
Employment status of the person with the main income per dwelling		
Employment status	Share	Represented in household
Retired	36%	v, viii
Employed	48%	i, ii, vi
Other	16%	iii, iv, vii

These profiles have different consumption patterns, which is due to different occupations; some people are at work, at school, at university or retired. This does not only change the electric energy consumption directly but also the water heating and space heating load. The electric energy consumption patterns for one week for different households (i-viii) are shown in Figure 3.6.

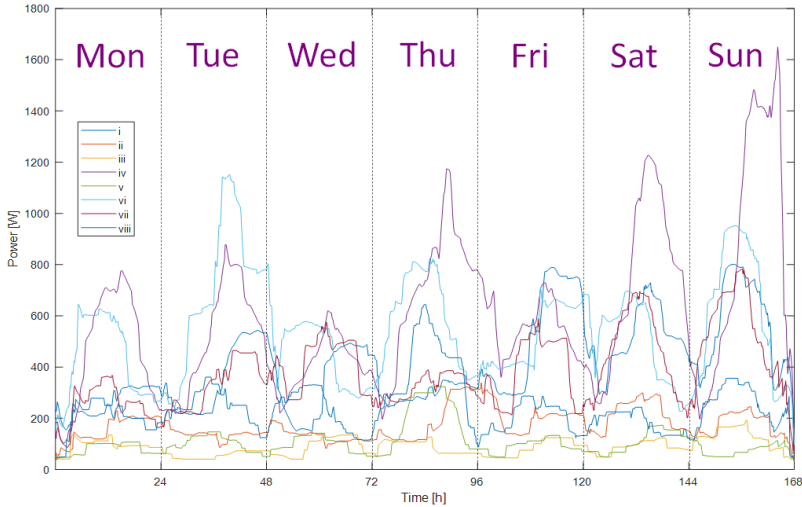


Figure 3.6: Electric energy consumption in households i-viii for 1 week [152], [153]

3.3 BESS and FESS model

The BESS and FESS models are based on existing objects and products. The FESS was modelled based on a device available in a laboratory at Tallinn University of Technology. The BESS is based on different datasheets from available lithium-ion batteries. The details about the models are shown in the following subsections.

3.3.1 FESS model with basic converter control

The FESS was modelled using Matlab/Simulink with the Simscape Electrical library [154], [159]. The model is based on the Rosseta Technik GmbH T3-15 FESS [69] with Unidrive SP2403 motor- and grid-side converters, located in Tallinn University of Technology. The relevant parameters for modelling are shown in Table 3.4.

Table 3.4: FESS parameters [159]

FESS Parameters	Value
Nominal Power	15 kVA
Energy Capacity	300 kW _s
Speed Range	500 – 6000 rpm
DC-link Capacitance	500 μ F
DC-link Voltage	700 V
Inverter Switching Frequency	16 kHz
LC Filter Parameters	Value
Filter Inductance	6.2 mH
Filter Capacitance	3 μ F

The modelled flywheel system includes an asynchronous machine, bidirectional AC-DC converters, a DC-link capacitor, and a LC filter at the front end.

The working principle of the flywheel storage system is shown in Figure 3.7.

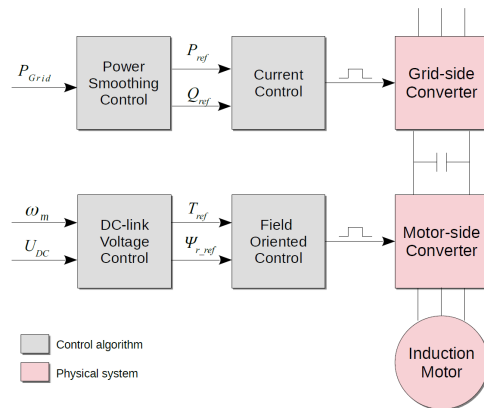


Figure 3.7: Schematic of flywheel storage system model control [154], [159]

The grid-side converter was used to exchange energy between the DC-link and the grid using current control. Due to the energy exchange with the grid, the voltage of the DC-link starts to increase or decrease. The resulting objective for the motor-side converter was to maintain the DC-link voltage within acceptable levels by supplying energy to or from the induction motor of the flywheel.

3.3.1.1 Current control

The power smoothing control, which is discussed in section 5.1, provides active (P_{ref}) and reactive (Q_{ref}) power control references to the current control block. The current control used the Clarke and Park transform [160] to convert the reference values from abc- to dq-domain. With the dq-domain reference values it is possible to calculate the output currents references of the grid-side converter using the grid voltage. A PI controller was used for minimizing the measured current and current reference difference. Considering the inductance from the LC-filter, the voltage difference signal of the PI controller and the measured voltage values, dq-voltage reference signals could be generated. This can be transformed back to $\alpha\beta$ -domain and used to implement a space vector pulse width modulation for switching the grid side converter transistors [161].

The schematic of the current control block is shown in Figure 3.8.

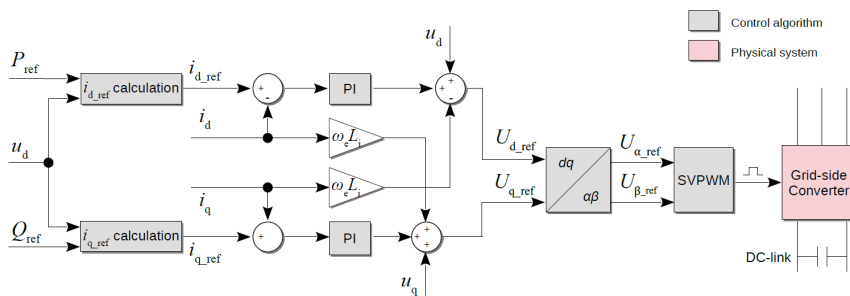


Figure 3.8: Flywheel current control block [154], [159]

3.3.1.2 DC-link voltage control

With the measured rotational speed ω_m and the DC-link voltage U_{DC} , the torque (T_{ref}) and flux ($\Psi_{r.ref}$) references for the field-oriented control can be calculated [162]. Therefore, two PI controllers, one to minimize the DC voltage difference and the other to minimize the rotational speed error, were used. The flux reference was calculated using the nominal flux and the nominal and measured rotational speed, as described in [163].

The DC-link voltage control schematic is shown in Figure 3.9.

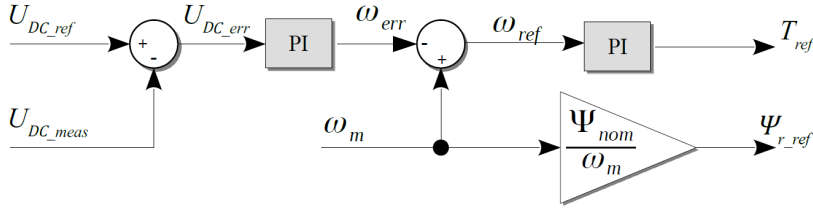


Figure 3.9: Flywheel DC-voltage control block [154], [159]

3.3.1.3 Field-oriented control

Since the rotor flux in the simulated model was not measured directly but estimated through the stator current, an indirect field-oriented control was implemented. With knowledge about the induction motor parameters, it is possible to derive the rotor flux Ψ_r , as shown in (3.2) [163]:

$$\frac{d}{dt} \Psi_r = -\left(\frac{R_r}{L_r}\right) \Psi_r + \left(\frac{L_m R_r}{L_r}\right) i_{ds} \quad (3.2)$$

where: R_r : Rotor resistance; L_r : Rotor inductance; L_m : mutual inductance; i_{ds} : flux forming current.

The control of the induction machine torque and flux can be decoupled by regulating the torque forming current i_{qs} and the flux forming current i_{ds} independently. The flux forming stator current reference $i_{ds.ref}$ could be evaluated using a PI controller by minimizing the error between the reference flux $\Psi_{r.ref}$ and the estimated flux. The torque forming current $i_{qs.ref}$ can be calculated using (3.3) [163]:

$$i_{qs.ref} = \frac{2}{3} \frac{L_r T_{ref}}{n_p L_m \Psi_r} \quad (3.3)$$

where: T_{ref} : Torque reference; L_r : Rotor inductance; L_m : mutual inductance; Ψ_r : rotor flux; n_p : number of motor poles pairs.

The stator voltage $U_{d.ref}, U_{q.ref}$ references are evaluated within the current controller block by minimizing the error between measured and reference stator currents, using PI controllers. Space vector pulse width modulation is used to generate switching for motor side converter transistors.

An overview of the field-oriented control block is shown in Figure 3.10.

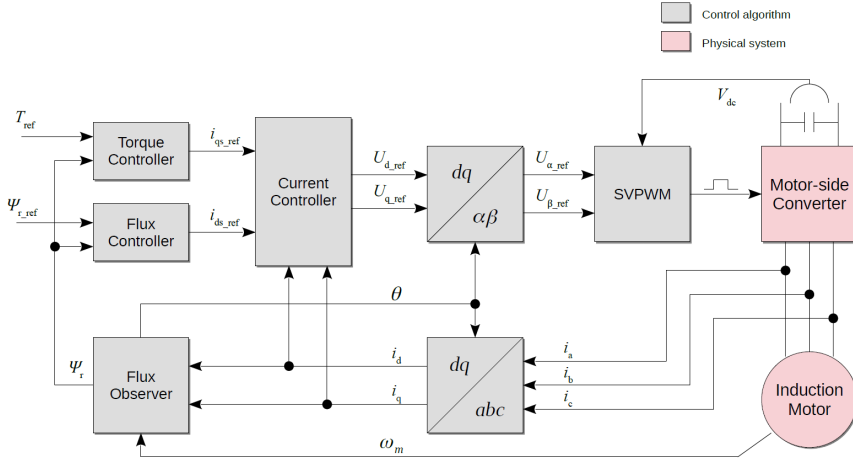


Figure 3.10: Flywheel field-oriented control block [154], [159]

3.3.2 BESS model

The model for the BESS is a simplified basic model based on [151], [164]; an extended model has been developed in [33], [148]. The model represents a lithium-ion based battery resp. battery cells, including a controller modelled on the datasheets of existing products.

The basic model of the battery itself consists of a SOC value and charging and discharging efficiencies. Based on the charging, respectively discharging current, the corresponding efficiencies, and the battery's nominal capacity, the SOC of the BESS can be calculated for each time step i (3.4):

$$SOC_{Bat}(i) = SOC_{Bat}(i - 1) + \frac{\eta_{cd} * \Delta t * I_{cd}(i)}{C_{Bat,nom}} \quad (3.4)$$

where: SOC_{Bat} : State of charge of the battery; η_{cd} : Charging resp. discharging efficiency [%]; Δt : Time step duration [h]; I_{cd} : Charging (>0) and discharging (<0) current [A]; $C_{Bat,nom}$: Nominal battery capacity [Ah].

Additionally, the self-discharge rate, which is relevant for long-term simulations [165], and a temperature dependence, which is relevant in environments with changing temperatures [166], have been added in the extended model presented in [33].

Lithium-ion batteries have a self-discharge rate of 5% within the first 24 hours and then 1-2% per month. This will remain reasonably steady throughout the service life. However, elevated temperatures and full SOC will cause an increasing self-discharge, as shown in Table 3.5. The self-discharge is implemented in the model with a linear approximation, which is shown in more detail in [33].

Table 3.5: Self-discharge per month for different temperatures and SOC's [165]

Temperature	0 °C	25 °C	60 °C
SOC = 1	6%	20%	35%
SOC = 0.5	2%	4%	15%

A BESS is affected by temperature changes as well, as the battery ages faster at higher temperatures and loses storage capacity temporarily at low temperatures. The simulations in this work were not conducted for such long-term timeframes that the aging due to temperature had to be considered. Thus, just the temporary capacity reduction due to lower temperatures is implemented in the model. The capacity retention at different temperatures is shown in Figure 3.11. [166]

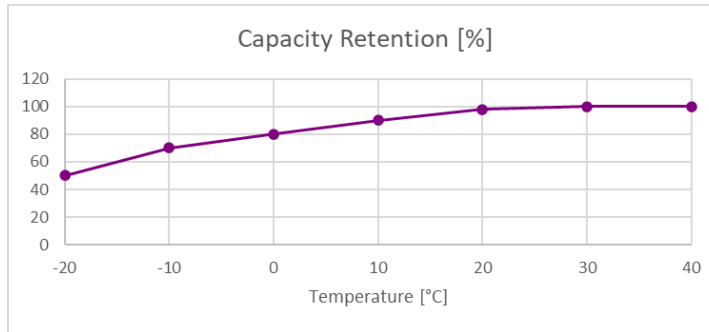


Figure 3.11: Battery capacity retention at different temperatures

The modelled batteries are based on the following available products, and their brochures and datasheets:

- Victron Energy LFP Smart Batteries (Nominal Capacity: 50 Ah - 300 Ah) [167]
- KOKAM SLPB120255255 (Nominal Capacity: 75 Ah) [168]
- KROS-H-2-222 (Nominal Capacity: 300 Ah) [169]

3.4 Freezer, water heater and simplified space heating model

The following simplified object models are based on the models presented in [10]. They use linear approximations for the temperature differences during the time step. Using such simplified models will reduce the calculation time compared to simulations with more detailed models, which is an important measure, especially for medium or large microgrid simulations. The accuracy resp. errors of these simplified models are determined and evaluated in the model validation in Chapter 4.

3.4.1 Freezer model

The freezer model is based on [10] and uses the temperature differences due to freezing, food exchange and ambient temperature for each time step i . All details about the model are shown in [151]. Since this model was developed for a chest type freezer, the temperature loss due to door opening was not considered in [10]. According to [170], this is an important parameter for the modelling of upright type refrigerators and freezers, which amounts to about 9 Wh for each door opening. Therefore, an additional temperature change due to door opening when exchanging food with an upright freezer is included in the freezer calculation (3.5) [151], [10]:

$$T(i + 1) = T(i) - dT_{freeze}(i) - dT_{food}(i) - dT_{amb}(i) - dT_{door}(i) \quad (3.5)$$

where: dT_{freeze} : Temperature change due to freezing [°C]; dT_{food} : Temperature change due to food exchange [°C]; dT_{amb} : Temperature change due to ambient losses [°C]; dT_{door} : Temperature change due to door opening [°C].

The temperature changes can be calculated as shown in (3.6)-(3.9) [151], [10]:

$$dT_{freeze}(i) = \beta * \Delta t * P_{el,f} * COP_f * y_i \quad (3.6)$$

$$dT_{food}(i) = \left(\frac{m_i(i)}{V_{Object} * \rho_x} \right) * (T(i) - T_{fc}) \quad (3.7)$$

$$dT_{amb}(i) = \beta * \Delta t * \alpha * (T_i - T_{amb}) \quad (3.8)$$

$$dT_{door}(i) = \beta * E_{door-loss} * d_i \quad (3.9)$$

where: Δt : Time step duration [h]; $P_{el,f}$: Electrical power of freezer [W]; COP_f : Coefficient of performance of freezer; y_i : Freezing/Heating status {0;1}; ρ_x : Density of material x [kg/m³]; $T_{f_corrected}$: Corrected food temperature [°C]; V_{Object} : Volume of object [m³]; c_{pi} : Specific heat capacity of ice [J/kgK]; $E_{door-loss}$: Energy loss for each door opening [Wh]; d_i : freezer door opened {0; 1}.

The coefficients α and β are shown in (3.10)-(3.11) [10]:

$$\alpha = U_{Object} * A_{Object} \quad (3.10)$$

$$\beta = \frac{1}{V_{Object} * \rho_x * c_{px}} \quad (3.11)$$

where: U_{Object} : U-value of the object [W/m²K]; A_{Object} : Surface area of the object [m²]; V_{Object} : Volume of the object [kg].

To use the specific heat coefficient of ice for the whole temperature spectrum of the food, the corrected food temperature $T_{f_corrected}$ for food warmer than 0 °C must be obtained with (3.12) [151]. For food below 0 °C, $T_{f_corrected}$ equals the actual food temperature T_{f_actual} .

$$T_{f_corrected} = T(i) - \frac{(m_i * c_{pi} * T(i)) + (m_i * c_{pw} * (-T_{f_actual}))}{m_i * c_{pi}} \quad (3.12)$$

where: T_{f_actual} : Actual food temperature [°C].

3.4.2 Water heater model

The water heater model is similar to the freezer model and is based on [10] as well. All the details of the model were presented in [151]. It uses the temperature changes due to heating with the heating element, exchange of water and ambient losses. The temperature of the water inside the boiler at the end of the time step is calculated as in (3.13) [151], [10]:

$$T(i + 1) = T(i) + dT_h(i) - dT_{cold_water}(i) - dT_{amb}(i) \quad (3.13)$$

where: dT_h : Temperature change due to heating [°C]; dT_{cold_water} : Temperature change due to water exchange [°C]; dT_{amb} : Temperature change due to ambient losses [°C].

The temperature changes can be calculated in the following way (3.14)-(3.16) [151], [10]:

$$dT_h(i) = \beta * \Delta t * P_{el,wh} * \eta_{wh} * y_i \quad (3.14)$$

$$dT_{cold_water}(i) = \left(\frac{V_i}{V_{Object}} \right) * (T(i) - T_{water_input}) \quad (3.15)$$

$$dT_{amb}(i) = \beta * \Delta t * \alpha * (T(i) - T_{amb}) \quad (3.16)$$

where: η_{wh} : Efficiency of water heater [%].

3.4.3 Simplified space heating model

The model for space heating and space cooling is similar to the freezer and water heater models; it is shown in detail in [151]. It was developed with equations, modelling techniques and typical values described by the American Society of Heating, Refrigerating and Air-Conditioning Engineers (ASHRAE) [171]. Since space heating is more complex to model than a water heater, there are more temperature influences for each time step i to calculate. These include the ventilation, occupancy, and sunlight irradiation through windows. The temperature for the next time step can be calculated as shown in (3.17) [151]:

$$T(i + 1) = T(i) + dT_h(i) - dT_{vent}(i) - dT_{amb}(i) + dT_{occ}(i) + dT_{rad}(i) \quad (3.17)$$

where: dT_h : Temperature change due to heating or cooling [°C]; dT_{vent} : Temperature change due to ventilation [°C]; dT_{amb} : Temperature change due to ambient losses [°C]; dT_{occ} : Temperature change due to room occupancy [°C]; dT_{rad} : Temperature change due to sun irradiation through windows [°C].

The temperature changes can be described with equations (3.18)-(3.22) [151]:

$$dT_h(i) = \beta * \Delta t * P_{el,sh} * COP_{sh} * y_i \quad (3.18)$$

$$dT_{vent}(i) = \left(\frac{V_i}{V_{Object}} \right) * (T(i) - T_{amb}) \quad (3.19)$$

$$dT_{amb}(i) = \beta * \Delta t * \alpha * (T(i) - T_{amb}) \quad (3.20)$$

$$dT_{occ}(i) = k_i * P_{Person} * \Delta t * \beta \quad (3.21)$$

$$dT_{rad}(i) = P_{el,solar} * \Delta t * \beta \quad (3.22)$$

where: k_i : Number of people in the room; P_{Person} : Typical heating power of one person [W].

Two different models were implemented based on this simplified space heating model. The first model is a simple room, which is modelled according to the civil engineering based simple room model shown in section 3.5.1. The second model is based

on a measured apartment located in the Kristiine district in Tallinn, Estonia, as presented in section 3.2. This apartment was selected due to several reasons:

- Measured electricity consumption data including separate devices was available for this apartment
- Measured food and hot water consumption data was available for this apartment
- The dwelling with 67.4 m² represents a typical dwelling for Germany/Estonia

The average dwelling size is 92.3 m² in Germany [158] and 66.7 m² in Estonia [172]. This includes family houses as well as apartments. Since the majority of people live alone, about 40% [173], the dwelling size per person should be considered as well. This is 44.8 m² in Germany [158] and 30.5 m² in Estonia [174]. Thus, the 67.4 m² apartment can be considered a typical dwelling. The modelling parameters to calculate the heating gains and losses for this apartment are shown in Table 3.6.

Table 3.6: Modelling variables for simplified space heating of an apartment

Variable	Value
Floor area	67.4 m ²
Roof area	67.4 m ²
Wall area	42.4 m ²
Window area (each direction)	7.2 m ² / 4.7 m ² / 0 m ² / 0 m ²
Cooling power	2000 W
Heating power	2000 W
U-value windows	0.6 W/m ² K
Relative volume of furniture	5%
Room height	2.5 m
U-value of wall insulation	27.0 W/m ² K
U-value of other wall materials	5.6 W/m ² K
Surface azimuth (each direction)	90° / 180° / -90° / 0°
Thickness of insulation	0.1 m
Thickness of other wall materials	0.25 m

3.5 Neural network-based space heating model

The neural network-based space heating models were created with an approach different from the previously described models. Pre-existing civil engineering models of a building created with IDA-ICE modelling software were used to create comprehensive datasets. These datasets could be used to train a neural network to behave like the IDA-ICE object model of the building within the defined limits. All details about the methodology were presented in [175].

With this methodology (c.f. Figure 3.12), it is possible to use building models from any civil engineering modelling software if the datasets from the simulation can be saved in a common file format. Additionally, the neural network model can be trained in any software which supports machine learning techniques like Matlab or Python. This provides more flexibility than co-simulations where certain communication standards must be met by both simulators.

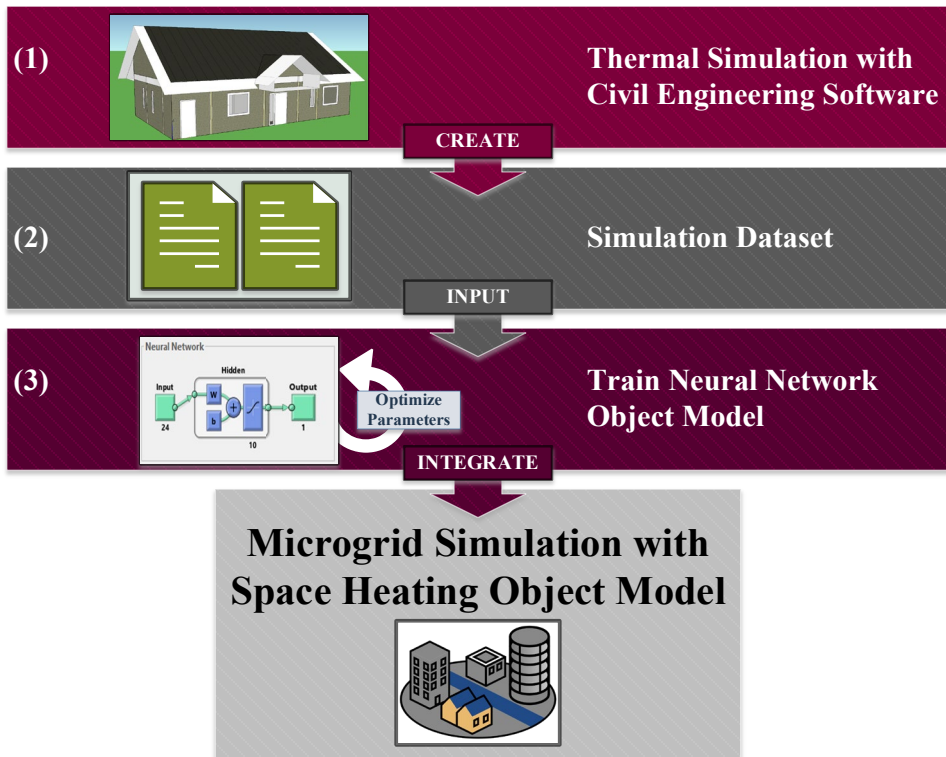


Figure 3.12: Methodology overview of the neural network-based space heating model

The creation of suitable datasets and training of the neural network model are described in more detail in the following subsections.

3.5.1 Description of used civil engineering models

The existing building models used for the creation of the datasets are modelled with IDA-ICE modelling software from Equa. It shows compliance with CEN standards EN 15255-2007, EN 15265-2007 and EN 13791, and with ASHRAE standard 140-2004 [176]. Three civil engineering models are used in this work. All of them have been described and validated in previous publications. The 3D-models are shown in Figure 3.13:

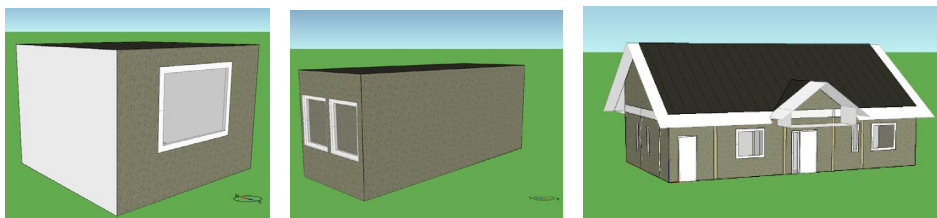


Figure 3.13: 3D view of used IDA-ICE building models; left: simple room; centre: control centre; right: single family house

3.5.1.1 Simple room

The first model is a simple room, which was chosen to represent a single room of a private house or an apartment building. It was previously published and validated in two conference papers [177], [178]. It used a 400 W electric radiator for heating, which was sized according to the Estonian heating design standard [179], including an added 20% power margin for safety. The thermostat was operating at 21 °C with a +/- 1 °C dead band. The implemented room was equipped with balanced heat recovery ventilation and the usage profiles for appliances, lights, and people were modelled as established for energy calculation of the apartment buildings by the Estonian law [180]. The Estonian test reference year data was used as weather data for this model [181]. This model was used for direct performance comparisons between the simplified space heating model, the civil engineering space heating model and the neural network-based space heating model.

3.5.1.2 Control centre

The second model is a control centre of the Energy Campus Wildpoldsried, which is located in the city of Wildpoldsried, Germany. Several measurements with the real object were done between 21st November and 3rd December 2019 in free-floating state and with an electric heater operated at 1300 W. [182]

The following data was logged:

- Temperature at several positions within and outside the control centre with four EL-USB-2 EH / Temp Data Loggers
- Outside temperature, global irradiation, air pressure, humidity, dew point, wind speed, and wind direction from a nearby weather station
- Power consumption of all active devices (including the electric heater) with portable power meters

With these measurements and the available construction data of the control centre, the IDA-ICE model could be created. With the free-floating measurements, the envelope could be calibrated and the heater measurement could be used to check the heat-up performance. The result of the calibration is shown in Figure 3.14. The average absolute error of the model compared to the measured data is 1.61 °C. This error is within the acceptable range, especially as the error during the independent test period is lower at 1.00 °C. Thus, the model is correctly calibrated and can be used for further research.

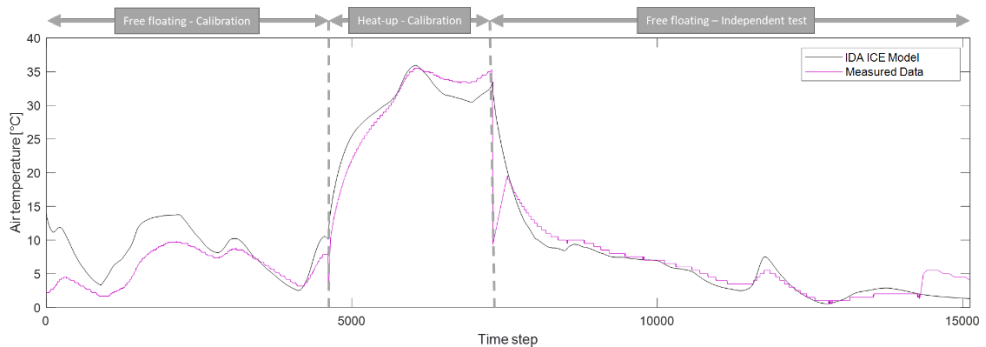


Figure 3.14: Air temperature behaviour of the IDA-ICE model compared to the measurements [182]

3.5.1.3 Single family house

The third model is a small single family house with one floor and a detached roof. It was used previously in a sample project for redefining the cost-optimality level of nearly zero energy buildings (nZEBs) for new residential buildings in Estonia [183]–[188]. The model development, validation and use are published in [189] and [190]. Like the simple room model, it uses the Estonian test reference year weather data [181]. The model is divided into 11 thermal zones/rooms (c.f. Figure 3.15) and is heated by underfloor heating at 100 W/m^2 . Each zone is controlled by a separate thermostat. All rooms except the attic were equipped with balanced heat recovery ventilation.

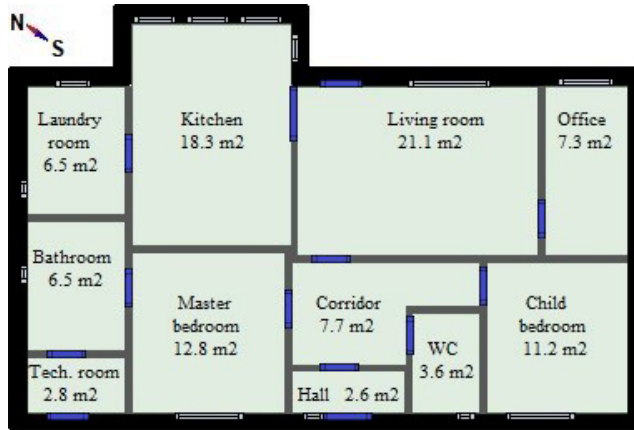


Figure 3.15: Floor plan of the single family house with area sizes; doors: blue; windows: light grey

As this model was intended to be used for flexibility simulations with variable set points for the thermostats, it was necessary to change the standard usage profiles for appliances, lights, and people to more realistic stochastic profiles. Like this, the created datasets will show more complexity regarding, e.g., the temperature set points or occupancy, which is necessary for a more dynamic behaviour and complexity of the neural network-based model.

To generate the occupancy profiles, the ProccS web tool [191] was used. It was developed, tested, and validated for a doctoral thesis at the Technical University of Denmark [192]. The profiles were generated for a family of two adults with one child. The adults go to work and the child to kindergarten/school [193]. The profiles were generated twice and the bathroom profile from the second run was used for the WC and the profile of the living room for the office. This introduces an error because up to five people can be in the house simultaneously; however, this can be even more realistic considering visiting guests. Rooms that are not often used (laundry room, technical room, corridor, hall) have no occupancy and are typically not heated specifically. Thus, they are excluded from the dataset creation.

3.5.2 Creation of comprehensive datasets with civil engineering models

To get the training datasets for the machine learning algorithm, it is necessary to do simulations with each model and log the relevant parameters. To obtain enough training data, the simulation period was chosen to be one year with 1 min output time step. This time step is small enough compared to the larger time constant of space heating systems. The whole year needs to be simulated to include different environmental

situations, like day/night, summer/winter, weather effects, etc. Otherwise, the neural network model will be limited to a certain season or weather conditions later.

To exemplify the single family house, the variables shown in Table 3.7 are logged. The room-based variables are only logged for the 7 relevant rooms with active heating and occupancy, as mentioned in the previous subsection.

Table 3.7: Variables for the neural network training dataset of a single family house [175]

General variables	Room-based variables
<ul style="list-style-type: none"> • Dry-bulb temperature [°C] • Relative humidity of air [%] • Direction of wind • Speed of meteorological wind [m/s] • Direct normal radiation [W/m²] • Diffuse radiation on horizontal surface [W/m²] 	<ul style="list-style-type: none"> • Mean air temperature [°C] • Heating energy [W]* • Ventilation [W]* • Infiltration and openings [W]* • Occupancy (Number of People) • Energy losses [W]* • Internal wall energy exchange [W]* • Equipment heat energy [W]* • Windows and solar gains [W]* • Cooling energy [W]* • Lighting energy [W]*

*sensible heat gains/losses

3.5.3 Development and training of neural network-based models

The following methodology was used for synthesizing the NN-based space heating model from the IDA-ICE simulation datasets.

The dataset needed to be pre-processed to be in the correct format for the neural network training. The neural network training parameters had to be chosen to achieve a model with good accuracy without over- or underfitting. Then the neural network model could be trained and tested. If the accuracy was not good enough, then the neural network training parameters had to be changed and the training had to be repeated. The process is shown in Figure 3.16 and described in more detail in the following subsections.

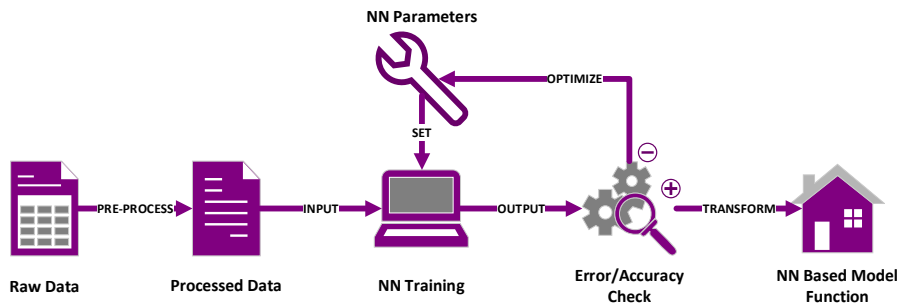


Figure 3.16: Overview of the neural network training process

3.5.3.1 Dataset pre-processing

First, it was required to add the temperature difference between the current and the previous time step to the dataset (3.23).

$$\Delta T(i) = T(i + 1) - T(i) \quad (3.23)$$

where: $T(i)$: Mean air temperature of time step i [°C]; $T(i + 1)$: Mean air temperature of time step $i+1$ [°C]; $\Delta T(i)$: Temperature difference between time step i and $i+1$ [°C].

Second, the weather data had to be changed. The source weather data that IDA-ICE was using was hourly data and therefore needed to be converted to minutely data. Typically, the values would be interpolated. But since the other variables in the IDA-ICE training data were based on the hourly weather values, it was more reasonable to duplicate the hourly values for each minute within the hour.

In a third step, the datasets needed to be normalized as this usually yields better results in the accuracy of the model because the influence of large fluctuating numbers dominating smaller numbers can be reduced. The input and target data for the neural network model were generated using (3.24) and (3.25).

$$X_{data,norm}(i, k) = \frac{X_{data}(i, k) - \mu(k)}{\sigma(k)} \quad (3.24)$$

$$T_{data,norm}(i, l) = \frac{T_{data}(i, l) - \mu(l)}{\sigma(l)} \quad (3.25)$$

where: $X_{data,norm}(i, k)$: Normalized input data of time step i and variable k ; $X_{data}(i, k)$: Input data of time step i and variable k ; $T_{data,norm}(i, l)$: Normalized target data of time step i and variable l ; $T_{data}(i, l)$: Target data of time step i and variable l ; μ : mean value of variable k resp. l ; σ : standard deviation of variable k resp. l .

3.5.3.2 Neural network training

To select and optimize the training parameters for the neural network model, the following error and accuracy metrics were considered:

- Root mean square error (RMSE) of the mean air temperature (3.26)
- RMSE of the heating power per square meter (3.27)
- Mean heating power difference (3.28)
- Percent of time steps with correctly estimated heating power (3.29)

$$RMSE_T = \sqrt{\mu((T_{CE} - \tilde{T})^2)} \quad (3.26)$$

where: μ : Mean value; T_{CE} : Civil engineering model mean air temperature [°C]; \tilde{T} : Test model mean air temperature [°C].

$$RMSE_P = \frac{\sqrt{\mu((P_{CE} - \bar{P})^2)}}{A_{Room}} \quad (3.27)$$

where: μ : Mean value; P_{CE} : Civil engineering model heating power [W]; \bar{P} : Test model heating power [W]; A_{Room} : Room area [m²].

$$\bar{P} = \frac{\mu(P_{CE}) - \mu(\bar{P})}{\mu(P_{CE})} * 100\% \quad (3.28)$$

$$TSA = \mu(\Delta P_E) * 100\% \quad (3.29)$$

where: TSA : time step accuracy; $\Delta P_E(i) = 1$ if $P_{CE}(i) - \bar{P}(i) = 0$; otherwise 0.

For a distinct representation of error metrics, one total error metric ($Error_{Total}$) is derived [194]. A weighting factor based on the importance of each error and accuracy metric for the overall use of the model was added. Since the model is included in an electric simulation, the temperature accuracy is less important. The most important values are the root mean square error and mean error for the power, resulting in the biggest weights. Additionally, the following limits and optimum values were chosen for the mapping to percentage values (c.f. Table 3.8):

Table 3.8: Error metric limits, optima, mapping factors and weighting factors [194]

Error	Limit	Optimum	Mapping factor	Weighting factor
$RMSE_T$	0.7 °C	0 °C	$1 - RMSE_T * \frac{0.1}{Limit}$	1/10
$RMSE_P$	300 W	0 W	$1 - RMSE_P * \frac{0.1}{Limit}$	4/10
\bar{P}	10 %	0 %	$1 - \bar{P} $	3/10
TSA	90 %	100 %	TSA	2/10

The limit value should be mapped to 90% and the optimum to 100%. The resulting total error metric can be calculated as follows (3.30) [194]:

$$Error_{Total} = \left[\left(\frac{1}{10} * \left(1 - RMSE_T * \frac{0.1}{0.7^\circ C} \right) \right) + \left(\frac{4}{10} * \left(1 - RMSE_P * \frac{0.1}{300W} \right) \right) + \left(\frac{3}{10} * (1 - |\bar{P}|) \right) + \left(\frac{2}{10} * TSA \right) \right] * 100\% \quad (3.30)$$

The most important training parameters for the selected algorithm are the number of neuron and layers, and the maximum number of epochs. The selected sizes for the hidden layers of the neural network models need to be chosen according to the complexity of the training data. As a rule of thumb, a good starting point for finding the optimum number of neurons can be chosen as 2/3 the size of the input layer. For the second hidden layer, half the size of the first hidden layer is commonly chosen. The optimum number of neurons can then be found by decreasing or increasing their number slowly and checking the corresponding accuracy of the model. In this stage, it is essential to make sure that

the model is neither underfitting with too few neurons nor overfitting with too many. From the training set, a ratio of 60% was used for training, 20% for cross-validation and 20% for testing. Fitting, cross-validation, and prediction tests were done internally within the Matlab training function. To be able to use the GPU computing capabilities, a scaled conjugate gradient algorithm [195], [196] had to be chosen as the other available algorithms are not compatible with GPU computing.

Table 3.9 shows the results obtained using the previously described metrics for a model with 17 input variables and different numbers of neurons for each layer.

Table 3.9: Results for different numbers of neurons per layer [194]

Neurons	[12 6]			[14 7]			[26 13]		
Test	1.1	1.2	1.3	2.1	2.2	2.3	3.1	3.2	3.3
$RMSE_T$ [$^{\circ}C$]	$3 \cdot 10^3$	0.71	0.67	2.81	$4 \cdot 10^3$	0.66	3.99	0.50	3.42
$RMSE_P$ [W]	407	288	288	406	533	267	247	308	278
\bar{P} [%]	53.73	-1.16	1.35	48.02	100.00	-4.87	13.00	-9.59	8.01
TSA [%]	96.27	98.13	98.13	96.27	93.59	98.39	98.62	97.85	98.26
Epochs	4243	803	909	2981	4146	1449	4407	1483	4190
Error_{Total}	$-5 \cdot 10^3$	94.83	94.83	76.04	$-5 \cdot 10^3$	94.08	87.27	92.29	89.12

These results demonstrate that the rule of thumb number for neurons with 12 in the first hidden layer and 6 in the second hidden layer gives the best total error metrics, as marked in bold in the table. It is evident as well that the best results are achieved with a lower number of training epochs. The typical behaviour where the validation error increases as the overfitting starts does not apply to the model, which can be the case for some datasets [197], [198]. Thus, the training cannot be stopped automatically. To select a suitable number to limit the epochs, it is necessary to look at the validation performance of the training. A too high number of epochs can be chosen for training to see the point where overfitting due to overtraining starts, as shown in Figure 3.17.

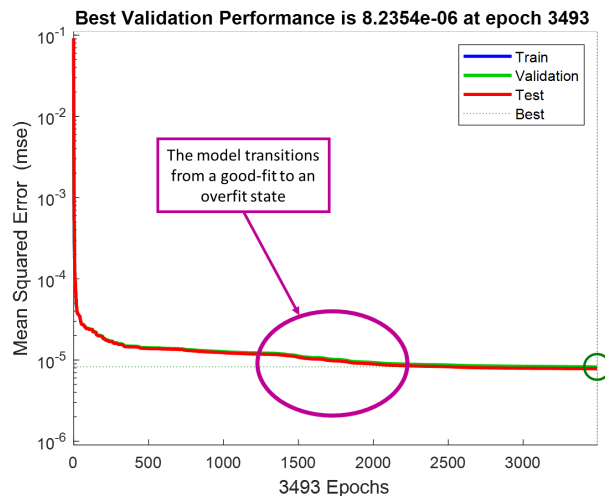


Figure 3.17: Evaluation of performance: Overfitted model [194]

The figure shows that the performance of the model reaches a good stable level at around 500 epochs. This will be referred to as the underfit marker. At around 1500 epochs, the overfitting transition due to overtraining starts, as marked by the purple circle. At this point, the model does not learn a general applicable solution anymore but learns the responses by heart. The maximum number of epochs should be limited between those two markers. To be sure not to overfit the model, a value of around 1/3 the difference between the over- and underfit marker is chosen: 850 epochs for this model.

Therefore, the chosen parameters for the model are:

- Neurons: Depending on input variables; according to the rule of thumb
- Maximum number of epochs: 1/3 the difference between the over- and underfit marker

The neural network model sizes are shown in Table 3.10 and visualized for the single family house in Figure 3.18.

Table 3.10: Neural network model sizes for different space heating models

Model	Input Variables	Hidden Layer 1	Hidden Layer 2	Output Variables	Epochs
Simple room	17	10	5	1	850
Control center	11	6	3	1	800
Single family house each room	17	12	6	1	850

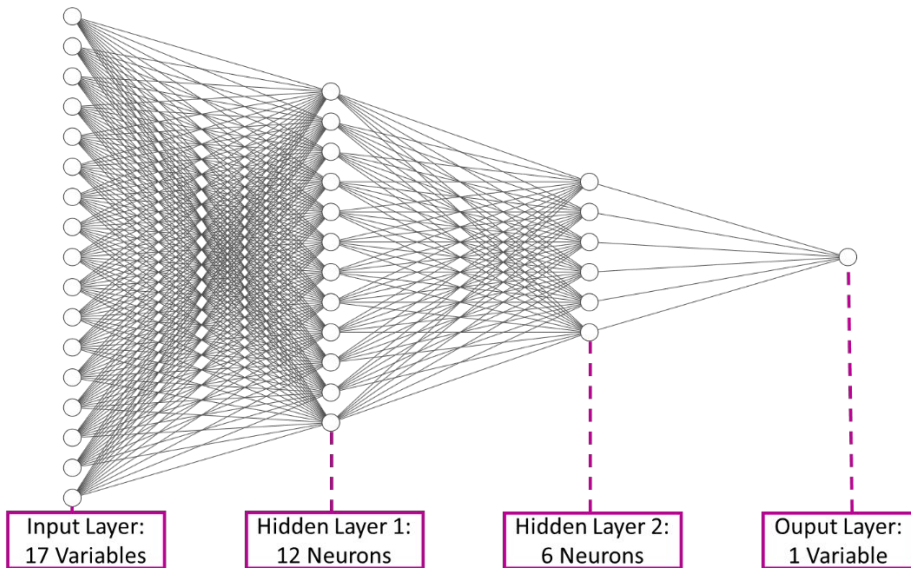


Figure 3.18: Visualization of neural network model used for each room of the single family house

The other training parameters of the training algorithm [195] do not necessarily need to be optimized as the variations between training with the same parameters have higher influence on the accuracy than the change of the parameters. An overview is presented in [194].

The training is much more stable when applying the optimized parameters, reducing the need for repeated trainings, as shown in Table 3.11. This can be seen by the comparison with the total error values for Test 1.1 presented in Table 3.9, where the training shows extremely bad results. Choosing a too large number of neurons and epochs does not improve the model, as it will regularly overfit (c.f. Table 3.9, Table 3.11).

Table 3.11: Comparison of optimized parameters to wrongly chosen parameters: mean total error values for multiple trainings

Evaluation criterion [%]	Mean Error_{Total} value
Optimized parameters:	92,03
Doubled neuron number; 5000 epochs	89,16

After the optimized training, the neural network model is converted and saved to a Matlab function instead of a neural network object. This has the advantage of higher compatibility, for example, if Matlab is used in combination with other software and higher calculation speed. The disadvantage is that the neural network cannot be additionally trained later with more input data but needs to be retrained completely. Applying this methodology to an existing civil engineering model to create a space heating model for a microgrid simulation can be achieved within 8 hours of active work for pre-processing and parameter adjustments. Additional computational time for pre-simulation and NN training in the background depends on the model size and detail and can take multiple hours. However, this does not account for active modelling time as it can be done in the background without supervision. This is a huge reduction by around 90% of active modelling time compared to more than 100 hours, as estimated by civil engineers.

3.6 Conclusions

To simulate the proposed system based on the conclusions of Chapter 2, models for the PV-system and loads, FESS and BESS, and TESs are necessary. For each of those models, either a measured profile or an object model has been presented. In summary, the following can be concluded for the used PV-system and load profiles used as input data for the simulations:

- For the PV-system model, measured profiles with resolutions of 1 minute and 1 second for Estonia and southern Germany were used. These PV-profiles were scaled to the specific application.
- Different load profiles for electrical and thermal loads were measured and artificially generated according to the foreseen simulated scenarios. To improve the results of the simulations, different dwelling occupancy profiles based on demographic statistics were selected to investigate the general applicability of the developed control algorithms in Chapter 5.

The energy storage systems were modelled with different methodologies. The following conclusions can be drawn from the modelling methodologies:

- The FESS model is modelled based on the available FESS at Tallinn University of Technology to enable validations of the model and control strategies with the physical object in Chapters 4 and 5.

- The BESS model is simplified to the basic function of a changing SOC. The behaviour is based on datasheet values. To improve this simple model, self-discharge and temperature dependent charge retention were implemented additionally.
- The freezer and water heater TES model are linear approximation models for the temperature changes inside the devices. Such models have been used in literature with similar microgrid level simulations with satisfying accuracy. To improve the freezer model, the additional losses during the door opening process of an upright-type freezer were added.
- The same approach was taken for the thermal model of a building. However, the literature analysis in Chapter 2 and the multitude of influences that need to be represented by a space heating model suggest that this model will not be accurate enough.
- To reduce the development and active modelling time and effort for detailed space heating objects, a novel methodology for the creation of NN-based space heating models was developed. With the correct pre-processing of data and training parameter selection, a NN-based space heating model that can be used as an object model in the microgrid simulations could be created. The active modelling time can be reduced with this methodology by around 90% from more than 100 hours to around 8 hours.

These models need to be validated next to ensure a good accuracy for the development of control strategies in Chapter 5, which will be the basis for the social and financial investigations in Chapter 6 and the microgrid development related recommendations in Chapter 7.

4 Validation of mathematical object models for storage systems

To get more insight into the quality of the presented modelled objects, it is necessary to validate the models and quantify the errors and accuracy. This is needed for the control strategy development in Chapter 5. Therefore, different validation methods are used for the different storage system models, as shown in more detail in the following subsections.

In the context of microgrid simulations, errors for the different storage systems should be kept within certain limits to ensure a valid simulation result. For the BESS, FESS and TESs, the mean error should be below 10%. For more complex models like space heating, a slightly higher error of up to 12% can be acceptable as well.

4.1 Validation of BESS and FESS models

The BESS and FESS models will introduce certain errors into the simulations. To decide whether the models are accurate enough and modelled properly, the following validation tests were conducted:

- Validation against measurement data
- Repeatability test of measurement data

4.1.1 Validation of FESS model

To be able to validate the flywheel model and later the corresponding control scenarios, it was necessary to modernize the available setup in the laboratory of Tallinn University of Technology.

Therefore, the existing PLC was replaced with a new Software-PLC, the Siemens AG ET 200SP Open Controller 2. This PLC enables real time simulations with Matlab in a PHIL setup. In this first step, the flywheel was connected to the PLC, but it is possible to connect more devices in future. The PHIL arrangement is depicted in Figure 2.15, a more detailed overview schematic for the validation is shown in Figure 4.1 and details about the implementation of the setup are presented in [64].

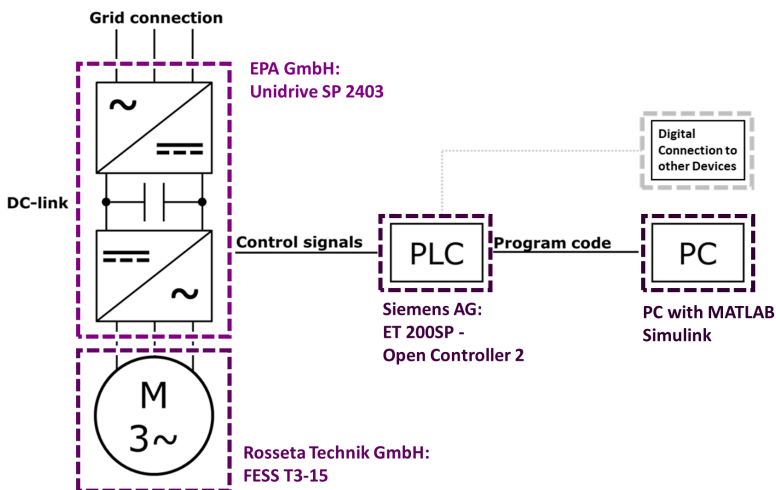


Figure 4.1: Schematic of the modernized flywheel validation setup [64]

With this setup it was possible to validate the FESS model and the implemented software power controller. The first test is a repeatability analysis, as shown in the next subsection, followed by a round trip efficiency validation.

4.1.1.1 Repeatability analysis

To know the accuracy of the flywheel power controller, a ramp shown in Figure 4.2 is applied. This charging and discharging test was performed for five times to analyse the deviation from the set ramp.

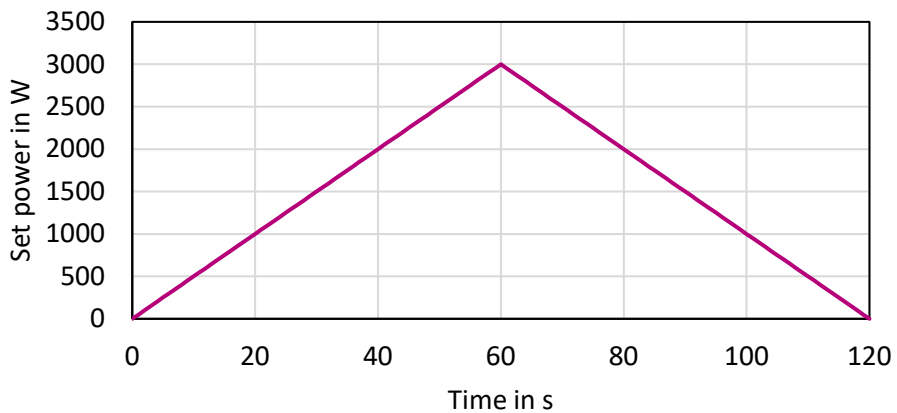


Figure 4.2: Flywheel storage repeatability profile [64]

The results for the power differences between set power and measured power are shown in Table 4.1. The RMSE is below 100 W across the whole spectrum and the other error metrics are small too. Thus, the power controller is working accurately.

Table 4.1: Results of flywheel storage repeatability [64]

Test	1 st	2 nd	3 rd	4 th	5 th	Overall
Average	-1.63W	0.25W	0.58W	0.00W	0.26W	-0.09W
Median	-4.68W	-0.83W	-3.40W	-7.14W	-5.46W	-3.97W
RMSE	94.06W	96.66W	98.25W	95.57W	100.91W	

4.1.1.2 Validation of round trip efficiency

The round trip efficiency typically shows how efficiently the storage system works. It is a good indicator for the model and setup quality as this value has been measured by the manufacturer and is available in the device documentation. Additionally, the simulation can be compared with the actual setup.

To get comparable results, the test is to be done as follows: first, the flywheel is at standstill. It is then charged with the maximum power of 15 kW until it is fully charged. Immediately after that, the flywheel is completely discharged with the maximum power of 15 kW. The consumed energy for charging and retrieved energy from discharging can then be compared to get the overall efficiency. The process is shown in Figure 4.3.

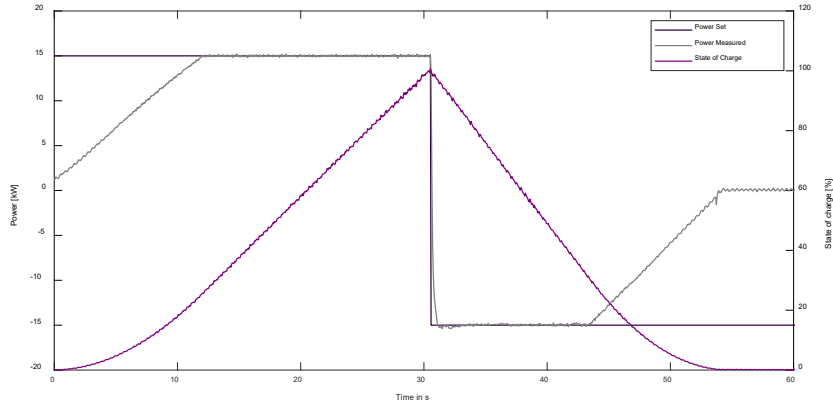


Figure 4.3: Flywheel storage round trip efficiency test

In total, 375 kW are charged in the test run while 269 kW are discharged. This results in a round-trip efficiency of 71.8% for the flywheel storage system, which is slightly lower than the provided value of 77.6% in the datasheet [69], which can indicate that a maintenance resp. balancing of this old device could be necessary. The modelled flywheel shows a slightly higher round trip efficiency value of 80.2%. The results are shown in Table 4.2.

Table 4.2: Efficiency errors of flywheel storage round trip

Round Trip Efficiency / Error	Datasheet	Simulation	Test
Datasheet	77.6%	-2.6%	+5.8%
Simulation	+2.6%	80.2%	+8.4%
Test	-5.8%	-8.4%	71.8%

These error values concerning the FESS model are within the acceptable range of less than 10%. The developed model for the FESS at Tallinn University of Technology can be used in the intended microgrid simulations.

4.1.2 Validation of BESS model

The battery models could be validated against measured data. The corresponding lithium-ion battery measurements were obtained from [199] and the batteries were modelled as shown in section 3.3 with their datasheet values.

The measurement data contained four lithium-ion battery data sets. The batteries were tested with different operational profiles for charging, discharging and impedance with detailed explanations of the methodology. The measured values for charging and discharging are:

- Voltage_measured: Battery terminal voltage [V]
- Current_measured: Battery output current [A]
- Temperature_measured: Battery temperature [°C]
- Current_charge: Current measured at load [A]
- Voltage_charge: Voltage measured at load [V]
- Time: Time vector for the cycle [s]
- Capacity: Battery capacity [Ah] for discharge until 2.7 V

Based on the methodology description and available measurements, the battery storage model was tested with suitable simulations. Comparison of the simulation results to the measured values shows that the charging current error is 11.6% and the discharging current error is 6.4%. Since these are errors for charging and discharging at maximum current, they will be smaller at partial load. Therefore, the BESS model has an acceptable accuracy, even though the charging current error is higher than the aimed 10% limit.

4.2 Validation of TES models

It is necessary to know the errors that are introduced into the simulation by each of the TES models. Thus, it is possible to decide if the models are accurate enough for the intended purpose and whether they are modelled correctly. The following validation methods are used for the simplified TES models:

- Design of experiment (DoE)
- Simulation with standardized conditions
- Validation against civil engineering models
- Validation against measurement data
- Uncertainty analysis

The validation details of the implemented storage system models are shown in the following subsections.

4.2.1 Validation of freezer model

The approach to verify the freezer object model is the following. First, the influence of the most significant parameters is confirmed with the design of the experiment (DoE) analysis. Second, simulations according to the requirements of the European Union commission delegated regulation (EU) No 1060/2010 with varied initial conditions are conducted. This can be used to analyse the error including the uncertainty.

4.2.1.1 Design of experiment for freezer model validation

Significant parameters based on typical implementations of a freezer model are the ambient temperature and the exchange of content in the freezer compartment [10]. To test if both of these values are significant in the simulation of the object model as well, a 2² factorial design was considered, as shown in Table 4.3. The high value for the ambient temperature is 23 °C, the low value 17 °C. The high and low values for the food exchange are 0.02 kg/5min and 0 kg/5min.

Table 4.3: Design of experiment: 2² factorial design for freezer verification

Experiment	T _{amb} = x _a	m _i = x _b
E1	23 °C	0.02 kg/5min
E2	17 °C	0.02 kg/5min
E3	23 °C	0 kg/5min
E4	17 °C	0 kg/5min

The results for experiments E1-E4 are shown in Table 4.4.

Table 4.4: Results for experiments E1-E4

T _{amb} /m _i	0.02kg/5min	0kg/5min
23 °C	E1 = 526.50 Wh	E3 = 470.25 Wh
17 °C	E2 = 456.75 Wh	E4 = 400.50 Wh

With those values it is possible to apply a simple regression model (4.5) using equations (4.1) - (4.4):

$$p_0 + p_A + p_B + p_{AB} = E1 = 526.50 \quad (4.1)$$

$$p_0 - p_A + p_B - p_{AB} = E2 = 456.75 \quad (4.2)$$

$$p_0 + p_A - p_B - p_{AB} = E3 = 470.25 \quad (4.3)$$

$$p_0 - p_A - p_B + p_{AB} = E4 = 400.50 \quad (4.4)$$

$$y = p_0 + p_A x_A + p_B x_B + p_{AB} x_A x_B \quad (4.5)$$

$$= 463.500 + 34.875x_A + 28.125x_B + 0.000x_A x_B$$

Using the sum of squares it is possible to determine the contribution of the two parameters (c.f. Table 4.5).

Table 4.5: Sum of squares for freezer parameters

Sum of squares	Equation	Contribution	% Contribution
SST	$4 * (p_A^2 + p_B^2 + p_{AB}^2)$	8029.1250	100
SSA	$4 * (p_A^2)$	4865.0625	61
SSB	$4 * (p_B^2)$	3164.0625	39
SSAB	$4 * (p_{AB}^2)$	0.0000	0

This shows that both parameters have significant influence on the simulation. In this case, the influence of the ambient temperature is higher than the food exchange rate. Both parameters are independent of each other due to the modelling.

4.2.1.2 Simulations with standardized conditions

The European Union commission delegated regulation (EU) No 1060/2010 [200] describes the standardized test parameters that need to be met to determine the official energy consumption values for a freezer for the EU energy label. Applying the same conditions to a simulation, which are typically applied in an experiment to the real object, will create comparable results for error analysis.

The simulation uses the following conditions:

- The set point is fixed to -18 °C
- The time step is 5 min
- The duration of the simulation is 24 h
- The food exchange is 3 times 0.3 kg in 24 h
- The temperature of the replacement food is 25 °C
- The ambient temperature is 25 °C
- The food exchange pattern is shifted 5 min for each simulation

With these simulations, a mean energy consumption of 442.9531 Wh/day with a standard deviation of 2.0144 Wh/day can be obtained. The uncertainty of the repeated simulations is of type A [201] and can be calculated like this (4.6):

$$u_f = \frac{\text{standard deviation}}{\sqrt{\# \text{ of simulations}}} = \frac{2.0144 \text{ Wh/day}}{\sqrt{288}} = 0.1187 \text{ Wh/day} \quad (4.6)$$

Matlab is calculating with 16 digits. The power consumption is in a range of 3 digits before the decimal point, leaving 13 digits after the decimal point. This yields the following uncertainty of type B [201] (4.7):

$$\begin{aligned} u_{MATLAB} &= \frac{\text{semi range}}{\sqrt{3}} = \frac{(0.0000000000001 \text{ Wh/day})/2}{\sqrt{3}} \\ &= 0.00000000000003 \text{ Wh/day} \end{aligned} \quad (4.7)$$

The combined uncertainty can be obtained with equation (4.8) [201]:

$$u_{total} = \sqrt{u_{pwr}^2 + u_{MATLAB}^2} = 0.1187 \text{ Wh/day} \quad (4.8)$$

Using a coverage factor $k=2$ for a confidence level of 95% yields that the freezer object model operates according to this simulation with a power consumption of 442.9531 +/- 0.2374 Wh/day. This corresponds to 161.677 +/- 0.0866 kWh/a compared to 174 kWh/a, as shown in the technical data for the selected freezer model [202]. This is an error of about 7%, which is acceptable for the microgrid simulations in this work, as it is below the chosen 10% error limit.

4.2.2 Validation of water heater model

The model for the water heater has been verified with a DoE analysis and measurements. For this purpose, the hot water consumption for a water heater in an apartment with the corresponding electrical energy consumption has been measured. The installed water heater in the apartment has a volume of 200 l and a power of 2100 W. All relevant parameters for the installed water heater are set according to the datasheet [203].

4.2.2.1 Design of experiment for water heater model validation

Typical models of water heaters show that the significant parameters are the ambient temperature and the water exchange [10]. A 2^2 factorial design for the DoE of the water heater model can be used to confirm the relevance of these, using the parameters shown in Table 4.6.

Table 4.6: Design of experiment: 2^2 factorial design for water heater verification

Experiment	$T_{amb} = x_a$	$V_i = x_b$
E1	26 °C	0.5l/5 min
E2	10 °C	0.5l/5 min
E3	26 °C	0l/5 min
E4	10 °C	0l/5 min

The ambient temperature changes for this DoE analysis are chosen more extremely than for the freezer, which is mostly placed in the basement with milder temperature changes. Despite that, the DoE analysis for the water heater shows that the ambient losses have a much lower influence on the model than the water exchange (c.f. Table 4.7). This is the result of better thermal design of a water heater without larger openings compared to a freezer, where the door is a strong thermal bridge, causing more ambient losses.

Table 4.7: Sum of squares for freezer parameters

Sum of squares	Contribution	% Contribution
SST	$4.97 * 10^6$	100
SSA	$0.13 * 10^6$	3
SSB	$4.84 * 10^6$	97
SSAB	0	0

4.2.2.2 Validation against measurement data

The measurements for the hot water and electrical energy consumption were done for 1 week with a 5 min time step. The resulting hot water pattern could then be applied to a simulation with the same ambient temperature that was present during the measurements. The average electrical power error of the simulated water heater is less than 6% compared to the measurements. This is well below the 10% error limit that was selected for the intended microgrid simulations.

4.2.3 Validation of the simplified space heating model

Since the simplifications for the simplified space heating model are extensive, it is necessary to determine whether the degree of abstraction is too high for the intended use in microgrid simulations.

Therefore, two validation methods were chosen to obtain quantitative error and accuracy values: First, the model was validated against the previously described civil engineering model of the simple room. Secondly, the model was compared to the measured data from the described 3-room apartment located in the Kristiine district in Tallinn.

4.2.3.1 Validation against civil engineering model

The simplified space heating model was validated against the simple room IDA-ICE model described in section 3.5. As mentioned, the civil engineering model had been validated previously. Thus, the additional error of the simplified space heating model, which is the test model in this case, could be verified against that model. A one-week simulation with one-minute time step was implemented for both models with the same environmental parameters as shown in Table 4.8. For the simulation results, the error and accuracy metrics from section 3.5 could be used for evaluation of the simplified space heating model:

- Root mean square error (RMSE) of the mean air temperature (3.26)
- RMSE of the heating power per square meter (3.27)
- Mean heating power difference (3.28)
- Percent of time steps with correctly estimated heating power (3.29)

Table 4.8: Environmental and model parameters for simplified space heating model validation against civil engineering simulation

Parameter	Value
Ambient air temperature	0.5 °C
Temperature set point	21 °C
Solar irradiation	Yes
Heating power	400 W
Structural dimensions and windows	According to civil engineering model
Occupancy	According to civil engineering model

The results for the error and accuracy metrics are the following:

- $RMSE_T$: 0.92 °C
- $RMSE_P$: 27.63 W/m²
- \bar{P} : 8.3%
- TSA : 63.54%

The error metrics are quite high and the accuracy is quite low, as the simulation errors for the civil engineering model need to be added as well. Those are around 5% according to [176], lifting the mean power error to 13.3%. Additionally, this model is quite simple compared to a regular apartment model, resulting in even higher expected errors for more complex rooms. The temperature RMSE is within a reasonable margin, the mean heating power error and heating power RMSE are too high, and the TSA is too low. The model is not within the 10% error margin, nor is it within the extended 12% error limit for complex models. Thus, the model can be useful for first general tests with different control algorithms, but the results should be verified with a more detailed model to ensure the correct behaviour of the control strategies in a specific case.

4.2.3.2 Validation against measurement data

Additionally, the simplified model was validated against the measurement data of the apartment in Kristiine district in Tallinn, as described in section 3.2. The validation time covers the complete week of the measurement data.

The model uses the parameters according to the conditions of the measurements presented in Table 4.9.

Table 4.9: Environmental and model parameters for simplified space heating model validation against measurements

Parameter	Value
Ambient air temperature	Fluctuating between -8 °C and +2 °C
Temperature set point	22 °C
Solar irradiation	Yes
Heating power	230 W
Structural dimensions and windows	According to apartment dimensions
Occupancy	According to apartment measurements

Unfortunately, the temperature in the apartment was not measured; thus, it is only possible to calculate the electrical power error between the model and the measurements. Due to the higher complexity of this model compared to the simple room model in the

previous validation, the mean power error increased in this test to 24%. This confirms, on the one hand, that the error increases with a more complex model, and on the other hand, that this simple modelling technique can only be used to get first indications about the behaviour of space heating for a general building. Thus, as mentioned before, the model can be only used for first control algorithm tests, but there is a need to verify the control strategy with a more detailed model for a specific case.

4.2.4 Validation of neural network space heating model

The neural network-based space heating model has been validated against the corresponding civil engineering models and against measurement data from the control center of the Energy Campus Wildpoldsried located in the city of Wildpoldsried, Germany. Like this, the different used models were all validated, and the errors of the different models can be compared. Additionally, an uncertainty analysis with the single family house model was conducted to see the stability of the neural network based models as a modelling quality indicator.

4.2.4.1 Validation against civil engineering model

For the validation of the neural network-based models, the error and accuracy metrics from section 3.5 could be used. The evaluation is presented in more detail in [175].

- Root mean square error (RMSE) of the mean air temperature (3.26)
- RMSE of the heating power per square meter (3.27)
- Mean heating power difference (3.28)
- Percent of time steps with correctly estimated heating power (3.29)

As described in more detail in [175], a simple simulation with the neural network-based model is created. Input data for a whole year with the different values are used as shown in Table 3.7. The simulation has a 1-min time step. The temperature calculated by the model for the end of a time step is used as input for the next time step. The resulting error metrics for this validation are shown in Table 4.10.

Table 4.10: Comparison of error and accuracy metrics between the neural network-based models and the civil engineering models [175]

Model	TSA [%]	\bar{P} [%]	$RMSE_P \left[\frac{W}{m^2} \right]$	$RMSE_T$ [°C]
Simple room (Simple Model)	63.54	8.3	27.63	0.92
Simple room (NN Model)	98.92	2.6	3.13	0.30
Single family house (NN Model): Average of 7 rooms	94.56	6.1	16.93	0.85

It can be observed that the accuracy and error metrics for the NN-based simple room model are much better than those for the simple space heating model of the simple room. The errors are lower, and the TSA is higher. For example, the mean power error is 5.7% lower. This clearly shows the superior modelling quality of the NN-based model over the simplified space heating model. The error metrics for the much more complex single family house model are better than the simple space heating model of a simple room. However, the more complex model shows slightly worse error metrics than the less complex simple room model. This indicates that a simplified model of the single family house would perform worse than the simplified simple room model.

Thus, improved space heating models are necessary to get more accurate simulation results. The mean air temperature validation result is shown visually for the single family house in Figure 4.4 and the related power consumption graph in Figure 4.5.

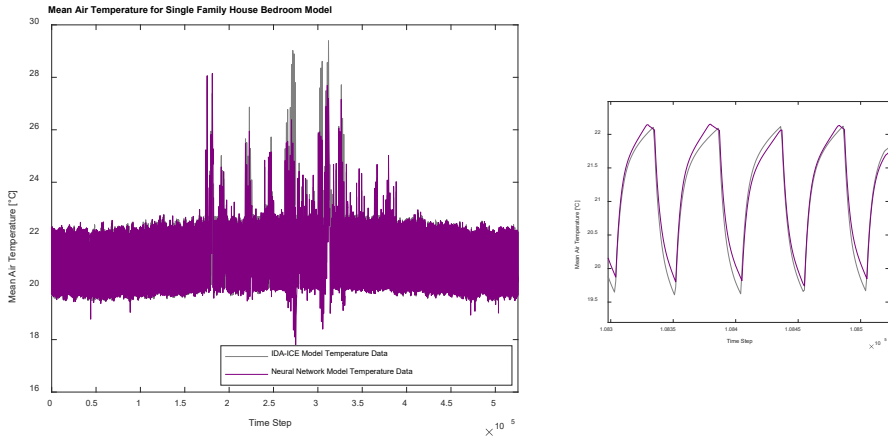


Figure 4.4: Mean air temperature comparison between civil engineering simulation and test simulation for single family house bedroom model in the test simulation with zoom-in [175]

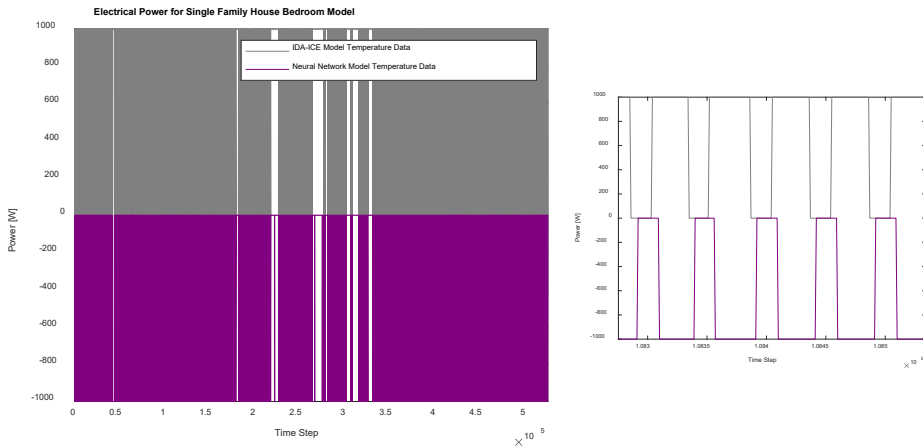


Figure 4.5: Power data comparison between civil engineering simulation and test simulation for single family house bedroom model (Calculated power data is shown in the negative y-direction) with zoom-in [175]

The high model quality for the NN-based models can be seen in both graphs, as the temperature and power consumption are close to the results for the civil engineering model. This is especially visible in the zoomed-in graphs on the right. Additionally, the model accuracy stays on the same level throughout the whole simulation of 1 year, as seen on the overview graphs on the left.

In summary, the NN-based space heating model for the more complex single family house does not quite reach the 10% error limit, but is well within the extended 12% error margin for complex models.

4.2.4.2 Validation against measurement data

Validation of the NN-based models against civil engineering models gives a good indication about the model quality. To have a comprehensive validation of the models, they need to be directly compared to measurements. Therefore, the control centre model of the Energy Campus Wildpoldsried was developed. With this model, it is possible to compare the NN-based model, the civil engineering model and the real object with each other and analyse the errors. Figure 4.6 shows the visual result for the comparison of the three models. The same input parameters that were measured for the real object have been used for the simulations. The NN-based model has been synthesized from the civil engineering model as described before.

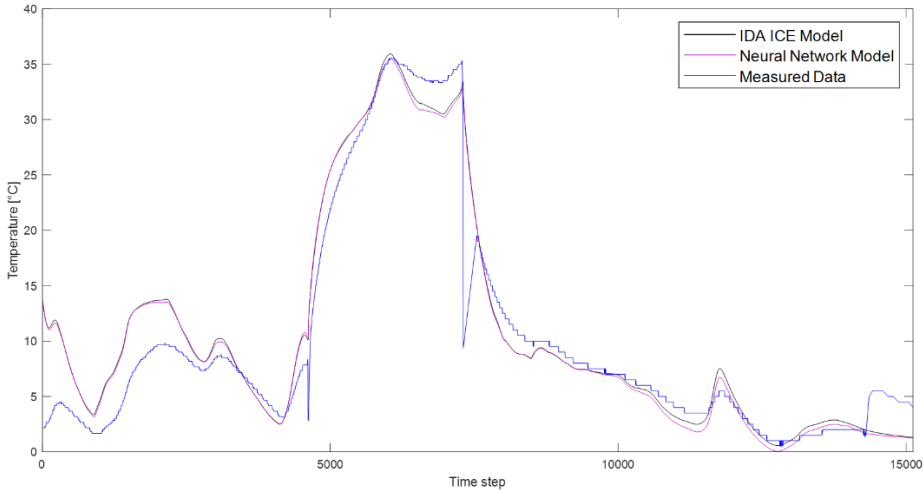


Figure 4.6: Model validation of neural network and IDA ICE control centre models with measured data

It can be observed that the temperature calculations for the two simulated models are closer to each other than to the measured data. This shows that the errors between the models are lower than to the real object. This is confirmed by the error calculations shown in Table 4.11.

Table 4.11: Error comparison between measurement and control centre models

Errors	NN vs. IDA ICE	NN vs. Measurement	IDA ICE vs. Measurement
RMSE [°C]	0.32	2.95	2.94
Mean Temperature error [°C]	1.93	4.98	7.05

The presented error metrics show error differences between the NN-based model and the civil engineering model. The errors between the civil engineering model and the measurements are much higher. The NN-based model presents higher error metrics as well. Interestingly, the RMSE is very similar to the civil engineering model, while the mean temperature error is even lower. This does not mean that the NN-based model is more accurate than the civil engineering model. Rather the errors between the measurements

and the civil engineering model, and the error between the civil engineering model and the NN-based model cancel each other out to a certain degree for the tested input data. With different input data, the results can differ. The NN-based model is within the set error margins and can therefore be used in the intended microgrid simulations.

To classify the results in relation to the other NN-based models, the temperature RMSE for the control centre, simple room and single family house model can be compared as shown in Table 4.12. The complexity of the control centre is slightly higher than the simple room model, which can be seen in the RMSE as well. The single family house model is more complex, as indicated by the higher RMSE, and the expected errors towards a real object should be considered higher than with the control centre consequently.

Table 4.12: Error comparison between NN-based models and civil engineering models

NN Based Models	Control Centre Model	Simple Room Model	Single Family House Model
RMSE [°C]	0.32	0.30	0.85

4.2.4.3 Validation with uncertainty analysis

Additionally, an uncertainty analysis was conducted as a model quality indicator. Therefore, multiple short simulations were run with the NN-based space heating model of the single family house, using a simulation time of 10 days with 1 min time steps. For each of the simulations, the initial parameters were varied slightly for each of the 7 rooms included in the model. This results in a total number of simulations of 1921, which can be used for the uncertainty analysis of the electrical power consumption of the space heating model, as this is the most relevant parameter for the intended purpose of the model. Based on the standard deviation between those simulations, the uncertainty could be calculated using (4.9):

$$u_{NN} = \frac{\text{standard deviation}}{\sqrt{\text{number of simulations}}} \quad (4.9)$$

The Matlab calculation uncertainty can be neglected in this case as Matlab calculates with 16 digits, as mentioned in section 4.2.1. This would result in an additional uncertainty, which is multiple magnitudes smaller than the space heating model uncertainty.

The standard deviation for the single family house model was 1.25% and as a result, the uncertainty of the model is 0.03% in these test simulations. This assures, on the one hand, the stability of the proposed modelling method and guarantees, on the other hand, the ability to handle small differences within the operational limits of the model.

4.3 Conclusions

The object models developed in Chapter 3 needed validation to obtain quantitative results for error metrics. This ensures good accuracy levels and a correct behaviour of the models for the control strategies that are developed next. For this purpose, validations with a PHIL setup against measurement data with standardized test conditions and against other detailed models were implemented. To ensure a good quality and accuracy of the simulations, a maximum mean error margin of 10% for most object models was chosen. As space heating models are much more complex due to all

the external influences than the other object models, an extended maximum error limit of 12% was chosen for the complex space heating models.

For the FESS model, validation with a PHIL setup was chosen, as the device is physically available at Tallinn University of Technology.

- A repeatability analysis to ensure the validity and stability of the other validation results showed that the system is working properly.
- The error margin for the round trip efficiency test was 8.4% between the measured object and the simulated model, which is well below the set 10% error margin. The error between the simulation and datasheet value is much smaller. This indicates that the physical object needs maintenance to reach the original measured efficiency level.

The BESS model was validated against measurement data. The mean discharging current error at maximum discharging rate was 6.4%, which is below the 10% error goal. The result for the mean charging current error at maximum charging rate was 11.6%. This is above the set 10% error limit. However, it can be considered that the battery will not be charged and discharged with the maximum allowed rate:

1. ... because the battery is charging and discharging according to the load needs, which are typically lower than the maximum allowed current level
2. ... because the BESS should be slightly over-dimensioned to increase the lifetime, as discussed in Chapter 2
3. ... because the control strategies should be designed to achieve a long lifetime by avoiding high currents

This means that the current error will be lower and within the set error margins most of the time.

The TESs were validated with the following results:

- The freezer model was validated according to standardized test conditions. The simulation was implemented exactly as the experimental setup used for obtaining the datasheet values. The mean power error obtained was 7%, which is below the set goal of a maximum of 10%.
- The water heater was validated against measurement data from the apartment in Kristiine district in Tallinn. The mean error was 6%, well below the set limit of 10%.
- The simplified space heating model was validated against the more accurate civil engineering model and against the measurement data from the measured apartment in Kristiine district in Tallinn. As expected, after adding the additional simulation error from the civil engineering model of 5%, the overall error for the simplified space heating model was 13.3% for the simple room. The error compared to the measured model was 24%, which is too high as well. Thus, the model can be used for first tests with control strategies, but the results should be verified with a more detailed model to ensure the correct behaviour of the control algorithms.
- The NN-based space heating model was validated against the civil engineering models and measurement data. The civil engineering model for this validation was the complex single family house model. Between the civil engineering model and the NN-based model, the mean power error was 6.1%, resulting in a total error of 11.1% if the civil engineering software error

is added. This value is slightly above the target of 10% maximum error, but since this is a complex model, the 12% error margin can be applied; thus, the model is accurate enough. The second validation against measured data of the control centre model confirmed that, showing an even lower mean power error of 5%, which is well below the set limit. The improvement of the mean power error compared to the simplified space heating model is 5.7%.

The error rates for all the storage system models are summarized in Table 4.13. FESS, BESS, freezer, water heater, and the NN-based space heating model can clearly be used for the development of control strategies, whereas the simplified model should be used for first general investigations.

Table 4.13: Overview of all object model errors

Object model	Mean error	Acceptable (10% / 12% limit)
FESS	8.4%	Yes / Yes
BESS	6.4% - 11.6%	Barely / Yes
Freezer	7%	Yes / Yes
Water heater	6%	Yes / Yes
Simplified space heating	>13.3%	No / No
NN-based space heating	5% - 11.1%	No / Yes

Additionally, during these validation tests, the simplified space heating model could be compared to the NN-based model further, as shown in Table 4.14. The tests showed not just different accuracy results, but also different calculation times and, as analysed in Chapter 2, different compatibilities. The reduction of calculation time during the microgrid simulation between a co-simulation and the NN-based model is 85%. Considering that in microgrid simulations, the simulations are repeated multiple times with different control strategies, the NN-based space heating model is most useful for the investigation of control strategies. Pre-training and data set creation is only necessary once and the reduction of calculation time and the compatibility issue compared to a co-simulation are therefore significant. As mentioned, the simplified model is only suitable for first general investigations on the control strategies, which is confirmed as the model is quickly calculated and highly compatible but has low accuracy.

Table 4.14: Overview of advantages and disadvantages for different space heating models in microgrid simulations [175]

Model	Advantages	Disadvantages
Simple model	<ul style="list-style-type: none"> • Fast to calculate during simulation (~3-min calculation time for complete single family house*) • No pre-training • Highly compatible (part of the microgrid simulation) 	<ul style="list-style-type: none"> • Low Accuracy
Civil engineering model (e.g., with co-simulation)	<ul style="list-style-type: none"> • Very good accuracy • No pre-training 	<ul style="list-style-type: none"> • High computational effort and slow during simulation (~20-min calculation time for complete single family house*) • Compatibility problems between simulators
NN- based model	<ul style="list-style-type: none"> • Fast to calculate during simulation (~3-min calculation time for complete single family house*) • Good accuracy within set limitations • Highly compatible (part of the microgrid simulation) 	<ul style="list-style-type: none"> • Pre-training (~6 min per room*) and creation of datasets (~20 min for complete single family house*)

*Intel Core i7 4770K CPU; Nvidia GeForce GTX 980Ti GPU

5 Research and development of control strategies for residential microgrids

In Chapter 2, the BESS, FESS and TES selected for investigations have been modelled and validated in Chapters 3 and 4. As a next step, control strategies for these storage systems need to be researched and developed to give recommendations and investigate the related user requirements and financial feasibility. In this regard, the BESS and FESS need to work with different control strategies than the TESs to cooperate efficiently and achieve the security of supply and financial feasibility improvement goals. The main goals in this regard are:

1. Increase of islanded operation duration (Security of supply parameter)
2. Increase of the cyclic lifetime of the BESS (Financial parameter)
3. Minimization of energy costs (Financial parameter)
4. Minimization of BESS capacity (Financial and security of supply parameter)

The first two goals, the cyclic lifetime and security of supply improvement, can be achieved with the FESS and BESS. The cyclic lifetime is a financial parameter, which influences the re-investment costs of the system when the BESS needs to be exchanged. The security of supply can be improved due to a prolonged islanded operation time with the additional FESS storage capacity. This is investigated in section 5.1.

The minimization of energy costs can be achieved with the TESs. In this case, the thermal energy is saved and released according to the electricity price in a real time price market scenario, as shown in section 5.2.

Minimizing the BESS capacity will reduce the investment costs for the system. This can be achieved by scheduling the TESs and therefore adjusting the consumption profile to the production, which can also increase the islanded operation duration. The development of these islanded control algorithms is described in section 5.3.

The latter two control strategies are dependent on the occupancy of the investigated dwelling as the thermal and electrical consumption patterns change. With this investigation, conclusions about the general applicability of the different algorithms can be drawn as shown in section 5.4.

5.1 Cyclic lifetime and security of supply improvement with FESS and BESS

As mentioned before, the primary goal of the FESS control system is to improve the power quality by reducing peaks and dips, which can help to increase the BESS lifetime as the number of charging and discharging cycles can be reduced with such a control. The control for the BESS itself is load following as it is the responsible device in the islanded operation to maintain voltage and frequency. As the FESS adds a small additional storage capacity to the system, the security of supply can be improved as well due to a longer islanded operation duration. The simulation topology is shown in Figure 5.1.

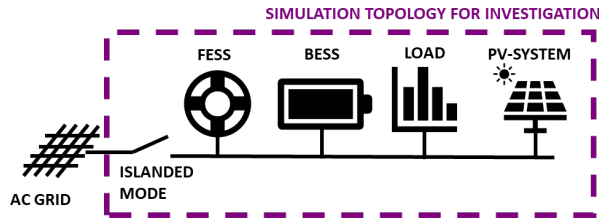


Figure 5.1: Simulation topology for islanded BESS and FESS investigation

5.1.1 FESS control

As mentioned in section 3.3, there is a power smoothing control implemented for the FESS. To smooth the load, a variety of different low pass filters can be used. As a first implementation, a moving average filter was selected, as shown in Figure 5.2. This control was implemented to change the active power reference for the current controller since the power smoothing operation is related to the active power.

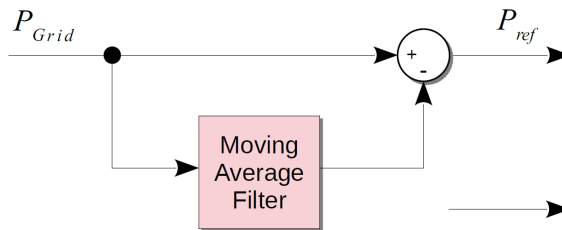


Figure 5.2: Schematic of FESS moving average control [154]

The length for this moving average filter was chosen to be 30 and 60 seconds. This length effects strongly how much the load profile is smoothed and therefore, how much stress will be put on the FESS. If the length chosen is too low, the profile will not be smoothed much, and the peaks and dips will remain. If the length chosen is too long, then the flywheel might not be able to work for extended time as it will be fully charged or discharged. The results for the power smoothing scenario for a small islanded microgrid are shown in Figure 5.3. The start-up phase for the flywheel in the first 30 s has been cut in the graph.

As the figure shows, the load in the microgrid is smoothed well with the moving average filter. The flywheel is balancing the peaks and dips in this simulation. However, it can be observed that the the rotational speed of the FESS is decreasing over time. This is an indication that the moving average filter length might be already too long for permanent operation of the selected flywheel. But it should also be mentioned that the selected flywheel, which is modelled based in the device in the laboratory, is an old device with lower efficiency and low capacity. A more modern FESS could perform better with this filter length.

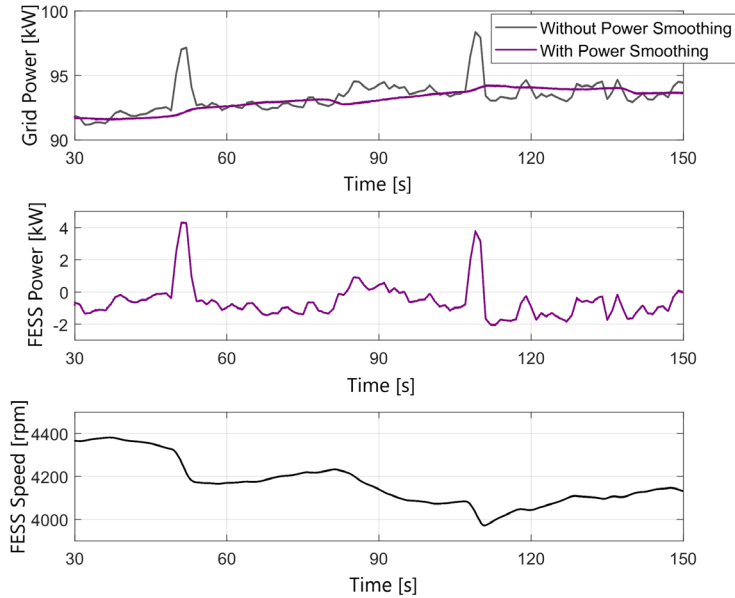


Figure 5.3: Main grid to microgrid power supply with and without power smoothing, FESS power and FESS rotational speed [154]

To verify these results, the same load profile is tested with the PHIL setup of the FESS. The result is shown in Figure 5.4.

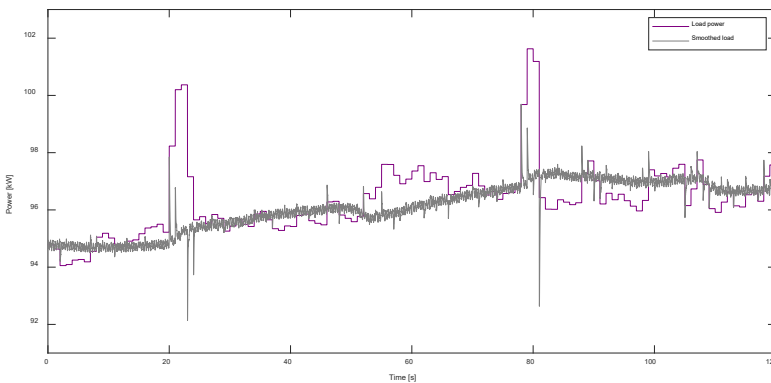


Figure 5.4: Load smoothing with FESS PHIL-setup moving average control with the test profile [64]

Like the results of the simulation in Figure 5.3, the real time simulation with the PHIL setup shows a smoothed load profile. The time resolution for the real time simulation is higher, which can be seen in the discretized graph for the original load profile. However, in this profile, a delay for the FESS power adjustment can be seen, as the controller and physical system have a certain reaction time constant. The FESS power controller has to adapt the set signal to the output signal. A more detailed graph for this delay is shown in Figure 5.5.

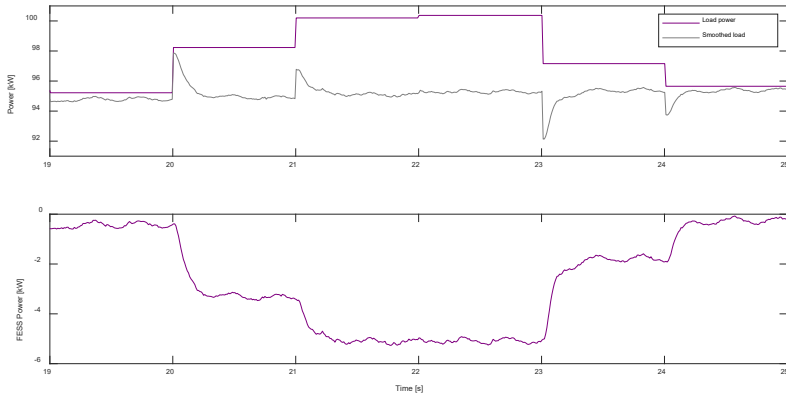


Figure 5.5: Detailed load smoothing with FESS PHIL-setup moving average control with the FESS power graph [64]

These peaks from the reaction time of the FESS controller can be positive and negative, but they are typically smaller in amplitude than the original step from the load signal that was sampled at 1 Hz. To see if the response of the flywheel can be optimized, a Butterworth filter was implemented additionally. The two different filter impulse responses are shown in Figure 5.6.

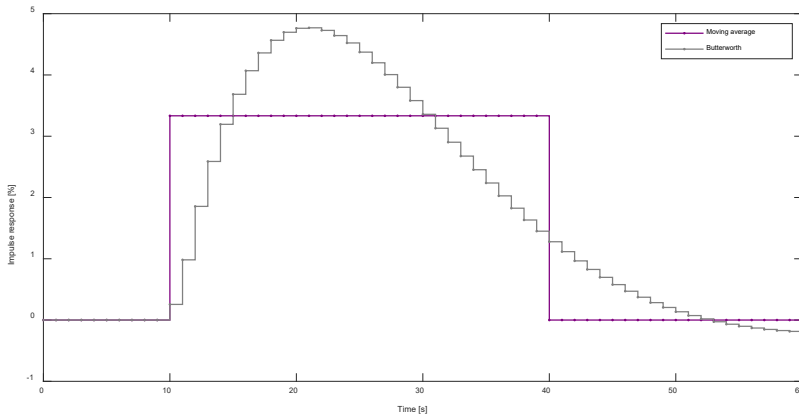


Figure 5.6: Impulse response for moving average and Butterworth filters [64]

The Butterworth filter is designed as a second order filter with a sampling frequency of 1 Hz and a cut-off frequency of 1/60 Hz. As shown in the figure, the moving average filter reacts first to the impulse and stays constant till the impulse passes the full filter. The Butterworth filter reacts less aggressively to the impulse but after some seconds, its response overshoots the moving average response. It is the first filter that starts to decrease and align to zero. However, the slope of the moving average filter reaches zero first. These properties of the Butterworth filter lead to a much better smoothing result. This can be seen even more detailed in the slope gradient of the smoothed load profile in Figure 5.7. The slope gradient is much smaller and smoother, which ensures a better power quality and more potential to reduce the charging and discharging cycles for the BESS.

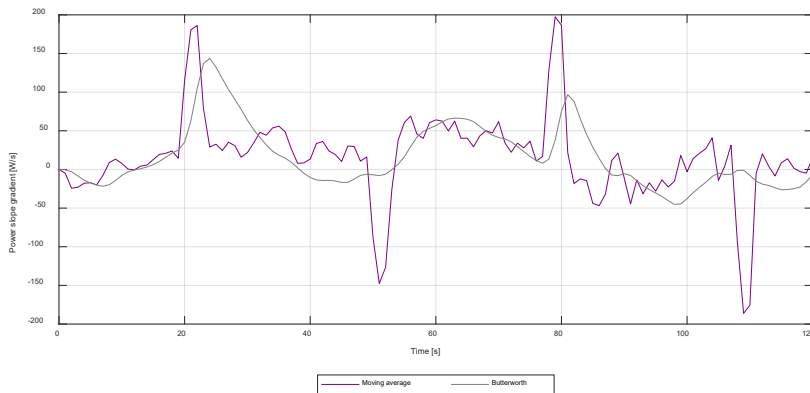


Figure 5.7: Power slope gradient for moving average and Butterworth filters with the test load profile [64]

A second implemented control algorithm is to charge the FESS in case the produced power from the PV-system exceeds the maximum charging power for the BESS. The charged energy can then be used to charge the BESS when the produced PV-power is reduced again. This can be implemented as shown on the flowchart in Figure 5.8.

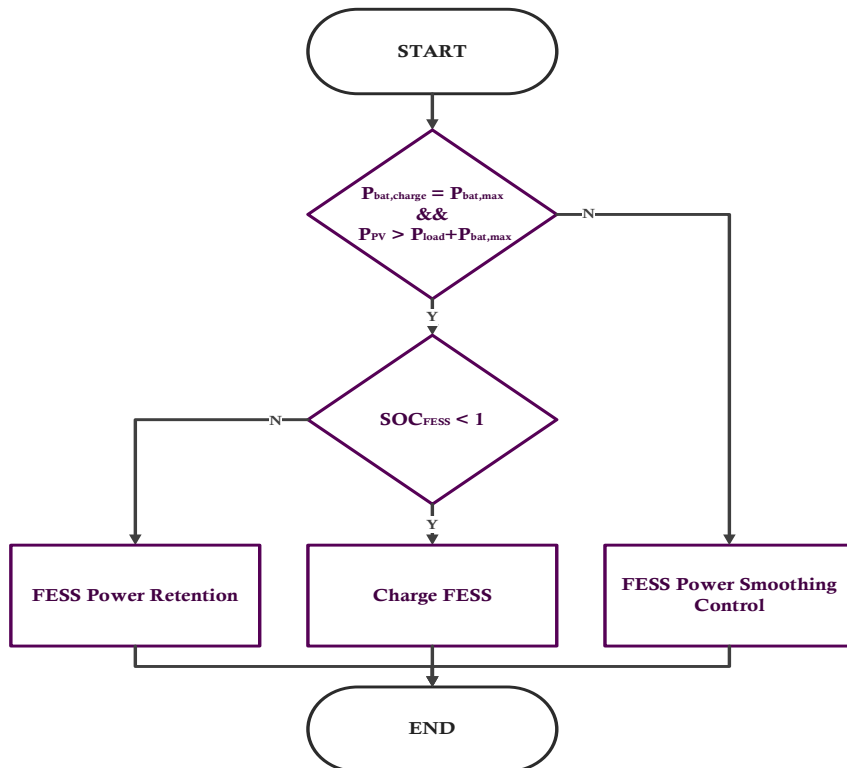


Figure 5.8: High PV-system production control strategy for FESS

5.1.2 BESS control

As the BESS is the grid forming device in the islanded operation mode, it needs to work in a load following way. This means that it needs to control the frequency and voltage for the microgrid according to the current load by charging and discharging the battery cells. Therefore, the following control principles have been implemented for the simulations [28], [38].

The integrated battery controller is assumed to limit the batteries SOC to a maximum value of 0.9 and a minimum value of 0.2 to reduce the degradation of the battery [68]. The inverter control model for the BESS reduces its basic working principle in the simulations [28], [38]:

- The inverter is modelled as an efficiency value.
- The typical inverter behaviour in the islanded mode is defined with the limits stated in grid standard EN 50160 in the following way:
 - The frequency in the islanded microgrid is kept constant in any case.
 - The voltage in the islanded microgrid is limited to the nominal root-mean-square (RMS) voltage of 230 V (VN) and cannot be exceeded. Thus, the energy production needs to be reduced.
 - Consequently, if the energy production cannot supply the demand, the voltage will drop and the microgrid will shut down in the islanded mode operation.

5.1.3 Results of cyclic lifetime and security of supply improvement control

As shown in [24], different scenarios with an islanded microgrid including a FESS and BESS were simulated. The islanded microgrid consists of the generated single family house load profile, the scaled Laastu Talu OÜ PV-system profile, the FESS model, and the BESS model. The first scenario was simulated without the FESS power smoothing control. The second scenario includes the moving average power smoothing control for the FESS. The simulation runs for 24 h even if the battery cannot maintain stable islanded operation anymore. The BESS SOC during the simulations is shown in Figure 5.9.

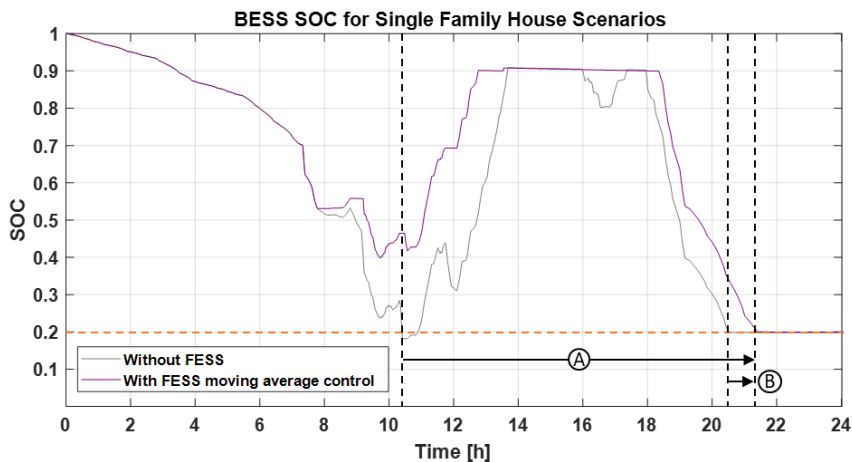


Figure 5.9: BESS SOC of an islanded microgrid system with and without supporting FESS for power smoothing; (A) Increase of islanded operation time with special case; (B) Increase of islanded operation time with typical cases [33], [24]

As indicated in the figure, the islanded operation time can be increased by more than 10 h 30 min or 50% because in the selected special case (Figure 5.9, (A)), a large dip was compensated by the flywheel. At around 10 hours of operation, the load of the single family house was draining the BESS below its minimum SOC because the sun was not shining strong enough for the PV-system to produce enough energy. With other load and PV-system profiles, there might appear similar cases where the islanded operation time is increased massively.

The increase of the islanded operation time without such a special case can be estimated from the figure as well (Figure 5.9, (B)). At the end of the simulation, the points in time when the final minimum SOC value is reached can be compared, assuming that the dip below the minimum SOC right after hour 10 did not take place. In this case, the increase would be around 45 min or 3%.

Based on the number of charging and discharging cycles within this 24-h simulation, it can be estimated by how much the cyclic lifetime can be increased with this control strategy. This estimation can be done using the maximum number of cycles given by the manufacturer’s datasheet for the BESS (5.1). This estimation can be compared to the SOLI test described in section 2.2.2.

$$t_{Bat,cyclic} = \frac{N_{cycles,24h} * 365}{N_{cycles,max}} \quad (5.1)$$

where: $t_{Bat,cyclic}$: Cyclic lifetime for BESS [a]; $N_{cycles,24h}$: Number of cycles in 24 h; $N_{cycles,max}$: Maximum number of cycles according to the datasheet.

This estimation includes the simplification of counting the partial cycles and adding them up to full cycles, even though they are less damaging for the BESS than full cycles [68]. The calculated cyclic lifetime values with the corresponding cycles per year and maximum islanded operation times are shown in Table 5.1.

Table 5.1: BESS cyclic lifetime estimation and maximum islanded operation time for microgrid system with and without FESS power smoothing [33], [24]

Scenario	Cycles/Year	Cyclic Lifetime	Maximum islanded operation time
Without FESS	542	8.3 a	10 h 22 min
With FESS moving average control	455	9.9 a	20 h 55 min

This reduced number of cycles per year by around 16% leads to an increase of the cyclic lifetime by 19% for the BESS, which is related to an increased service life of the battery with longer periods before re-investments for replacement devices. Of course, the microgrid is not operating in the islanded mode permanently, but these results apply to a very similar maximum self-consumption BESS control strategy in the grid-connected mode as well.

For the second control approach regarding improved energy use and self-consumption, which is especially useful during the islanded operation, a real time simulation with the PHIL setup was used. A combined load and PV-system profile and a BESS model were implemented in Matlab and the response of the real FESS was measured and included in

the microgrid simulation in real time. In this scenario, the produced power during the daytime of the PV-system is exceeding the maximum charging power for the BESS. In this case, the FESS is charged with the excess-energy. The load profile power, BESS charging power and FESS power are shown in Figure 5.10, including the stored FESS energy. In the last few minutes, the energy stored in the FESS is used to charge the BESS even more for later use of the energy when the PV-production is lower. In this case, more than 200 kW_s could be additionally stored. However, due to the low efficiency of the old FESS system, about 90% of the excess energy is lost due to high self-discharge of the device. A more modern device could show more significant results with an improved performance and efficiency.

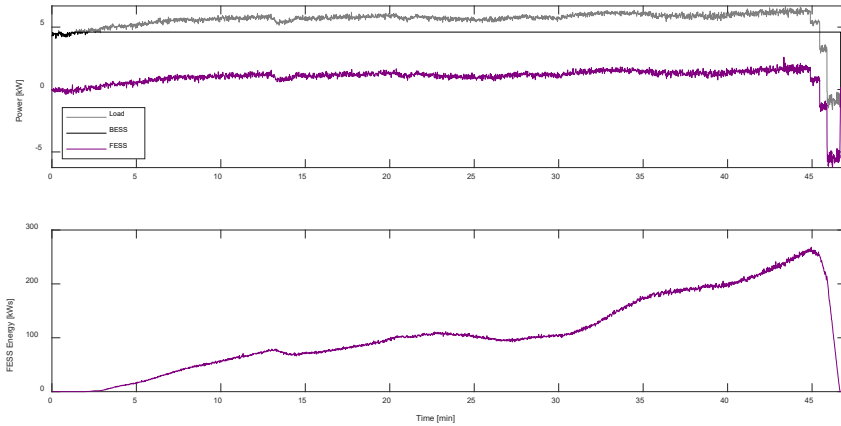


Figure 5.10: Flywheel and battery storage control with PHIL setup for exceeding the PV-power scenario [25]

5.2 Energy cost minimization with TES

In the grid-connected operation, the TES has to work with an energy cost minimization control strategy to reduce the cost for energy exchange to and from the grid. The price-based control algorithms depend on the real time electricity price or day-ahead electricity prices. Example price patterns have been obtained from the Nord Pool website [77] for the corresponding times and dates of the other used profiles. The simulation topology is shown in Figure 5.11.

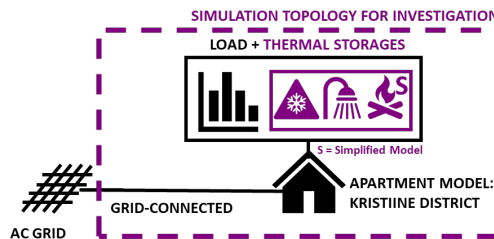


Figure 5.11: Simulation topology for grid-connected TES investigation

5.2.1 Price-based control algorithm description

The general working principle of the price-based control algorithms is the following: if the electricity price is high, then it is required to choose a low consumption set point:

- For heating devices, a low temperature set point
- For cooling devices, a high temperature set point

If the electricity price is low, a higher consumption set point can be chosen:

- For heating devices, a high temperature set point
- For cooling devices, a low temperature set point

In total, 7 different price-based algorithms have been implemented based on [85], [84] and [10]. The algorithms are shown in Table 5.2.

Table 5.2: Price-based control algorithm description; Cooling = Freezer; Heating = Water heater and space heating [10], [85], [84]

#	Description of set point calculation algorithm
A	Cooling: $T_{set} = T_{set,min} + C_{user} * (Pr - Pr_{min}) * \frac{T_{set,max} - T_{set,min}}{Pr_{max} - Pr_{min}}$ Heating: $T_{set} = T_{set,max} - C_{user} * (Pr - Pr_{min}) * \frac{T_{set,max} - T_{set,min}}{Pr_{max} - Pr_{min}}$
B	Cooling: $T_{set} = T_{goal} + C_{user} * (Pr - Pr_{avg}) * \frac{ T_{set,max} - T_{goal} }{Pr_{dev}}$ Heating: $T_{set} = T_{goal} - C_{user} * (Pr - Pr_{avg}) * \frac{ T_{set,min} - T_{goal} }{Pr_{dev}}$
C	Cooling: $T_{set} = T_{goal} + C_{user} * (Pr - Pr_{avg}) * \frac{T_{set,max} - T_{goal}}{Pr_{max} - Pr_{avg}}$ Heating: $T_{set} = T_{goal} - C_{user} * (Pr - Pr_{avg}) * \frac{T_{set,min} - T_{goal}}{Pr_{min} - Pr_{avg}}$
D	Cooling: $T_{set} = T_{goal} + C_{user} * (Pr - Pr_{min}) * \frac{T_{set,max} - T_{goal}}{Pr_{max} - Pr_{avg}}$ Heating: $T_{set} = T_{goal} - C_{user} * (Pr - Pr_{min}) * \frac{T_{set,min} - T_{goal}}{Pr_{min} - Pr_{avg}}$
E	Cooling: $T_{set} = T_{goal} + C_{user} * (Pr - Pr_{avg}) * \frac{T_{set,max} - T_{set,min}}{Pr_{max} - Pr_{min}}$ Heating: $T_{set} = T_{goal} - C_{user} * (Pr - Pr_{avg}) * \frac{T_{set,max} - T_{set,min}}{Pr_{max} - Pr_{min}}$
F	Cooling: $T_{set} = T_{goal} + C_{user} * (Pr - Pr_{min}) * \frac{T_{set,max} - T_{set,min}}{Pr_{max} - Pr_{min}}$ Heating: $T_{set} = T_{goal} - C_{user} * (Pr - Pr_{min}) * \frac{T_{set,max} - T_{set,min}}{Pr_{max} - Pr_{min}}$
G	Cooling: $Pr \geq Pr_{avg} \rightarrow T_{set} = T_{set,max}$; <i>Otherwise</i> $\rightarrow T_{set} = T_{set,min}$; Heating: $Pr \geq Pr_{avg} \rightarrow T_{set} = T_{set,min}$; <i>Otherwise</i> $\rightarrow T_{set} = T_{set,max}$;

where: T_{set} : Chosen set point for TES [°C]; $T_{set,min}$: Minimum set point temperature [°C]; $T_{set,max}$: Maximum set point temperature [°C]; T_{goal} : Goal temperature [°C]; C_{user} : User comfort related scaling factor; Pr : Current electricity price [€/kWh]; Pr_{min} : Minimum electricity price [€/kWh]; Pr_{max} : Maximum electricity price [€/kWh]; Pr_{avg} : Average electricity price [€/kWh]; Pr_{dev} : Electricity price deviation [€/kWh].

All these algorithms have slightly different methods for choosing the set point between the minimum and maximum consumption. The selection is based on different quantities related to the electricity price. As an additional scaling factor, C_{user} is introduced. For most simulations, the factor is set to 1. If the factor is selected higher, the set point variation is more aggressive and should reduce the user comfort. If it is chosen lower than 1, the set point variation is less aggressive and the user comfort should increase. The results for the scaling of this factor are presented in more detail in [38]. The general relation between the chosen set point and the electricity price is shown for all the algorithms in the example of the water heater model in Figure 5.12. It can be seen that the algorithms have different linear and non-linear behaviour, which causes different results regarding the cumulative price and the user comfort based on the temperature selection.

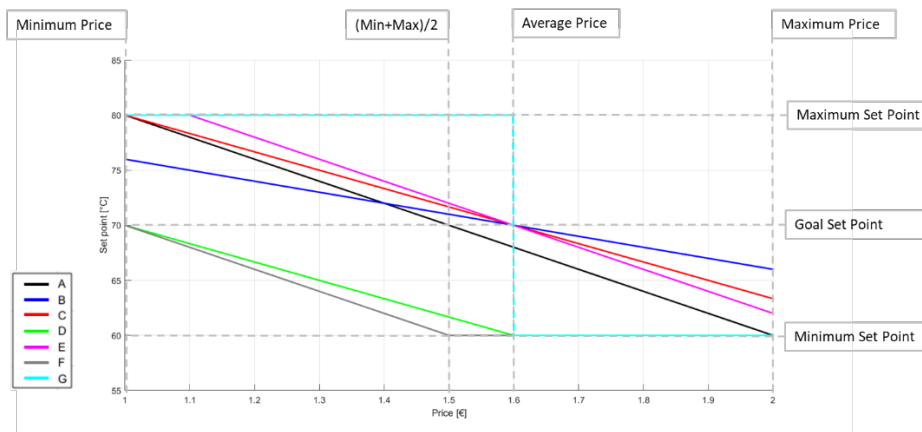


Figure 5.12: Price-based control algorithm visualization: Example with the water heater [30]

5.2.2 Results of price-based control algorithms

Typical cost reductions with such price-based algorithms are in a range of 5-30% [10], [85]. For 1-week simulations with each of the algorithms the cost reductions presented in Table 5.3 could be achieved. The simulation focuses on the TESs. The BESS, FESS and PV-system are not considered in this case to have results comparable to the previously presented scientific literature. More detailed influences from changing different parameters have been published in [38]. As it can be seen, these values are within the same range as other published scientific work. However, these studies did not consider space heating as the thermostatically controllable load that has the biggest potential for cost saving as the results clearly show. The combined case with all 3 TESs shows lower relative cost savings than the case with only space heating because the freezer and water heater show lower cost reductions. This results in lower total relative cost savings compared to a fixed set point control. In general, algorithms D and F show the best performance for most cases.

Table 5.3: Cost reductions for price-based control algorithms compared to FSP control [38]

#	Freezer	Water heater	Simplified Space heating	Combined
A	-5%	-7%	-13%	-8%
B	-14%	-9%	-13%	-10%
C	-10%	-9%	-15%	-10%
D	-11%	-19%	-22%	-20%
E	-14%	-10%	-15%	-11%
F	-11%	-19%	-22%	-19%
G	-15%	-6%	-2%	-5%

So far, these control algorithms have only been applied to one specific household configuration. It is required to determine the influence of different household occupancies well, to find out which control algorithm is the most efficient in different occupancy cases. This is shown in section 5.4. Additionally, the magnitude of the influence of different space heating model complexities on the results needs to be determined. Then it is possible to confirm the conclusions about the accuracy of the space heating model from Chapter 4 and improve the reliability of the results, as shown in the next section.

5.2.3 Comparison of space heating model complexities

As mentioned in Chapter 4, the space heating model complexity has an influence on the model accuracy. Therefore, it was concluded in that chapter that it is reasonable to use the simplified space heating model only for first general investigations and a more complex model for a specific case. To confirm and strengthen those conclusions, the influence of the different models on the control strategies needs to be determined. Therefore, the simplified space heating model is compared to the civil engineering model regarding the performance with the price-based algorithms presented in the previous sections. The simulation topologies are depicted in Figure 5.13.

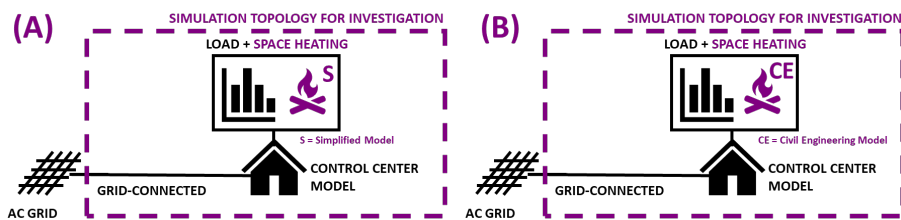


Figure 5.13: Simulation topologies for investigation of space heating model complexity with the simplified (A) and civil engineering (B) models

The selected model is the control centre of the Energy Campus Wildpoldsried. As published in more detail in [57], the selected timeframe for the simulation with price-based control algorithms was from November 22nd until December 2nd, 2019, with the corresponding prices from the Nord Pool Website [77]. The same price-based algorithms A-G and FSP control were used with each model. For an easier comparison, in Table 5.4, the qualitative cost reductions of each model and algorithm are compared to the FSP control.

Table 5.4: Comparison of cost savings of the civil engineering and the simplified space heating model for the price-based algorithms A-G [57]

Algorithm	Cost Reduction with Civil Engineering Model	Cost Reduction with Simplified Model
A	--	+
B	-	+
C	-	+
D	++	++
E	+	+
F	++	++
G	0	0

++ highest; + high; 0 none; - lower; -- lowest;

The results of the simulations show that the models behave similarly for algorithms D-G. The cost reductions are comparable between the models. However, it can clearly be seen that with different models, algorithms A-C behave differently. With the more detailed civil engineering model, they show worse performance than the FSP control while with the simplified model, they show cost reductions. This shows that the model complexity has an influence on the performance of the control algorithms, which leads to the same conclusion as in chapter 4. The simplified space heating model should only be used for a first general investigation. For accurate analysis in a specific case, a complex space heating model is necessary. However, as the system in this work is not a specific planned microgrid, the general results from the simplified space heating model will be sufficient as a basis for the financial feasibility analysis in chapter 6.

Additionally, the NN-based space heating model of the single family house is investigated in more detail regarding the behaviour with small control variations. This will show whether it is necessary to run multiple slightly different simulations to achieve a more accurate forecast of the system behaviour to improve the choice of the price-control algorithm financially. Therefore, flexibility analysis is implemented with a large number of simulations, which is possible even with the more complex NN-based model, as shown in section 4.3. Each simulation has a length of 240 h, and the total number of simulations is 481. The available set points are the following:

- Low set point of 21 °C
- Regular set point of 22 °C
- High set point of 23 °C

The simulations are then conducted with the topology shown in Figure 5.14 according to the following process [80]:

- In the 1st simulation, each hour has the regular set point of 22 °C.
- In the 2nd simulation, the first hour has a lower set point of 21 °C while the other hours are set to the regular set point of 22 °C
- In the 3rd simulation, the second hour has a lower set point of 21 °C while the other hours are set to the regular set point of 22 °C
- ...
- In the 481st simulation, the last hour has a higher set point of 23 °C while the other hours are set to the regular set point of 22 °C

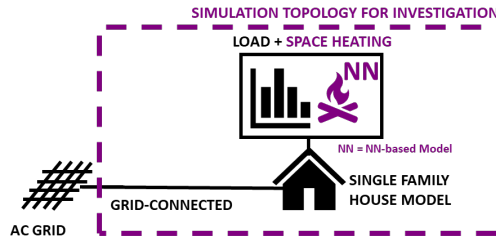


Figure 5.14: Simulation topology for investigations of space heating model behaviour

With these simulations it is possible to analyse the intra-interval and long-term flexibility with the space heating model. Consequently, the behaviour of the complex space heating model can be investigated with such a simple control strategy. The intra-interval flexibility using the NN based single family house model is shown in Figure 5.15. The graph shows the energy consumption within each hour for each selected set point.

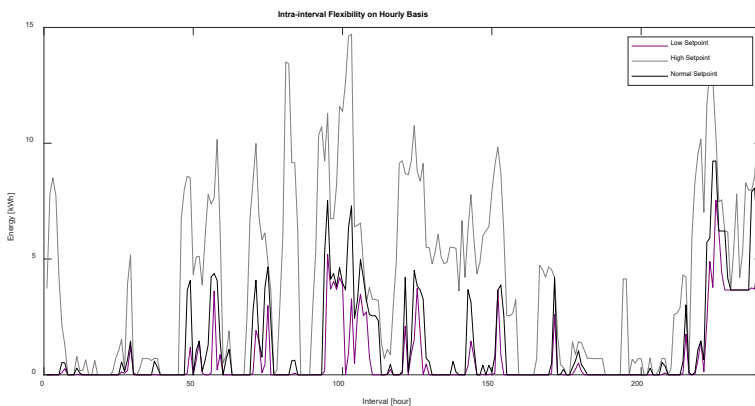


Figure 5.15: Intra-interval flexibility for 240 h on an hourly basis [80]

As expected, the energy consumption within each interval is higher if a high set point is chosen, lower if a lower set point is chosen, and inbetween for the regular set point. If the cumulated energy consumption over the whole 240-h-simulation is investigated, the results look different, as shown in Figure 5.16. This long-term flexibility is shown for each of the changed intervals in the graph. It can be observed that when selecting a high set point in one interval, it does not necessary lead to an overall higher energy consumption, like for interval 91. Vice versa, if a low set point is chosen for one interval, it does not necessary lead to a lower overall energy consumption, like for interval 57. This indicates that space heating is a very complex system that does not always behave as expected. Therefore, to make accurate predictions in a specific case, a numerous slightly varied simulations are necessary. This is only possible with an accurate model that can be calculated with low computational effort, like the proposed NN based model. Thus, it is recommended in the case of a specific planned microgrid to run multiple variations of the control strategy simulations with an NN-based space heating model for more accurate estimations of the space heating behaviour and control strategy performance that can be expected. More details about the setup of the simulations and a more detailed result analysis have been published in [80].

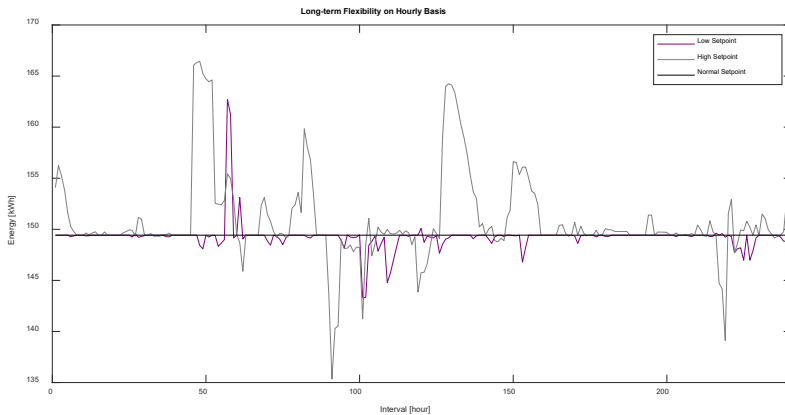


Figure 5.16: Long-term flexibility for 240 h on an hourly basis [80]

5.3 BESS capacity minimization with TESs

In the islanded operation mode, the TESs need to be controlled with a different control strategy as the electricity price is not relevant without power exchange to and from the grid. Therefore, other available values of the microgrid components need to be used as a reference to adjust the temperature set point of the TESs in an optimal and efficient way to minimize the necessary BESS capacity and therefore the investment costs for the system. The simulation topology is depicted in Figure 5.17.

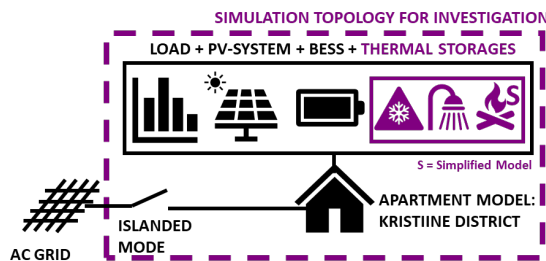


Figure 5.17: Simulation topology for islanded TES investigation

5.3.1 Islanded control algorithm description

There are two different devices available within the proposed microgrid structure that can be used as reference points for the set point selection:

1. PV-system
2. BESS

The FESS is not a good reference as it works quite arbitrarily in power smoothing operation and has lower relevance for the long-term islanded operation due to its high self-discharge rate. Similarly, the load is not a suitable reference point on its own as it does not give any information about the stored or available energy in the microgrid.

The general working principle of the PV-power-based control algorithms is the following. If the available PV-power is high, then it is required to choose a high consumption set point:

- For heating devices, a high temperature set point
- For cooling devices, a low temperature set point

If the available PV-power is low or 0, a low consumption set point must be chosen:

- For heating devices, a low temperature set point
- For cooling devices, a high temperature set point

Firstly, 7 different PV-power-based algorithms have been implemented, like the price-based algorithms presented in section 5.2. More details have been published in [28], [38]. An overview of these algorithms is shown in Table 5.5.

Table 5.5: PV-power-based control algorithm description; Cooling = Freezer; Heating = Water heater and space heating [28]

#	Description of set point calculation algorithm
A	Cooling: $T_{set} = T_{set,max} - C_{user} * (Pwr - Pwr_{min}) * \frac{T_{set,max} - T_{set,min}}{Pwr_{max} - Pwr_{min}}$ Heating: $T_{set} = T_{set,min} + C_{user} * (Pwr - Pwr_{min}) * \frac{T_{set,max} - T_{set,min}}{Pwr_{max} - Pwr_{min}}$
B	Cooling: $T_{set} = T_{goal} - C_{user} * (Pwr - Pwr_{avg}) * \frac{ T_{set,min} - T_{goal} }{Pwr_{dev}}$ Heating: $T_{set} = T_{goal} + C_{user} * (Pwr - Pwr_{avg}) * \frac{ T_{set,max} - T_{goal} }{Pwr_{dev}}$
C	Cooling: $T_{set} = T_{goal} - C_{user} * (Pwr - Pwr_{avg}) * \frac{T_{set,min} - T_{goal}}{Pwr_{min} - Pwr_{avg}}$ Heating: $T_{set} = T_{goal} + C_{user} * (Pwr - Pwr_{avg}) * \frac{T_{set,max} - T_{goal}}{Pwr_{max} - Pwr_{avg}}$
D	Cooling: $T_{set} = T_{goal} - C_{user} * (Pwr - Pwr_{min}) * \frac{T_{set,min} - T_{goal}}{Pwr_{min} - Pwr_{avg}}$ Heating: $T_{set} = T_{goal} + C_{user} * (Pwr - Pwr_{min}) * \frac{T_{set,max} - T_{goal}}{Pwr_{max} - Pwr_{avg}}$
E	Cooling: $T_{set} = T_{goal} - C_{user} * (Pwr - Pwr_{avg}) * \frac{T_{set,max} - T_{set,min}}{Pwr_{max} - Pwr_{min}}$ Heating: $T_{set} = T_{goal} + C_{user} * (Pwr - Pwr_{avg}) * \frac{T_{set,max} - T_{set,min}}{Pwr_{max} - Pwr_{min}}$
F	Cooling: $T_{set} = T_{goal} - C_{user} * (Pwr - Pwr_{min}) * \frac{T_{set,max} - T_{set,min}}{Pwr_{max} - Pwr_{min}}$ Heating: $T_{set} = T_{goal} + C_{user} * (Pwr - Pwr_{min}) * \frac{T_{set,max} - T_{set,min}}{Pwr_{max} - Pwr_{min}}$
G	Cooling: $Pwr \geq Pwr_{avg} \rightarrow T_{set} = T_{set,min}; \text{ Otherwise } \rightarrow T_{set} = T_{set,max};$ Heating: $Pwr \geq Pwr_{avg} \rightarrow T_{set} = T_{set,max}; \text{ Otherwise } \rightarrow T_{set} = T_{set,min};$

where: T_{set} : Chosen set point for TES [°C]; $T_{set,min}$: Minimum set point temperature [°C]; $T_{set,max}$: Maximum set point temperature [°C]; T_{goal} : Goal temperature [°C]; C_{user} : User comfort related scaling factor; Pwr : Current power [W]; Pwr_{min} : Minimum power [W]; Pwr_{max} : Maximum power [W]; Pwr_{avg} : Average power [W]; Pwr_{dev} : Power deviation [W].

As with the price-based algorithms, all these algorithms have slightly different methods, choosing the set point between the minimum and maximum consumption as well. The selection is based on different quantities related to the available PV-power instead of the electricity price. The user comfort, respectively the aggressivity of the set point variation, C_{user} is included in these algorithms as well but it is set to 1 for most of the simulations. The results for the scaling of this factor are presented in more detail in [38]. The visual representation for all the algorithms with the example of the water heater model is shown in Figure 5.18. The algorithms show linear and non-linear behaviour according to their general working principles, which leads to different results in the energy consumption adjustment during islanded operation.

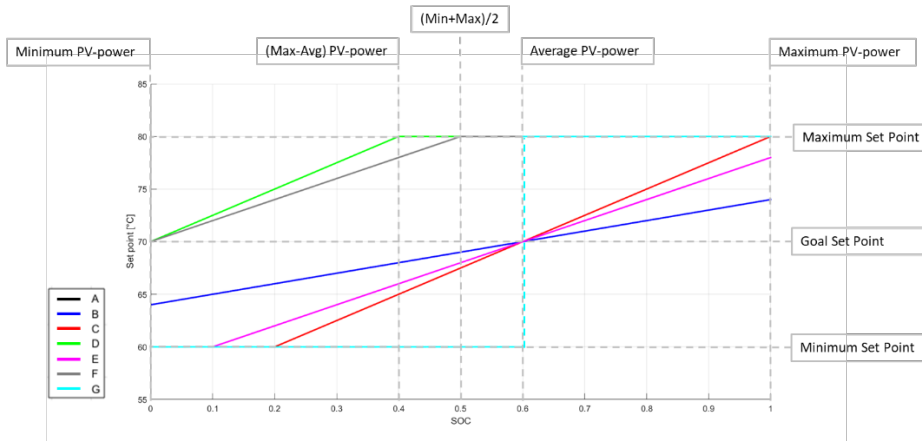


Figure 5.18: PV-power-based control algorithm visualization: Example with the water heater [29]

Secondly, four additional algorithms were implemented, as shown in Table 5.6. Algorithm H is indirectly related to the battery SOC. As mentioned in section 5.1, the stability of the microgrid can be determined by the voltage as the frequency is assumed to be kept constant in any case. Algorithm H uses this property, as the set point is chosen as the goal set point if the microgrid voltage is not dropping to the minimum desired voltage. This only happens if the SOC of the BESS is reaching the minimum while a powerful load is active. The other three algorithms are directly related to different BESS SOC properties. Algorithm J includes the user comfort scaling factor as the price- and PV-power-based algorithms.

The algorithms show linear and non-linear behaviour with the set point selection, as shown with the example of the water heater model in Figure 5.19. This leads to different energy consumption adjustments than with the PV-power-based algorithms and therefore, to other overall performance results.

Table 5.6: SOC-based control algorithm description; Cooling = Freezer; Heating = Water heater and space heating [28]

#	Description of set point calculation algorithm
H	Cooling: $T_{set} = T_{goal}$; If $V_{MG} \leq V_{MG,min}$ then $T_{set} = T_{set,max}$ Heating: $T_{set} = T_{goal}$; If $V_{MG} \leq V_{MG,min}$ then $T_{set} = T_{set,min}$
I	Cooling: $SOC_{Bat} \geq SOC_{Bat,min} + 0.2 \rightarrow T_{set} = T_{goal}$; Otherwise $\rightarrow T_{set} = T_{set,max}$; Heating: $SOC_{Bat} \geq SOC_{Bat,min} + 0.2 \rightarrow T_{set} = T_{goal}$; Otherwise $\rightarrow T_{set} = T_{set,min}$;
J	Cooling: $T_{set} = T_{set,max} - C_{user} * (SOC_{Bat} - SOC_{Bat,min}) * \frac{T_{set,max} - T_{set,min}}{DOD_{Bat,max}}$ Heating: $T_{set} = T_{set,min} + C_{user} * (SOC_{Bat} - SOC_{Bat,min}) * \frac{T_{set,max} - T_{set,min}}{DOD_{Bat,max}}$
K	Cooling: $SOC_{Bat} \geq (1 + SOC_{Bat,min})/2 \rightarrow T_{set} = T_{set,max}$; Otherwise $\rightarrow T_{set} = T_{set,min}$; Heating: $SOC_{Bat} \geq (1 + SOC_{Bat,min})/2 \rightarrow T_{set} = T_{set,min}$; Otherwise $\rightarrow T_{set} = T_{set,max}$;

where: T_{set} : Chosen set point for TES [°C]; $T_{set,min}$: Minimum set point temperature [°C]; $T_{set,max}$: Maximum set point temperature [°C]; T_{goal} : Goal temperature [°C]; V_{MG} : Microgrid voltage [V]; $V_{MG,min}$: Minimum desired microgrid voltage [V]; C_{user} : User comfort related scaling factor; SOC_{Bat} : SOC of BESS; $SOC_{Bat,min}$: Minimum acceptable SOC of BESS; $DOD_{Bat,max}$: Maximum DOD of BESS.

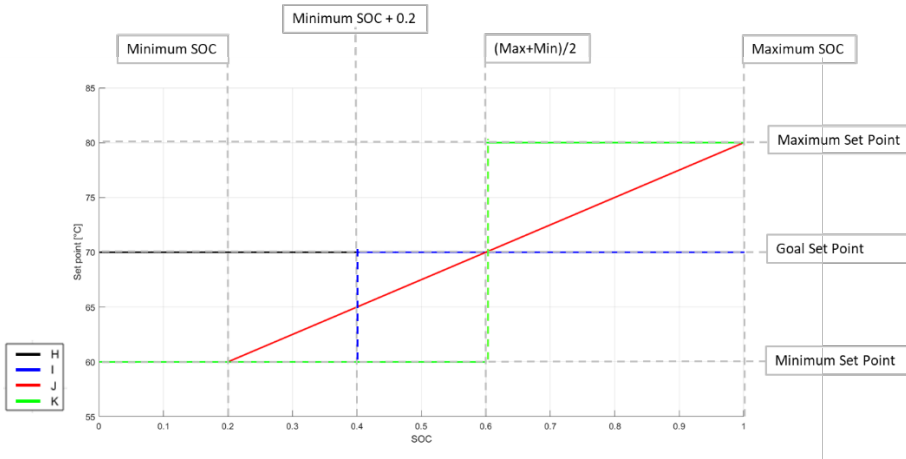


Figure 5.19: SOC-based control algorithm visualization: Example with the water heater [29]

5.3.2 Results of islanded control algorithms

The simulations in the islanded mode were designed to find the minimum BESS capacity for the microgrid to be able to operate for 1 week in the islanded mode. The simulations include the BESS and PV-system, while the FESS is not included to reduce the simulation complexity and use a larger time step of 5 min. This time step is sufficient for the TESs as they have a large time constant for reactions and minimum switching cycle times of several minutes. Compressors in heat pumps and freezers have minimum run (typically 3 min) and pause times (30 s to 15 min), as shown in datasheets [206], [207], [208]. This was confirmed in correspondence with heat pump manufacturers and measurements of a Sharp heat pump. The results for each of the PV-power-based algorithms in comparison to a FSP control are presented in Table 5.7. More detailed influences from changing different parameters have been published in [38].

Table 5.7: Minimum BESS capacity for PV-power-based control algorithms compared to FSP control [38]

#	Freezer	Water heater	Simplified Space heating	Combined
A	0%	-1%	0%	-12%
B	0%	-21%	0%	-30%
C	0%	-25%	-24%	-35%
D	0%	-21%	+3%	-36%
E	0%	-1%	0%	-12%
F	0%	-21%	0%	-30%
G	0%	-25%	-24%	-35%

The freezer alone does not provide a reduction in the BESS capacity, as seen in the table. The energy consumption of the freezer itself is relatively low, while it cannot store the energy for extended amounts of time. This results in low amounts of energy that can be stored and shifted, which has a small influence on the minimum required BESS capacity. Another significant result can be seen with algorithm D and the space heating model. This leads to a higher required minimum BESS capacity than with the FSP control. One reason for this is the complexity of the space heating model, where small influences can make large differences, as described in more detail in section 5.4. Another reason is the possibility of having a small influence at the wrong time, as presented in section 5.1, where a small change at a BESS SOC dip can result in huge differences. The BESS capacity reductions with the combined use of all 3 TESs show impressive margins of more than 1/3 of BESS capacity reduction. This presents generally a huge potential to operate microgrids in the islanded mode more efficiently. The simulation results for the SOC-based control algorithms are shown in Table 5.8.

For the freezer model as well as the water heater, the SOC-based control seems to work better than the PV-power-based one. Space heating results are like in the PV-power-based control but there is no case of a necessary BESS capacity increase. The results for the combined case are in the same range as with the PV-power-based algorithms. Thus, in general the same BESS capacity reductions seem to be achievable with a slight advantage for the SOC-based algorithms considering single devices.

Table 5.8: Minimum BESS capacity for SOC-based control algorithms compared to FSP control [38]

#	Freezer	Water heater	Simplified Space heating	Combined
H	0%	-15%	0%	-18%
I	-3%	-30%	0%	-27%
J	-3%	-31%	-30%	-35%
K	0%	-36%	-4%	-30%

So far, the control strategies for the TESs have only been applied to one specific household configuration and the influence of different household occupancies needs to be determined to find out which control algorithm is the most efficient in general or under a specific occupancy case. This is shown in the following section.

5.4 Cost and capacity minimization with different dwelling occupancies

The dwelling occupancy is an important parameter for the simulation of the household, which can influence the results for the TES control strategies. This applies to the previously described energy cost minimization control strategy as well as to the BESS capacity minimization control strategy. This additional investigation improves the understanding of the already obtained results and enables conclusions about the general applicability or case specific use of the different presented and developed algorithms from sections 5.2 and 5.3.

The described models of the measured 3-room apartment in Kristiine district in Tallinn or the single family house described in section 3.5.1 can be occupied by different demographic groups, such as young families, elderly people or students. These people have different daily schedules as they go working, studying, or for example, to a bingo game.

These different activities at different times have direct influence on the energy consumption. TV sets are turned on at different times, computers are used during home office times, and time preferences regarding cooking are different. This changes the electricity profile for the same physical object, as devices are actively turned on or off. Additionally, these different habits influence the thermal load of the freezer, water heater and space heating. Every person inside the apartment is emitting heat, which changes the space heating energy consumption. People are eating and cooking at different times, influencing the amount of food they put in and take out of the freezer. Different people have different personal hygiene patterns, influencing the amount of water that needs to be heated for hot showers or baths. The overall electricity consumption depends strongly on the number of people living in the household, as shown in Figure 3.6. To investigate the influence of these differences, the previously described households i-vii are used in simulations where the different presented algorithms are applied:

1. For price-based algorithms A-G
2. For PV-power-based algorithms A-G
3. For SOC-based algorithms H-K

Figure 5.20 shows the simulation topologies for these investigations.

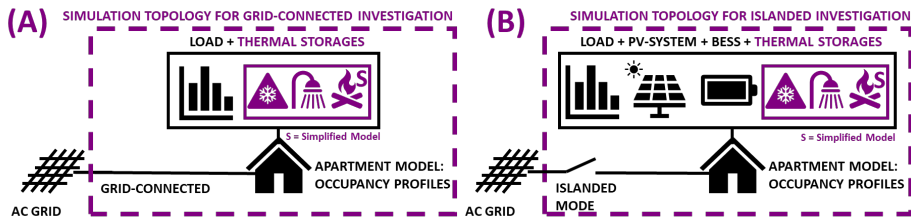


Figure 5.20: Simulation topologies for investigations of dwelling occupancy influence on price-based (A) and islanded (B) control algorithm performance

First, the price-based simulations are implemented with the following conditions:

- Used models: Freezer, water heater, simplified space heating, and thermal and electrical patterns for household i-vii
- Simulation time is 1 week with a time step of 5 min
- Prices are taken from the Nord Pool Webpage [77]
- Price-based algorithms A-G and the FSP control are implemented

The results for these simulations are shown in Figure 5.21. More details about the simulations have been published in [30].

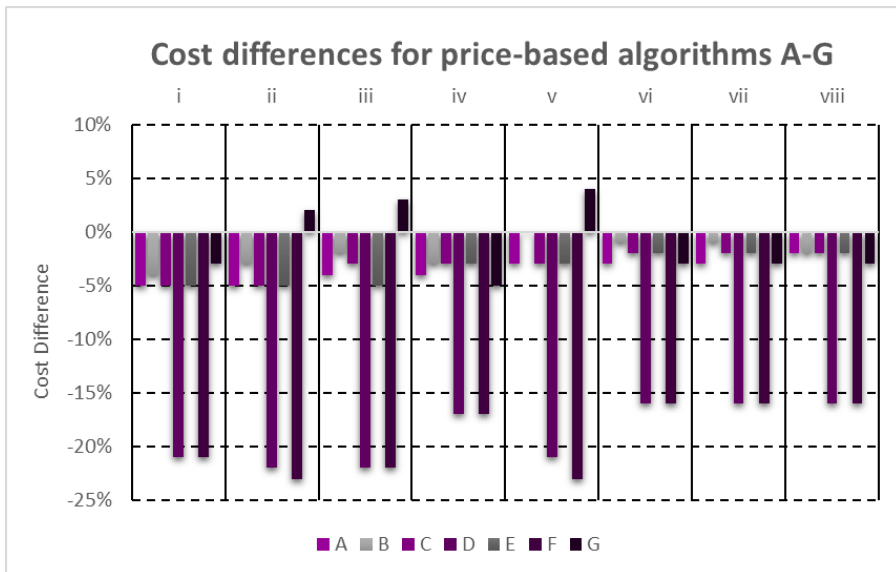


Figure 5.21: Electricity cost differences for algorithms A-G in households i-viii in percent compared to FSP control

The results show that there are not always cost reductions with algorithm G. With some households, the costs are increased compared to FSP control, which is not desirable. The reason for this is the binary behaviour of the algorithm. As it can be seen in Figure 5.12 and Table 5.9, the algorithm does not have a goal set point and can only change between maximum and minimum consumption set point.

The best cost savings are achieved for households i, ii, iii, and v. These are the households with a low number of occupants. The algorithms are working better for a lower number of occupants as they put a lower total thermal load on the devices.

The most significant observation is the extremely good cost reduction for algorithms D and F for all households. These algorithms are scaling between minimum consumption and goal set point instead of minimum and maximum consumption set point like the other algorithms, as shown in Figure 5.12 previously. The consequences of this behaviour will be analysed in more detail in section 6.1.1. To simplify and summarize the results for all households, a qualitative cost reduction classification shown in Table 5.9 is used.

Table 5.9: Qualitative cost savings classification with description for goal set point operation for price-based algorithms A-G [30]

Algorithm	Goal Set Point Operation	Cost Savings
A	(Max. Price + Min. Price)/2	+
B	Average Price	+
C	Average Price	+
D	Minimum Price	++
E	Average Price	+
F	Minimum Price	++
G	Never	0

++ highest; + high; 0 none; - lower; -- lowest;

Second, the PV-power-based simulations are implemented with the following conditions:

- Used models: Freezer, water heater, simplified space heating, basic BESS, PV-system pattern, and thermal and electrical patterns for household i-vii
- Simulation time is 1 week with a time step of 5 min
- PV-power-based algorithms A-G and the FSP control are implemented
- As in section 5.3, the simulation searches for the minimum BESS capacity for stable 1 week operation of the microgrid

Additional information about the simulations has been published in [29]. As a reference, the minimum BESS capacities for the households with a FSP control are shown in Table 5.10. The households with more occupants, and consequently a higher electricity consumption, need a larger BESS capacity, even though they are living in the same physical object. In comparison, the relative minimum BESS changes for each household and algorithm are presented in Figure 5.22.

Table 5.10: Minimum battery storage capacities for households i-viii with a fixed set point control [29]

Household	i	ii	iii	iv	v	vi	vii	viii
Battery Capacity [kWh]	5.7	1.3	0.6	9.6	0.8	16.8	13.8	11.4

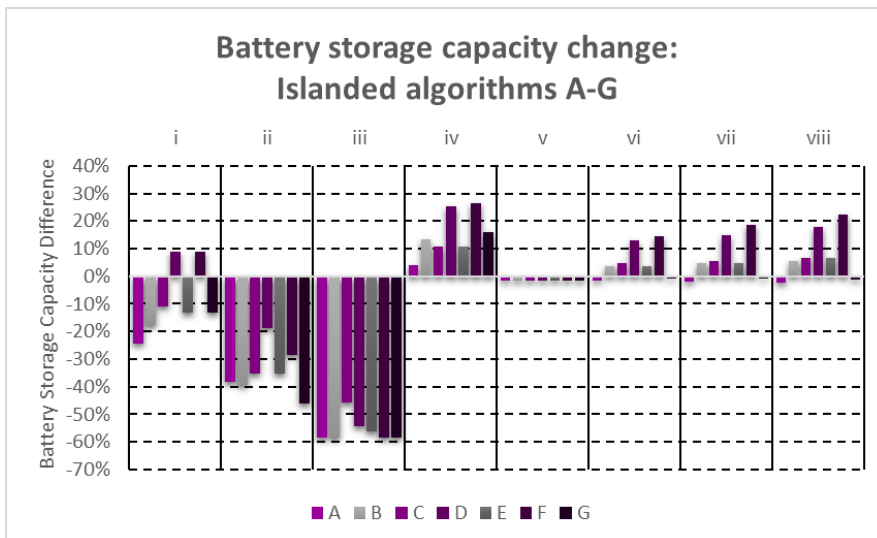


Figure 5.22: Battery capacity differences for islanded algorithms A-G in households i-viii in percent compared to FSP control [29]

It is significant that the minimum BESS capacity cannot be reduced for all households with the PV-power-based algorithms. For households iv, vi, vii, and viii, the BESS capacity must be increased. The same holds for household i with algorithm D or F. Closer investigations on the households show that those are the households with higher energy consumptions. Since the simulations are based on the same physical objects, it can be concluded that the behaviour originates from the PV-system. The PV-system size has been scaled to the largest household consumption. The PV-power-based algorithms cannot scale well in this situation as they only work well if the PV-system is over-dimensioned for the household.

It can be seen as well that algorithms D and F show the worst performance regarding BESS capacity reduction. This is the opposite behaviour compared to the price-based algorithms. Since the PV-power-based algorithms are based on the inverted logic of the price-based algorithms, algorithms D and F can only scale between maximum consumption and goal set point, as can be seen in Figure 5.18. For household iii, with the lowest energy consumption, all algorithms work extremely well and achieve BESS capacity reductions around 50%.

Third, the SOC-based simulations are implemented with the following conditions:

- Used models: Freezer, water heater, simplified space heating, basic BESS, PV-system pattern, and thermal- and electrical patterns for households i-vii
- Simulation time is 1 week with a time step of 5 min
- SOC-based algorithms H-K and FSP control are implemented
- As in section 5.3, the simulation searches for the minimum BESS capacity for stable 1 week operation of the microgrid

More details about the implementation and results have been published in [29]. The relative minimum BESS changes for each household and algorithm compared to FSP control shown in Table 5.10 are presented in Figure 5.23.

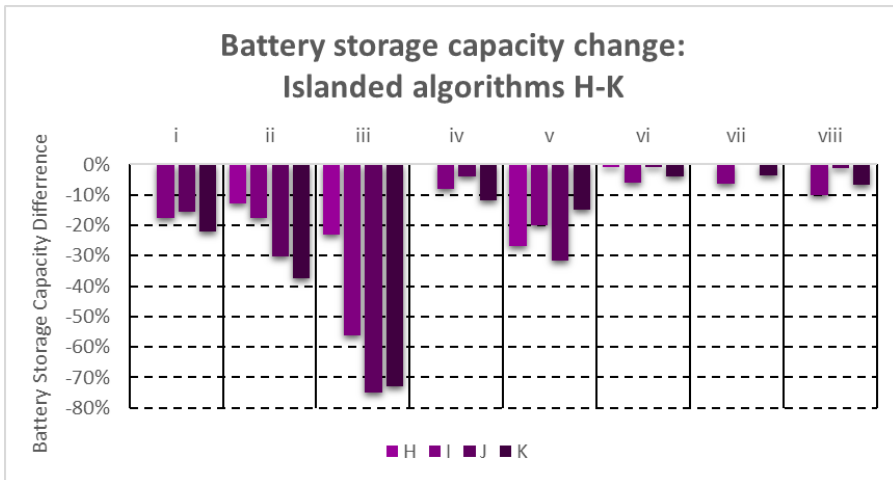


Figure 5.23: Battery capacity differences for islanded algorithms H-K in households i-viii in percent compared to FSP control [29]

It can be observed that no algorithm creates BESS capacity increases for any households. This is a very positive result regarding the stability and reliability of those algorithms. It can be seen as well that for households with lower energy consumption the best results can be achieved. This is related to the PV-system over-sizing, as mentioned before. A larger PV-system compared to the energy consumption enables more control freedom for the algorithms. Further, the extremely simple algorithm H shows good performance for households ii, iii and v. Algorithm K presents good results for all households and is the most constant overall even though it does not always show the best result for the household. The BESS capacity reductions that can be achieved are around 4-70%.

5.5 Conclusions

The modelled and validated storage systems need to be controlled with different control strategies to achieve certain defined goals. Therefore, different simulations with control strategies for the storage systems have been developed and tested. The following four goals for the control strategies were investigated:

1. Increase of islanded operation duration (Security of supply parameter)
2. Increase of the cyclic lifetime of the BESS (Financial parameter)
3. Minimization of energy costs (Financial parameter)
4. Minimization of BESS capacity (Financial and security of supply parameter)

From the cyclic lifetime and security of supply improvement control strategy with the BESS and FESS, the following main conclusions can be drawn:

- The BESS cyclic lifetime can be improved by around 19% with a cycle reduction of 16%.
- The islanded operation time for the microgrid could be improved by up to 50%. This result, however, is not generally applicable, as the FESS managed to bridge a short power shortage.
- An increase of around 3% in the islanded operation time is a general applicable value.

The energy cost minimization control strategy for the TESs achieved the following:

- The cost reductions are in a range around 5%-30%.
- The highest cost reductions could be achieved with algorithms D and F for all different tested dwelling occupancies.
- Comparing the cost reductions between the simplified and a more complex space heating model showed different results for some algorithms. Thus, the conclusion from Chapter 4 is confirmed that the simplified model should only be used for a general investigation and a complex model is needed for better accuracy and recommendations in a specific case.

With the TESs it was also possible to achieve the minimization of the BESS capacity:

- The minimum required BESS capacity for the islanded operation could be reduced by 10-36%.
- The results for the PV-power-based algorithms showed that they seem to work only with dwelling occupancies where the PV-production is over dimensioned compared to the household's energy consumption. This is not a desirable behaviour.
- The SOC-based algorithms showed more stable results with BESS capacity reductions in all cases around 4-70%.
- In this regard, for low-budget upgrades of existing systems, algorithm H can be recommended as it needs no additional communication, while algorithm K should be used in all other cases due to the most stable performance.

The results and conclusions from these investigations are used in the next chapter as a basis for studying user requirements and as input for the financial feasibility analysis.

6 Analysis of social and financial feasibility

Since the proposed setup is technically feasible, as shown in the previous chapters, additional investigations are required to cover financially and socially relevant aspects as well. If a system is not financially feasible, then the interest in the technology will be low despite its technical feasibility. Additionally, it should be considered whether the system has the potential to be accepted by the designated users. Therefore, the following sections will investigate the social acceptability and financial feasibility in more detail.

6.1 Social acceptance analysis

A technology that is not acceptable for the potential customers has a small chance of widespread use and will stay a niche product [209]. Therefore, an analysis regarding the social acceptability of the proposed setup has been done. Two main factors were selected for this investigation: the potential concerns regarding the user comfort interference and the users' privacy concerns. If these concerns can be reduced, the technology has a higher potential for general acceptance.

6.1.1 Concerns regarding user comfort interference

The user comfort is an important acceptance parameter. If the user comfort is reduced, the technology is unlikely to be adopted. As the state-of-the-art analysis in chapter 2 showed, it is first necessary to define the user comfort for the different devices and operation modes. Then the limits need to be determined and selected based on certain standards. Afterwards, additional boundaries for evaluation can be chosen.

For the grid-connected operation, the temperatures of the TESs are the measurements for user comfort. The control algorithms for the TESs are influencing the temperature set points of the freezer, water heater and space heating. As mentioned in chapter 5, maximum and minimum set points for the algorithms can be set. Users can change the settings in case the standard values are not fitting and out of their comfort range. Additionally, a preferred goal set point inbetween can be selected. This is especially important for the space heating control, as people feel comfortable at slightly different temperatures [210]. The comfort interference for changing the temperature set point of the freezer and water heater is very low if it is done within reasonable limits. The user typically cannot determine the difference between 60 or 70 °C hot water temperature, as it is mixed with cold water during a shower anyway. Similarly, the temperature difference between -21 and -20°C in the freezer compartment does not cause the frozen food to go bad immediately.

Revisiting the simulations from section 5.4, the indoor air temperature development for the different price-based control algorithms during the simulation can be visualized as shown in Figure 6.1.

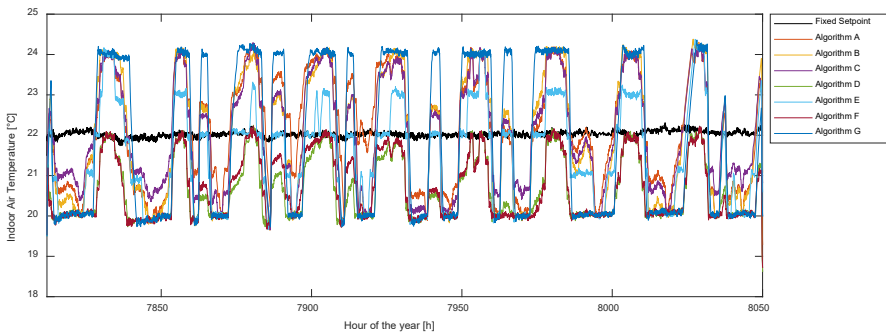


Figure 6.1: Indoor air temperature results for price-based set point calculation algorithms A-G and a fixed set point for the civil engineering space heating model [57]

As space heating can influence the comfort feeling of humans much easier, a difference of 1-2 °C can already cause discomfort [210]. The indoor air temperature graphs show a temperature range of 4 °C. The goal set point selected by the user would be 22 °C, the same as the FSP control. If 22 °C is the perfect temperature, larger variations from this value can be considered as a reduced user comfort. In this regard, mean temperature deviations from this goal set point are considered a large discomfort as well.

The user comfort for the grid-connected system is therefore defined as:

- “More and larger temperature fluctuations and mean temperature deviations of the room temperature equal less user comfort.”

It can be observed in the figure that algorithms D and F are always below the goal set point. This creates a large discomfort. Algorithm G is switching between the extreme values, which is not desirable in terms of user comfort either. Algorithms A, B and C are fluctuating between the maximum and minimum, creating only a small comfort reduction compared to an FSP. Algorithm E behaves similarly, but it tends to vary less than algorithms A, B and C, reducing the user comfort less consequently.

These findings in relation to the cost reductions for each algorithm, as presented in Chapter 5, are summarized in Table 6.1.

Table 6.1: Cost savings and user comfort classification for price-based algorithms A-G

Algorithm	User Comfort	Cost Reductions with Detailed Model
A	+	--
B	+	-
C	+	-
D	--	++
E	+(+)	+
F	--	++
G	-	0
FSP	++	0

++ highest; + higher; 0 none; - lower; -- lowest;

The table reveals that algorithms D and F, which provide the highest electricity cost reductions, create the highest user discomfort. Algorithm G does not show any benefits over an FSP control. Algorithms A, B and C do not reduce the user comfort significantly, but do not provide cost savings with space heating either. Algorithm E shows good performance in cost reductions and additionally has a small impact on the user comfort. Thus, algorithm E would be the preferred algorithm if the user comfort is prioritized over cost reductions.

For islanded operation, the thermal user comfort plays a much smaller role, as stable operation of the microgrid is more important. If the microgrid management cannot maintain stable operation, it must turn off the energy supply during islanded operation, which causes a larger discomfort for the user than a temperature deviation. Therefore, the temperature related user comfort of the islanded set point control algorithms does not need to be investigated as detailed as for the grid-connected operation. Thus, a longer islanded operation time and therefore better security of supply is the main measurement for user comfort in the islanded operation mode.

The user comfort for the islanded operation mode is defined as:

- “A longer islanded operation duration improves the user comfort more than fluctuations of the room temperature reduce it as a blackout is a much larger inconvenience for the user.”

Considering this, it is evident that the FESS and BESS control strategy in section 5.1, which shows that such a control can prolong the islanded mode operation by 3%-50%, improves the user comfort significantly by increasing the security of supply. Following the results presented in section 5.3.2, the performance of the islanded TES control needs to be evaluated as well. Considering the SOC-based algorithms H and K, it is evident that the user comfort from the temperature comfort point of view is reduced. However, the results show that the necessary BESS capacity could be reduced, respectively, the islanded operation time could be increased with the same BESS capacity. Since this is more important than the temperature comfort, the overall user comfort for this control strategy is improved. Thus, the FESS and BESS, and the islanded TES control strategy should be implemented for improved user comfort in islanded operation mode. These aspects are summarized in Table 6.2.

Table 6.2: User comfort classification for islanded control strategies

Control Strategy	Results	Overall User Comfort
Without FESS	Regular Islanded Operation Time	0
FESS Power Smoothing	Increased Islanded Operation Time (3%-50%)	++
TESs: FSP	Optimal Temperature with Regular Islanded Operation Time	0
TESs: SOC-based Algorithm H/K	Reduced Temperature Comfort with Increased Islanded Operation Time	+

++ large increase; + small increase; 0 regular level;

In Chapter 5, a user comfort scaling factor was introduced for some of the price-based and islanded algorithms. If the factor is selected higher, the set point variation is more aggressive, reducing the user comfort. If it is chosen lower than 1, the set point variation is less aggressive, and the user comfort increases. The results for the investigation of this user comfort-based scaling show inconclusive results for values larger than 1. The user comfort gains with values lower than 1 are quite low, while the performance regarding BESS capacity reduction and cost saving drops sharply. Therefore, the user comfort scaling factor was set to 1 for all other simulations. The basic control selection considering the user comfort should be made based on the algorithm. The user comfort scaling is more suitable for small optimization adjustments in a specific case. The results for the other user comfort scaling factors compared to a scaling factor of 1 can be summarized as shown in Table 6.3.

Table 6.3: Relative cost savings with different user comfort scaling factors; $C_{user} = 2$: more aggressive scaling; $C_{user} = 0.5$: less aggressive scaling

Algorithm type	Scalable algorithms	$C_{user} = 2$	$C_{user} = 0.5$
Price-based	A, D, F	+	-
	C, E	-	-
PV-power-based	A, B, C, D, E, F	+	-
SOC-based	J	-	-

+ better performance; - worse performance;

As a side aspect of user comfort, it can be noted that the islanded BESS and FESS control strategy, in combination with the TES control in islanded mode, reduces the size of the necessary BESS and prolongs its lifetime, as shown in Chapter 5. This increases the sustainability of such a system because less rare materials need to be used to produce BESSs in case they are not already in use in the microgrid as a second life. Many users welcome this higher environmental friendliness and feel more comfortable additionally.

6.1.2 Concerns regarding privacy

Data privacy concerns regarding the proposed system in this work may seem to be neglectable on first sight if the system is designed for just one household. The whole control can be implemented in a local home energy management system. Additionally, traditional, robust algorithms are used for control, which do not collect data.

However, if the system is designed for a multi household building or even multiple buildings, there will be a dataflow between the households. This can already create concerns with some users. Multiple buildings can be considered a microgrid if they have a common point of coupling or are connected on the same feeder. In this case, the local DSO is already involved in the microgrid design. The next step would be the interconnection of multiple microgrids to form a so-called smart city. In this case, data will be transferred across multiple layers, like the already existing AMI. A common AMI configuration as described in chapter 2 with the AMI surfaces that can lead to privacy concerns is shown in Figure 6.2. Thus, the scalability of the proposed system can raise user concerns regarding their privacy.

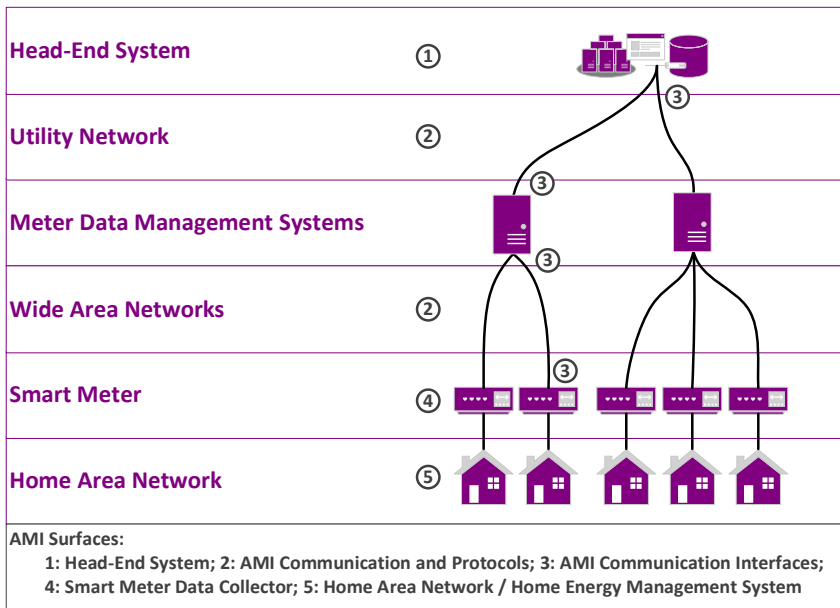


Figure 6.2: Common AMI configuration, based on [53]

Another aspect that can create data privacy related concerns is the further development of such systems. The proposed system is using mostly traditional, robust control algorithms with a low amount of processed data. As shown in Chapter 2, machine learning is becoming more common in the microgrid context. Additional data input from machine learning methods, like PV-power production predictions and load predictions, can be beneficial for optimizing the control strategies further. For example, model predictive control or reinforcement learning control can be implemented instead of traditional algorithms. Most user concerns will be raised in this regard with the analysis of their load patterns. Non-intrusive load monitoring (NILM) is a technique that is based on machine learning. It can disaggregate the load profile of a smart meter to learn switching patterns for single devices. This can be used to determine the users' behaviours on the one hand; on the other hand, it is extremely useful to optimize the control of schedulable devices.

To determine the privacy concerns that could be raised with the proposed system, the AMI related user concerns were identified in literature. The results can be transferred to a large-scale version of the proposed system. The identified concerns are shown in Table 6.4.

Consecutively, as it is a likely that the proposed system will be optimized in future with predictions, the most concerning technique, NILM, is analysed step by step regarding the identified concerns. As mentioned in Chapter 2, the used data sets in different NILM publications are quite large. This means that a lot of training data is used for the machine learning methods to get good results at accuracy. An overview of the data set sizes is presented in Table 6.5.

Table 6.4: Residential user concerns regarding the AMI and ML algorithms [53], [47], [51], [49], [81], [82], [83], [84], [45], [85]

Concern	Description
Privacy	
Price discrimination	Variance in consumer pricing based on consumer profile
Denial of consumer services	Denied access to consumer services due to unsuitable consumer profile
Target to excessive advertisements	Increased advertisements, since consumer identified as target group by consumer profile
Identification of home appliances	Unwanted identification of individual home appliances through NILM
Exhibition of user habits and lifestyle	Exposure of sensitive data regarding consumer habits through NILM
Exhibition of illnesses and disabilities	Exposure of sensitive health data through NILM
Personification of anonymous data	The personification of data deemed to be collected anonymously through ML algorithms
Cyber Security	
Disconnection of home appliances	The manipulation of demand response (DR) programs through the tampering of ML training and input data
Burglary, arson, vandalism etc.	Increased threat through occupancy information gained by NILM
Attractive target to burglary	Increased likelihood of burglary due to identification of attractive appliances through NILM
Target to kidnapping	Possibility to use NILM for identifying persons in vulnerable situations
Denial of personal mobility	The manipulation of DR programs through the tampering of ML training and input data to deny charging of electric vehicles

Table 6.5: Overview of training data sets with literature examples [CSW]

Dataset	Duration/Resolution	Publication
Pecan Street	4 years / 1 minute	[133], [87], [88]
REDD	2-4 weeks / ≤ 4 seconds	[88], [115], [90]
UK-DALE	655 days / ≤ 6 seconds	[115], [137], [237]
ECO	8 months / 1 second	[238], [239]
BLUED	1 week / ≤ 1 seconds	[140]
Challekere Campus	7 days / 2 minutes	[139]
Private Dataset	1 months / 10 seconds	[138]
Private Dataset	1 month / 30 minutes	[136]

Analysing the sizes of the used data sets and the presented accuracy of the disaggregation shows that there is a correlation between the data set size and the accuracy, as with nearly all ML methods. The more data, including additional measurements, like mentioned in Chapter 2, the better the accuracy of the NILM process.

This leads to a tendency of using as much data as possible, raising concerns regarding the users' privacy.

To complement the analysis, the corresponding legal documents that are relevant in this regard have been mapped to the identified concerns regarding whether:

- ... the current EU legislation protects the prosumer's data and privacy rights, using [240], [241]
- ... the EU regulatory framework addresses the prosumer's concerns in the area of cyber-security, using [240], [241], [242], [243]

The results are presented in Table 6.6. It is intended to be used as a tool to guide the future development of the proposed system and to avoid complications regarding privacy concerns from a legal and users' point of view. The tool can be used during the development of an application that makes use of NILM or operates at any surface of the AMI to determine cyber-security and data privacy requirements that need to be prioritized. This is transferrable to the microgrid development as well. A flowchart is presented in Figure 6.3 to provide an example for the use of the developed tool. More details were published in [53].

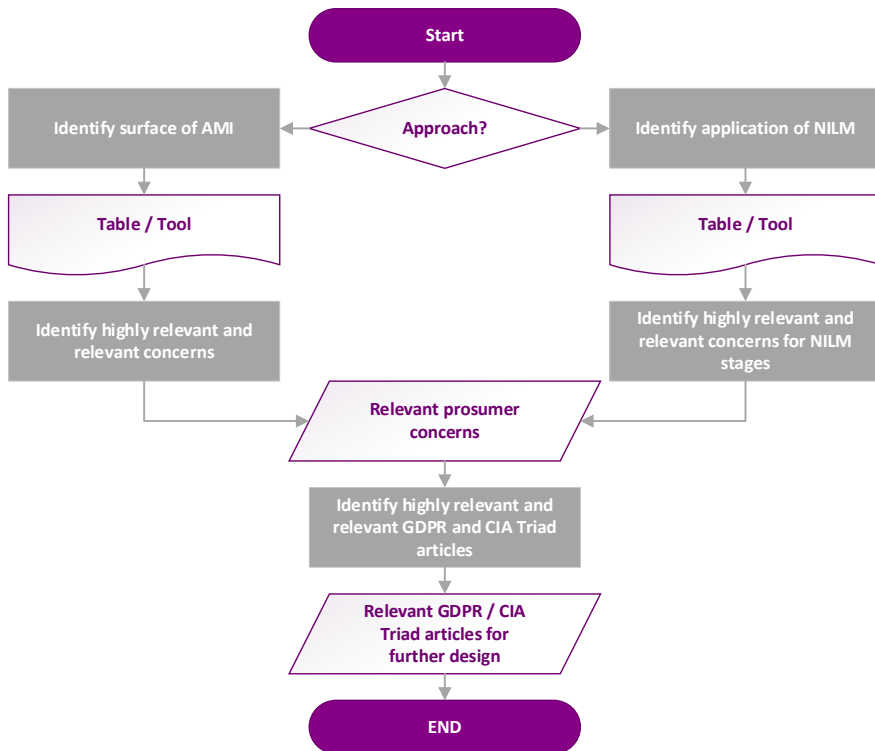


Figure 6.3: Flowchart for the use of the provided tool

Evaluating the proposed and investigated system in this work with the tool showed no privacy concerns because there is no data stored or analysed with the implemented control algorithms. However, the cyber-security concerns apply here as in nearly all cyber-physical systems. As mentioned before, this can change if the system is extended to multiple households or uses data analysis-based control or prediction methods.

Table 6.6: Mapping of ML angles via prosumer concerns based on relevance: Technical and legal views [53]

		Prosumer Concerns													
		Price discrimination	Denial of prosumer services	Target to excessive advertisements	Identification of home appliances	Exhibition of user habits and lifestyle	Exhibition of illnesses and disabilities	Personification of anonymous data	Disconnection of home appliances	Burglary, arson, vandalism etc.	Attractive target to burglary	Target to kidnapping	Denial of personal mobility		
Technical	Surfaces of AMI	Home Area Network	0	0	++	++	++	++	++	++	++	++	++	++	
		Smart Meter	+	0	+	++	++	++	++	+	++	++	++	++	
		Smart Meter Data Collector	0	0	++	+	+	+	+	+	+	+	+	+	
		AMI Networks	0	0	+	+	+	+	+	+	+	+	+	+	
		AMI Protocols	0	0	+	+	+	+	+	+	+	+	+	+	
		Head-End Management System	++	++	++	++	++	++	++	+	+	+	+	+	
	Applications of NILM	Home Energy Management System	a			c		0							
		Ambient Assisted Living Recommender System	0	a, e	a, e	0	e	e	a, e	a, b, c, d, e	d, e	c, d	d, e	a, b, c, d, e	
		Fault Diagnostics	a			c		0							
			0			0		0							
	Legal	Data Protection and Privacy (I)	GDPR Art. 5(1)(a)	++	++	++	++	++	++	++	+	+	+	+	+
			GDPR Art. 5(1)(b)	++	++	++	++	++	++	++	+	+	+	+	+
			GDPR Art. 5(1)(c)	++	++	++	++	++	++	++	+	+	+	+	+
			GDPR Art. 5(1)(d)	+	+	+	+	+	+	+	+	+	+	+	+
GDPR Art. 5(1)(e)			+	+	+	+	+	+	+	+	+	+	+	+	
GDPR Art. 5(1)(f)			+	+	+	++	++	++	+	++	++	++	++	++	
GDPR Art. 5(1)(g)			++	++	++	++	++	++	++	++	++	++	++	++	
Data Protection and Privacy (II)		GDPR Art. 12	++	++	++	++	++	++	++	+	+	+	+	+	
		GDPR Art. 13, 14, 15	++	++	++	++	++	++	++	+	+	+	+	+	
		GDPR Art. 16, 17, 18, 19, 20	++	++	++	+	+	+	+	0	0	0	0	0	
		GDPR Art. 21, 22	++	++	++	++	++	++	++	0	0	0	0	0	
Data Protection and Privacy (III)		GDPR Art. 24	++	++	++	++	++	++	++	++	++	++	++	++	
		GDPR Art. 28	++	++	++	++	++	++	++	+	+	+	+	+	
		GDPR Art. 32	+	+	+	++	++	++	+	++	++	++	++	++	
Cyber-security: CIA Triad		Confidentiality	0	0	0	0	0	0	0	0	++	++	++	0	
		Integrity/Authenticity	0	0	0	0	0	0	0	++	0	0	0	0	
		Availability	0	0	0	0	0	0	0	0	0	0	0	++	

++ = highly relevant; + = relevant; 0 = not relevant/applicable; a = Metering NILM stage; b = Event detection NILM stage; c = Feature extraction NILM stage; d = Classification NILM stage; e = Analysis of classification NILM stage

6.2 Financial feasibility analysis

To complement the social and technical analysis, a financial investigation is needed. Even if a system works technically well and has a general social acceptance, it still needs financial feasibility to be successful on the market. This investigation is divided into two parts:

- A general financial analysis of the complete proposed system with BESS, FESS and TESS
- Additional investigations regarding FESS and the separate influence of each of the TESS

Based on these two investigations, it is possible to give recommendations about the microgrid design from the financial point of view.

6.2.1 Financial investigation for the complete proposed system

An important metric from the investment point of view is the time until the invested money is completely recovered, and the implemented system shows profits compared to regular operation without the added devices. This return of investment time is the comparison basis for different control strategies in the grid-connected mode and should be below 10 years considering the component lifetimes. As mentioned earlier, the islanded control methods can be applied in the grid-connected operation for maximum self-consumption as well. The price-based control strategies are relevant for times when electricity is needed from the main grid. In the first step, the current average supply interruption times per year should be evaluated to estimate the share of the islanded operation per year.

The System Average Interruption Duration Index (SAIDI) is the average outage duration for each customer, measured in minutes per year. The average SAIDI values for Estonia and Germany for the year 2020 are shown in Table 6.7. As the table shows, the current supply interruption levels make a very low share of the whole year. Thus, these interruptions have a neglectable average impact on the financial calculations for such a system. But supply interruptions can have a very high case specific value, e.g., for microgrids with hospitals or other service providers that must not be interrupted at all.

Table 6.7: Disturbance metrics for DE and EE for 2020 [226], [227]

Country	SAIDI 2020 [minutes/year]	Share of the year [%]
DE	2.11	0.0004
EE	157.9	0.03

Thus, for the financial analysis, different self-consumption levels will be investigated, which make use of the described islanded control methods. The system that is investigated financially consists of all the described components with their related financial aspects. This includes FESS, BESS, PV-system, and TESSs. The different aspects that are relevant for the financial investigation are listed in Table 6.8.

These aspects include consumption and production values, component dimensioning values, component costs, installation costs, electricity prices, subsidy rates, and other values from the technical calculations.

Table 6.8: Considered aspects for financial analysis of a hybrid storage system for a typical single family house

Aspect	Unit	Single Family House	Description / Details
Power consumption	kWh/year	3987.97	
Typical regional solar generation EE	kWh/kWp	864	Based on PVGIS [150]
Total generated PV-power per day	W	819446	24 th Sep. of the Laastu Talu OÜ PV-profile
Min. basic required PV-system output	kWp	4.62	
Surcharge for losses (25%)	kWh/year	997	BESS self-discharge and other losses [149]
Power consumption with surcharge	kWh/year	4985	
Min. required PV-system output with surcharge	kWp	5.77	
Required energy generation per day	kWh	13.66	
kW per day	kW	819	
Power of one PV-module	Wp	330	Typical value between 300 Wp – 400 Wp
Area of one PV-module	m ²	2	Typical area of PV-module
Required amount of PV-modules	pcs	17	
Required total roof area	m ²	29.37	
Electricity price DE (2021)	EUR/kWh	0.33	End of 2021 prices [228]
Electricity price EE (2021)	EUR/kWh	0.14	End of 2021 prices [229]
BESS capacity	kWh	3.88	Example: Kokam SLPB120255255 [168]
BESS costs per kWh	EUR/kWh	1000	Beginning of 2022 average end-user price [230]
BESS costs total	EUR	3880	
FESS capacity	kWh	10	Minimum offered by e.g., Energiestro [231]
FESS costs per kWh	EUR/kWh	250	2021 Estimation [232], [233]
FESS costs total	EUR	2500	
Price of one PV-module	EUR	150	Beginning of 2022 average prices [234]
Price for all PV-modules	EUR	2623	

PV-inverter costs	EUR	1574	50%-60% of module costs (Beginning 2022) [235]
Small parts	EUR	1000	Cables etc.
Installation and commissioning (BESS+FESS+PV-system)	EUR	900	Medium installation effort [230]
Control system for TEs	EUR	100	Small devices, e.g., Raspberry Pi, Cables, ...
Installation and commissioning (TEs)	EUR	100	Low installation effort
BESS capacity reductions (Max. reduced BESS capacity for new systems)	%	15%	SOC-based Algorithm K; Average for different dwelling occupancies
BESS capacity reductions (Reduced BESS capacity for existing systems)	%	4%	SOC-based Algorithm H; Average for different dwelling occupancies
Consumption reductions (Comfort oriented)	%	4%	Price-based Algorithm E; Average for different dwelling occupancies
Consumption reductions (Price oriented)	%	17%	Price-based Algorithm D/F; Average for different dwelling occupancies
Subsidy rate DE	EUR/kWh	0.0653	Value for 22 April 2022 [236]
Subsidy rate EE	EUR/kWh	0.0537	[237]
Additional renewable support programmes	EUR	0	Programmes are regional and temporary → Not included

The financial analysis will be carried out for the following cases to compare the main control strategies during grid-connected operation with differently dimensioned systems:

- Case 1: Typical grid-connected operation with regular dimensioning of components leads to approx. 38% self-consumption [149].
- Case 2: It is assumed that at least 80% self-consumption can be achieved with BESS in maximum self-consumption operation mode for reduced PV-system size (like islanded operation).
- Case 3: It is assumed that at least 80% self-consumption can be achieved with TEs and reduced BESS capacity in maximum self-consumption operation mode for reduced PV-system size (like islanded operation).
- Case 4: It is assumed that the PV-system and BESS are 50% too small to cover the self-consumption. Additional energy is consumed from the grid.
- Case 5: It is assumed that the PV-system and BESS are 50% too small to cover the self-consumption. The TEs work with price-based control algorithms D/F for the consumed energy from the grid.

The benefits for extended islanded operation, which depend on the microgrid consumers, are not considered, and can be added for each case additionally. These are reduced loss of revenue due to devices and computers not working and other cases. Details for the component dimensioning for the cases are shown in Table 6.9.

Table 6.9: Changed aspects for self-consumption cases for financial analysis

Aspect	Unit	Case 1	Case 2	Case 3	Case 4	Case 5
Self-consumption rate	%	38	80	80	100	100
PV-system output	kWp	5.77	2.74	2.74	1.8	1.8
PV-system costs	EUR	2623	1200	1200	600	600
BESS capacity	kWh	3.88	3.88	3.30	1.6	1.6
BESS costs	EUR	3880	3880	3300	1600	1600
Feed-in (Power) per day	W	508057	77847	77847	0	0
Feed-in (Energy) per day	Wh	8468	1297	1297	0	0
TES Algorithm	-	-	-	K	-	D/F
Self-consumption (Power) per day	W	311389				
Self-consumption (Energy) per day	Wh	5190				

To calculate the investment return time, it is necessary to consider the initial investment cost and the yearly returns, as shown in Table 6.10. The initial investment costs differ for the 5 presented cases due to the sizing of the BESS and PV-system. The yearly returns contain the cost savings on electricity that would have to be bought if there was no self-consumption. This value is smaller if electricity consumption from the grid was necessary. Additionally, the yearly subsidy for feeding energy into the main grid is added. These yearly returns depend on the country as the subsidy rates and electricity prices differ.

The table shows that the investment return for Germany is the best for case 3 at 6 years. This means that the components are sized for a very high self-consumption rate with as little main grid interaction as possible and optimized self-consumption control methods for BESS, FESS and TESs. It includes medium investment costs and medium investment return rates, which is the best compromise based on the German pricing system. This is a good investment return time as it is smaller than the lifetime of the installed components. The BESS capacity minimization strategy improves the return of invest compared to case 2.

For Estonia, case 1 shows the fastest return of investment at 11.8 years. This is due to the high subsidy rates compared to the electricity prices, where an over-dimensioned system benefits from selling a lot of energy to the main grid. However, the investment return time is quite high as it can be longer than the lifetime of the BESS system, which means additional investments. This will be investigated in more detail in the following subchapter. Independently, it can be observed from the results for case 2 and 3 that using the BESS capacity minimization strategy can improve the return of investment additionally and should therefore be applied to case 1 as well.

Cases 4 and 5 show the worst investment return times for both countries. Thus, the system components should rather be over-dimensioned than too small.

Table 6.10: Financial analysis of a hybrid storage system for a single family house

	Unit	Case 1	Case 2	Case 3	Case 4	Case 5
Investment costs						
Components (BESS, FESS, PV-system, etc.)	EUR	11677	9400	8818	6160	6160
Installation and commissioning	EUR	1000	1000	1000	1000	1000
Sum of investment costs:	EUR	12677	10400	9818	7160	7160
Yearly returns:						
Consumption cost reduction DE	EUR	1563	1563	1563	977	1076
Subsidy DE	EUR	505	77	77	0	0
Yearly sum of returns DE:	EUR	2067	1640	1640	997	1076
Consumption cost reduction EE	EUR	663	663	663	414	457
Subsidy EE	EUR	415	64	64	0	0
Yearly sum of returns EE:	EUR	1078	727	727	414	457
Investment return DE	Years	6.1	6.3	6.0	7.3	6.7
Investment return EE	Years	11.8	14.3	13.5	17.3	15.7

As shown in [33], the investment return time can be reduced by up to 50% depending on the selected components, necessary investment cost and cost reductions for cases with microgrids or complete settlements. This should be investigated in more detail in the future work.

6.2.2 Financial investigation regarding flywheel and TESs

This general financial analysis does not provide enough details about the financially related behaviour of the FESS and each of the TESs separately. To give better recommendations from the financial point of view, the following aspects are investigated and presented additionally:

- Investment return time behaviour with and without FESS
- Financial analysis of the previously mentioned long-term prediction challenges of space heating
- Consumption cost and BESS investment cost behaviour for each TES separately

For the first additional financial analysis, it is assumed that the FESS does not contribute as additional storage or self-consumption device but only supports the lifetime of the BESS. The investment return-calculations with and without additional FESS show the results presented in Figure 6.4 for the Estonian case and for the German case. Based on [33], the BESS has a cyclic lifetime of 4500 cycles according to the datasheet

[168] or 8.3 years with the proposed microgrid operation. After this time, the BESS needs to be replaced. This can be increased using an additional FESS by 19% to 9.9 years, using the calculation method presented in section 5.1. The FESS cyclic lifetime is around 10^5 cycles or more with low maintenance costs, as mentioned in chapter 2. Therefore, the replacement and maintenance costs can be neglected for the FESS for this calculation. TESSs have lifetimes of 10-20 years [164], but this is not considered as the control does not shorten the lifetime and the device would have to be replaced independent of the control system. The used investment return times are based on case 3 for DE and case 1 for EE, as these show the lowest investment return periods. Both cases are recalculated without FESS to obtain the correct investment costs and investment return times.

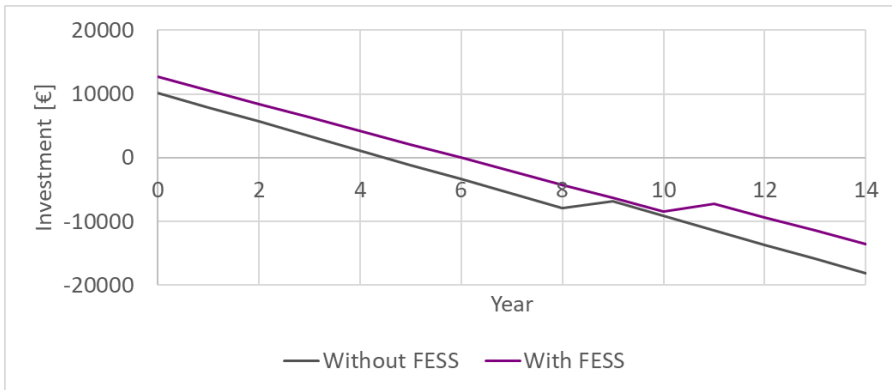


Figure 6.4: Investment return calculations with re-investments for BESS for DE

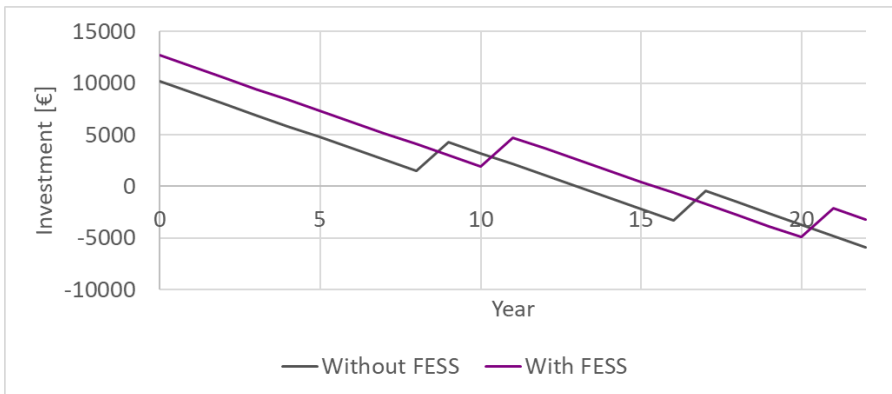


Figure 6.5: Investment return calculations with re-investments for BESS for EE

The figures show that from a purely financial point of view, it does not make sense to include a FESS in the system as the return of investment costs is reached earlier without FESS in both cases for DE and EE. However, in the case of Estonia, the investment curve without the FESS nearly crosses the zero-line again after 17 years. The development of storage system prices could lead to an actual crossing of the zero-line, making a system with a FESS storage more attractive. The additional benefits for increased islanded operation time and short-term storage are not taken into account in this financial investigation.

As mentioned in section 5.4, the behaviour of space heating can be challenging to predict regarding the long-term behaviour. The long-term flexibility results presented in Figure 5.16 show the following:

- The long-term energy consumption for 10 days is at 149 kWh, resulting in costs of approximately 49€ in DE and 21€ in EE.
- With a higher set point as described, these costs can increase for the same timeframe by 12%, respectively decrease by 9%, depending on the chosen time of the changed set point.
- For the same timeframe, changing the set point to a lower one can increase the costs by 9%, respectively decrease them by 3%.

This behaviour strengthens the previously mentioned need for detailed models and predictions of space heating for microgrid simulations for their financially and technically efficient operation planning, which is recommended for accurate investigations in a specific case.

To find out the influence of each of the three investigated common household TESs on the financial investigations, a more detailed analysis of the reduction of consumption costs and BESS investment costs is shown in Table 6.11. Different algorithms and household occupancies are considered for averaging the numbers. It can be seen that the water heater has the biggest share in both cases, followed by space heating with a significantly smaller share. These modelled shares correspond to the shares presented in Figure 2.10 well. The share of the freezer is low. Regarding the consumption cost reductions, the freezer has the highest relative improvement but the impact of space heating and especially the water heater is much higher in the end due to their significantly higher price shares. For the case of the BESS capacity, regarding investment cost reductions, the freezer influence is neglectable while the water heater and space heating show a similarly high average impact. Thus, it can be concluded that the water heater and space heating should be prioritized from a financial point of view as they have a much higher influence on both types of costs.

Table 6.11: Influence on consumption costs and BESS investment for each TES [152], [153], [164]

TES	Share of total price	Average reduction potential for price share	Share of BESS capacity use	Average reduction potential for BESS capacity resp. costs
Freezer	2%	10%	1%	0%
Water heater	54%	7%	63%	20%
Space heating and cooling	15%	7%	9%	20%

As an example, the consumption costs for space heating are investigated in more detail to see the influence of the different price-based algorithms on the example previously shown in section 5.4 and section 6.1. The costs are shown in Table 6.12. In this case, the price shares are slightly below the average shown in Table 6.11. With these exact numbers, the recommendation from the financial point of view is to use algorithm D or F, as indicated in previous chapters. Algorithm E presents less cost reductions but

achieves around 1/3 of cost reductions compared to algorithm D or F. The other algorithms are not desirable from a financial point of view.

Table 6.12: Cumulative costs and cost savings for price-based algorithms A-G for an electric heater [182]

Algorithm	Cumulative Costs [€]	Difference compared to FSP Control
A	8.65	+1.3%
B	8.56	+0.2%
C	8.59	+0.6%
D	7.76	-9.1%
E	8.27	-3.2%
F	7.80	-8.7%
G	8.53	-0.1%
FSP	8.54	---

6.3 Conclusions

Based on the selected, modelled, and validated storage systems, control strategies were developed and simulated in the previous chapters. Based on the results from the control strategies, it could be concluded that the proposed system is technically feasible. Accordingly, it was necessary to evaluate the social acceptance and financial feasibility of the system. The user comfort and privacy as social factors were investigated and different financial analyses were made in this chapter to give recommendations for choice of a control strategy in different scenarios.

Regarding the user comfort, the following conclusions can be made:

- A novel method to evaluate the user comfort for the islanded and the grid-connected operation was developed. The user comfort definitions are based on temperature limits, temperature fluctuations, and security of supply.
- Temperatures of TESs can be directly noticed by the users. In this context, it is most important to investigate space heating as users typically do not notice smaller temperature deviations in frozen food or hot water supply.
- The space heating simulations showed that the algorithms with the highest cost reductions using price-based control, algorithm D and F, show the lowest user comfort levels. These algorithms are recommended from a financial point of view.
- Algorithm E showed moderate cost reductions while maintaining a similar user comfort level as a FSP control and is therefore the recommendation from the user comfort point of view.
- In temporary islanded mode operation, the user comfort is more determined by having electricity at all than by discomfort due to temperature deviations. Therefore, the algorithm with the best performance from the technical point of view should be recommended, which is algorithm H for low budget upgrade projects and algorithm K for all other cases, as mentioned in chapter 5.
- The FESS control strategy providing 3-50% prolonged islanded operation time provides increased user comfort in this regard as well.

Since data collection is becoming more common today, investigations on possible user concerns regarding their private data are more relevant. Therefore, the AMI infrastructure was used as an example to analyse the user concerns.

- The concept of NILM has been investigated regarding the privacy concerns, as this poses the most profound data collection technique. These investigations showed 13 privacy and cyber-security related concerns of users for different surfaces of the AMI and applications of NILM.
- The results were mapped to each other in a table, adding the corresponding GDPR and CIA Triad articles for reference on mitigating the problems from a legal point of view. This developed table should be used as a novel tool to evaluate the users' privacy concerns.
- Based on this tool, the proposed system poses low risk for privacy concerns, as it is implemented on a household level as shown in the simulations, and the used algorithms do not collect and store data about the user.
- If the system is expanded to the building, microgrid or even multi-microgrid level, the data needs to flow through the different levels, as shown in Chapter 2, or if the control algorithms of the proposed system will be optimized with additional data collection for predictions, the tool needs to be used to design the system according to the relevant legal norms.

From a financial point of view, to estimate the average necessary yearly islanded operation time, the SAIDI values for Germany and Estonia are used. Since the interruption times are multiple magnitudes below 1%, there is no need to separately investigate the islanded operation mode financially. Instead, the islanded control strategies are used for maximum self-consumption in the grid-connected mode. Therefore, five different cases were defined to represent different self-consumption and component dimensioning situations:

- Case 1: Over-dimensioning of components with 38% self-consumption
- Case 2: Reduced PV-system size with 80% self-consumption
- Case 3: Reduced PV-system and BESS size with 80% self-consumption
- Case 4: PV-system and BESS are 50% under-dimensioned leading to electricity consumption costs
- Case 5: PV-system and BESS are 50% under-dimensioned with price-based control algorithms for reduced electricity consumption costs

Considering the investment costs and investment returns for a system with all components, the different cases showed the following results:

- For Germany, case 3 shows the fastest investment return of 6 years which is a good overall result as it is well below 10 years. Using the BESS capacity minimizing control strategy for the TESs reduces the investment return time compared to case 2 and should therefore be applied in any case.
- Relatively high subsidy rates lead to the best result with case 1 for Estonia with 11.8 years. Independently, this could be additionally reduced with the BESS capacity minimizing control strategy.
- The result of 11.8 years is too high as this exceeds the lifetime of some components, which leads to re-investments and therefore even longer investment return times. It should be below 10 years.

- Cases 4 and 5 have the slowest return rates. Thus, the components should be rather over-dimensioned than under-dimensioned.

From a purely financial point of view, it is not recommended to use a FESS in the system as the investment return rate is longer for the DE and EE case. Without a FESS, the EE case manages to stay with re-investments below the maximum acceptable investment return time of 15 years. Depending on the development of storage prices, a system with a FESS might lead to a faster investment return in Estonia.

Investigating each TES financially showed the following:

- The space heating model must be very detailed as the previously mentioned prediction challenges can lead to strong undesirable financial differences.
- The freezer has a low influence as a TES from a financial point of view. This is valid for the energy consumption price reduction as well as the BESS investment cost reduction.
- Water heater and space heating have a much higher financial influence as TESs and should therefore be preferred. This is valid for the energy consumption price reduction as well as the BESS investment cost reduction.
- Algorithm D and F show the highest energy consumption price reductions as mentioned previously. The comfort-oriented control algorithm E shows about 1/3 of these cost reductions while the other algorithms are not desirable at all.

As an overview, a decision tree based on these financial investigation conclusions, is shown in Figure 6.6.

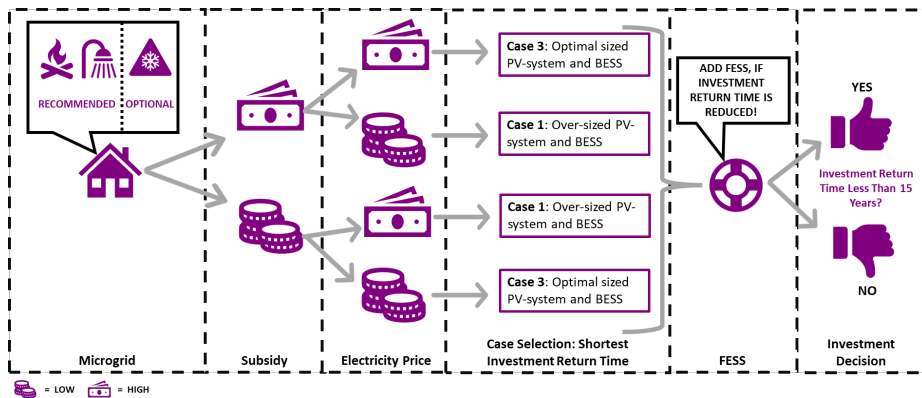


Figure 6.6: Investment-based decision tree

In the following chapter, these conclusions can be used in combination with the findings from the previous chapters, to give comprehensive recommendations to microgrid designers, microgrid and building managers, and homeowners regarding the development of new and existing microgrid systems.

7 Conclusions, recommendations and future work

Based on a state-of-the-art review, a microgrid system topology was proposed to improve the security of supply and financial feasibility for the users. This system consists of a BESS, FESS, and nZEBs with PV-systems and common household TESs. The proposed system with the simulation framework is depicted in Figure 7.1.

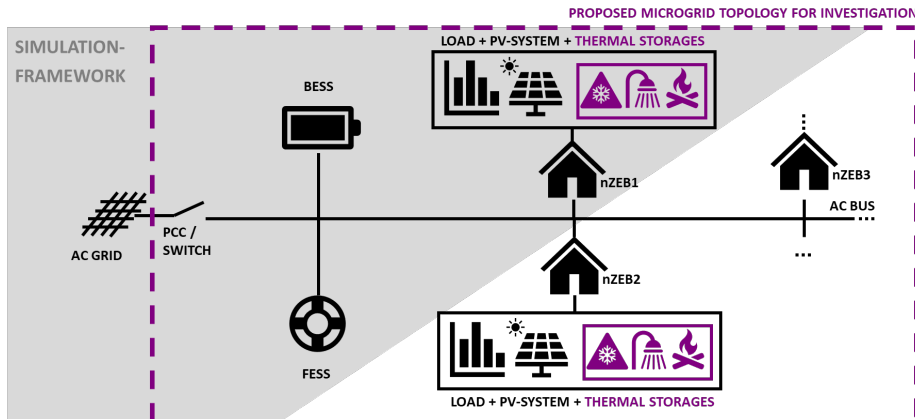


Figure 7.1: Proposed microgrid topology with simulation framework

The thermal and electrical load patterns and the PV-system could be modelled as measured and artificially generated profiles. The BESS, FESS and TESs were modelled as object models. These models were simplified to a reasonable level for microgrid simulations, as e.g., detailed chemical or cell controller research for BESS is out of the scope of this work. For most models, the set mean power error limit of 10%, respectively 12% for complex models, could be achieved during the object model validation. The simplified space heating model could not reach the target and a second modelling methodology was developed for a more accurate NN-based space heating model. The improvements of the different modelling are presented in the next subchapter in more detail.

For these validated models, different control strategies with different aims were developed and simulated. An overview is shown in Table 7.1. For these different control strategies, various control algorithms were researched, developed, and tested with different scenarios. This investigation includes the technical performance as well as a consideration of the user comfort and financial aspects. Relevant conclusions are shown in section 7.2.

The complete technical investigation with social acceptance and financial feasibility analyses was developed to give comprehensive recommendations to microgrid planners, building and dwelling owners. Optimal solutions from each of those three viewpoints and the overall recommendations are presented in section 7.3.

Lastly, recommendations for future work are described in section 7.4.

Table 7.1: Devices used in software simulations with time steps and control aim

Object Models	Δt	Control aim
•FESS	1s	•Power smoothing
•FESS •BESS	1min	•BESS lifetime improvement •Islanded operation duration increase
•Freezer •Water heater •Simplified space heating	5min	•Cost reduction •Minimum BESS capacity reduction
•Freezer •Water heater •Simplified space heating •Different occupancy profiles	5min	•Influence of occupancy
•Simplified space heating •Civil engineering space heating	1min	•Influence of complex space heating models
•NN-based space heating	1min	•Influence of complex space heating models

7.1 Modelling techniques for space heating

Space heating models for buildings are quite complex and time consuming to create. Civil engineers are dedicated to developing detailed thermal models of buildings with a high level of detail and complexity, using their own special software tools. These tools have limited capabilities regarding electrical engineering control strategies. Integrating space heating into electrical microgrid simulations turns into an interdisciplinary challenge, where the most useful modelling technique needs to be determined for the intended application. Three categories of modelling techniques could be identified in literature:

- Complex thermal models with limited electrical and control engineering capabilities from the civil engineering domain
- Complex control strategies with strongly simplified thermal models for the electrical power engineering domain
- Co-simulations with detailed thermal and control models but compatibility problems and computational overhead

As this work is placed in the field of electrical power engineering, the first investigated model was a simplified thermal model that uses linearized approximations for temperature changes. Validating the accuracy of this model showed that the errors introduced by such a simplified model were 3.3% higher than the set error limits for the intended use in a microgrid simulation. However, such a model proved to be quick to calculate, which is useful for repeated control optimization simulations typically used in microgrid simulations. Second, co-simulations with a civil engineering model were investigated. The advantage is good accuracy, however, there are compatibility problems with time step width and communication combined with a high computational burden. Thus, on the other hand, there is a need for a different modelling method that is accurate enough for microgrid simulations, on the other hand, higher compatibility and lower computational power than the existing methods can provide are required.

For the proposed novel ML-based model in this work, the following methodology was developed:

1. A pre-validated civil engineering model is used to create comprehensive data sets that include all necessary information.
2. The data sets are pre-processed to fit the needs for the ML training algorithm.
3. Training parameters are chosen and optimized to avoid over- and underfitting of the model.
4. The NN is trained with the pre-processed data.
5. The obtained NN object can be transformed into a function in Matlab, which can be used as a space heating object model in microgrid simulations.

This methodology could reduce the active modelling and development time and effort for a detailed space heating object in electrical engineering software by around 90% from more than 100 hours to 8 hours. An overview of all three different space heating modelling methods discussed in this work is shown in Figure 7.2.

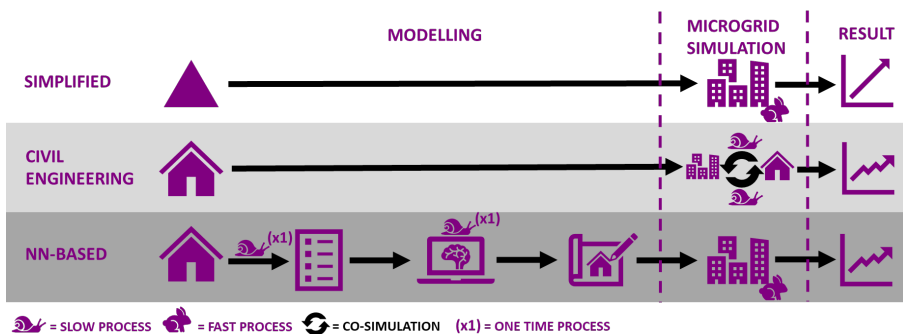


Figure 7.2: Comparison of space heating modelling and simulation

A disadvantage of the NN-based model is that the pre-simulation with the civil engineering model and pre-training of the algorithm are necessary. This is a time-consuming process (c.f. Table 4.14). However, the pre-simulation and pre-training are only necessary once. Since there are typically multiple runs for microgrid simulations for control optimization purposes, these one-time pre-calculations have a much lower weight than the repeated high computation effort for every run of a co-simulation. Further, the NN-based model cannot be more accurate than the civil engineering model it is based on.

As an advantage, the NN-based model can be calculated as fast as the simplified model during microgrid simulation and 85% faster compared to a very slow co-simulation (c.f. Table 4.14). Simultaneously, the model shows a more than 5% higher accuracy than the simplified model (c.f. Table 4.10).

Thus, comparisons show that the proposed NN-based model is the best compromise of accuracy, calculation speed and compatibility. It achieves an error of less than 12%, which was the set goal accuracy for such a complex model. Simulations with the simplified and more detailed space heating model showed that the model accuracy can have an influence on the control algorithm results. This is due to the high complexity of building thermal dynamics where small changes can show their influences later. This strengthens the necessity for the more accurate and quickly calculated NN-based space heating model further.

7.2 Control algorithm selection in different scenarios

The developed and validated models for the proposed system were simulated with different control strategies for different scenarios. These scenarios have been investigated from a technical, social, and financial point of view. The conclusions from the respective chapters are connected and summarized in the following.

The occupancy of a dwelling can change due to, for example, a landlord renting out an apartment to a different demographic group. The investigation showed that even with different occupancies, there are specific algorithms for the TESs that seem to be generally working better in all cases. For a price-based control situation, algorithms D and F are providing the best cost reductions. However, if the user comfort is the main priority, then algorithm E is the preferred solution for space heating, as it keeps the room temperature within more comfortable limits. In the islanded control scenario, which is also valid as a maximum self-consumption scenario in the grid-connected mode, the PV-power based algorithms could not be recommended in general as they did not show good results with households where the PV-system was not over-sized. However, from the SOC-based control algorithms, algorithm K can be recommended for all households, especially if it is implemented in a new microgrid, where some communication infrastructure can be added in the design stage. For existing microgrids, algorithm H without communication needs is better suitable from an investment point of view. This is valid for all TESs. Connecting these findings leads to the following decision tree (c.f. Figure 7.3), which can be used for recommendations.

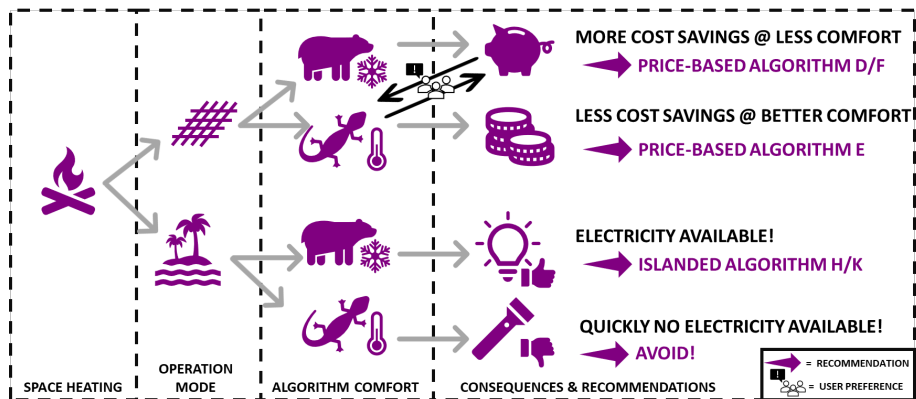


Figure 7.3: User comfort-based decision tree for TES control algorithms

7.3 Recommendations for microgrid designers, building and dwelling owners

To give suitable recommendations to microgrid designers, building and dwelling owners, it is necessary to analyse all the conclusions from the technical, social, and financial investigations. Based on this, it is possible to draw overall conclusions and formulate recommendations. For a better overview and understanding, the recommended decisions are visualized using a decision tree. This complete decision tree for the selection of the components and control strategies is shown in Figure 7.4. As mentioned, this decision tree is based on the conclusions and recommendations developed on the proposed system in this work. The recommendations can be transferred to design or

upgrade a microgrid, a smart building or a dwelling. Some additional remarks regarding the three main branches of the decision tree are the following:

- The BESS and PV-system sizing is based on the financial conclusions presented in Figure 6.6. As shown in section 5.4, the occupancy of an apartment influences the sizing of components as well because the islanded control algorithms for TEs work more effectively with an over-sized PV-system. This means an additional benefit for case 1.
- With the TEs, it is required to determine whether a new microgrid is designed or an existing one is upgraded to select an islanded control strategy. Algorithm K shows better performance but needs some communication with the BESS, while algorithm H does not need additional communication, thus no additional investment.
- Adding a FESS to the system as proposed will improve the user comfort in the islanded mode additionally, as the islanded operation time is improved by 3-50%. This can be of additional financial interest in microgrids where the power supply must never be interrupted.

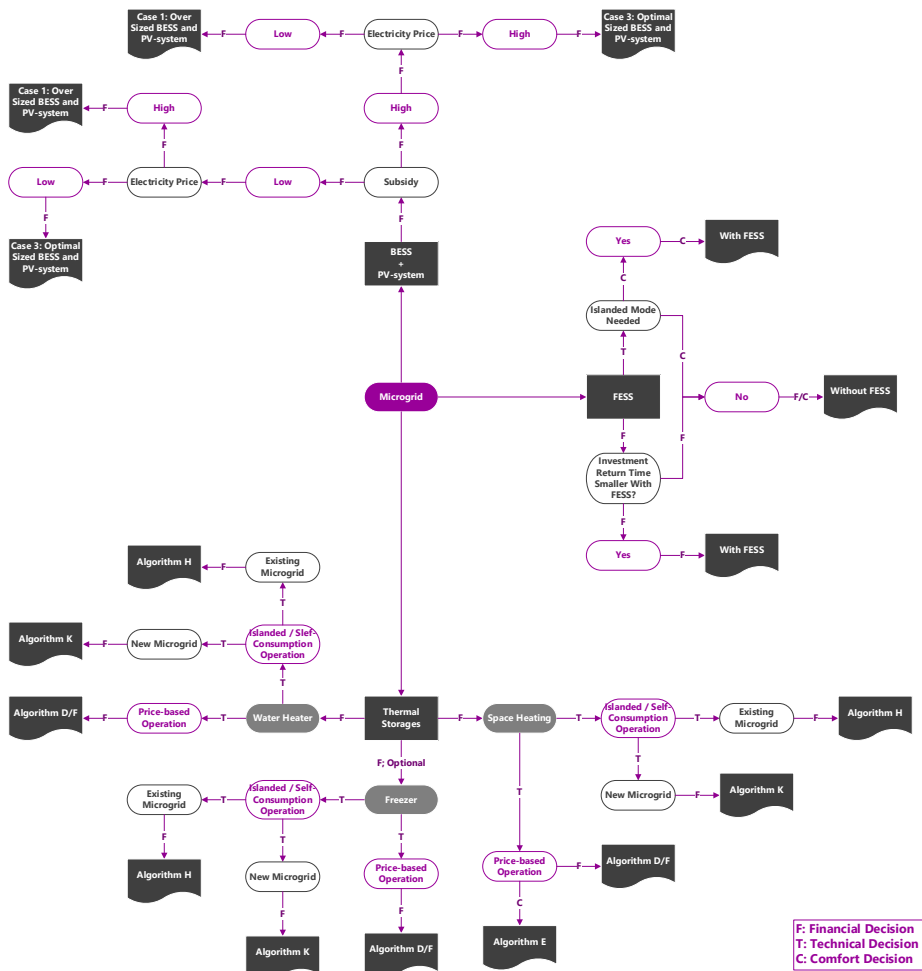


Figure 7.4: Complete decision tree based on technical, financial and comfort decisions

For further development of this decision tree and applying the findings to extended systems, it is recommended to assess first the legal dimension with the provided tool (c.f. Table 6.6). Figure 7.5 shows the recommended approach in a simplified way:

- If data driven control strategies are implemented in the system, the legal norms should be assessed based on the provided tool.
- If the proposed system is extended to the building, microgrid or smart city level, the legal norms should be assessed based on the provided tool as well.

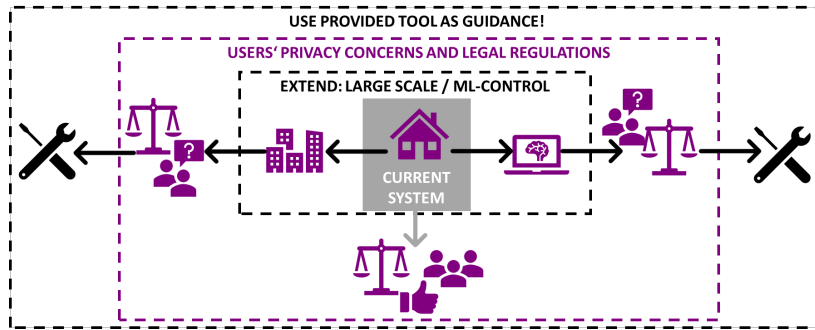


Figure 7.5: User privacy tool use cases

7.4 Future work

To improve the developed models, control strategies and system topology, the following aspects can be researched and developed further:

- In addition to the FESS or as an alternative for the FESS, supercapacitors could be investigated to optimize the proposed system technically or financially further.
- The developed PHIL-setup should be extended with additional components, as intended in the initial design. This work has already been started by a student under the author's supervision.
- The NN-based space heating model should be developed further with different machine learning techniques to improve the accuracy. In addition, models for different kinds of buildings, including larger residential buildings, commercial buildings, etc., should be tested.
- As the control strategies for the TESs and FESS are traditional and simple approaches, they could be improved with reinforcement learning based control, especially for the design in new microgrids with more communication and data analysis possibilities.
- The financial analysis can be calculated for more countries to provide better country specific recommendations.
- The financial benefits for different specific critical system examples that must not be interrupted could be calculated to give more specific recommendations on the financial benefit of the extended islanded operation time.
- The proposed system is investigated and modelled for the size of a single family house. It should be extended to multi-household buildings, microgrids or even smart cities to include aggregation challenges and influences. This includes technical, social, and financial investigations.

List of figures

Figure 1.1: General content of this thesis	14
Figure 2.1: General microgrid topology	19
Figure 2.2: AC microgrid topology	19
Figure 2.3: DC microgrid topology	20
Figure 2.4: Hybrid microgrid topology	20
Figure 2.5: Microgrid power sources [33]	21
Figure 2.6: Schematic of the grid-connected (A) and the islanded (B) operation mode for a microgrid	23
Figure 2.7: Basic schematic of primary, secondary and tertiary control reserve [40]	25
Figure 2.8: Overview of energy storage systems [33]	30
Figure 2.9: Schematic of a FESS [64], [69]	32
Figure 2.10: Share of household loads; purple: TESs; grey: other [82]	34
Figure 2.11: Load forecast for the Estonian grid [118]	37
Figure 2.12: Training and use of ML-based object model	38
Figure 2.13: Typical reinforcement learning based control	38
Figure 2.14: Machine learning based coordination methods	39
Figure 2.15: PHIL example schematic [64]	41
Figure 2.16: Topology of the proposed microgrid system for investigation	43
Figure 3.1: Example day from the measured PV-system profile in Estonia	44
Figure 3.2: Example day from the measured PV-system profile in southern Germany..	45
Figure 3.3: Example segment of the measured NRG-Building load profile	46
Figure 3.4: Measured total energy, food and hot water consumption	47
Figure 3.5: Example day from a single family house load profile	48
Figure 3.6: Electric energy consumption in households i-viii for 1 week [152], [153]	49
Figure 3.7: Schematic of flywheel storage system model control [154], [159]	50
Figure 3.8: Flywheel current control block [154], [159]	50
Figure 3.9: Flywheel DC-voltage control block [154], [159]	51
Figure 3.10: Flywheel field-oriented control block [154], [159]	52
Figure 3.11: Battery capacity retention at different temperatures	53
Figure 3.12: Methodology overview of the neural network-based space heating model .	57
Figure 3.13: 3D view of used IDA-ICE building models; left: simple room; centre: control centre; right: single family house	57
Figure 3.14: Air temperature behaviour of the IDA-ICE model compared to the measurements [182]	58
Figure 3.15: Floor plan of the single family house with area sizes; doors: blue; windows: light grey	59
Figure 3.16: Overview of the neural network training process	60
Figure 3.17: Evaluation of performance: Overfitted model [194]	63
Figure 3.18: Visualization of neural network model used for each room of the single family house	64
Figure 4.1: Schematic of the modernized flywheel validation setup [64]	67
Figure 4.2: Flywheel storage repeatability profile [64]	68
Figure 4.3: Flywheel storage round trip efficiency test	69
Figure 4.4: Mean air temperature comparison between civil engineering simulation and test simulation for single family house bedroom model in the test simulation with zoom-in [175]	76

Figure 4.5: Power data comparison between civil engineering simulation and test simulation for single family house bedroom model (Calculated power data is shown in the negative y-direction) with zoom-in [175]	76
Figure 4.6: Model validation of neural network and IDA ICE control centre models with measured data	77
Figure 5.1: Simulation topology for islanded BESS and FESS investigation.....	83
Figure 5.2: Schematic of FESS moving average control [154]	83
Figure 5.3: Main grid to microgrid power supply with and without power smoothing, FESS power and FESS rotational speed [154]	84
Figure 5.4: Load smoothing with FESS PHIL-setup moving average control with the test profile [64]	84
Figure 5.5: Detailed load smoothing with FESS PHIL-setup moving average control with the FESS power graph [64].....	85
Figure 5.6: Impulse response for moving average and Butterworth filters [64].....	85
Figure 5.7: Power slope gradient for moving average and Butterworth filters with the test load profile [64].....	86
Figure 5.8: High PV-system production control strategy for FESS	86
Figure 5.9: BESS SOC of an islanded microgrid system with and without supporting FESS for power smoothing; (A) Increase of islanded operation time with special case; (B) Increase of islanded operation time with typical cases [33], [24]	87
Figure 5.10: Flywheel and battery storage control with PHIL setup for exceeding the PV-power scenario [25]	89
Figure 5.11: Simulation topology for grid-connected TES investigation	89
Figure 5.12: Price-based control algorithm visualization: Example with the water heater [30].....	91
Figure 5.13: Simulation topologies for investigation of space heating model complexity with the simplified (A) and civil engineering (B) models	92
Figure 5.14: Simulation topology for investigations of space heating model behaviour	94
Figure 5.15: Intra-interval flexibility for 240 h on an hourly basis [80].....	94
Figure 5.16: Long-term flexibility for 240 h on an hourly basis [80]	95
Figure 5.17: Simulation topology for islanded TES investigation.....	95
Figure 5.18: PV-power-based control algorithm visualization: Example with the water heater [29]	97
Figure 5.19: SOC-based control algorithm visualization: Example with the water heater [29].....	98
Figure 5.20: Simulation topologies for investigations of dwelling occupancy influence on price-based (A) and islanded (B) control algorithm performance	101
Figure 5.21: Electricity cost differences for algorithms A-G in households i-viii in percent compared to FSP control.....	101
Figure 5.22: Battery capacity differences for islanded algorithms A-G in households i-viii in percent compared to FSP control [29]	103
Figure 5.23: Battery capacity differences for islanded algorithms H-K in households i-viii in percent compared to FSP control [29].....	104
Figure 6.1: Indoor air temperature results for price-based set point calculation algorithms A-G and a fixed set point for the civil engineering space heating model [57]	107
Figure 6.2: Common AMI configuration, based on [53].....	110
Figure 6.3: Flowchart for the use of the provided tool.....	112
Figure 6.4: Investment return calculations with re-investments for BESS for DE.....	119

Figure 6.5: Investment return calculations with re-investments for BESS for EE	119
Figure 6.6: Investment-based decision tree.....	123
Figure 7.1: Proposed microgrid topology with simulation framework	124
Figure 7.2: Comparison of space heating modelling and simulation	126
Figure 7.3: User comfort-based decision tree for TES control algorithms.....	127
Figure 7.4: Complete decision tree based on technical, financial and comfort decisions .	128
Figure 7.5: User privacy tool use cases	129

List of tables

Table 2.1: Advantages and disadvantages of different microgrid topologies [28], [27], [33]..	22
Table 2.2: TSOs and DSOs in Germany and Estonia	24
Table 2.3: Surfaces for intrusion and cyber-attacks of the AMI [53]	26
Table 2.4: Comparison of renewable energy source characteristics [36], [60].....	29
Table 2.5: Comparison of energy storage technologies [64]	30
Table 2.6: NILM process stages [132], [53]	40
Table 3.1: Overview of load profiles with relevant parameters [148], [151], [152], [153], [154]	46
Table 3.2: Description of generated occupancy profiles with average electrical energy consumption per day [152], [153]	48
Table 3.3: Occupancy profile selection criteria with typical shares [152], [153]	48
Table 3.4: FESS parameters [159]	49
Table 3.5: Self-discharge per month for different temperatures and SOCs [165]	52
Table 3.6: Modelling variables for simplified space heating of an apartment.....	56
Table 3.7: Variables for the neural network training dataset of a single family house [175]..	60
Table 3.8: Error metric limits, optima, mapping factors and weighting factors [194]	62
Table 3.9: Results for different numbers of neurons per layer [194]	63
Table 3.10: Neural network model sizes for different space heating models	64
Table 3.11: Comparison of optimized parameters to wrongly chosen parameters: mean total error values for multiple trainings.....	65
Table 4.1: Results of flywheel storage repeatability [64].....	68
Table 4.2: Efficiency errors of flywheel storage round trip.....	69
Table 4.3: Design of experiment: 2 ² factorial design for freezer verification	70
Table 4.4: Results for experiments E1-E4	71
Table 4.5: Sum of squares for freezer parameters.....	71
Table 4.6: Design of experiment: 2 ² factorial design for water heater verification.....	72
Table 4.7: Sum of squares for freezer parameters.....	73
Table 4.8: Environmental and model parameters for simplified space heating model validation against civil engineering simulation	74
Table 4.9: Environmental and model parameters for simplified space heating model validation against measurements.....	74
Table 4.10: Comparison of error and accuracy metrics between the neural network-based models and the civil engineering models [175]	75
Table 4.11: Error comparison between measurement and control centre models.....	77
Table 4.12: Error comparison between NN-based models and civil engineering models .	78
Table 4.13: Overview of all object model errors.....	80
Table 4.14: Overview of advantages and disadvantages for different space heating models in microgrid simulations [175].....	81
Table 5.1: BESS cyclic lifetime estimation and maximum islanded operation time for microgrid system with and without FESS power smoothing [33], [24].....	88
Table 5.2: Price-based control algorithm description; Cooling = Freezer; Heating = Water heater and space heating [10], [85], [84].....	90
Table 5.3: Cost reductions for price-based control algorithms compared to FSP control [38]	92
Table 5.4: Comparison of cost savings of the civil engineering and the simplified space heating model for the price-based algorithms A-G [57]	93

Table 5.5: PV-power-based control algorithm description; Cooling = Freezer; Heating = Water heater and space heating [28]	96
Table 5.6: SOC-based control algorithm description; Cooling = Freezer; Heating = Water heater and space heating [28]	98
Table 5.7: Minimum BESS capacity for PV-power-based control algorithms compared to FSP control [38]	99
Table 5.8: Minimum BESS capacity for SOC-based control algorithms compared to FSP control [38]	100
Table 5.9: Qualitative cost savings classification with description for goal set point operation for price-based algorithms A-G [30]	102
Table 5.10: Minimum battery storage capacities for households i-viii with a fixed set point control [29]	102
Table 6.1: Cost savings and user comfort classification for price-based algorithms A-G...	107
Table 6.2: User comfort classification for islanded control strategies.....	108
Table 6.3: Relative cost savings with different user comfort scaling factors; $C_{user} = 2$: more aggressive scaling; $C_{user} = 0.5$: less aggressive scaling	109
Table 6.4: Residential user concerns regarding the AMI and ML algorithms [53], [47], [51], [49], [81], [82], [83], [84], [45], [85]	111
Table 6.5: Overview of training data sets with literature examples [CSW]	111
Table 6.6: Mapping of ML angles via prosumer concerns based on relevance: Technical and legal views [53].....	113
Table 6.7: Disturbance metrics for DE and EE for 2020 [226], [227].....	114
Table 6.8: Considered aspects for financial analysis of a hybrid storage system for a typical single family house	115
Table 6.9: Changed aspects for self-consumption cases for financial analysis	117
Table 6.10: Financial analysis of a hybrid storage system for a single family house	118
Table 6.11: Influence on consumption costs and BESS investment for each TES [152], [153], [164].....	120
Table 6.12: Cumulative costs and cost savings for price-based algorithms A-G for an electric heater [182].....	121
Table 7.1: Devices used in software simulations with time steps and control aim	125

References

- [1] V. Masson-Delmotte *et al.*, "Climate Change 2021: The Physical Science Basis. Contribution of Working Group I to the Sixth Assessment Report of the Intergovernmental Panel on Climate Change," 2021.
- [2] United Nations, "Paris Agreement," 2016.
- [3] European Union, "Communication From The Commission To The European Parliament, The European Council, The Council, The European Economic And Social Committee And The Committee Of The Regions - The European Green Deal."
- [4] European Union, "Directive Of The European Parliament And Of The Council - amending Directive (EU) 2018/2001 of the European Parliament and of the Council, Regulation (EU) 2018/1999 of the European Parliament and of the Council and Directive 98/70/EC of the European Parliament and of the Council as regards the promotion of energy from renewable sources, and repealing Council Directive (EU) 2015/652."
- [5] "NetZeroCities - Energy Cities." <https://energy-cities.eu/project/netzerocities/> (accessed Dec. 27, 2021).
- [6] "Decarb City Pipes 2050 - Energy Cities." <https://energy-cities.eu/project/decarb-city-pipes-2050/> (accessed Dec. 27, 2021).
- [7] "FinEst Twins | FinEst Centre." <https://www.finestcentre.eu/finesttwins> (accessed Dec. 27, 2021).
- [8] European Union, "Directive 2010/31/EU of the European Parliament and of the Council of 19 May 2010 on the energy performance of buildings."
- [9] S. H. Rouhani, R. Ahmadihangar, T. Haring, and A. Rosin, "Improving Dynamic Stability of deregulated power system," Nov. 2020. doi: 10.1109/RTUCON51174.2020.9316618.
- [10] A. Rosin, S. Link, M. Lehtla, J. Martins, I. Drovtar, and I. Roasto, "Performance and feasibility analysis of electricity price based control models for thermal storages in households," *Sustainable Cities and Society*, vol. 32, pp. 366–374, Jul. 2017, doi: 10.1016/j.scs.2017.04.008.
- [11] North American Electric Reliability Corporation, "Accommodating High Levels of Variable Generation," *North American Electric Reliability Corporation (NERC)*, no. April, p. 104, 2009, [Online]. Available: https://docs.wind-watch.org/NERC-accommodating-variable-generation_17Nov08.pdf
- [12] M. H. Roos, P. H. Nguyen, J. Morren, and J. G. Slootweg, "Aggregation of component-based grid-feeding DER and load models for simulation of microgrid islanding transients," *Electric Power Systems Research*, vol. 189, p. 106759, Dec. 2020, doi: 10.1016/J.EPSR.2020.106759.
- [13] E. Imaie, A. Sheikholeslami, and R. A. Ahangar, "Improving Short-Term Wind Power Prediction with Neural Network and ICA Algorithm and Input Feature Selection," *Journal of Advances in Computer Research*, vol. 5, no. 3, pp. 13–34, 2014.
- [14] R. Ahmadihangar *et al.*, "Flexibility investigation of price-responsive batteries in the microgrids cluster," in *Proceedings - 2020 IEEE 14th International Conference on Compatibility, Power Electronics and Power Engineering, CPE-POWERENG 2020*, Jul. 2020, pp. 456–461. doi: 10.1109/CPE-POWERENG48600.2020.9161667.

- [15] M. B. Sanjareh, M. H. Nazari, G. B. Gharehpetian, R. Ahmadihangar, and A. Rosin, "Optimal scheduling of HVACs in islanded residential microgrids to reduce BESS size considering effect of discharge duration on voltage and capacity of battery cells," *Sustainable Energy, Grids and Networks*, vol. 25, p. 100424, Mar. 2021, doi: 10.1016/J.SEGAN.2020.100424.
- [16] "Traditional vs Modern Approaches to Product Development." <https://www.designrule.co.uk/traditional-vs-modern> (accessed Dec. 27, 2021).
- [17] A. Mosavi, M. Salimi, S. Faizollahzadeh Ardabili, T. Rabczuk, S. Shamshirband, and A. Varkonyi-Koczy, "State of the Art of Machine Learning Models in Energy Systems, a Systematic Review," *Energies (Basel)*, vol. 12, no. 7, p. 1301, Apr. 2019, doi: 10.3390/en12071301.
- [18] R. AhmadiAhangar, A. Rosin, A. N. Niaki, I. Palu, and T. Korötko, "A review on real-time simulation and analysis methods of microgrids," *International Transactions on Electrical Energy Systems*, vol. 29, no. 11, Nov. 2019, doi: 10.1002/2050-7038.12106.
- [19] F. Puschmann, "Sicheres Testen durch Power-Hardware-in-the-Loop-Systeme," *ATZelextronik 2021 16:7*, vol. 16, no. 7, pp. 52–55, Jul. 2021, doi: 10.1007/S35658-021-0645-4.
- [20] M. H. Chen, H. Y. Wang, and M. C. Wang, "Knowledge sharing, social capital, and financial performance: the perspectives of innovation strategy in technological clusters," <https://doi.org/10.1080/14778238.2017.1415119>, vol. 16, no. 1, pp. 89–104, Jan. 2018, doi: 10.1080/14778238.2017.1415119.
- [21] F. Almeshqab and T. S. Ustun, "Lessons learned from rural electrification initiatives in developing countries: Insights for technical, social, financial and public policy aspects," *Renewable and Sustainable Energy Reviews*, vol. 102, pp. 35–53, Mar. 2019, doi: 10.1016/J.RSER.2018.11.035.
- [22] B. M. Buchholz and Z. Styczynski, "Smart grids - Fundamentals and technologies in electricity networks," *Smart Grids - Fundamentals and Technologies in Electricity Networks*, vol. 9783642451201, pp. 1–396, Mar. 2014, doi: 10.1007/978-3-642-45120-1.
- [23] "Here's What Caused the Texas Electricity Blackout | IE." <https://interestingengineering.com/what-caused-the-texas-electricity-blackout> (accessed Dec. 21, 2021).
- [24] "The Day Europe's Power Grid Came Close to a Massive Blackout - Bloomberg." <https://www.bloomberg.com/news/articles/2021-01-27/green-shift-brings-blackout-risk-to-world-s-biggest-power-grid> (accessed Dec. 21, 2021).
- [25] A. Ali, W. Li, R. Hussain, X. He, B. W. Williams, and A. H. Memon, "Overview of Current Microgrid Policies, Incentives and Barriers in the European Union, United States and China," *Sustainability 2017, Vol. 9, Page 1146*, vol. 9, no. 7, p. 1146, Jun. 2017, doi: 10.3390/SU9071146.
- [26] D. T. Ton and M. A. Smith, "The U.S. Department of Energy's Microgrid Initiative," *The Electricity Journal*, vol. 25, no. 8, pp. 84–94, Oct. 2012, doi: 10.1016/J.TEJ.2012.09.013.
- [27] P. Ray and M. Biswal, "Microgrid: Operation, Control, Monitoring and Protection," vol. 625, 2020, doi: 10.1007/978-981-15-1781-5.

- [28] T. Funabashi, "Integration of Distributed Energy Resources in Power Systems: Implementation, Operation and Control," *Integration of Distributed Energy Resources in Power Systems: Implementation, Operation and Control*, pp. 1–309, Mar. 2016, doi: 10.1016/C2014-0-03911-1.
- [29] I. Roasto, O. Husev, M. Najafzadeh, T. Jalakas, and J. Rodriguez, "Voltage source operation of the energy-router based on model predictive control," *Energies (Basel)*, vol. 12, no. 10, 2019, doi: 10.3390/EN12101892.
- [30] E. Unamuno and J. A. Barrena, "Hybrid ac/dc microgrids—Part I: Review and classification of topologies," *Renewable and Sustainable Energy Reviews*, vol. 52, no. C, pp. 1251–1259, Aug. 2015, doi: 10.1016/J.RSER.2015.07.194.
- [31] Siemens AG, "Warum Microgrids die Zukunft des Energie- managements sind."
- [32] A. Choulot, "Hydropower: Small hydro & hidden hydro - Overview of Switzerland situation (and abroad)," 2021.
- [33] N. Cinay, "Energiasalvestite juhtimisstrateegiate uurimine ja arendamine saartalitluses mikrovõrgule," M.Sc.Eng. Thesis, Supervision: T. Häring and H.Biechl, Tallinn, 2020.
- [34] International Energy Agency, *Harnessing Variable Renewables - A Guide to the Balancing Challenge*. OECD/IEA, 2011. Accessed: Mar. 26, 2020. [Online]. Available: www.iea.org/about/copyright.asp
- [35] "On-Grid und Off-Grid Photovoltaik." <https://www.photovoltaiik.org/wissen/on-grid-und-off-grid> (accessed Dec. 21, 2021).
- [36] Asian Development Bank, "Handbook on Microgrids for Power Quality and Connectivity," Aug. 2020, doi: 10.22617/TIM200182-2.
- [37] R. Sabzehgar, "Overview of Technical Challenges, Available Technologies and Ongoing Developments of AC/DC Microgrids," *Development and Integration of Microgrids*, Aug. 2017, doi: 10.5772/INTECHOPEN.69400.
- [38] T. Wu, G. Bao, Y. Chen, and J. Shang, "A review for control strategies in microgrid," *Chinese Control Conference, CCC*, vol. 2018-July, pp. 30–35, Oct. 2018, doi: 10.23919/CHICC.2018.8482549.
- [39] Y. Zahraoui *et al.*, "Energy Management System in Microgrids: A Comprehensive Review," *Sustainability 2021, Vol. 13, Page 10492*, vol. 13, no. 19, p. 10492, Sep. 2021, doi: 10.3390/SU131910492.
- [40] D. R. Graeber, "Handel mit Strom aus erneuerbaren Energien," 2014, doi: 10.1007/978-3-658-05941-5.
- [41] "Electricity market | Ministry of Economic Affairs and Communications." <https://www.mkm.ee/en/objectives-activities/energy-sector/electricity-market> (accessed Dec. 23, 2021).
- [42] T. Häring, "Netzstabilisierung durch Laufwasserkraftwerke," B.Eng. Thesis, Supervision: M. König and F. Fischer, Kempten (Allgäu), 2016.
- [43] Bundesministerium der Justiz und für Verbraucherschutz, "EnWG - Gesetz über die Elektrizitäts- und Gasversorgung." https://www.gesetze-im-internet.de/enwg_2005/BJNR197010005.html (accessed Dec. 23, 2021).
- [44] F. Al-Turjman and M. Abujubbeh, "IoT-enabled smart grid via SM: An overview," *Future Generation Computer Systems*, vol. 96, pp. 579–590, Jul. 2019, doi: 10.1016/j.future.2019.02.012.
- [45] M. Wigan, "User issues for smart meter technology," *IEEE Technology and Society Magazine*, vol. 33, no. 1, pp. 49–53, Mar. 2014, doi: 10.1109/MTS.2014.2301856.

- [46] D. L. S. Mendes, R. A. L. Rabelo, A. F. S. Veloso, J. J. P. C. Rodrigues, and J. v. dos Reis Junior, "An adaptive data compression mechanism for smart meters considering a demand side management scenario," *Journal of Cleaner Production*, vol. 255, May 2020, doi: 10.1016/j.jclepro.2020.120190.
- [47] J. E. Rubio, C. Alcaraz, and J. Lopez, "Recommender system for privacy-preserving solutions in smart metering," *Pervasive and Mobile Computing*, vol. 41, pp. 205–218, Oct. 2017, doi: 10.1016/j.pmcj.2017.03.008.
- [48] L. Wei, L. P. Rondon, A. Moghadasi, and A. I. Sarwat, "Review of Cyber-Physical Attacks and Counter Defense Mechanisms for Advanced Metering Infrastructure in Smart Grid," *Proceedings of the IEEE Power Engineering Society Transmission and Distribution Conference*, vol. 2018-April, May 2018, Accessed: Apr. 22, 2020. [Online]. Available: <http://arxiv.org/abs/1805.07422>
- [49] CEN-CENELEC-ETSI, "Functional architecture for communications in smart metering systems," pp. 1–70, 2011, [Online]. Available: ftp://ftp.cen.eu/cen/Sectors/List/Measurement/Smartmeters/CENCLCETSI_TR5_0572.pdf
- [50] D. Jacobson and L. Dickerman, "Distributed intelligence: A critical piece of the microgrid puzzle," *Electricity Journal*, vol. 32, no. 5, pp. 10–13, Jun. 2019, doi: 10.1016/j.tej.2019.05.001.
- [51] S. Tonyali, K. Akkaya, N. Saputro, A. S. Uluagac, and M. Nojournian, "Privacy-preserving protocols for secure and reliable data aggregation in IoT-enabled Smart Metering systems," *Future Generation Computer Systems*, vol. 78, pp. 547–557, Jan. 2018, doi: 10.1016/j.future.2017.04.031.
- [52] J. Foreman and D. Gurugubelli, "Cyber Attack Surface Analysis of Advanced Metering Infrastructure," 2016.
- [53] A. Antonov, T. Häring, T. Korötko, A. Rosin, T. Kerikmäe, and H. Biechl, "Pitfalls of Machine Learning Methods in Smart Grids: A Legal Perspective," *2021 International Symposium on Computer Science and Intelligent Controls (ISCSIC)*, pp. 248–256, 2021, doi: 10.1109/ISCSIC54682.2021.00053.
- [54] European Commission, "Study on "Residential Prosumers in the European Energy Union"," 2017.
- [55] C. Ochsenbein, "First Around The World By Solar Energy," 2021.
- [56] T. Schott, U. Muntwyler, and E. Schüpbach, "Long-term Measurements of PV Installations," 2021.
- [57] G. Favaro, "PhD Summer School Mont Soleil 2021: Wind Turbine Design and Repowering - Technological development in the JUVENT wind farm 1996-2019," 2021.
- [58] M. Pfisterer, "Wind energy in practice – Partnership or legal proceedings," 2021.
- [59] S. Koller, "Wind Assessment in Complex Terrain - PhD summer school Mont-Soleil," 2021.
- [60] J. Lepik, "Power Hardware-In-The-Loop Setup For Research And Development Of Islanded Microgrid Control Scenarios," M.Sc.Eng. Thesis, Supervision: T. Häring and A. Rosin, Tallinn, 2022.
- [61] M. Sterner and I. Stadler, "Handbook of Energy Storage," *Handbook of Energy Storage*, 2019, doi: 10.1007/978-3-662-55504-0.
- [62] N. W. A. Lidula and A. D. Rajapakse, "Microgrids research: A review of experimental microgrids and test systems," *Renewable and Sustainable Energy Reviews*, vol. 15, no. 1, pp. 186–202, Jan. 2011, doi: 10.1016/J.RSER.2010.09.041.

- [63] A. M. R. Lede, M. G. Molina, M. Martinez, and P. E. Mercado, "Microgrid architectures for distributed generation: A brief review," *2017 IEEE PES Innovative Smart Grid Technologies Conference - Latin America, ISGT Latin America 2017*, vol. 2017-January, pp. 1–6, Dec. 2017, doi: 10.1109/ISGT-LA.2017.8126746.
- [64] L. Link, "Reaalajasimulaatori rakenduse väljatöötamine hooratas-energiasalvesti juhtimisstsenaariumite uurimiseks," M.Sc.Eng. Thesis, Supervision: T. Häring and H. Biechl, Tallinn, 2022.
- [65] sonnen GmbH, "Technische Daten sonnenBatterie 10." <https://www.sparemitsolar.de/upload/41243371-sonnenBatterie-10-Datenblatt.pdf> (accessed Dec. 22, 2021).
- [66] LG Electronics, "LG Energiespeichersysteme." https://www.tritec.ch/pdf/produkte/LG_ESS-Home-8-10_D_de.pdf (accessed Dec. 22, 2021).
- [67] "Battery Test Methods - Battery University." <https://batteryuniversity.com/article/battery-test-methods> (accessed Dec. 22, 2021).
- [68] "How to make Batteries more Reliable and Longer Lasting - Battery University." <https://batteryuniversity.com/article/how-to-make-batteries-more-reliable-and-longer-lasting> (accessed Dec. 22, 2021).
- [69] Rosseta Technik GmbH, "Flywheel storage system T3-15 - Technical documentation."
- [70] GE Power Conversion, "Rotating Stabilisers: CO2 free, high-inertia machines to help stabilise weak grids and enable higher penetration of renewable energy".
- [71] M. E. Amiryar and K. R. Pullen, "A Review of Flywheel Energy Storage System Technologies and Their Applications," *Applied Sciences 2017, Vol. 7, Page 286*, vol. 7, no. 3, p. 286, Mar. 2017, doi: 10.3390/APP7030286.
- [72] A. A. K. Arani, H. Karami, G. B. Gharehpetian, and M. S. A. Hejazi, "Review of Flywheel Energy Storage Systems structures and applications in power systems and microgrids," *Renewable and Sustainable Energy Reviews*, vol. 69, pp. 9–18, Mar. 2017, doi: 10.1016/J.RSER.2016.11.166.
- [73] STORNETIC, "Powerful Storage System for Grid Services," 2018.
- [74] B. Bolund, H. Bernhoff, and M. Leijon, "Flywheel energy and power storage systems," *Renewable and Sustainable Energy Reviews*, vol. 11, no. 2, pp. 235–258, Feb. 2007, doi: 10.1016/J.RSER.2005.01.004.
- [75] B. Zohuri, "Energy Storage Technologies and Their Role in Renewable Integration," *Hybrid Energy Systems*, pp. 213–255, 2018, doi: 10.1007/978-3-319-70721-1_8.
- [76] M. Hedlund, J. Lundin, J. de Santiago, J. Abrahamsson, and H. Bernhoff, "Flywheel Energy Storage for Automotive Applications," *Energies 2015, Vol. 8, Pages 10636-10663*, vol. 8, no. 10, pp. 10636–10663, Sep. 2015, doi: 10.3390/EN81010636.
- [77] "Siemens Energy's grid stabilizer technology to help Irish grid exceed renewables penetration limit | Press | Siemens Energy." <https://press.siemens-energy.com/global/en/pressrelease/siemens-energy-grid-stabilizer-technology-help-irish-grid-exceed-renewables> (accessed Dec. 22, 2021).
- [78] N. D. Rahate and N. Kinhekar, "Demand side management for household equipment's," *IEEE International Conference on Information, Communication, Instrumentation and Control, ICICIC 2017*, vol. 2018-January, pp. 1–5, Feb. 2018, doi: 10.1109/ICOMICON.2017.8279108.

- [79] N. Good, K. A. Ellis, and P. Mancarella, "Review and classification of barriers and enablers of demand response in the smart grid," *Renewable and Sustainable Energy Reviews*, vol. 72, pp. 57–72, May 2017, doi: 10.1016/J.RSER.2017.01.043.
- [80] I. Roasto, T. Lehtla, T. Moller, and A. Rosin, "Control of Ultracapacitors Energy Exchange," pp. 1401–1406, Feb. 2009, doi: 10.1109/EPEPMC.2006.4778599.
- [81] A. Rahmoun, A. Armstorfer, J. Helguero, H. Biechl, and A. Rosin, "Mathematical modeling and dynamic behavior of a Lithium-Ion battery system for microgrid application," *2016 IEEE International Energy Conference, ENERGYCON 2016*, Jul. 2016, doi: 10.1109/ENERGYCON.2016.7513977.
- [82] A. Rosin, T. Moller, M. Lehtla, and H. Hoimoja, "Analysis of Household Electricity Consumption Patterns and Economy of Water Heating Shifting and Saving Bulbs," *Scientific Journal of Riga Technical University. Power and Electrical Engineering*, vol. 26, no. 1, pp. 15–20, Jan. 2011, doi: 10.2478/V10144-010-0013-3.
- [83] "Average Life Span of Homes, Appliances, and Mechanicals – ATD Home Inspection." <https://www.atdhomeinspection.com/advice/average-product-life/> (accessed Dec. 21, 2021).
- [84] D. J. Hammerstrom *et al.*, "Pacific Northwest GridWise™ Testbed Demonstration Projects, Volume I: The Olympic Peninsula Project." 2007.
- [85] C. H. K. Goh and J. Apt, "Consumer Strategies for Controlling Electric Water Heaters under Dynamic Pricing," *Carnegie Mellon Electricity Industry Center Working Paper*, pp. 1–8, 2005.
- [86] R. Bálint, A. Fodor, K. M. Hantos, and A. Magyar, "Cost-optimal model predictive scheduling of freezers," *Control Engineering Practice*, vol. 80, pp. 61–69, Nov. 2018, doi: 10.1016/J.CONENGP.2018.08.009.
- [87] L. Aleixo, A. Rosin, H. Sæle, A. Z. Morch, O. S. Grande, and I. P. Sintef, "Ecogrid EU project - Real time price based load control and economic benefits in a wind production based system," *IET Conference Publications*, vol. 2013, no. 615 CP, 2013, doi: 10.1049/CP.2013.1253.
- [88] V. Kapsalis, G. Safouri, and L. Hadellis, "Cost/comfort-oriented optimization algorithm for operation scheduling of electric water heaters under dynamic pricing," *Journal of Cleaner Production*, vol. 198, pp. 1053–1065, Oct. 2018, doi: 10.1016/J.JCLEPRO.2018.07.024.
- [89] K. Masaba, A. Ntakirutimana, and T. S. Ustun, "Design and implementation of a load scheduling embedded system for off grid solar power systems," *IEEE PES Innovative Smart Grid Technologies Conference Europe*, Jul. 2016, doi: 10.1109/ISGTEUROPE.2016.7856282.
- [90] I. Aldaouab and M. Daniels, "Microgrid battery and thermal storage for improved renewable penetration and curtailment," *IESC 2017 - International Energy and Sustainability Conference*, vol. 2017-December, pp. 1–5, Dec. 2017, doi: 10.1109/IESC.2017.8167472.
- [91] M. J. Goldsworthy and S. Sethuvenkatraman, "The off-grid PV-battery powered home revisited; the effects of high efficiency air-conditioning and load shifting," *Solar Energy*, vol. 172, pp. 69–77, Sep. 2018, doi: 10.1016/J.SOLENER.2018.02.051.
- [92] M. Roux, M. Apperley, and M. J. Booyesen, "Comfort, peak load and energy: Centralised control of water heaters for demand-driven prioritisation," *Energy for Sustainable Development*, vol. 44, pp. 78–86, Jun. 2018, doi: 10.1016/J.ESD.2018.03.006.

- [93] Statista / Bloomberg, "Lithium Battery Prices Plunge." <https://www.statista.com/chart/23807/lithium-ion-battery-prices/> (accessed Dec. 23, 2021).
- [94] O. Kilkki, A. Alahäivälä, and I. Seilonen, "Optimized control of price-based demand response with electric storage space heating," *IEEE Transactions on Industrial Informatics*, vol. 11, no. 1, pp. 281–288, Feb. 2015, doi: 10.1109/TII.2014.2342032.
- [95] B. Feron and A. Monti, "Integration of space heating demand flexibility in a home energy management system using a market-based multi agent system," in *IEEE Power and Energy Society General Meeting*, Jan. 2018, vol. 2018-Janua, pp. 1–5. doi: 10.1109/PESGM.2017.8273810.
- [96] M. Pau, J. L. Cremer, F. Ponci, and A. Monti, "Impact of customers flexibility in heat pumps scheduling for demand side management," Jul. 2017. doi: 10.1109/EEEIC.2017.7977681.
- [97] P. Bacher, H. Madsen, H. A. Nielsen, and B. Perers, "Short-term heat load forecasting for single family houses," *Energy and Buildings*, vol. 65, pp. 101–112, Oct. 2013, doi: 10.1016/j.enbuild.2013.04.022.
- [98] L. Georges, M. Thalfeldt, Ø. Skreiberg, and W. Fornari, "Validation of a transient zonal model to predict the detailed indoor thermal environment: Case of electric radiators and wood stoves," *Building and Environment*, vol. 149, pp. 169–181, Feb. 2019, doi: 10.1016/j.buildenv.2018.12.020.
- [99] J. Clauß and L. Georges, "Model complexity of heat pump systems to investigate the building energy flexibility and guidelines for model implementation," *Applied Energy*, vol. 255, p. 113847, Dec. 2019, doi: 10.1016/j.apenergy.2019.113847.
- [100] R. E. Hedegaard, M. H. Kristensen, T. H. Pedersen, A. Brun, and S. Petersen, "Bottom-up modelling methodology for urban-scale analysis of residential space heating demand response," *Applied Energy*, vol. 242, pp. 181–204, May 2019, doi: 10.1016/j.apenergy.2019.03.063.
- [101] M. Vogt, F. Marten, and M. Braun, "A survey and statistical analysis of smart grid co-simulations," *Applied Energy*, vol. 222. Elsevier Ltd, pp. 67–78, Jul. 15, 2018. doi: 10.1016/j.apenergy.2018.03.123.
- [102] K. Wang, P. O. Siebers, and D. Robinson, "Towards Generalized Co-simulation of Urban Energy Systems," in *Procedia Engineering*, Jan. 2017, vol. 198, pp. 366–374. doi: 10.1016/j.proeng.2017.07.092.
- [103] S. Huang and D. Wu, "Validation on aggregate flexibility from residential air conditioning systems for building-to-grid integration," *Energy and Buildings*, vol. 200, pp. 58–67, Oct. 2019, doi: 10.1016/j.enbuild.2019.07.043.
- [104] F. Pallonetto, E. Mangina, F. Milano, and D. P. Finn, "SimApi, a smartgrid co-simulation software platform for benchmarking building control algorithms," *SoftwareX*, vol. 9, pp. 271–281, Jan. 2019, doi: 10.1016/j.softx.2019.03.003.
- [105] P. Palensky, A. A. van der Meer, C. D. López, A. Joseph, and K. Pan, "Cosimulation of Intelligent Power Systems: Fundamentals, Software Architecture, Numerics, and Coupling," *IEEE Industrial Electronics Magazine*, vol. 11, no. 1. Institute of Electrical and Electronics Engineers Inc., pp. 34–50, Mar. 01, 2017. doi: 10.1109/MIE.2016.2639825.

- [106] T. Q. Péan, J. Salom, and J. Ortiz, "Potential and optimization of a price-based control strategy for improving energy flexibility in Mediterranean buildings," *Energy Procedia*, vol. 122, pp. 463–468, Sep. 2017, doi: 10.1016/J.EGYPRO.2017.07.292.
- [107] G. Gholamibozanjani and M. Farid, "Peak load shifting using a price-based control in PCM-enhanced buildings," *Solar Energy*, vol. 211, pp. 661–673, Nov. 2020, doi: 10.1016/J.SOLENER.2020.09.016.
- [108] D. Wu, B. Wang, D. Precup, and B. Boulet, "Multiple Kernel Learning-Based Transfer Regression for Electric Load Forecasting," *IEEE Transactions on Smart Grid*, vol. 11, no. 2, pp. 1183–1192, Mar. 2020, doi: 10.1109/TSG.2019.2933413.
- [109] R. Ahmadiyahangar, T. Häring, A. Rosin, T. Korötke, and J. Martins, "Residential Load Forecasting for Flexibility Prediction Using Machine Learning-Based Regression Model," in *Proceedings - 2019 IEEE International Conference on Environment and Electrical Engineering and 2019 IEEE Industrial and Commercial Power Systems Europe, IEEEIC/I and CPS Europe 2019*, Jun. 2019, pp. 1–4. doi: 10.1109/EEEIC.2019.8783634.
- [110] P. Prashanthi and K. Priyadarsini, "A Comparative Study of the Performance of Machine Learning based Load Forecasting Methods," *Proceedings - International Conference on Artificial Intelligence and Smart Systems, ICAIS 2021*, pp. 132–136, Mar. 2021, doi: 10.1109/ICAIS50930.2021.9395834.
- [111] P. Bacher, H. Madsen, and H. A. Nielsen, "Online short-term solar power forecasting," *Solar Energy*, vol. 83, no. 10, pp. 1772–1783, Oct. 2009, doi: 10.1016/j.solener.2009.05.016.
- [112] Y. Du and F. Li, "Intelligent Multi-Microgrid Energy Management Based on Deep Neural Network and Model-Free Reinforcement Learning," *IEEE Transactions on Smart Grid*, vol. 11, no. 2, pp. 1066–1076, Mar. 2020, doi: 10.1109/TSG.2019.2930299.
- [113] X. Lei, Z. Yang, J. Yu, J. Zhao, Q. Gao, and H. Yu, "Data-Driven Optimal Power Flow: A Physics-Informed Machine Learning Approach," *IEEE Transactions on Power Systems*, vol. 36, no. 1, pp. 346–354, Jan. 2021, doi: 10.1109/TPWRS.2020.3001919.
- [114] Y. Ye, D. Qiu, M. Sun, D. Papadaskalopoulos, and G. Strbac, "Deep Reinforcement Learning for Strategic Bidding in Electricity Markets," *IEEE Transactions on Smart Grid*, vol. 11, no. 2, pp. 1343–1355, Mar. 2020, doi: 10.1109/TSG.2019.2936142.
- [115] M. A. Mengistu, A. A. Girmay, C. Camarda, A. Acquaviva, and E. Patti, "A Cloud-Based On-Line Disaggregation Algorithm for Home Appliance Loads," *IEEE Transactions on Smart Grid*, vol. 10, no. 3, pp. 3430–3439, May 2019, doi: 10.1109/TSG.2018.2826844.
- [116] H. Patel, M. Pandya, and M. Aware, "Short term load forecasting of Indian system using linear regression and artificial neural network," Apr. 2016. doi: 10.1109/NUICONE.2015.7449617.
- [117] I. el Kafazi, R. Bannari, A. Abouabdellah, M. O. Aboutafail, and J. M. Guerrero, "Energy Production: A Comparison of Forecasting Methods using the Polynomial Curve Fitting and Linear Regression," Sep. 2018. doi: 10.1109/IRSEC.2017.8477278.
- [118] T. Haring, R. Ahmadiyahangar, A. Rosin, T. Korotko, and H. Biechl, "Accuracy Analysis of Selected Time Series and Machine Learning Methods for Smart Cities based on Estonian Electricity Consumption Forecast," in *Proceedings - 2020 IEEE 14th International Conference on Compatibility, Power Electronics and Power Engineering, CPE-POWERENG 2020*, Aug. 2020, pp. 425–428. doi: 10.1109/cpe-powereng48600.2020.9161690.

- [119] M. Imani, "Long short-term memory network and support vector regression for electrical load forecasting," Aug. 2019. doi: 10.1109/PGSRET.2019.8882730.
- [120] R. K. Agrawal, F. Muchahary, and M. M. Tripathi, "Long term load forecasting with hourly predictions based on long-short-term-memory networks," in *2018 IEEE Texas Power and Energy Conference, TPEC 2018*, Mar. 2018, vol. 2018-Febru, pp. 1–6. doi: 10.1109/TPEC.2018.8312088.
- [121] J. S. Wang and Q. W. Zhu, "Short-term electricity load forecast performance comparison based on four neural network models," in *Proceedings of the 2015 27th Chinese Control and Decision Conference, CCDC 2015*, Jul. 2015, pp. 2928–2932. doi: 10.1109/CCDC.2015.7162426.
- [122] L. Buşoniu, T. de Bruin, D. Tolić, J. Kober, and I. Palunko, "Reinforcement learning for control: Performance, stability, and deep approximators," *Annual Reviews in Control*, vol. 46. Elsevier Ltd, pp. 8–28, Jan. 01, 2018. doi: 10.1016/j.arcontrol.2018.09.005.
- [123] T. Wu and J. Wang, "Artificial intelligence for operation and control: The case of microgrids," *The Electricity Journal*, vol. 34, no. 1, p. 106890, Jan. 2021, doi: 10.1016/J.TEJ.2020.106890.
- [124] E. Samadi, A. Badri, and R. Ebrahimpour, "Decentralized multi-agent based energy management of microgrid using reinforcement learning," *International Journal of Electrical Power & Energy Systems*, vol. 122, p. 106211, Nov. 2020, doi: 10.1016/J.IJEPES.2020.106211.
- [125] P. Kofinas, A. I. Dounis, and G. A. Vouros, "Fuzzy Q-Learning for multi-agent decentralized energy management in microgrids," *Applied Energy*, vol. 219, pp. 53–67, Jun. 2018, doi: 10.1016/J.APENERGY.2018.03.017.
- [126] F. D. Li, M. Wu, Y. He, and X. Chen, "Optimal control in microgrid using multi-agent reinforcement learning," *ISA Transactions*, vol. 51, no. 6, pp. 743–751, Nov. 2012, doi: 10.1016/J.ISATRA.2012.06.010.
- [127] T. A. Nakabi and P. Toivanen, "Deep reinforcement learning for energy management in a microgrid with flexible demand," *Sustainable Energy, Grids and Networks*, vol. 25, p. 100413, Mar. 2021, doi: 10.1016/J.SEGAN.2020.100413.
- [128] C. Guo, X. Wang, Y. Zheng, and F. Zhang, "Optimal energy management of multi-microgrids connected to distribution system based on deep reinforcement learning," *International Journal of Electrical Power & Energy Systems*, vol. 131, p. 107048, Oct. 2021, doi: 10.1016/J.IJEPES.2021.107048.
- [129] L. Yin and S. Li, "Hybrid metaheuristic multi-layer reinforcement learning approach for two-level energy management strategy framework of multi-microgrid systems," *Engineering Applications of Artificial Intelligence*, vol. 104, p. 104326, Sep. 2021, doi: 10.1016/J.ENGAPPAL.2021.104326.
- [130] M. M. Morato, J. Vergara-Dietrich, E. A. Esparcia, J. D. Ocon, and J. E. Normey-Rico, "Assessing demand compliance and reliability in the Philippine off-grid islands with Model Predictive Control microgrid coordination," *Renewable Energy*, vol. 179, pp. 1271–1290, Dec. 2021, doi: 10.1016/J.RENENE.2021.07.012.
- [131] T. Panapongpakorn and D. Banjerdpongchai, "Model Predictive Control of Energy Management System for Economic Dispatch with Application to MHS Microgrid in Normal Operation," in *2019 19th International Conference on Control, Automation and Systems (ICCAS)*, Oct. 2019, vol. 2019-October, pp. 1281–1286. doi: 10.23919/ICCAS47443.2019.8971734.

- [132] A. Ruano, A. Hernandez, J. Ureña, M. Ruano, and J. Garcia, "NILM techniques for intelligent home energy management and ambient assisted living: A review," *Energies*, vol. 12, no. 11. MDPI AG, Jun. 10, 2019. doi: 10.3390/en12112203.
- [133] J. Cho, Z. Hu, and M. Sartipi, "Non-Intrusive A/C Load Disaggregation Using Deep Learning," in *2018 IEEE/PES Transmission and Distribution Conference and Exposition (T&D)*, Apr. 2018, vol. 2018-April, pp. 1–5. doi: 10.1109/TDC.2018.8440358.
- [134] R. G. Rajasekaran, S. Manikandaraj, and R. Kamaleshwar, "Implementation of Machine Learning Algorithm for predicting user behavior and smart energy management," in *2017 International Conference on Data Management, Analytics and Innovation (ICDMAI)*, Feb. 2017, pp. 24–30. doi: 10.1109/ICDMAI.2017.8073480.
- [135] L. Pereira and N. Nunes, "Performance evaluation in non-intrusive load monitoring: Datasets, metrics, and tools—A review," *Wiley Interdisciplinary Reviews: Data Mining and Knowledge Discovery*, vol. 8, no. 6, Nov. 2018, doi: 10.1002/widm.1265.
- [136] A. Miyasawa, Y. Fujimoto, and Y. Hayashi, "Energy disaggregation based on smart metering data via semi-binary nonnegative matrix factorization," *Energy and Buildings*, vol. 183, pp. 547–558, Jan. 2019, doi: 10.1016/j.enbuild.2018.10.030.
- [137] M. Devlin and B. P. Hayes, "Non-Intrusive Load Monitoring using Electricity Smart Meter Data: A Deep Learning Approach," in *2019 IEEE Power & Energy Society General Meeting (PESGM)*, Aug. 2019, vol. 2019-Augus, pp. 1–5. doi: 10.1109/PESGM40551.2019.8973732.
- [138] G. Tang, Z. Ling, F. Li, D. Tang, and J. Tang, "Occupancy-aided energy disaggregation," *Computer Networks*, vol. 117, pp. 42–51, Apr. 2017, doi: 10.1016/j.comnet.2016.11.019.
- [139] G. A. Raiker, B. Subba Reddy, L. Umanand, A. Yadav, and M. M. Shaikh, "Approach to Non-Intrusive Load Monitoring using Factorial Hidden Markov Model," in *2018 IEEE 13th International Conference on Industrial and Information Systems (ICIIS)*, Dec. 2018, pp. 381–386. doi: 10.1109/ICIINF5.2018.8721436.
- [140] T. Bernard, M. Verbunt, G. vom Bogel, and T. Wellmann, "Non-Intrusive Load Monitoring (NILM): Unsupervised Machine Learning and Feature Fusion : Energy Management for Private and Industrial Applications," in *2018 International Conference on Smart Grid and Clean Energy Technologies (ICSGCE)*, May 2018, pp. 174–180. doi: 10.1109/ICSGCE.2018.8556735.
- [141] J. Bélanger, P. Venne, and J.-N. Paquin, "The What, Where and Why of Real-Time Simulation," 2010, Accessed: Dec. 23, 2021. [Online]. Available: https://blob.opal-rt.com/medias/L00161_0436.pdf
- [142] E. García-Martínez, J. F. Sanz, J. Muñoz-Cruzado, and J. M. Perié, "A Review of PHIL Testing for Smart Grids—Selection Guide, Classification and Online Database Analysis," *Electronics 2020, Vol. 9, Page 382*, vol. 9, no. 3, p. 382, Feb. 2020, doi: 10.3390/ELECTRONICS9030382.
- [143] O. Tremblay, "Contribution to the design of the closed-loop control of a real-time power simulator," Dec. 2020.
- [144] E. De *et al.*, "European White Book on Real-Time Powerhardware-in-the-Loop testing".

- [145] H. Kikusato *et al.*, “Integrated Power Hardware-in-the-Loop and Lab Testing for Microgrid Controller,” *2019 IEEE PES Innovative Smart Grid Technologies Asia, ISGT 2019*, pp. 2743–2747, May 2019, doi: 10.1109/ISGT-ASIA.2019.8881576.
- [146] C. Seitzl, J. Kathan, G. Lauss, and F. Lehfuss, “Power hardware-in-The-loop implementation and verification of a real time capable battery model,” *IEEE International Symposium on Industrial Electronics*, pp. 2285–2290, 2014, doi: 10.1109/ISIE.2014.6864974.
- [147] H. Fakham, O. Ducarme, and M. Legry, “Development of a power hardware in the loop simulation of an islanded microgrid”.
- [148] N. Cinay, T. Haring, A. Rosin, T. Korotko, R. Ahmadiyahangar, and H. Biechl, “Lifetime-Oriented Control Strategies for Hybrid Energy Storage Systems in an Islanded Microgrid,” in *2021 22nd IEEE International Conference on Industrial Technology (ICIT)*, Mar. 2021, pp. 1267–1272. doi: 10.1109/ICIT46573.2021.9453617.
- [149] L. Czarnecki, *Photovoltaik*, 1st ed. bookboon.com, 2018. Accessed: Nov. 11, 2021. [Online]. Available: <https://bookboon.com/en/photovoltaik-ebook>
- [150] “Photovoltaic Geographical Information System (PVGIS) | EU Science Hub.” <https://ec.europa.eu/jrc/en/pvgis> (accessed Nov. 11, 2021).
- [151] T. Häring, A. Rosin, and H. Biechl, “Using common household thermal storages to support the PV- and battery system in nearly zero energy buildings in off-grid mode,” *Sustainable Energy Technologies and Assessments*, vol. 35, no. May, pp. 12–24, Oct. 2019, doi: 10.1016/j.seta.2019.05.014.
- [152] T. Häring, R. Ahmadiyahangar, A. Rosin, and H. Biechl, “Impact of Load Matching Algorithms on the Battery Capacity with different Household Occupancies,” in *IECON 2019 - 45th Annual Conference of the IEEE Industrial Electronics Society*, Oct. 2019, pp. 2541–2547. doi: 10.1109/IECON.2019.8927495.
- [153] T. Haring, R. Ahmadiyahangar, A. Rosin, H. Biechl, and T. Korotko, “Comparison of the impact of different household occupancies on load matching algorithms,” in *2019 Electric Power Quality and Supply Reliability Conference (PQ) & 2019 Symposium on Electrical Engineering and Mechatronics (SEEM)*, Jun. 2019, pp. 1–6. doi: 10.1109/PQ.2019.8818270.
- [154] F. Plaum, T. Haring, R. Ahmadiyahangar, and A. Rosin, “Power Smoothing in Smart Buildings using Flywheel Energy Storage,” in *Proceedings - 2020 IEEE 14th International Conference on Compatibility, Power Electronics and Power Engineering, CPE-POWERENG 2020*, Jul. 2020, pp. 473–477. doi: 10.1109/CPE-POWERENG48600.2020.9161458.
- [155] N. Pflugradt, “LoadProfileGenerator.” <https://www.loadprofilegenerator.de/> (accessed Sep. 07, 2021).
- [156] N. Pflugradt, J. Teuscher, B. Platzer, and W. Schufft, “Analysing low-voltage grids using a behaviour based load profile generator,” *Renewable Energy and Power Quality Journal*, vol. 1, no. 11, pp. 361–365, Mar. 2013, doi: 10.24084/REPQJ11.308.
- [157] Finnish Meteorological Institute, “Download observations.” <https://en.ilmatietaenlaitos.fi/download-observations#!/> (accessed Sep. 07, 2021).
- [158] Statistisches Bundesamt, “Haushalte und Familien - Ergebnisse des Mikrozensus - Fachserie 1 Reihe 3 – 2017,” 2017.

- [159] F. Plaum, "Hooratas-energiasalvesti juhtimisstrateegiate arendamine mikroõrgu tasakaalustamiseks," M.Sc.Eng. Thesis, Supervision: T. Häring and A. Rosin, Tallinn, 2019.
- [160] "Clarke and Park Transforms - MATLAB & Simulink." <https://se.mathworks.com/solutions/power-electronics-control/clarke-and-park-transforms.html> (accessed Dec. 23, 2021).
- [161] A. K. Gupta and A. M. Khambadkone, "A space vector PWM scheme for multilevel inverters based on two-level space vector PWM," *IEEE Transactions on Industrial Electronics*, vol. 53, no. 5, pp. 1631–1639, Oct. 2006, doi: 10.1109/TIE.2006.881989.
- [162] "Field-Oriented Control (FOC) - MATLAB & Simulink - MathWorks Nordic." <https://se.mathworks.com/help/mcb/gs/implement-motor-speed-control-by-using-field-oriented-control-foc.html> (accessed Dec. 23, 2021).
- [163] N. P. Quang and J.-A. Dittrich, "Vector control of three-phase AC machines : system development in the practice".
- [164] T. Häring, "Research And Development Of Thermal Storage Control Models," M.Sc.Eng. Thesis, Supervision: A. Rosin and H. Biechl, Tallinn, 2018. Accessed: Feb. 20, 2020. [Online]. Available: <https://digikogu.taltech.ee/en/Item/e58d6aaa-37ff-449a-99a0-4d951d0c09e2>
- [165] "BU-802b: What does Elevated Self-discharge Do? - Battery University." <https://batteryuniversity.com/article/bu-802b-what-does-elevated-self-discharge-do%C2%A0> (accessed Dec. 14, 2021).
- [166] D. Yan, L. Lu, F. Jiang, and M. Ouyang, "Comparing the performances of different energy storage cells for hybrid electric vehicle," 2015.
- [167] Victron Energy B.V., "Off-grid, backup & island systems," 2021. https://www.victronenergy.com/upload/documents/Brochure-Off-Grid-backup-and-island-systems_EN_web.pdf (accessed Dec. 13, 2021).
- [168] Kokam, "KBM SERIES MODULE: KBM255 14S Gen 1.0," 2018. <https://battery-manufacturing.com/wp/wp-content/uploads/2020/12/Kokam-Battery-Module-255-series-Brochure.pdf> (accessed Dec. 14, 2021).
- [169] Kokam, "System Integrator - Energy Storage Solution Provider: 35MW/11MWh ESS Project in Western Australia," 2018. https://kokam.com/data/filebox/ess_brochure.pdf (accessed Dec. 14, 2021).
- [170] R. Saidur, H. H. Masjuki, and I. A. Choudhury, "Role of ambient temperature, door opening, thermostat setting position and their combined effect on refrigerator-freezer energy consumption," *Energy Conversion and Management*, vol. 43, no. 6, pp. 845–854, Apr. 2002, doi: 10.1016/S0196-8904(01)00069-3.
- [171] American Society of Heating Refrigerating and Air-Conditioning Engineers, *2009 ASHRAE Handbook: Fundamentals*. American Society of Heating, Refrigeration and Air-Conditioning Engineers, 2009.
- [172] Eurostat, "Average size of dwelling by household type and degree of urbanisation," 2012. https://appsso.eurostat.ec.europa.eu/nui/show.do?dataset=ilc_hcmh02&lang=en (accessed Sep. 07, 2021).
- [173] Statistisches Bundesamt, "Datenreport 2018," 2018.
- [174] Statistikaamet, "Eesti Statistika," 2013. https://www.stat.ee/65359?parent_id=32784 (accessed Apr. 16, 2019).

- [175] T. Häring, T. M. Kull, R. Ahmadihangar, A. Rosin, M. Thalfeldt, and H. Biechl, "Microgrid Oriented modeling of space heating system based on neural networks," *Journal of Building Engineering*, vol. 43, p. 103150, Nov. 2021, doi: 10.1016/j.jobe.2021.103150.
- [176] "Validation & certifications - Simulation Software | EQUA." <https://www.equa.se/en/ida-ice/validation-certifications> (accessed Aug. 05, 2021).
- [177] T. M. Kull, R. Simson, M. Thalfeldt, and J. Kurnitski, "Influence of time constants on low energy buildings' heating control," in *Energy Procedia*, 2017, vol. 132. doi: 10.1016/j.egypro.2017.09.640.
- [178] T. M. Kull, R. Simson, and J. Kurnitski, "Setback Efficiency of Limited-Power Heating Systems in Cold Climate," 2019, pp. 87–95. doi: 10.1007/978-3-030-00662-4_8.
- [179] *EESTI STANDARD HOONETE KÜTTE PROJEKTEERIMINE Design of heating for buildings*. 2016.
- [180] "Estonian Regulation No 58: Methodology for calculating the energy performance of buildings." Ministry of Economic Affairs and Communications, 2015.
- [181] T. Kalamees and J. Kurnitski, "Estonian test reference year for energy calculations," *Proc. Estonian Acad. Sci. Eng*, vol. 12, pp. 40–58, 2006.
- [182] T. Häring, A. Rosin, T. M. Kull, J. Helguero, and H. Biechl, "Thermal Modelling of a Control Center for Flexibility Analysis in nZEB Nanogrids," *61st Annual International Scientific Conference on Power and Electrical Engineering of Riga Technical University (RTU CON)*, Nov. 2020, doi: 10.1109/RTU CON51174.2020.9316568.
- [183] "Liginullenergia eluhooned. Väikemajad," 2017.
- [184] HEVAC OÜ, "Liginullenergia eluhooned. Väike eramu Soojusvarustus, küte ja ventilatsioon," 2017.
- [185] Roofit Solar Energy OÜ, "Liginullenergia eluhooned. Väike eramu. Päikese-elektrisüsteem ja tugevvool, variant 1," 2017.
- [186] TalTech, "Liginullenergia eluhooned. Väike eramu. Energiatõhusus," 2017.
- [187] H. OÜ and R. OÜ, "Liginullenergia eluhooned. Väike eramu. Päikese-elektrisüsteem ja tugevvool, variant 2," 2017.
- [188] Roofit Solar Energy OÜ, EVAC OÜ, and RAUSI OÜ, "Liginullenergia eluhooned. Väike eramu. Päikese-elektrisüsteem ja tugevvool, variant 2," 2017.
- [189] R. Simson, E. Arumägi, K. Kuusk, and J. Kurnitski, "Redefining cost-optimal nZEB levels for new residential buildings," *E3S Web of Conferences*, vol. 111, no. 2019, 2019, doi: 10.1051/e3sconf/201911103035.
- [190] R. Simson et al., "The Impact of Infiltration on Heating Systems Dimensioning in Estonian Climate," in *E3S Web of Conferences, 12th Nordic Symposium on Building Physics*, 2020, p. to be published.
- [191] S. Wolf, D. Cali, and H. Madsen, "ProccS," 2019. <https://www.proccs.org/>
- [192] S. Wolf, "Modelling Building Occupant Behaviour Using Hidden Markov Models," Technical University of Denmark, 2019.
- [193] S. Wolf et al., "Room-level occupancy simulation model for private households," *Journal of Physics: Conference Series*, vol. 1343, no. 1, 2019, doi: 10.1088/1742-6596/1343/1/012126.

- [194] M. Petrõkin, "Närvivõrgustiku õppimisparameetrite optimeerimine küttekeha masinõppemudeli sünteesimiseks," B.Sc.Eng. Thesis, Supervision: T. Korõtko and T. Häring, Tallinn, 2021.
- [195] "Scaled conjugate gradient backpropagation - MATLAB trainscg - MathWorks Nordic." <https://se.mathworks.com/help/deeplearning/ref/trainscg.html> (accessed May 23, 2020).
- [196] M. F. Møller, "A scaled conjugate gradient algorithm for fast supervised learning," *Neural Networks*, vol. 6, no. 4, pp. 525–533, Jan. 1993, doi: 10.1016/S0893-6080(05)80056-5.
- [197] L. Prechelt, "Early Stopping - But When?," pp. 55–69, 1998, doi: 10.1007/3-540-49430-8_3.
- [198] "A Gentle Introduction to Early Stopping to Avoid Overtraining Neural Networks." <https://machinelearningmastery.com/early-stopping-to-avoid-overtraining-neural-network-models/> (accessed Dec. 23, 2021).
- [199] B. Saha and K. Goebel, "Battery Data Set," *NASA Ames Prognostics Data Repository*. <http://ti.arc.nasa.gov/project/prognostic-data-repository> (accessed Dec. 14, 2021).
- [200] European Union, "Commission Delegated Regulation (EU) No 1060/2010 of 28 September 2010 supplementing Directive 2010/30/EU of the European Parliament and of the Council with regard to energy labelling of household refrigerating appliances," 2010.
- [201] European Federation of National Associations of Measurement, "Testing and Analytical Laboratories Guide to the Evaluation of Measurement Uncertainty for Quantitative Test Results," 2006.
- [202] Robert Bosch Hausgeräte GmbH, "GSN51AW41 Produktdatenblatt nach Verordnung (EU) Nr. 1060/2010."
- [203] "VEEBOILERITE PAIGALDUS-JA KASUTUSJUHEND (ACI HÜBRIIDANOOD)".
- [204] "Market data | Nord Pool." <https://www.nordpoolgroup.com/Market-data1/Dayahead/Area-Prices/EE/Hourly/?view=table> (accessed Feb. 20, 2020).
- [205] T. Haring, R. Ahmadiyahangar, A. Rosin, and H. Biechl, "Machine Learning Approach for Flexibility Characterisation of Residential Space Heating," *IECON 2021 – 47th Annual Conference of the IEEE Industrial Electronics Society*, pp. 1–6, Oct. 2021, doi: 10.1109/IECON48115.2021.9589216.
- [206] Panasonic, "Service Manual CS-CZ / CU-CZ".
- [207] Mitsubishi Electric, "Service Technical Guide MSC / MS/ MSH / MSZ / MLZ / MU / MUH / MUZ / MXZ".
- [208] Daikin, "Manual FTXTM30M2V1B / FTXTM40M2V1B."
- [209] H. H. Bauer, T. Reichardt, S. J. Barnes, and M. M. Neumann, "DRIVING CONSUMER ACCEPTANCE OF MOBILE MARKETING: A THEORETICAL FRAMEWORK AND EMPIRICAL STUDY," *Journal of Electronic Commerce Research*, vol. 6, no. 3, 2005.
- [210] J. F. Nicol and M. A. Humphreys, "Adaptive thermal comfort and sustainable thermal standards for buildings," *Energy and Buildings*, vol. 34, no. 6, pp. 563–572, Jul. 2002, doi: 10.1016/S0378-7788(02)00006-3.
- [211] M. Bae, K. Kim, and H. Kim, "Preserving privacy and efficiency in data communication and aggregation for AMI network," *Journal of Network and Computer Applications*, vol. 59, pp. 333–344, Jan. 2016, doi: 10.1016/j.jnca.2015.07.005.

- [212] N. Fadhel, F. Lombardi, L. Aniello, A. Margheri, and V. Sassone, "Towards a semantic modelling for threat analysis of IoT applications: A case study on transactive energy," in *IET Conference Publications*, 2019, vol. 2019, no. CP756. doi: 10.1049/cp.2019.0147.
- [213] G. Giaconi, D. Gunduz, and H. V. Poor, "Smart Meter Privacy with Renewable Energy and an Energy Storage Device," in *IEEE Transactions on Information Forensics and Security*, Jan. 2018, vol. 13, no. 1, pp. 129–142. doi: 10.1109/TIFS.2017.2744601.
- [214] M. S. Piscitelli, S. Brandi, and A. Capozzoli, "Recognition and classification of typical load profiles in buildings with non-intrusive learning approach," *Applied Energy*, vol. 255, p. 113727, Dec. 2019, doi: 10.1016/j.apenergy.2019.113727.
- [215] S. Yussof, M. E. Rusli, Y. Yusoff, R. Ismail, and A. A. Ghapar, "Financial impacts of smart meter security and privacy breach," *Conference Proceedings - 6th International Conference on Information Technology and Multimedia at UNITEN: Cultivating Creativity and Enabling Technology Through the Internet of Things, ICIMU 2014*, pp. 11–14, 2015, doi: 10.1109/ICIMU.2014.7066595.
- [216] A. U. Rehman, T. Tjing Lie, B. Valles, and S. R. Tito, "Low Complexity Non-Intrusive Load Disaggregation of Air Conditioning Unit and Electric Vehicle Charging," in *2019 IEEE Innovative Smart Grid Technologies - Asia (ISGT Asia)*, May 2019, pp. 2607–2612. doi: 10.1109/ISGT-Asia.2019.8881113.
- [217] S. Singh and A. Majumdar, "Deep Sparse Coding for Non-Intrusive Load Monitoring," *IEEE Transactions on Smart Grid*, vol. 9, no. 5, pp. 4669–4678, Sep. 2018, doi: 10.1109/TSG.2017.2666220.
- [218] M. Aiad and P. H. Lee, "Unsupervised approach for load disaggregation with devices interactions," *Energy and Buildings*, vol. 116, pp. 96–103, Mar. 2016, doi: 10.1016/j.enbuild.2015.12.043.
- [219] T.-T.-H. Le, J. Kim, and H. Kim, "Classification performance using gated recurrent unit recurrent neural network on energy disaggregation," in *2016 International Conference on Machine Learning and Cybernetics (ICMLC)*, Jul. 2016, vol. 1, pp. 105–110. doi: 10.1109/ICMLC.2016.7860885.
- [220] S. Hosseini, N. Henao, S. Kelouwani, K. Agbossou, and A. Cardenas, "A Study on Markovian and Deep Learning Based Architectures for Household Appliance-level Load Modeling and Recognition," in *2019 IEEE 28th International Symposium on Industrial Electronics (ISIE)*, Jun. 2019, vol. 2019-June, pp. 35–40. doi: 10.1109/ISIE.2019.8781186.
- [221] P. A. Schirmer, I. Mporas, and M. Paraskevas, "Evaluation of Regression Algorithms and Features on the Energy Disaggregation Task," in *2019 10th International Conference on Information, Intelligence, Systems and Applications (IISA)*, Jul. 2019, pp. 1–4. doi: 10.1109/IISA.2019.8900695.
- [222] European Union, "Regulation (EU) 2016/679 of the European Parliament and of the Council of 27 April 2016 on the protection of natural persons with regard to the processing of personal data and on the free movement of such data, and repealing Directive 95/46/EC (General Data Protection Regulation)."
- [223] European Union, "Directive (EU) 2019/944 of the European Parliament and of the Council of 5 June 2019 on common rules for the internal market for electricity and amending Directive 2012/27/EU."

- [224] European Union, “Directive (EU) 2016/1148 of the European Parliament and of the Council of 6 July 2016 concerning measures for a high common level of security of network and information systems across the Union.”
- [225] European Union, “Regulation (EU) 2019/881 of the European Parliament and of the Council of 17 April 2019 on ENISA (the European Union Agency for Cybersecurity) and on information and communications technology cybersecurity certification and repealing Regulation (EU) No 526/2013 (Cybersecurity Act).”
- [226] Majandus- ja Kommunikatsiooniministeerium, “Energieetika tulemusvaldkonna 2020.aasta aruanne”.
- [227] “Bundesnetzagentur - Auswertung Strom.”
https://www.bundesnetzagentur.de/DE/Sachgebiete/ElektrizitaetundGas/Unternehmen_Institutionen/Versorgungssicherheit/Versorgungsunterbrechungen/Auswertung_Strom/start.html (accessed Feb. 28, 2022).
- [228] “BMWK - Der Strompreis.”
<https://www.bmwi.de/Redaktion/DE/Artikel/Energie/strompreise-bestandteile.html> (accessed Mar. 01, 2022).
- [229] “Electricity price statistics - Statistics Explained.”
https://ec.europa.eu/eurostat/statistics-explained/index.php?title=Electricity_price_statistics (accessed Mar. 01, 2022).
- [230] “Kosten für Stromspeicher - Wirtschaftlichkeit und Preise.”
<https://www.energieheld.de/solaranlage/photovoltaik/stromspeicher/kosten> (accessed Feb. 28, 2022).
- [231] “Energistro - The ecological and sustainable energy storage | Energistro Flywheel, ecological, economical and sustainable energy storage.”
<https://energistro.net/> (accessed Mar. 01, 2022).
- [232] “Concrete flywheel storage system for residential PV – pv magazine International.” <https://www.pv-magazine.com/2021/06/21/concrete-flywheel-storage-system-for-residential-pv/> (accessed Mar. 01, 2022).
- [233] “Flywheel Energy Storage — AMT, Inc.” <https://american-maglev.com/fess> (accessed Mar. 01, 2022).
- [234] “Preisentwicklung Photovoltaik 2022, Preise, Module, Speicher, Prognose.”
<https://photovoltaik.one/photovoltaik-preise> (accessed Mar. 01, 2022).
- [235] “Preise Solarmodule: Kosten & Vergleich [2022] | Echtsolar.”
<https://echtsolar.de/preise-solarmodule/> (accessed Mar. 01, 2022).
- [236] “Bundesnetzagentur 2022”.
- [237] “Bundesministerium für Umwelt, Naturschutz und Reaktorsicherheit 2022”.

Acknowledgements

Foremost, I would like to thank my family for believing in me and backing up my decisions in the last 10 years to achieve my ambitious goal of earning a doctoral degree. Thank you to all my loved family members in Germany and Estonia for your relentless support, understanding and patience. I could not have finished this work without you and all the conversations, discussions, and daily adventures that supported and distracted me regularly which helped me re-focus on my work with a fresh mindset.

I would like to thank both of my supervisors for their continuous counselling and support, especially Prof. Argo Rosin for his day-to-day mentoring and guidance during the curriculum of my doctoral studies in Tallinn.

Thank you to all my colleagues from Tallinn University of Technology and University of Applied Sciences Kempten, who provided helpful input for my work through cooperation, meaningful conversations, and interesting discussions and provided a pleasant work environment.

This research was supported by the Estonian Centre of Excellence in Zero Energy and Resource Efficient Smart Buildings and Districts, ZEBE (grant No. 2014-2020.4.01.15-0016), by the programme Mobilitas Pluss (Grant No – 2014-2020.4.01.16-0024, MOBTP88) funded by the European Regional Development Fund, by the Estonian Research Council (grant No. PSG409), by the Estonian Research Council grant PUT (PUT1680), and by the European Commission through the H2020 project Finest Twins (grant No. 856602).

I would like to thank the Archimedes Foundation for their support with the "Smart Specialisation Scholarship".

Abstract

Research and development of energy storage control strategies for residential area microgrids

Due to the rising concerns regarding climate change, there are multiple national and international agreements to reduce greenhouse gas emissions, e.g., the European Green Deal. To achieve the goal of these agreements, the share of renewable energy sources needs to be increased while reducing the dependence on fossil energy sources. This transition can be accomplished with microgrids as they can balance demand and supply of renewable generation already locally with demand side management strategies and storage systems. For such microgrids, the control possibilities for hybrid energy storage systems, including household appliances as supporting thermal storages, as well as the related user acceptance and financial feasibility, need additional research, especially for the islanded operation mode.

Thus, this work aims to research and develop object models with improved accuracy and control strategies for hybrid energy storage systems to improve supply reliability and financial feasibility in residential microgrids to provide recommendations for the development of microgrids.

First, the current state of the art regarding smart grid topologies and components, including building requirements, storage systems, energy sources, and modelling and experimental setup design, like machine learning and hardware-in-the-loop-setups, was investigated.

On these bases, it was possible to improve and develop object models for flywheel energy storage, battery energy storage, and common household thermal storages, namely freezer, water heater and space heating. For the space heating model, a novel neural network-based methodology was developed to compensate either high computational time or low accuracy of existing modelling techniques.

These models were then validated to ensure good accuracy levels for the microgrid simulations with error rates for all object models below 12% mean error.

With the validated models, it was possible to develop control strategies for supply reliability and financial feasibility improvements: The energy costs could be reduced by more than 10% and the battery storage capacity, representing investment costs, by 4%. Simultaneously, the battery storage cyclic lifetime could be increased by 19% and the islanded operation duration as a supply reliability parameter by more than 3%.

Lastly, a social acceptance evaluation methodology and privacy mapping tool were developed to address the user satisfaction and privacy concerns more effectively and thereby improve the microgrid development and planning quality. A consecutive financial analysis showed that the investment return time of the system is 6 years in Germany and 13 years in Estonia for different component dimensioning strategies.

In conclusion, the set goals were achieved. Based on the technical, social, and financial feasibility analyses discussed in this thesis it was possible to develop a decision tree as an applicable guidance tool for recommendations on the design of microgrids to simplify the work for microgrid planners and designers. The developed solutions will increase the supply reliability and profitability of microgrids with renewable energy sources and hybrid energy storage systems and ensure social acceptance in the development of future microgrids.

Lühikokkuvõte

Energiasalvestite juhtimisstrateegiate uurimine ja arendamine elamupiirkondade mikrovõrkudele

Seoses kliimamuutustega on kasvuhoonegaaside heitkoguste vähendamine järjest olulisem, milleks on sõlmitud mitmeid riiklikke ja rahvusvahelisi lepinguid, sh Euroopa roheline kokkulepe. Lepingutes sätestatud eesmärkide saavutamiseks tuleb suurendada taastuvate energiaallikate osakaalu, vähendades samaaegselt sõltuvust fossiilsetest energiaallikatest. Seda üleminekut toetavad nutikad mikrovõrgud, kus on võimalik juhuslikku taastuenergia tootmist ja tarbimist tasakaalustada nutikate juhtimise strateegiate ja salvestussüsteemidega. Selliste mikrovõrkude puhul vajavad täiendavat uurimist hübriid-energiasalvestussüsteemide juhtimine sh kodumasinat kui toetavate soojussalvestite juhtimisvõimalused. Samuti mikrovõrkude vaates olulisel kohal kasutajamugavuse hindamine, eriti saartalitluse puhul.

Käesoleva töö eesmärk on uurida ja arendada täiustatud objektide mudelid ja hübriid-energiasalvestite juhtimisstrateegiaid, et parandada elamupiirkondade mikrovõrkude varustuskindlust ja kulutõhusust. Lisaks analüüsitakse investeeingu-tasuvust ning lõppkasutaja privaatsus- ja mugavusnõudeid, et tõsta sotsiaalse heakskiidu taset ja anda soovitusi tulevaste mikrovõrkude arendamiseks.

Esmaalt viidi läbi tehnika- ja teadustaseme hetkeolukorra kaardistus tarkvõrgu topoloogiate, komponentide, sh salvestussüsteemide, energiaallikate, objektide mudelid, masinõppemudelid ja katseseadmete (PHIL) osas, et väljatöötada raamistik edasiste uuringute ja arendustöö jaoks. Analüüsi põhjal töötati välja ja täiustati hooratta, akude ja kodumajapidamistes kasutatavate soojust salvestavate seadmete (sügavkülmik, veeboiler, ruumiküte) mudelid. Näiteks, ruumi küttemudeli jaoks töötati välja uudne närvivõrgupõhine meetodika, et kompenseerida olemasolevate modelleerimistehnikate suurt ajamahukust või madalat täpsust.

Töö järgmises etapis mudelid valideeriti, et tagada mikrovõrgu simulatsioonide puhul soovitud täpsus ehk keskmine objektimudelite summaarne viga oleks alla 12%. Valideeritud mudelite abil töötati välja hübriidsalvestuslahendusele juhtimisstrateegiaid varustuskindluse ja kulutõhususe parandamiseks, mille tulemusel oli võimalik vähendada energiakulusid enam kui 10% ja aku salvestusmahtu 4%. Samaaegselt võimaldasid juhtimisstrateegiaid pikendada aku salvestamise tsüklilist eluiga 19% ja tööaega enam kui 3%.

Töö viimases etapis töötati välja sotsiaalse heakskiidu hindamismetoodika, mille abil saab tõhusamalt arvestada kasutaja rahulolu ja privaatsusprobleemidega ning seeläbi parandada tulevaste mikrovõrkude arendamise ja planeerimise kvaliteeti. Samuti koostati investeeingu tasuvusanalüüs, mis näitas, et süsteemi investeeingu tasuvusaeg on sõltuvalt erinevate komponentide dimensioneerimisest Saksamaal 6 aastat ja Eestis 13 aastat.

Kokkuvõtteks võib öelda, et püstitatud eesmärgid said täidetud. Doktoritöös käsitletud tehniliste lahenduste, sotsiaalsete mõjude ja tasuvuse analüüsi baasil on loodud mikrovõrkude kavandamiseks ja soovitude andmiseks tööriist ehk otsustuspuu, mis lihtsustab mikrovõrkude planeerijate ja projekteerijate tööd. Väljatöötatud lahendused võimaldavad parandada taastuenergiaallikate ja hübriid-energiasalvestuslahendustega mikrovõrkude varustuskindlust, tasuvust ning tagada sotsiaalne heakskiit tulevaste mikrovõrkude arendamisel.

Appendix

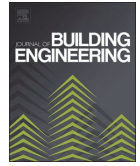
Publication I

T. Häring, T. M. Kull, R. Ahmadiyahangar, A. Rosin, M. Thalfeldt, and H. Biechl, "Microgrid Oriented modeling of space heating system based on neural networks," *Journal of Building Engineering*, vol. 43, p. 103150, Nov. 2021, doi: 10.1016/j.job.2021.103150.



Contents lists available at ScienceDirect

Journal of Building Engineering

journal homepage: www.elsevier.com/locate/job

Microgrid Oriented modeling of space heating system based on neural networks

Tobias Häring^{a,b,*}, Tuule Mall Kull^c, Roya Ahmadihangar^{a,b}, Argo Rosin^{a,b},
Martin Thalfeldt^c, Helmuth Biechl^{a,b,d}

^a Department of Electrical Power Engineering and Mechatronics, School of Engineering, Tallinn University of Technology, Ehitajate Tee 5, 19086, Tallinn, Estonia

^b Smart City Center of Excellence (Finest Twins), Tallinn University of Technology, Estonia

^c Department of Civil Engineering and Architecture, School of Engineering, Tallinn University of Technology, Ehitajate Tee 5, 19086, Tallinn, Estonia

^d Institute of Electrical Power Systems (IEES), University of Applied Sciences Kempten, Bahnhofstraße 61, 87435 Kempten (Allgäu), Germany

ARTICLE INFO

Keywords:

Machine learning
Modeling
Thermostatic load
Microgrid
nZEB
Smart city

ABSTRACT

Balancing the energy production and consumption is a huge challenge for future smart grids. In this context, many demand-side management programs are being developed to achieve flexibility from different loads like space heating. As space heating models for flexibility simulations are an interdisciplinary field of work, complex civil engineering thermal models need to be combined with complex electrical engineering control simulations in different software frameworks. Traditionally used methods have shortcomings in one of those two domains as the publications that provide complex control strategies for demand response are lacking complex thermal models and vice versa. Co-simulations overcome this problem but are computationally expensive and have compatibility limitations. Thus, the aim of this work is to develop a methodology for designing space heating/cooling models, intended for positive energy district- or smart city simulations, which provide high accuracy at low computational expense. This could be achieved by synthesizing neural network object models from IDA-ICE civil engineering models in Matlab. These machine learning models showed improvements of more than 30% in different error metrics and a simulation time reduction of more than 80% compared to other methods, making them suitable for use in microgrid simulations, including flexibility analyses.

1. Introduction

In recent years, the share of renewable energy production has been increasing worldwide. This is a great development in terms of sustainability and environmental friendliness. Nevertheless, a higher share of renewables, which typically have a volatile and hardly predictable energy generation, leads to various challenges for grid operators as the operational complexity increases [1]. Even with accurate production predictions for photovoltaics (PV) or wind power systems [2], their maximum production cannot be increased during high demand and vice versa it would be a waste of energy to reduce their electricity production if the demand is low.

Thus, it is necessary to extend the traditional balancing approach of variable energy production to smart grids [3] with storage systems, like battery storage systems (BESS) [4] or thermal storage systems [5], in combination with demand-side management (DSM) applications [6], to have a variable consumption as well [7]. All these DSM programs can be

used in future smart cities to achieve higher flexibility [8] of the system. There are many devices in the residential sector, which can be controlled in a DSM manner, like dishwashers, washing machines [9], water heaters [10], or freezers [11]. More complicated to model, are heating, ventilation, and air conditioning (HVAC) systems [12,13]. Since these systems are relevant in the residential, commercial and industrial sectors, they are amongst the biggest consumers of indoor electricity in the EU [14], making them interesting investigation objects for DSM and flexibility concepts. Modeling these systems is an interdisciplinary approach, thus, there are typically 3 different kinds of models: Complex control models with simplified thermal models, complex thermal models with simple control strategies, or co-simulation between different modeling software.

Complex Control Strategies: Several publications with simplified thermal models for heating demand estimation can be found in literature, like [15], where the authors use a minimalistic model of space heating. It is assumed to be a certain percentage of the overall energy

* Corresponding author. University of Technology, Ehitajate tee 5, 19086, Tallinn, Estonia.
E-mail address: tobias.haring@taltech.ee (T. Häring).

<https://doi.org/10.1016/j.job.2021.103150>

Received 27 April 2021; Received in revised form 8 August 2021; Accepted 16 August 2021

Available online 17 August 2021

2352-7102/© 2021 Elsevier Ltd. All rights reserved.

consumption, and based on that, a price-based control strategy is proposed. A multi-agent system with a simple aggregated model of the space heating/cooling is used in Ref. [16] to show DSM strategies. In Ref. [17] price-based control algorithms are shown depending on the occupancy in the rooms. Nevertheless, the used thermal model is very simplified. Similarly, in Ref. [18] a DSM approach for assessing the flexibility of heat pumps is shown with simple thermal models for the houses and heat pumps. Additionally [19], shows, that such DSM strategies are not limited to grid-connected systems but can be utilized in (temporarily) islanded microgrids as well. The proposed thermal models are simplified temperature-difference-based models.

Complex Thermal Models: Other papers present quite accurate thermal models, but do not take into account the electrical control strategies or only in a limited way. The authors of [20] for example have a linear time-series model based on historical measurement data. This model is computationally quite inexpensive and shows good results, but there are no considerations about possible control strategies for DSM. Similarly, authors of other publications, like [21], do not consider DSM methods at all but can present very detailed thermal models. A very detailed heat pump model is presented in Ref. [22], but the proposed control strategies are quite simple and do not provide the full flexibility potential, which could be achieved. The authors of [23] present detailed thermal models of buildings. The proposed DSM control strategies however are limited to a simple pre-charging of thermal storages for expected peaks and do not show the anticipated results for peak reduction without additional constraints. Similarly in Ref. [24] the thermal model is quite accurate, but the control is quite static as it is based on a day-ahead price pattern.

Co-Simulation: Another possibility to enable the simulation of complex DSM control strategies with complex thermal models is the application of co-simulation software. Civil engineering software often does not provide sufficient tools to create a complex DSM control and electrical engineering software has only limited capabilities for thermal models, respectively, implementation of such is very time-consuming in both cases. Thus, co-simulation is a viable solution to bring both simulations together [25] and use the complexity and detail of each simulator. One way for co-simulation is the functional mock-up interface (FMI) or functional mock-up units (FMU) that are supported by some simulators like Matlab or Python, like shown in Ref. [26]. Similarly, this is presented in Ref. [27], where the building is modelled in EnergyPlus and the control is modelled in Modelica. The building model and control are connected in Ref. [28] with the SimAPI software platform to enable co-simulation. A good overview of co-simulation is presented in Ref. [29], where fundamental disadvantages of co-simulation, slow speed and limited compatibility, are shown, which apply to the above-mentioned publications [25–28] as well:

- Additional overhead for coordinating and synchronizing
- Initialization of some simulators for each macro time step
- Limited communication and data exchange between simulators
- Complicated implementation in real-time simulations

Thus, the publications that provide complex control strategies for demand-side management with space heating/cooling are lacking complex thermal models and rely on simplified temperature difference based or aggregated models. Vice versa, articles presenting complex space heating/cooling models can provide very detailed models in the thermal domain, but the control strategies are limited to fixed setpoint control or other simple methods if they are considered at all. In the field of co-simulation, there are other limitations, like connection, communication, and compatibility issues. A communications overhead can slow those simulations down as well.

Another trend in the field of smart grids apart from flexibility analysis is the use of machine learning methods due to the increasing number of smart meters and their collected data. An overview of the different possible applications of machine learning in smart grids is given in

Ref. [30]. A very popular application is the forecasting of residential loads, like shown in Ref. [31], often in the context of flexibility considerations [32] or load modeling [33]. The second important application is control, e.g. energy management in general [34], power flow control [35], or bidding strategies [36]. But modeling a space heating object with machine learning algorithms for DSM simulations has not been researched in detail yet.

Considering this, the aim of this work is to develop a methodology for designing space heating/cooling models, with high accuracy at low computational expense which can be used for smart city simulations. The novel proposed method for creating a space heating model in electrical engineering software presented in Section 2 in this work is the following: Since detailed measurement data, like in Ref. [37], is often not available, simulation data from accurate models, like [21], is used for training of a neural network (NN) to create an object model of space heating. This pre-trained model is more accurate than a simplified thermal model and can be calculated multiple times faster in a smart grid simulation than a co-simulation, while providing a similar level of complexity within its defined framework. An additional benefit is the integration of the model into e.g. real-time simulations [38] without additional changes to the Matlab model.

2. Material and methods

The final aim of the work is to develop a methodology for designing space heating/cooling models intended for smart grid simulations, which provide high accuracy and compatibility while being computationally light. This can be achieved by using a machine learning algorithm to synthesize a space heating model from simulation data of an accurate, pre-validated civil engineering model. Different time series and machine learning-based algorithms, like multivariate adaptive regression splines (MARS), linear regression, NN or gene expression programming (GEP), could be used for this purpose, which will show minor differences in their performance. Of those algorithms, the NN has been selected to show the major differences in performance of this novel modeling method compared to a simple white box model and co-simulation because it is a commonly used algorithm. These NN-based models can include rooms, apartments, or whole buildings for micro-grid simulations using complex civil engineering models as a basis. To achieve this, the following approach is taken in this work:

- In Section 2.1, the first stage of the approach is described. A suitable, existing thermal model of a room, apartment or building, which can

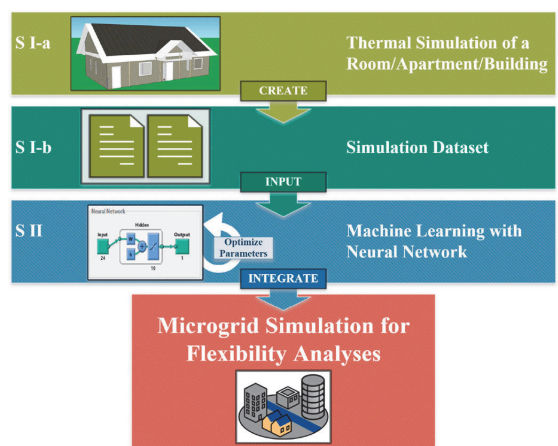


Fig. 1. Generalized methodology overview.

be implemented in any civil engineering software, is used as a starting point to create datasets (c.f. Fig. 1: S I-a). In this case, the room and building models are built in IDA ICE 4.8. SP1, Expert edition [39]. It is a validated building energy simulation software [40,41] using a numerical solver with a changing time step [42]. The created datasets need to include all possible environmental influences to enable the development of a comprehensive machine learning model. A suitable time step needs to be chosen for the data as well as a general supported file format of the dataset. The datasets can then be used as the input data for the training of the machine learning algorithm (c.f. Fig. 1: S I-b).

- The second stage (c.f. Fig. 1: S II), which is described in Section 2.2, is the training and optimization of the neural network model. For creating a neural network model, a suitable and commonly used software in electrical engineering, like Python, could be used. In this case, Matlab R2019a [43] with the Deep Learning [44] and Parallel Computing [45] toolboxes is selected for the machine learning model and microgrid simulation. Using the datasets from the first stage as input for training, cross-validation, and test, it is possible to see the accuracy of the created machine learning model. If the accuracy is not high enough, then the parameters for the neural network can be changed to optimize the model. If the accuracy is good, then the machine learning model can be converted to a function and it be integrated into an electrical microgrid simulation.

The generalized overview of the methodology is given in Fig. 1.

2.1. Creation of datasets with thermal models in IDA ICE software

The documentation of IDA ICE shows compliance to CEN standards EN 15255–2007 and EN 15265–2007 and is validated against several other standards such as CEN Standard EN 13791 and ASHRAE Standard 140–2004 [46], which is needed as a basis for properly validated civil engineering models. Different existing and pre-validated IDA-ICE objects have been used in this work. The first one is a model of a simple room, which was used to be able to compare it with a simple white-box model. This white-box model has been developed based on temperature differences in previous studies [11]. A model of a single-family house, which represents a typical building in many suburbs, is used to compare more complex room models of such a house to the model of the simple room. This small house model is extended with more realistic stochastic usage profiles to be able to create more comprehensive datasets, which are necessary for flexibility simulations in Microgrids.

2.1.1. Simple room model

As the first civil engineering model, a simple room model was chosen for representing a room of an apartment building or a private house. This room model has been previously described and validated in two conference papers [47,48].

An electric radiator of 400 W heats the room. The radiator has been sized according to the Estonian heating design standard [49], with an added 20% power for a safety margin. A thermostat with ± 1 °C dead-band controls the radiator valve to maintain a constant air temperature setpoint of 21 °C. The building has balanced mechanical heat recovery ventilation, which is practically compulsory in new buildings in Estonia to meet the energy performance requirements. The room usage profiles (schedules for appliances, lights, and people) have been modelled as foreseen for energy calculation of the apartment buildings by the Estonian law [50].

2.1.2. Small house model

The house model represents a small single-family home with one floor and a detached roof. This is one of the sample houses used for redefining the cost-optimality level of nearly zero energy buildings (nZEBs) for new residential buildings in Estonia [51]. The model has been validated for the sample project and the documentation of the

project is available online [52–56]. The building and its model have been developed, validated and used by Simson et al. in several previous studies [57,58]. The 100 m² large ground floor was modelled as 11 thermal zones (c.f. Fig. 2). The rooms have electric underfloor heating (UFH) with 100 W/m² installed power. The power output of such a system is several times higher than the needed power, but this is a common solution as the UFH circuit is installed over the entire floor. The electric UFH circuits were controlled by thermostats zone by zone. The upper floor was modelled free-floating i.e. unheated and as one zone. All rooms except the attic were equipped with balanced heat recovery ventilation.

2.1.3. Small house model (stochastic)

In the stochastic cases, more realistic usage profiles are generated for the rooms in the small house model. Stochastic profiles improve the complexity of the machine learning model as well as providing data for different setpoint- and temperature levels. This is necessary for simulations with changing setpoints, like flexibility analyses. In the typical case, the usage schedules were the same as in the simple room, but the maximum powers were adapted so that the stochastic and typical scenarios had an equal annual sum of internal gains.

The occupancy profiles were generated in the ProccS web tool [59] for a family of 2 adults and one child. This tool has been developed, tested and validated in a doctoral thesis [60]. The profile generator assumes that the adults go to work and the child to school/kindergarten on weekdays [61]. The profiles were generated twice and used the bathroom profile from the second run for the WC and the profile of the living room for the office. This can result in up to five people in the house, but this can be even more realistic considering guests. Rooms that are not often used (laundry room, technical room, corridor, hall) have no occupancy.

The lights are switched on when people are in the room and the direct solar radiation outdoors is less than 150 W/m² on a plane normal to solar rays. In bedrooms, additional off-times for lights were defined. For the master bedroom, this is 12 p.m. to 6 a.m. and for the child bedroom, it is 9.30 p.m. to 7 a.m. In the rooms that would not be used often, standard light profiles were applied as in simple test room energy calculation [50]. Standard profiles and powers were used for appliances the same way as in the typical case for all rooms.

Room temperature setpoints were varied according to typical usage. The setpoint was at 22 °C on weekdays from 6 to 8 a.m. and 5–9 p.m. and on weekends from 8 a.m. to 10 p.m. At other times, the setpoint was set to 18 °C to include nighttime temperature reductions for sleeping

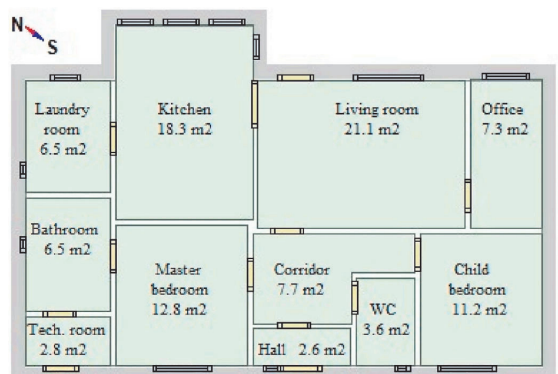


Fig. 2. Floor plan of the small house, doors are denoted with yellow, windows with blue color, floor area of each room is noted, master bedroom geometry is similar to the simple room model. (For interpretation of the references to color in this figure legend, the reader is referred to the Web version of this article.)

comfort and energy saving.

2.1.4. Creation of comprehensive datasets

To create a machine learning model in Matlab, a suitable dataset for the training of the algorithm is necessary. Therefore, simulations with each of the models, a simple room, a small house, and a small house (stochastic) model, are conducted. To get a suitable amount of training data, the simulation period is 1 year with a 1-min output time step. Since the time constant for space heating systems is typically quite large, the 1-min time step is sufficiently small to cover the dynamics of the heating system. The period of 1 year ensures, that all the different environmental situations are covered in the training data. This means cold temperatures in winter, high temperatures in summer, day and night cycles, different wind and irradiation conditions, heating/standby cycles of the heating system, different occupancy situations, etc. are included. The relevant variables for each of the models are presented in Table 1. For the small house model and the small house (stochastic) model, only the 7 relevant rooms (c.f. Table 6) with occupancy profiles are included. The other rooms can be omitted to reduce the training time, as these rooms are typically not occupied or actively heated in most households. Thus, they do not have an active energy consumption for heating and their internal influence on the other rooms will be automatically included in the machine learning model.

2.2. Development of space heating models based on neural networks

In this section, the different developed machine learning models are described. As the datasets from the simple room and the small house model only contain data with a fixed setpoint, the resulting machine learning models will also just represent this fixed setpoint and are therefore just suitable for validation and error comparison purposes. In a flexibility analysis, it is necessary to change the setpoint. This is possible with the small house (stochastic) model dataset, as it contains data with changing setpoints. The neural network model can learn the setpoint changes as well as different setpoint- and indoor air temperature levels. These small house (stochastic) machine learning models can be used in microgrid simulations for flexibility analyses. The flowchart for the whole process is shown in Fig. 3.

2.2.1. Proposed dataset pre-processing

To have suitable data for the training of the NNs, it is necessary to import and pre-process the data stored in the IDA ICE simulation output files and the weather-data file, which was used for the previous simulations. The variables are shown in Table 1.

Table 1

Relevant variables for the machine learning model creation for each model, that were logged in the dataset creation simulations.

General variables
• Dry-bulb temperature [°C]
• Relative humidity of air [%]
• Direction of wind
• Speed of meteorological wind [m/s]
• Direct normal radiation [W/m ²]
• Diffuse radiation on horizontal surface [W/m ²]
Room-based variables
• Mean air temperature [°C]
• Heating energy [W] ^a
• Ventilation [W] ^a
• Infiltration and openings [W] ^a
• Occupancy (Number of People)
• Energy losses [W] ^a
• Internal wall energy exchange [W] ^a
• Equipment heat energy [W] ^a
• Windows and solar gains [W] ^a
• Cooling energy [W] ^a
• Lighting energy [W] ^a

^a Sensible heat gains/losses.

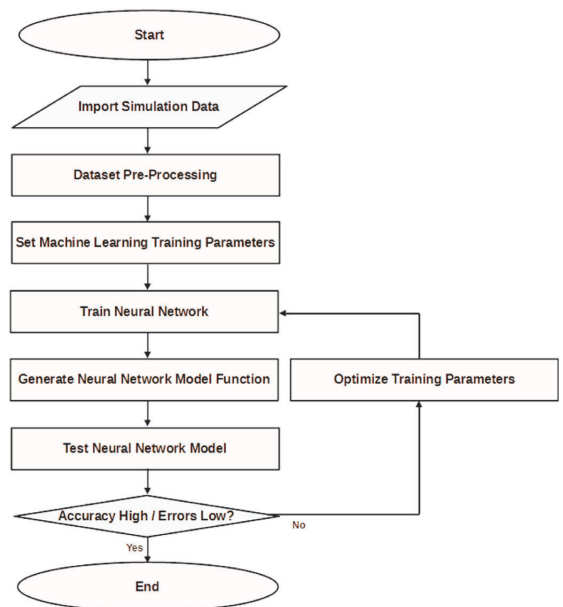


Fig. 3. Flowchart for the development of the neural network models.

The temperature difference between the time steps is calculated (1), which is necessary as the target vector respectively array for training the machine learning model.

$$\Delta T(i) = T(i+1) - T(i) \quad (1)$$

Using: $T(i)$: Mean air temperature of time step i [°C]; $T(i+1)$: Mean air temperature of time step $i+1$ [°C]; and $\Delta T(i)$: Temperature difference between time step i and $i+1$ [°C];

Additionally, the weather data needs to be added to the input data array. After importing the hourly weather data, it is necessary to convert the data into minute data to fit the time step of the heating-simulation output files. Therefore, each value is duplicated 59 times to have one value for each minute. Typically, a linear interpolation would be more reasonable in this case and lead to better results. However, the model is supposed to be useable in a real-time prediction context (e.g. 1 min/5 min/15 min ahead prediction) as well, where often hourly weather data is available. In this case, there won't be a linear interpolation between the values and a model already trained with non-interpolated data will be more suitable. In total, the input array contains the variables shown in Table 1 and the target vector respectively array contains the temperature differences for training the correct output of the NN. To reduce the calculation time of the machine learning training, the variables, which are 0 over the whole dataset, are removed.

The input and target data need to be added for all the rooms, which

Table 2

Selected neural network models.

Model	Sub-model	Description
Simple room	–	1 NN model for the simple room
Small house	1 room	1 NN model for the living room
	7 rooms	1 NN model for all 7 rooms
	7 rooms, separate	7 NN models for 7 rooms (1 NN for each room)
Small house (stochastic)	1 room	1 NN model for the living room
	7 rooms	1 NN model for all 7 rooms
	7 rooms, separate	7 NN models for 7 rooms (1 NN for each room)

are represented by one machine learning model. For the simulations, the chosen models are shown in Table 2.

As training with machine learning algorithms is more efficient with normalized data, all the input and target variables are normalized (2), (3).

$$X_{data, norm}(i, k) = \frac{X_{data}(i, k) - \mu(k)}{\sigma(k)} \quad (2)$$

$$T_{data, norm}(i, l) = \frac{T_{data}(i, l) - \mu(l)}{\sigma(l)} \quad (3)$$

Using: $X_{data, norm}(i, k)$: Normalized input data of time step i and variable k ; $X_{data}(i, k)$: Input data of time step i and variable k ; $T_{data, norm}(i, l)$: Normalized target data of time step i and variable k ; $T_{data}(i, l)$: Target data of time step i and variable k ; μ : mean value of variable k resp. l ; and σ : standard deviation of variable k resp. l ;

The detailed flowchart for this process is shown in Fig. 4.

2.2.2. Training of the neural network models

The selected sizes for the two hidden layer networks of the different models are shown in Table 3 and the selected architecture is shown in

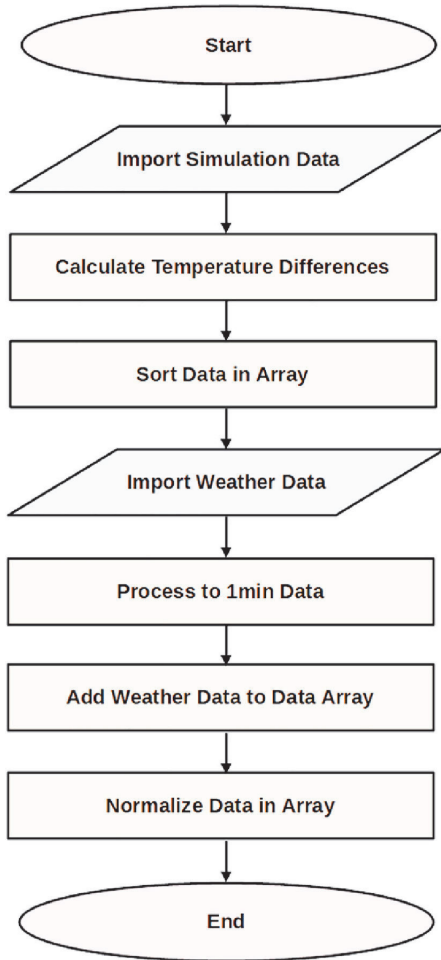


Fig. 4. Flowchart for dataset pre-processing.

Fig. 5 on the example of the 1-room model of the small house (stochastic). These values have been found with a structured optimization and showed good results for the different models (c.f. Section 3): The best starting point for finding the optimum number of neurons is chosen as 2/3 the size of the input layer for the first hidden layer, and half the size of the first hidden layer for the second hidden layer. The optimum number can then be found by decreasing or increasing the number of neurons slowly and checking if the accuracy of the model improved. If the model is underfitting with too few neurons, the accuracy will be bad as it cannot represent the data sufficiently. On the other hand, with an overfit model, with too many neurons, the accuracy is bad as well, because the model can only represent the training samples but not the variations in the cross-validation and test data.

From the input training set, a ratio of 60% for training, 20% for cross-validation and 20% for testing is selected. Fitting, cross-validation and prediction tests are done internally within the Matlab training function. To speed up the training of the machine learning model, GPU computing is enabled. This only supports the scaled conjugate gradient algorithm [62] for training. After training is finished the NN is saved as a separate function, which can be used in other scripts. This function can be calculated faster by Matlab and has better compatibility for use in combination with other software, for example in real-time simulations.

2.2.3. Validation of neural network models with test-simulations

To validate the machine learning model, the input data is loaded and normalized again as described previously. The input dataset for each time step is sent to the machine learning model to calculate the temperature difference to the next time step (4). This temperature difference is then added after denormalization to the mean air temperature of the input data (5) and can be compared to the actual mean air temperature $T(i+1)$ of the next time step.

$$\Delta \tilde{T}_{norm}(i) = NN(X_{data, norm}(i)) \quad (4)$$

$$\tilde{T}(i+1) = T(i) + \left(\left(\Delta \tilde{T}_{norm}(i) * \sigma \right) + \mu \right) \quad (5)$$

Using: $\Delta \tilde{T}_{norm}(i)$: normalized calculated temperature difference between time step i and $i+1$ [°C]; $NN()$: neural network function; $\tilde{T}(i+1)$: Calculated mean air temperature for time step $i+1$ [°C];

Next, this calculated mean air temperature is normalized and replaces the pre-simulated mean air temperature of time step $i+1$ in the input data. Additionally, the same thermostatic 2-step controller like in the pre-simulations with a ± 1 °C deadband is implemented to control the heating of the rooms according to their calculated mean air temperature. The output of this controller $\{0; 1\}$ multiplied by the maximum heating energy replaces the heating energy in the input data continuously for each time step. Losses from that heating energy to e.g. the ground, which never reach the room for heating, are already included in the machine learning model, as it was trained with such data. This results in a simple simulation with the same framework as the pre-simulations with the civil engineering model. Thus, these models can directly be compared to each other in a quantitative way.

The selected comparison metrics are the following:

- Root mean square error (RMSE) of the mean air temperature (6)
- RMSE of the heating power per square meter (7)
- Mean heating power difference (8)
- Percent of time steps with correctly estimated heating power (9)

$$RMSE_T = \sqrt{\mu \left((T - \tilde{T})^2 \right)} \quad (6)$$

Using: μ : Mean value; T : Pre-simulated mean air temperature [°C]; \tilde{T} : Calculated mean air temperature [°C];

Table 3
Neural network layer sizes for the different models.

Model	Number of rooms	Input Variables	Neurons Hidden Layer 1	Neurons Hidden Layer 2	Target/Output Variables
Simple room	1	17	10	5	1
Small house	1	17	10	5	1
	7	82	70	50	7
Small house (stochastic)	1	17	20	10	1
	7	82	90	50	7

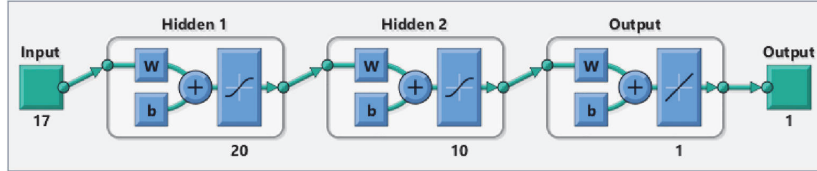


Fig. 5. Neural network architecture for the 1-room model of the small house (stochastic).

$$RMSE_P = \frac{\sqrt{\mu((P - \tilde{P})^2)}}{A_{Room}} \quad (7)$$

Using: μ : Mean value; P : Pre-simulated heating power [W]; \tilde{P} : Calculated heating power [W]; A_{Room} : Room area [m²];

$$\bar{P} = \frac{\mu(P) - \mu(\tilde{P})}{\mu(P)} * 100\% \quad (8)$$

$$TSA = \mu(\Delta P) * 100\% \quad (9)$$

Using: TSA : time step accuracy; $\Delta P(i) = 1$ if $P(i) - \tilde{P}(i) = 0$; otherwise 0;

These metrics are compared for all models (simple room, small house and small house (stochastic)), including their sub-models with the different numbers of rooms (1 and 7 rooms). Additionally, a simplified model of the simple room, based on the model in Ref. [11], is added to the comparison. The temperature difference model can be described with (10).

$$T(i+1) = T(i) + T_h(i) - T_{vent}(i) - T_{amb}(i) + T_{occ}(i) + T_{rad}(i) \quad (10)$$

Using: T_h : Temperature change due to heating [°C]; T_{vent} : Temperature change due to ventilation [°C]; T_{amb} : Temperature change due to ambient losses [°C]; T_{occ} : Temperature change due to room occupancy [°C]; T_{rad} : Temperature change due to sun irradiation through windows [°C];

The calculation of these temperature difference values is shown in detail in Ref. [11]. The values have been adapted to the same conditions as the simple room model.

As an additional model quality indicator, an uncertainty analysis was conducted. For this purpose, multiple simulations like the simulations described for the evaluation of the error metrics were set up. The total simulation time for each of the simulations were 10 days with 1min time steps and for each of the simulations the initial parameters are varied slightly for all 7 included rooms. This led to a total number of simulations of 1921 with a simulation time of 10 days each. The uncertainty analysis was carried out for the electrical power consumption of the space heating model because that is the most relevant parameter for an electrical power flow simulation. Therefore, the standard deviation between those 1921 simulations could be obtained and the uncertainty for the neural network-based models could be calculated with (11):

$$u_{NN} = \frac{\text{standard deviation}}{\sqrt{\text{number of simulations}}} \quad (11)$$

The uncertainty of the Matlab calculation itself can be neglected in

this case, as Matlab calculates with 16 digits, resulting in an additional uncertainty several magnitudes smaller than the model uncertainty.

2.2.4. Documentation about input and output parameters and data for each methodology step

All main steps of the methodology process are summarized in Table 4 in chronological order for a 1-room model of the small house (stochastic). The input and output parameters and data are documented in the table for each step of the proposed method.

3. Results

After training the different machine learning models and sub-models, it is necessary to evaluate and compare them to estimate their performance and errors. Based on this it is possible to select the best model to use in a microgrid simulation. The uncertainty analysis for the neural network-based space heating models shows a standard deviation of 1.25%. This corresponds to an uncertainty of 0.03% for these test simulations, which proves the stability of the proposed modeling method and the ability to handle small differences within the operational limits of the model.

3.1. Simple room model

The test simulation with error calculations is carried out for the simple room model to have quantitative values for comparison with the simplified model from Ref. [11]. The results of the temperature and power calculations are shown in Fig. 6 and Fig. 7, and the errors are shown in Table 5. The temperature and power graphs show good results, which is confirmed by the error metrics. The time step accuracy (TSA) is high, which means that the power is calculated correctly for most of the time steps. The mean power is very close to the actual value with a 2.6% error. Additionally, it can be seen that the machine learning model is more accurate than the simplified model from Ref. [11], as all the error metrics are better for the machine learning model.

3.2. Small house model

The temperature and power graphs for the small house model, 1 room sub-model are shown in Fig. 8 and Fig. 9. The error metrics are included in Table 5. The living room is chosen, as it is a more complex and larger room, and the bedroom is similar to the simple room. The graphs and metrics show, that the models for both rooms of the small house model show slightly worse performance than the simple room machine learning model. To be able to compare the two machine

Table 4
Input and output documentation for each step of proposed methodology for a 1-room model of the small house (stochastic).

Main methodology process	Input data	Output data
Dataset creation, dataset pre-processing and neural network training Simulation with civil engineering model & logging of relevant variables	<ul style="list-style-type: none"> Pre-validated civil engineering model 	<ul style="list-style-type: none"> 3 files with 11 room-based variables with 525,600 1min time steps 1 file with 6 weather data variables with 8760 1h time steps 11x525,600 input data array
Import dataset of 11 room-based variables	<ul style="list-style-type: none"> 3 files with 11 room-based variables with 525,600 1min time steps 	<ul style="list-style-type: none"> 11x525,600 input data array
Calculate temperature changes between time steps & add create target data array	<ul style="list-style-type: none"> 11x525,600 target data array 	<ul style="list-style-type: none"> 1x525,600 target data array
Import weather data, convert it to 1min data & add it to input data array	<ul style="list-style-type: none"> 1 file with 6 weather data variables with 8760 1h time steps 11x525,600 input data array 17x525,600 input data array 	<ul style="list-style-type: none"> 17x525,600 input data array
Normalize data in arrays	<ul style="list-style-type: none"> 1x525,600 target data array 17x525,600 normalized input data array 1x525,600 normalized target data array 	<ul style="list-style-type: none"> 17x525,600 normalized input data array 1x525,600 normalized target data array
Create and train NN	<ul style="list-style-type: none"> 17x525,600 normalized input data array 1x525,600 normalized target data array 	<ul style="list-style-type: none"> 1 neural network model with 17 inputs, 20 neurons in 1st hidden layer, 10 neurons in 2nd hidden layer and 1 output
Convert NN-model to function	<ul style="list-style-type: none"> 1 neural network model with 17 inputs, 20 neurons in 1st hidden layer, 10 neurons in 2nd hidden layer and 1 output 	<ul style="list-style-type: none"> 1 NN-function with 17 input parameters and 1 output parameter
Validation of neural network models with test simulations		
Import dataset of 11 room-based variables	<ul style="list-style-type: none"> 3 files with 11 room-based variables with 525,600 1min time steps 	<ul style="list-style-type: none"> 11x525,600 input data array
Import weather data, convert it to 1min data & add it to input data array	<ul style="list-style-type: none"> 1 file with 6 weather data variables with 8760 1h time steps 11x525,600 input data array 17x525,600 input data array 	<ul style="list-style-type: none"> 17x525,600 input data array
Normalize data in arrays and remove temperature and power values	<ul style="list-style-type: none"> 17x525,600 input data array 15x525,600 input data array 	<ul style="list-style-type: none"> 15x525,600 normalized input data array 17x525,600 output data array
Evaluate each row of the input data array (+calculated temperature and power values) with the NN-function; calculate temperature and power values for next time step with output from the previous row evaluation	<ul style="list-style-type: none"> 15x525,600 input data array 	<ul style="list-style-type: none"> 17x525,600 output data array
Evaluate errors of temperature and power variables in output array compared to input data array	<ul style="list-style-type: none"> 17x525,600 input data array 17x525,600 output data array 	<ul style="list-style-type: none"> 4 error metrics

learning models directly, the same number of neurons was chosen for both models (c.f. Table 3). The small house models are more complex than the small room model and therefore the machine learning model should have more neurons to efficiently learn from the dataset. The performance metrics are still sufficient. The TSA is much higher than with the simplified model and the mean power error is even better than with the simple room machine learning model. The RMSE for the power is higher for the small house models than for the simple room model but better than the simplified model. This results in a higher absolute RMSE with about the same relative error. The RMSE for the temperature is twice as high.

The combined 7-room sub-model (c.f. Table 6) seems to have worse error metrics than the 1-room model in Table 5. This suggests that a higher number of rooms in one neural network model increases the complexity and reduces the model accuracy.

Comparing the combined and separate 7-room sub-models for the small house, the following observations can be made (c.f. Table 6):

- The TSA for the combined model is worse than with separate models
- The mean power error is significantly smaller for the separate models compared to the combined model
- The RMSE for the power is lower for the separate models
- The RMSE for the temperature seems to be better for the combined model.

A higher number of rooms as input data increases the complexity that needs to be learnt by one neural network. This does not only lead to an increased training time with a significant increase of neurons but also reduces the overall accuracy of the space heating models of the rooms.

These observations suggest that the use of separate models for the rooms is preferable, as all metrics for the electrical power are better, which are more important in a microgrid simulation in the field of electrical engineering than the exact temperature prediction.

3.3. Small house (stochastic) model

Comparing the small house (stochastic) 1-room sub-model to the other 1-room models shows a good performance for this machine learning model (c.f. Table 5). It is evident, that the error metrics are even better than with the small house model. This is due to the increased number of neurons that can represent this more complex model (c.f. Table 3). The TSA is nearly as good as for the simple room machine learning model and the mean power error is extremely low. The RMSE for the power is higher for the small house (stochastic) models than for the simple room model but better than the simplified model and the small house model. The RMSE temperature value is between the simple room and the small house model.

Comparing the 1- and 7-room sub-models, the same conclusion as with the small house model can be drawn. The more rooms are included in the model, the lower the TSA, mean power error, RMSE for power and RMSE for temperature. The combined and separate 7-room sub-models for the small house (stochastic) model show mostly the same behavior as the corresponding small house models (c.f. Table 7). In the case of the small house (stochastic) models, all error metrics are better for the separate models compared to the combined one. Comparing the small house (stochastic) models with the small house models (c.f. Table 6) shows, that, apart from the mean power error, all metrics are better. It can be concluded that the overall results for the small house (stochastic) are better than for the small house. The selected number of neurons fits better the selected data than in the case of the small house model. As mentioned before, only the separate 7-room small house (stochastic) models can be used for microgrid simulations.

4. Discussion, limitations and future work

The machine learning models themselves are showing good results. The error metrics that have been presented (c.f. Table 8), clearly show

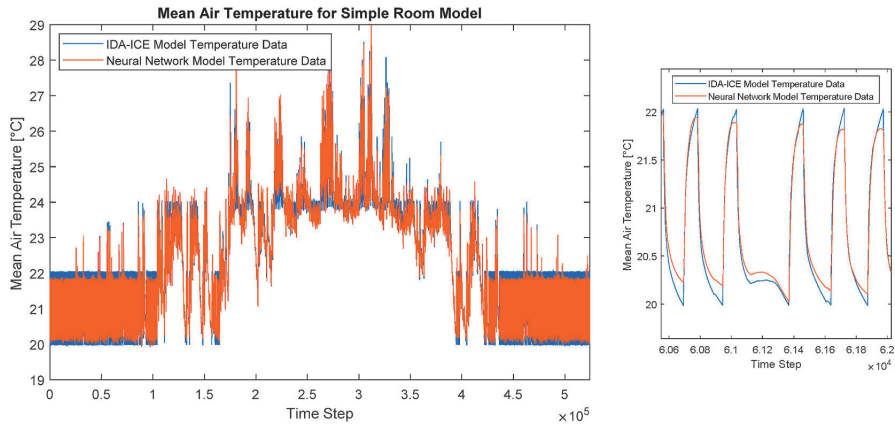


Fig. 6. Mean air temperature for simple room model in the test simulation with zoom-in.

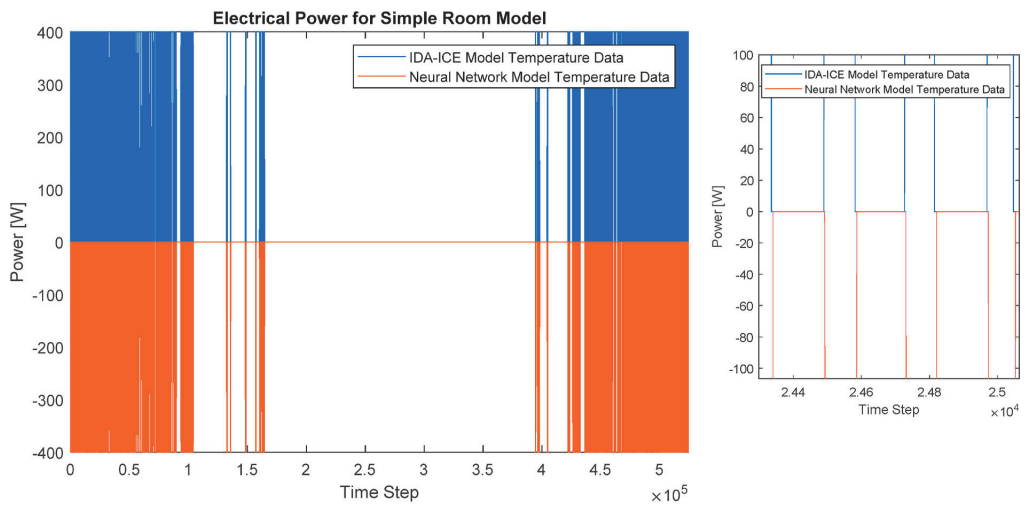


Fig. 7. Power data comparison between pre-simulation data and test simulation for simple room model (Calculated power data is shown in the negative y-direction) with zoom-in.

an improvement in accuracy for separate neural network models for each room compared to other methods used in literature. The other presented methods have been used for microgrid simulations with sufficient accuracy, therefore, the developed neural network models are suitable for microgrid simulations as well and even provide an improvement in accuracy. The results for separate models for each room of a building instead of one large neural network model for all rooms is preferable as the accuracy is higher and training time resp. need for computational resources for several small neural networks is less than for one large neural network model (c.f. Table 8).

However, additional effort is necessary to create training data, train the neural network models, and test and optimize them until they show desirable results. This is clearly a disadvantage compared to the simple models that are presented in other publications, like for example aggregated models.

On the other hand, the computational effort and time for the microgrid simulations can be reduced by a lot with the pre-trained neural network models, as a co-simulation with a detailed thermal model can take multiple amounts of those resources. This is especially

true if large simulations with multiple buildings and apartments are done. The computational effort with accurate thermal models can be too high. Then the neural network models present more accurate results than aggregated models, while keeping the computational effort on acceptable levels.

An overview of these advantages and disadvantages for the different modeling methods is shown in Table 9.

As mentioned before, the presented neural network models have low error margins. The accuracy compared to the simple model could be improved by 35–89%, depending on the different error metrics. These models were based on 1 year of 1-min simulation data. As with all machine learning algorithms, increasing this amount of data can improve the accuracy even more, but will as well increase the training time. Depending on the application, this additional training and accuracy might be an advantage. Another advantage is the low runtime during microgrid simulations. The neural network object models can be calculated as fast as the simple model. This is a reduction of calculation time of more than 80% compared to a co-simulation model without overhead.

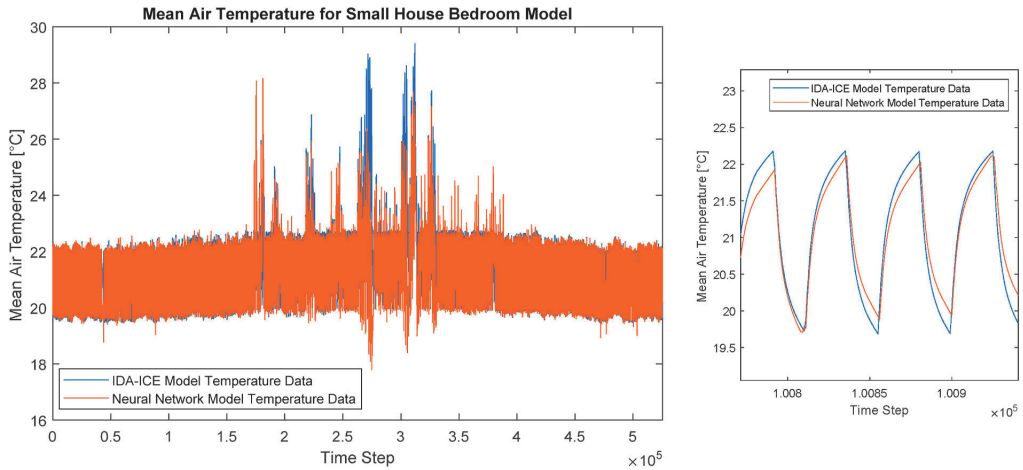


Fig. 8. Mean air temperature for small house bedroom model in the test simulation with zoom-in.

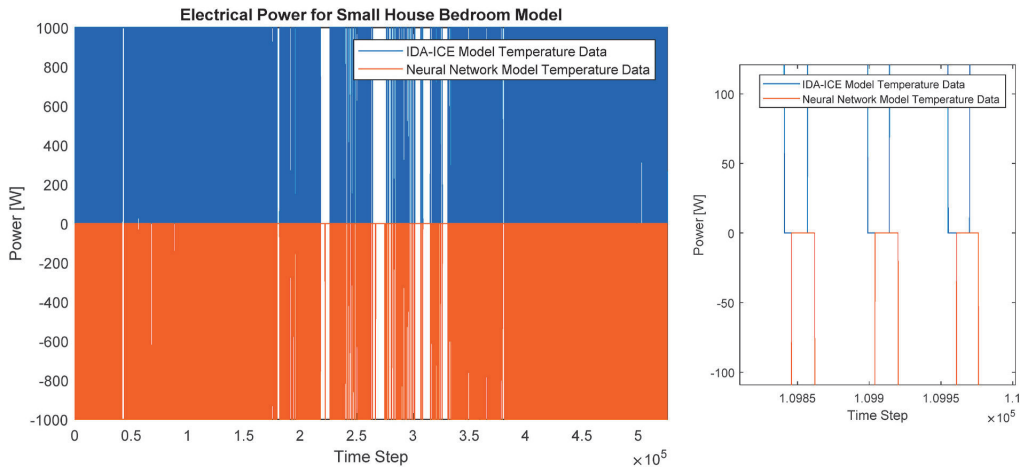


Fig. 9. Power data comparison between pre-simulation data and test simulation for small house bedroom model (Calculated power data is shown in the negative y-direction) with zoom-in.

Table 5
Comparison of errors for all 1-room models.

Model	TSA [%]	\bar{P} [%]	$RMSE_p$ [$\frac{W}{m^2}$]	$RMSE_T$ [°C]
Simple Room: Simple Model [11]	63.54	8.3	27.63	0.92
Simple Room: ML Model	98.92	2.6	3.13	0.30
Small House: Living room	95.84	2.1	19.36	2.13
Small House: Bedroom	85.80	0.1	29.56	2.29
Small House (Stochastic): Living room	97.24	0.5	16.61	1.06
Small House (Stochastic): Bedroom	97.65	0.7	15.33	0.99

The big disadvantage of the neural network object models is the one-time dataset creation and pre-training, which amounts to about 62min. This means that you can only gain a time advantage if you do 4 or more microgrid simulations with this model compared to a co-simulation without overhead. But usually, microgrid simulations need to be run

multiple times for control optimizations. The second disadvantage is that the accuracy is lower than with a co-simulation.

Another limitation of the neural network-based models is the operational range. The model can only present reliable results within the limits that it has been trained in. If the model has only been trained with data for the summer season, then it cannot predict the behavior during wintertime well. Thus, it is necessary to create suitable training data and check the training data limits to determine the operational range for the model.

The quality of the training data is essential for the quality of the neural network prediction. Thus, to get a good NN-based model, the civil engineering model needs to be properly pre-validated. The accuracy of the neural network model is limited by the accuracy of the civil engineering model and software that was used for the dataset creation.

For future work, the NN-based models need to be used in microgrid and smart city simulations with other devices and different control strategies, like reinforcement learning, to control the setpoints and do for example flexibility analyses. Different types of neural networks and

Table 6
Comparison of errors for combined and separate 7-room sub-models for the small house.

Small house	7 Rooms	Living Room	Office	Kitchen	Bedroom	Child-Room	Bathroom	Toilet	Average
TSA [%]	Combined	92.75	48.41	92.60	77.59	79.89	84.12	86.26	80.23
	Separate	95.84	77.42	93.90	85.80	89.32	88.37	92.05	88.96
\bar{P} [%]	Combined	2.5	8.2	2.5	8.2	3.7	1.2	2.4	4.1
	Separate	2.1	0.9	2.3	0.1	0.1	0.3	0.1	0.8
$RMSE_p \left[\frac{W}{m^2} \right]$	Combined	25.55	98.72	29.72	37.13	40.15	30.79	31.25	41.90
	Separate	19.36	65.31	26.97	29.56	29.25	26.38	23.76	31.51
$RMSE_T [^\circ C]$	Combined	1.23	1.40	1.55	1.59	1.73	1.41	1.27	1.45
	Separate	2.13	2.00	2.45	2.29	1.68	2.31	1.30	2.02

Table 7
Comparison of errors for combined and separate 7-room sub-models for the small house (stochastic).

Small house (stochastic)	7 Rooms	Living Room	Office	Kitchen	Bedroom	Child-Room	Bathroom	Toilet	Average
TSA [%]	Combined	91.07	92.32	88.37	96.47	91.28	87.30	92.83	91.38
	Separate	97.24	93.53	92.75	97.65	96.86	91.59	92.16	94.56
\bar{P} [%]	Combined	22.6	50.5	46.3	59.8	0.2	9.7	12.1	28.7
	Separate	0.5	11.4	0.1	0.7	7.6	3.4	6.1	6.1
$RMSE_p \left[\frac{W}{m^2} \right]$	Combined	29.88	24.39	34.10	18.79	29.53	33.74	15.94	26.62
	Separate	16.61	10.30	26.92	15.33	17.73	15.25	16.49	16.95
$RMSE_T [^\circ C]$	Combined	1.45	1.03	1.33	1.26	1.29	0.84	0.78	1.14
	Separate	1.06	0.56	1.17	0.99	0.72	0.37	1.27	0.85

Table 8
Overview of error metrics for selected presented models.

Model	TSA [%]	\bar{P} [%]	$RMSE_p \left[\frac{W}{m^2} \right]$	$RMSE_T [^\circ C]$	
Simple room [11]	63.54	8.3	27.63	0.92	
Simple room ^a	98.92	2.6	3.13	0.30	
Small house	1 room (bedroom) ^a	85.80	0.1	29.56	2.29
	7 rooms combined ^a	80.23	4.1	41.90	1.45
	7 rooms separate ^a	88.96	0.8	31.51	2.02
Small house (stochastic)	1 room (bedroom) ^a	97.65	0.7	15.33	0.99
	7 rooms combined ^a	91.38	28.7	26.62	1.14
	7 rooms separate ^a	94.56	6.1	16.93	0.85

^a Neural network model.

other time series and machine learning-based methods, like MARS or GEP, will show performance differences and should be compared in future work as well. Additionally, more buildings should be tested with this modeling approach, including different heating systems like heat pumps. Since there had to be some simplifications with the internal wall energy exchange for the simulation, a prediction model based on a neural network for the internal wall energy exchange should be added for better accuracy.

5. Conclusions

Space heating is a suitable thermal storage that can be utilized for flexibility or demand side management strategies. To run microgrid simulations for these strategies, it is necessary to have accurate and computationally inexpensive models for space heating. As this is an interdisciplinary research field, complex models of civil engineering and electrical engineering need to be brought together from different simulation software to avoid too many simplifications in space heating models. As co-simulation is often limited, this paper proposed a new methodology of using machine learning models to convert the civil engineering models into an electrical simulation framework.

An overview of the advantages and disadvantages of the different

Table 9
Overview of advantages and disadvantages for different modeling methods.

Model	Advantages	Disadvantages
Simplified white-box model	<ul style="list-style-type: none"> Fast to calculate during simulation (~3min calculation time for complete small house^a) No pre-training Highly compatible (part of the microgrid simulation) 	<ul style="list-style-type: none"> Lower Accuracy
Complex white-box models with co-simulation	<ul style="list-style-type: none"> Very good accuracy No pre-training 	<ul style="list-style-type: none"> High computational effort and slow during simulation (~20min calculation time for complete small house) Compatibility problems between simulators
Proposed machine learning based model	<ul style="list-style-type: none"> Fast to calculate during simulation (~3min calculation time for complete small house^a) Good accuracy within set limitations Highly compatible (part of the microgrid simulation) 	<ul style="list-style-type: none"> Pre-training (~6min per room^a) and creation of datasets (~20min for complete small house^a)

^a Intel Core i7 4770K CPU; Nvidia GeForce GTX 980Ti GPU.

methods is shown in Table 9. The neural network object model could improve the accuracy by more than 30% for all presented error metrics compared to a simple model and reduce the simulation time by more than 80% compared to a co-simulation without overhead. The big disadvantage of dataset creation and pre-training is only relevant if less than 4 microgrid simulations are done with the model.

Including multiple rooms in one neural network showed, that the accuracy is decreasing with the number of rooms. Therefore, it is advisable to create one machine learning model for each room of a building rather than including all the rooms in one large model. Table 8 presents a quantitative overview, showing improvements for the presented metrics of 3% for the TSA up to 80% for the RMSEp for this aspect.

Author statement

Tobias Häring: Conceptualization, Methodology, Software,

Validation, Investigation, Writing – original draft, Writing – review & editing, Visualization, Tuule Mall Kull: Methodology, Software, Validation, Resources, Writing – original draft, Writing – review & editing, Visualization, Roya Ahmadihangar: Conceptualization, Writing – review & editing, Argo Rosin: Conceptualization, Writing – review & editing, Supervision, Martin Thalfeldt: Resources, Writing – review & editing, Supervision, Helmuth Biechl: Writing – review & editing, Supervision

Declaration of competing interest

The authors declare that they have no known competing financial interests or personal relationships that could have appeared to influence the work reported in this paper.

Acknowledgements

This research was supported by the Estonian Centre of Excellence in Zero Energy and Resource Efficient Smart Buildings and Districts, ZEBE (grant No. 2014-2020.4.01.15-0016) and the programme Mobilitas Pluss (Grant No – 2014-2020.4.01.16-0024, MOBTP88) funded by the European Regional Development Fund, by the Estonian Research Council (grant No. PSG409), and by the European Commission through the H2020project Finest Twins (grant No. 856602).

References

- [1] D.E. Olivares, et al., Trends in microgrid control, *IEEE Trans. Smart Grid* 5 (4) (Jul. 2014) 1905–1919.
- [2] E.B. Iversen, J.M. Morales, J.K. Møller, P.-J. Trombe, H. Madsen, Leveraging stochastic differential equations for probabilistic forecasting of wind power using a dynamic power curve, *Wind Energy* 20 (1) (Jan. 2017) 33–44.
- [3] M. Stephant, D. Abbes, K. Hassam-Ouari, A. Labrumie, B. Robyns, Distributed optimization of energy profiles to improve photovoltaic self-consumption on a local energy community, *Simulat. Model. Pract. Theor.* 108 (Apr. 2021) 102242.
- [4] A. Rahmoun, A. Armstorfer, J. Helguero, H. Biechl, A. Rosin, Mathematical modeling and dynamic behavior of a Lithium-Ion battery system for microgrid application., *IEEE International Energy Conference (ENERGYCON)*, 2016, pp. 1–6, 2016.
- [5] A. Rosin, S. Link, M. Lehtla, J. Martins, I. Drovtar, I. Roasto, Performance and feasibility analysis of electricity price based control models for thermal storages in households, *Sustain. Cities Soc.* 32 (Jul. 2017) 366–374.
- [6] S. Sharda, M. Singh, K. Sharma, Demand side management through load shifting in IoT based HEMS: overview, challenges and opportunities, *Sustain. Cities Soc.* 65 (Oct. 2020), 102517.
- [7] F.S. El-Faouri, M.W. Alzahlan, M.G. Batarseh, A. Mohammad, M.E. Za’ter, “Modeling of a microgrid’s power generation cost function in real-time operation for a highly fluctuating load, *Simulat. Model. Pract. Theor.* 94 (Jul. 2019) 118–133.
- [8] F. Lu, Z. Yu, Y. Zou, and X. Yang, “Cooling system energy flexibility of a nearly zero-energy office building using building thermal mass: potential evaluation and parametric analysis,” *Energy Build.*, vol. 236, p. 110763, Apr. 2021.
- [9] S. Mishra, H. Koduvere, I. Palu, R. Kuhl-Thalfeldt, A. Rosin, “Assessing Demand Side Flexibility with Renewable Energy Resources,” in *IEEE 16th International Conference on Environment and Electrical Engineering (EEEIC)*, 2016, pp. 1–6.
- [10] G. Shen, Z.E. Lee, A. Amadeh, K.M. Zhang, A data-driven electric water heater scheduling and control system, *Energy Build.* 242 (Jul. 2021) 110924.
- [11] T. Haring, A. Rosin, H. Biechl, Using common household thermal storages to support the PV- and battery system in nearly zero energy buildings in off-grid mode, *Sustain. Energy Technol. Assessments* 35 (May) (Oct. 2019) 12–24.
- [12] V. Maask, T. Haring, R. Ahmadihangar, A. Rosin, T. Korotko, Analysis of ventilation load flexibility depending on indoor climate conditions. In *2020, IEEE International Conference on Industrial Technology (ICIT)*, 2020, pp. 607–612.
- [13] A. Belahsen, H. Dagdougui, Aggregated short-term load forecasting for heterogeneous buildings using machine learning with peak estimation, *Energy Build.* 237 (Apr. 2021) 110742.
- [14] European Commission, Ventilation units [Online]. Available: https://ec.europa.eu/info/energy-climate-change-environment/standards-tools-and-labels/products-labelling-rules-and-requirements/energy-label-and-codesign/energy-efficient-products/ventilation-units_en.
- [15] O. Kilkki, A. Alahäivälä, I. Seilonen, Optimized control of price-based demand response with electric storage space heating, *IEEE Trans. Ind. Informatics* 11 (1) (Feb. 2015) 281–288.
- [16] B. Feron, A. Monti, Integration of space heating demand flexibility in a home energy management system using a market-based multi agent system, in *IEEE Power and Energy Society General Meeting 2018-Janua* (2018) 1–5.
- [17] T. Haring, R. Ahmadihangar, A. Rosin, H. Biechl, T. Korotko, “Comparison of the Impact of Different Household Occupancies on Load Matching Algorithms,” in *2019 Electric Power Quality and Supply Reliability Conference (PQ) & 2019 Symposium on Electrical Engineering and Mechatronics, SEEM*, 2019, pp. 1–6.
- [18] M. Pau, J.L. Cremer, F. Ponci, A. Monti, impact of customers flexibility in heat pumps scheduling for demand side management. In *Conference Proceedings - 2017 17th IEEE International Conference on Environment and Electrical Engineering and 2017 1st IEEE Industrial and Commercial Power Systems Europe, IEEEIC/1 and CPS Europe 2017*, 2017.
- [19] T. Haring, R. Ahmadihangar, A. Rosin, H. Biechl, Impact of load matching algorithms on the battery capacity with different household occupancies. In *IECON 2019 - 45th Annual Conference of the, IEEE Industrial Electronics Society*, 2019, pp. 2541–2547.
- [20] P. Bacher, H. Madsen, H.A. Nielsen, B. Perers, Short-term heat load forecasting for single family houses, *Energy Build.* 65 (Oct. 2013) 101–112.
- [21] L. Georges, M. Thalfeldt, Ø. Skreiberg, V. Fornari, Validation of a transient zonal model to predict the detailed indoor thermal environment: case of electric radiators and wood stoves, *Build. Environ.* 149 (Feb. 2019) 169–181.
- [22] J. Clauß, L. Georges, Model complexity of heat pump systems to investigate the building energy flexibility and guidelines for model implementation, *Appl. Energy* 255 (Dec. 2019) 113847.
- [23] R.E. Hedegaard, M.H. Kristensen, T.H. Pedersen, A. Brun, S. Petersen, Bottom-up modelling methodology for urban-scale analysis of residential space heating demand response, *Appl. Energy* 242 (May 2019) 181–204.
- [24] T. Haring, A. Rosin, T.M. Kull, J. Helguero, H. Biechl, “Thermal Modelling of a Control Center for Flexibility Analysis in nZEB Nanogrids,” in *2020 IEEE 61st Annual International Scientific Conference on Power and Electrical Engineering of Riga Technical University, RTUCON 2020 - Proceedings*, 2020.
- [25] M. Vogt, F. Marten, and M. Braun, “A survey and statistical analysis of smart grid co-simulations,” *Applied Energy*, vol. vol. 222. Elsevier Ltd, pp. 67–78, 15-Jul-2018.
- [26] K. Wang, P.O. Siebers, D. Robinson, Towards generalized Co-simulation of urban energy systems, in *Procedia Engineering* 198 (2017) 366–374.
- [27] S. Huang, D. Wu, Validation on aggregate flexibility from residential air conditioning systems for building-to-grid integration, *Energy Build.* 200 (Oct. 2019) 58–67.
- [28] F. Pallonetto, E. Mangina, F. Milano, D.P. Finn, SimApi, a smartgrid co-simulation software platform for benchmarking building control algorithms, *SoftwareX* 9 (Jan. 2019) 271–281.
- [29] P. Palensky, A. A. Van Der Meer, C. D. López, A. Joseph, and K. Pan, “Cosimulation of Intelligent Power Systems: Fundamentals, Software Architecture, Numerics, and Coupling,” *IEEE Industrial Electronics Magazine*, vol. vol. 11, no. 1, Institute of Electrical and Electronics Engineers Inc., pp. 34–50, 01-Mar-2017.
- [30] A. Mosavi, M. Salimi, S. Faizollahzadeh Ardabili, T. Rabczuk, S. Shamsirband, A. Varkonyi-Koczy, State of the art of machine learning models in energy systems, a systematic review, *Energies* 12 (7) (Apr. 2019) 1301.
- [31] D. Wu, B. Wang, D. Precup, and B. Boulet, “Multiple Kernel learning-based transfer regression for electric load forecasting,” *IEEE Trans. Smart Grid*, vol. 11, no. 2, pp. 1183–1192, Mar. 2020.
- [32] R. Ahmadihangar, T. Haring, A. Rosin, T. Korotko, J. Martins, Residential load forecasting for flexibility prediction using machine learning-based regression model. In *Proceedings - 2019 IEEE International Conference on Environment and Electrical Engineering and 2019 IEEE Industrial and Commercial Power Systems Europe, IEEEIC/1 and CPS Europe*, 2019, pp. 1–4, 2019.
- [33] P. Prashanthi, K. Priyadarshini, A comparative study of the performance of machine learning based load forecasting methods, *Proc. - Int. Conf. Artif. Intell. Smart Syst. ICAIS (2021)* 132–136, Mar. 2021.
- [34] Y. Du and F. Li, “Intelligent multi-microgrid energy management based on Deep neural network and model-free reinforcement learning,” *IEEE Trans. Smart Grid*, vol. 11, no. 2, pp. 1066–1076, Mar. 2020.
- [35] X. Lei, Z. Yang, J. Yu, J. Zhao, Q. Gao, H. Yu, Data-Driven optimal power flow: a physics-informed machine learning approach, *IEEE Trans. Power Syst.* 36 (1) (Jan. 2021) 346–354.
- [36] Y. Ye, D. Qiu, M. Sun, D. Papadaskalopoulos, and G. Strbac, “Deep reinforcement learning for strategic bidding in electricity markets,” *IEEE Trans. Smart Grid*, vol. 11, no. 2, pp. 1343–1355, Mar. 2020.
- [37] M. Rätz, A. P. Javadi, M. Baranski, K. Finkbeiner, and D. Müller, “Automated data-driven modeling of building energy systems via machine learning algorithms,” *Energy and Buildings*, vol. vol. 202. Elsevier Ltd, p. 109384, 1-Nov-2019.
- [38] R. Ahmadihangar, A. Rosin, A.N. Niaki, I. Palu, T. Korotko, “A review on real-time simulation and analysis methods of microgrids, *Int. Trans. Electr. Energy Syst.* 29 (11) (Nov. 2019).
- [39] IDA ICE 4.8 SP1, Expert edition (2019).
- [40] S. Kropf, G. Zweifel, “Validation of the Building Simulation Program IDA-ICE According to CEN 13791 “Thermal Performance of Buildings - Calculation of Internal Temperatures of a Room in Summer without Mechanical Cooling - General Criteria and Validation Procedures”, 2001.
- [41] A.B. Equa Simulation, Validation of IDA Indoor Climate and Energy 4.0 Build 4 with Respect to ANSI/ASHRAE Standard 140-2004. , 2010.
- [42] A.B. Bris Data, “IDA Solver User’s Guide, no. October, 1999.
- [43] MATLAB - MathWorks - MATLAB & Simulink [Online]. Available: <https://se.mathworks.com/products/matlab.html>.
- [44] Deep Learning Toolbox - MATLAB [Online]. Available: <https://se.mathworks.com/products/deep-learning.html>.
- [45] Parallel Computing Toolbox - MATLAB [Online]. Available: <https://se.mathworks.com/products/parallel-computing.html>.
- [46] Validation & Certifications - Simulation Software | EQUA [Online]. Available: <https://www.equa.se/en/ida-ice/validation-certifications>.

- [47] T.M. Kull, R. Simson, M. Thalfeldt, J. Kurnitski, "Influence of time constants on low energy buildings' heating control, in *Energy Procedia* 132 (2017).
- [48] T.M. Kull, R. Simson, J. Kurnitski, Setback Efficiency of Limited-Power Heating Systems in Cold Climate, 2019, pp. 87–95.
- [49] EESTI STANDARD HOONETE KÜTTE PROJEKTEERIMINE Design of Heating for Buildings, 2016.
- [50] "Estonian Regulation No 58, Methodology for calculating the energy performance of buildings," Ministry of Economic Affairs and Communications, 2015.
- [51] Liginullenergia Eluhooned, Väikemajad, ", 2017.
- [52] O.Ü. Timbeco Woodhouse, Liginullenergia eluhooned, Väike eramu. Arhitektuur (2017).
- [53] TalTech, Liginullenergia eluhooned. Väike Eramu, Energiatöhusus, ", 2017.
- [54] O.Ü. Hevac, "Liginullenergia eluhooned, Väike Eramu Soojusvarustus, Küte Ja Ventilatsioon, ", 2017.
- [55] Roofit Solar Energy Oü, "Liginullenergia eluhooned, Väike Eramu. Päikese-Elektristüsteem Ja Tugevpool, variant 1, 2017.
- [56] Hevac Oü, Roofit Solar Energy Oü, Liginullenergia Eluhooned. Väike Eramu. Päikese-Elektristüsteem Ja Tugevpool, variant 2, 2017.
- [57] R. Simson, E. Arumägi, K. Kuusk, J. Kurnitski, Redefining cost-optimal nZEB levels for new residential buildings, *E3S Web Conf.* 111 (2019).
- [58] R. Simson, et al., "The Impact of Infiltration on Heating Systems Dimensioning in Estonian Climate," in *E3S Web of Conferences, 12th Nordic Symposium on Building Physics*, 2020 to be published.
- [59] S. Wolf, D. Cali, H. Madsen, Proccs, 2019 [Online]. Available: <https://www.proccs.org/>.
- [60] S. Wolf, Modelling Building Occupant Behaviour Using Hidden Markov Models, " Technical University of Denmark, 2019.
- [61] S. Wolf, et al., Room-level occupancy simulation model for private households, *J. Phys. Conf. Ser.* 1343 (1) (2019).
- [62] M.F. Møller, A scaled conjugate gradient algorithm for fast supervised learning, *Neural Network.* 6 (4) (Jan. 1993) 525–533.

Publication II

A. Antonov, T. Häring, T. Korötko, A. Rosin, T. Kerikmäe and H. Biechl, "Pitfalls of Machine Learning Methods in Smart Grids: A Legal Perspective," 2021 International Symposium on Computer Science and Intelligent Controls (ISCSIC), 2021, pp. 248–256, doi: 10.1109/ISCSIC54682.2021.00053.

Pitfalls of Machine Learning Methods in Smart Grids: A Legal Perspective

Alexander Antonov¹, Tobias Häring^{2,3}, Tarmo Korõtko^{2,3}, Argo Rosin^{2,3}, Tanel Kerikmäe¹, Helmuth Biechl^{2,3,4}

1- Department of Law, Tallinn University of Technology, Tallinn, Estonia

2- Department of Electrical Power Engineering and Mechatronics, Tallinn University of Technology, Tallinn, Estonia

3- Smart City Center of Excellence (Finest Twins)

4- Institute of Electrical Power Systems (IEES), University of Applied Sciences Kempten, Kempten, Germany
+372 6202002
alanto@ttu.ee

ABSTRACT

The widespread implementation of smart meters (SM) and the deployment of the advanced metering infrastructure (AMI) provide large amounts of fine-grained data on prosumers. Machine learning (ML) algorithms are used in different techniques, e.g. non-intrusive load monitoring (NILM), to extract useful information from collected data. However, the use of ML algorithms to gain insight on prosumer behavior and characteristics raises not only numerous technical but also legal concerns. This paper maps electricity prosumer concerns towards the AMI and its ML based analytical tools in terms of data protection, privacy and cybersecurity and conducts a legal analysis of the identified prosumer concerns within the context of the EU regulatory frameworks. By mapping the concerns referred to in the technical literature, the main aim of the paper is to provide a legal perspective on those concerns. The output of this paper is a visual tool in form of a table, meant to guide prosumers, utility, technology and energy service providers. It shows the areas that need increased attention when dealing with specific prosumer concerns as identified in the technical literature.

Keywords

Machine Learning, GDPR, Cybersecurity, EU, Smart City, Smart Grid

1. INTRODUCTION

Within the context of the Third Energy package and the latest Clean Energy for all Europeans Package, the EU made the roll out of smart meters (SM) mandatory to enable residential end-users a better overview of their energy consumption and raise energy efficiency [1]. However, the transformation of energy systems raises various legal concerns, specifically in terms data protection, privacy and cybersecurity [1]. While the deployment of SM allows for real-time tracking of individual households' energy consumption, it might bear reverse effects on their autonomy and potentially affect their fundamental rights in the areas of data protection and privacy.

This is especially evident in applications such as pattern-recognition and profiling which machine learning (ML) facilitates. Latest increases in malicious cyber operations by state proxies against states' critical infrastructure or "essential services" [2], which includes electricity grids, pose an additional challenge to the application of SM.

Smart appliances and home energy management systems (HEMS) are gaining popularity in smart grids in the EU. Renewable energy sources of buildings are typically connected to a HEMS, which shifts the building from a passive role as electricity consumer into an active role as prosumer [3] [4]. To facilitate prosumer needs for auxiliary electricity services, the distribution system operator (DSO) is required to install SM.

Compared to legacy metering equipment, SMs enable improved measurements at shorter sampling intervals and provide additional functionality. Along with enhanced data collection and analysis tools, SMs are part of the advanced metering infrastructure (AMI), which is an essential component of modern electricity grids and smart cities. The fine-grained measurements and increased amounts of data enable the implementation of machine learning (ML) based analytical tools for various purposes e.g. energy flexibility analysis [5], non-intrusive load monitoring (NILM) [6] etc.

Although the analysis of AMI data enables efficient optimization methods, it is also recognized to raise numerous privacy and security issues [7], [8], [9]. Widespread use of ML algorithms further increases end-user concerns, since technical publications about machine learning approaches to NILM, e.g. Factorial Hidden Markov Models (FHMM) [10] or Neural Networks (NN) [11], rarely take privacy or cyber security aspects into account. Some publications even suggest the breach of end-user privacy through the implementation of additional occupancy monitoring measures [12].

Against this backdrop, it is identified that there is a need to map electricity prosumer concerns towards the AMI and its ML based analytical tools and analyze how these concerns could be addressed from a legal perspective with a view to raising ethical and legal awareness about potential pitfalls of ML methods, specifically from the perspective of accountability for potential data and cybersecurity breaches. Taking the latest regulatory initiatives of the EU in the areas of data protection, privacy and cybersecurity into account, the General Data Protection Regulation (GDPR) in particular, the paper is predicated on the assumption that the EU's approach towards the governance of new technologies such as SM presents a unique case in addressing these concerns.

Having mapped prosumer concerns towards the AMI, a technical analysis of the identified prosumer concerns in terms of the ML based analytical tools is conducted. The concerns identified in the technical literature are then analyzed from a legal perspective. For

this purpose, pertinent EU legislative frameworks and deliverables by the European Commission’s Smart Grid Task Force 2 (SGTF) are consulted [13], [14]. The authors suggest a visual tool in form of a table to provide guidance to prosumers, utility, technology and energy service providers for identifying and addressing prosumer concerns mapped in the technical literature.

The terms prosumer and active customer are applied interchangeably in this paper. The latter term is defined in Electricity Directive (ED), Art. 2(8) [15]. This paper treats prosumers and active customers as a special category of consumers.

The paper is organized as follows: The analysis of general user concerns for AMI are presented in Section 2. In Section 3 the technically relevant concerns are identified and then connected to relevant regulatory frameworks in Section 4. Finally, the conclusions with general recommendations are presented in Section 5.

2. Analysis of user concerns for AMI and ML in general

The AMI is a common application of electricity smart grids, which spreads across all its fields and domains and integrates relevant technologies for bidirectional communication between utilities and prosumers [16], [17], [18], [19], [20]. The AMI provides services for customers, suppliers and network operators and is used for automated meter reading, billing, information provision, event management, device configuration etc. A common configuration of the AMI is depicted on Figure 1. Common components of the AMI include SMs, hierarchically disposed communication networks, Meter Data Management Systems (MDMS) and Head-End Systems (HES). The HES is a central data system for exchanging data of various meters in its service area. The communication network of the AMI is primarily divided into three sections: home area networks (HAN), wide area networks (WAN), and the utility network. The MDMSs act as meter data concentrators and as gateways between the WAN and utility network. SMs are the coupling points of users into the AMI, which provide enhanced metering capabilities, data communication and optional auxiliary functions, e.g. the adjustment of energy use based on cost and

availability [21], [22], [23]. SMs are used to report, measure and monitor power quality metrics, as well as loading conditions and power flows, which make them essential operational components and data sources for analytics.

The availability to utilize ML algorithms on fine-grained data at different parts of the AMI raises numerous concerns for residential prosumers. A literature survey was carried out to gain insight into the concerns of electricity end-users regarding the AMI and ML based analytical tools and more prominent concerns are outlined in Table 1. Additional concerns of electricity prosumers, which do not utilize ML algorithms, include theft of data, eavesdropping, denial of ICT services, compromise of data integrity, hijacking of home appliances, energy theft, tampering of SMs and denial of power.

To address individual concerns, it is necessary to identify their origin. The AMI is a complex technological system, which reveals several surfaces for intrusion or other forms of cyber-attacks. For the classification of the origin of prosumer concerns, surfaces for cyber-attacks in the AMI, identified in [24], are adopted. The following surfaces of the AMI for cyber-attacks are distinguished in Table 2.

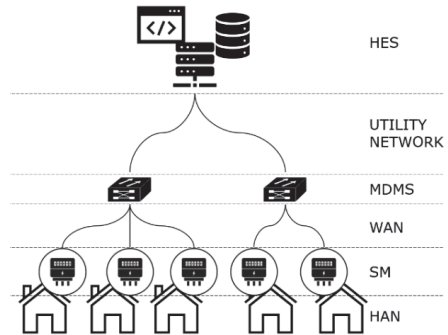


Figure 1. Common AMI configuration.

Table 1. Residential prosumer concerns regarding the AMI and ML algorithms [19], [20], [23], [25], [26], [27], [28], [29], [30]

Prosumer concern	Description	ID
Privacy		
Price discrimination	Variance in consumer pricing based on consumer profile	P1
Denial of consumer services	Denied access to consumer services due to unsuitable consumer profile	P2
Target to excessive advertisements	Increased advertisements, since consumer identified as target group by consumer profile	P3
Identification of home appliances	Unwanted identification of individual home appliances through NILM	P4
Exhibition of user habits and lifestyle	Exposure of sensitive data regarding consumer habits through NILM	P5
Exhibition of illnesses and disabilities	Exposure of sensitive health data through NILM	P6
Personification of anonymous data	The personification of data deemed to be collected anonymously through ML algorithms	P7
Cyber Security		
Disconnection of home appliances	The manipulation of demand response (DR) programs through the tampering of ML training and input data	C1
Burglary, arson, vandalism etc.	Increased threat through occupancy information gained by NILM	C2
Attractive target to burglary	Increased likelihood of burglary due to identification of attractive appliances through NILM	C3
Target to kidnapping	Possibility to use NILM for identifying persons in vulnerable situations	C4
Denial of personal mobility	The manipulation of DR programs through the tampering of ML training and input data to deny charging of electric vehicles	C5

Table 2. Surfaces of AMI

Abbr.	Description
HAN	the consumer side of the AMI. A consumer gateway acts as a bridge between the smart meter and the consumer's home devices
SM	the primary point of data collection for power grid energy consumption. Physical access to the meter is considered a vulnerable attack surface
SM data collector (SMDC)	a hardware computing device aggregating real-time data from multiple smart meters and providing a data collection and management point for the utility. An integral part of the MDMSs
AMI comm. interfaces and network	the network along with used communication interfaces linking the smart meter and the SMDCs. The AMI communications network exists alongside the power grid and can be scaled to serve millions of smart meters
AMI comm. protocols and software	the communication links and protocols utilized by the AMI
HES	the AMI management platform at the utility installation. Provides data warehousing for collected data and centralized management of the AMI

An estimation about the relevance of each listed surface regarding each individual problem is provided in Table 8. To evaluate the user concerns stemming from increased use of ML algorithms in the AMI, the technical process enabling such actions needs to be studied.

3. Analysis of technical process of ML in AMI and identification of related prosumer concerns

The basic process behind the disaggregation of load patterns from smart meter data, or NILM, is shown in Table 3.

It is the same for all different proposed ML methods, like FHMMs, NNs or Support Vector Machines, the main differences can be found in the amount, resolution and detail of the collected data, the amount of auxiliary data measurements of additional information, and the way the obtained data is intended to be used after the identification of the loads.

3.1 Differences in data collection

For many publications on NILM different public datasets are used. A detailed overview of the differences is shown in [31]. Some publications rely on their own measurement data, which makes comparisons of the performance more difficult. Table 4 shows an overview of the used datasets in selected recent publications.

If a typical percentage of 60-70% of the datasets was used for the training of the ML algorithms, it can be seen from Table 4 that in most publications the data amount is large. Months and years of training data with small resolutions of less than 5min, thus high detail on the time of the energy consumption, are used. Only few datasets contain less than a month of data and/or a resolution of

more than 5min. It should be noted that none of these technical papers discuss privacy concerns about the collected data and their use.

3.2 Additional data acquisition and additionally proposed features

Some of the recent publications on NILM present the use of some additional data measurements to improve the disaggregation results. In [32] an additional voluntary user feedback about the disaggregated data is added. Authors of [12] propose the use of cameras, motion sensors and smartphone apps, to track the occupancy of the household. An additional smartphone application is developed in [33] to display the results to the prosumers in a structured way. In [10] a cloud based on-line monitoring approach is presented. The authors of [34] show a novelty detection function for their ML method for new appliances. Future research of [35] includes classifying the prosumer activities for better accuracy and in [36] the authors' future goal is to influence the prosumers' behavior to increase energy efficiency. Privacy and cyber security are not discussed in any of these publications.

3.3 Comparison based on metrics

Since the metrics for measuring the accuracy of the different NILM methods is not unified and the publications use different datasets for training and testing of their proposed methods, direct comprehensive comparisons can be more difficult. Additionally, different devices in the datasets result in different accuracies.

Table 3. NILM process stages [37]

Stage	Description
Metering	Data is collected from smart meters and sometimes additional measurement equipment, typically with a low frequency (including current, voltage and power data)
Event detection	Events are detected within the data sets: e.g. an appliance changed its state
Feature extraction	Every appliance has a certain load signature and features, by which it can be distinguished from others
Classification	Load identification by a classification procedure to determine the times or periods a device was operating
Analysis of classification	Based on the application the NILM-process is used for, the classification can be analyzed

Table 4. Overview of training datasets

Dataset	Duration/Resolution	Publication
Pecan Street	4Y/1min	[38], [39], [40]
REDD	2-4W/<=4s	[10], [36], [40]
UK-DALE	655D/<=6s	[35], [41], [10]
ECO	8M/1s	[11], [42]
BLUED	1W/<=1s	[34]
Challekere Campus	7D/2min	[33]
Private Dataset	1M/10s	[12]
Private Dataset	1M/30min	[32]

Measuring privacy is not unified as well. It usually has qualitative and quantitative aspects which makes it difficult to use some simple scoring system. Literature proposes either complicated quantitative methods or qualitative methods for privacy evaluation [43].

Therefore, a simplified scoring system has been developed to provide a rough overview of the correlation between the accuracy of ML methods and their privacy. The framework is not based on specific standards but aims to provide a quick categorization of ML techniques for NILM.

The privacy score is designed to have 6 levels from -10 to -35. The best achievable privacy score is -10 and the worst is -35. The privacy level is estimated by the amount of used data for training the algorithm and additional data acquisition methods. A low amount of used data is considered to have a lower impact on the prosumers' privacy. Therefore, the score is -5. If the used amount of data is higher, then the score is -10. The threshold for this is chosen to be 1 month of data. Many prosumers do not like their data to be processed in a cloud, so this gives an additional score of -5. Additional occupancy monitoring with cameras is considered a huge violation of privacy and therefore gets an additional score of -10.

The accuracy of the ML methods is usually shown as an accuracy value (ACC) or F1 score (F1). The two values are shown with different colors in Figure 2 as they are being calculated differently and therefore cannot be compared directly.

The metrics are shown in Table 5 and the simple privacy score in connection with a simplified accuracy and F1 score is shown in Figure 2.

As a result for the general process of NILM, the two figures show clearly that the accuracy of the NILM methods is directly correlated to the reduction of privacy. A higher amount of data that can be used as a training set improves the accuracy of ML methods but reduces the privacy and of the prosumer as more data is stored. Additional available data can also improve the accuracy but for the example of occupancy monitoring [12] it reduces the privacy level.

Table 5. Privacy metrics for comparison

Measure	Privacy Score	Otherwise
Dataset < 1 Month	-5	-10
Resolution of Data > 5min	-5	-10
Occupancy Monitoring	-10	0
Cloud Processing	-5	0

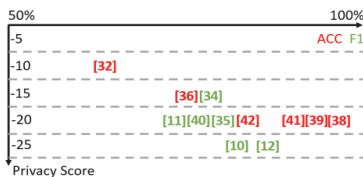


Figure 2. ACC and F1 score compared to proposed privacy score for selected publications.

3.4 Proposed applications for NILM

NILM methods are used for different purposes and applications in Smart Grids. HEMS, ambient assisted living (AAL), recommender systems (RS) and fault diagnostics (FD) are the most common implementations [37]. The goal and purpose of NILM is different for each of these applications. Sometimes power on/off detection or power estimations are necessary [38], sometimes predictions for more efficient home energy management are needed [44]. Sometimes the goal is a recommendation on more efficient energy consumption or faults and unusual behavior can be detected in the ambient assisted living context [37]. For all these specific applications the privacy and cyber security concerns are identified individually, based on the stages of the NILM ML process considering implementation on different surfaces of AMI. This is shown in Table 8.

4. Legal view on concerns identified in technical literature: The EU regulatory framework

Against the backdrop of the concerns identified in the technical literature, the following analysis is geared to address two questions: How does current EU legislation protect the prosumer's data and privacy rights? How does the EU regulatory framework address the prosumer's concerns in the area of cybersecurity? For the first dimension, GDPR [45] and ED [15] are consulted; for the second, GDPR [45], ED [15], the NIS Directive (NIS) [2] and the Cybersecurity Act (CA) [46].

4.1 Data protection and privacy

Since SM help aggregate vast amounts of personal data of prosumers, data protection is a prevalent concern. As of 25 May 2018, GDPR governs the processing of an EU citizen's personal data. Potential personal data breaches by controllers or processors ensuing from the processing of a natural person's data can fall within the scope of GDPR [45].

This paper applies the definition of SM stipulated in ED, which establishes common rules for the EU internal market for electricity [15]. ED also includes the protection of prosumer rights and in the context of this paper is to be read together with GDPR [15], [45]. In this regard, a SM is defined as "an electronic system that is capable of measuring electricity fed into the grid or electricity consumed from the grid, providing more information than a conventional meter, and that is capable of transmitting and receiving data for information, monitoring and control purposes, using a form of electronic communication"[15].

Pursuant to Art. 4(1) of GDPR, prosumers in private households can be considered "natural persons", thus falling within the scope of "data subjects" [45]. In this case, any information processed by SM, which helps identify a natural person directly or indirectly by an identifier such as name, an identification number, location data, an online identifier or by other identifiers pertaining to the physical, psychological, genetic, mental, economic, cultural or social identity of that natural person, classifies as "personal data" [45].

ML generates profiles of prosumers. Without obtaining granular consent for the processing of personal data for "one or more specific purposes" in electronic communication or in form of an electronic or written contract from the data subject, GDPR renders

processing of personal data generally illegal, except for situations allowed by law (Art. 6(1)(c-f); Art. 23(1)) [45]. The preconditions of receiving consent are stipulated in Art. 6(1), Art. 7 and Art. 12 [45]. Recital 32 clarifies consent as “a clear affirmative act establishing a freely given, specific, informed and unambiguous indication of the data subject’s agreement to the processing of personal data” [47]. Against this backdrop, the controller would be required to explain the prosumer in an electronic or written contract “using clear and plain language” for which purposes SM gather personal data and which measures are taken by the operator to safeguard the prosumer’s rights in compliance with the GDPR [45].

GDPR Art. 5 is instrumental in understanding the key principles regarding the processing of personal data. Without respecting these principles, SM would infringe upon the prosumer’s autonomy (for an overview of GDPR principles, see Table 6) [45].

GDPR makes a distinction between data controllers (Art. 4(7): “natural or legal person, public authority, agency or other body which, alone or jointly with others, determines the purposes and means of the processing of personal data”) and data processors (Art. 4(8): “natural or legal person, public authority, agency or other body which processes personal data on behalf of the controller”) [45], where different obligations for each of these two actors are set out in Art. 24-43 (for an overview of the rights of the data subject and the obligations of the controller and processor, see Table 7). The multitude of actors involved in the design and operation of the smart grid system, however, complicates a clear identification of both data controller and data processor, thus posing challenges in terms of the attribution of duties and ensuing accountability requirements set out by GDPR [45] and ED [15] (for an overview of potential operators, consider [13], p. 9).

Table 6. Data protection and privacy (I). GDPR: Principles [45]

Principles	Article
Lawfulness, fairness and transparency	5(1)(a)
Purpose limitation	5(1)(b)
Data minimisation	5(1)(c)
Accuracy	5(1)(d)
Storage limitation	5(1)(e)
Integrity and confidentiality	5(1)(f)
Accountability	5(1)(g)

Table 7. GDPR: Rights of the data subject and obligations of the controller and processor [45]

Rights	Article(s)
Transparent information, communication and modalities	12
Information and access to personal data	13;14;15
Rectification and Erasure	16;17;18;19;20
Right to object and automated individual decision-making	21;22
Obligations	Article
Responsibility of the Controller	24
Processor	28
Security of processing	32

GDPR Art. 22 (“Automated individual decision-making, including profiling”) [45] presents a key prosumer right by obligating data controllers to implement measures that allow data subjects to intervene in automated decision-making procedures. In the context of this paper, this implies that a prosumer is granted the right to contest any automated decision facilitated by SM that entailed legal consequences for the data subject. However, the complexity of actors raises questions in terms of identifying and establishing accountability for GDPR breaches in cases such as denial of services, target to excessive advertisements or exhibition of prosumer habits and lifestyle. This could equally apply to scenarios in which e.g. electricity bills are sent out automatically to the prosumer based on potentially flawed data processed by SM, which result in e.g. price discrimination (for a legal view on all identified prosumer concerns, see Table 8). It follows that national supervisory authorities play a central role in identifying operators and processors to be able to allocate their legal responsibilities in the smart grid.

4.2 Cybersecurity

According to GDPR Art. 5(1)(f), personal data must be processed in a manner which ensures appropriate security [45]. Here, security is mainly understood as the controller’s duty to implement mechanisms which can appropriately mitigate a “personal data breach”, more precisely “accidental or unlawful destruction, loss, alteration, unauthorized disclosure of, or access to, personal data transmitted, stored or otherwise processed” [45]. In the context of this paper, the term security refers to the security of personal data processed by SM in smart grids. Since this process takes place in the information and communication technology environment, the security of data would be generally governed by the framework of cybersecurity. Hence, NIS [2] and the latest adoption of CA [46] are instrumental in understanding how data security applies to SM. Consequently, cybersecurity forms one part of the understanding of security spelled out in ED, which refers to “security” as the “security of supply and provision of electricity and technical safety” [15].

Art. 2(1) of CA defines cybersecurity as “activities necessary to protect network and information systems, the users of such systems, and other persons affected by cyber threats” [46]. SM can be considered network and information systems. This can be deduced from NIS Art. 4(1), which delineates the parameters of “network and information systems” [2]. A threat against i.a. SM is described as “any potential circumstance, event or action that could damage, disrupt or otherwise adversely impact” (Art. 2(8), CA) these systems [46].

Cyberthreats against network and information systems in energy systems can be mitigated provided operators/processors of personal data are able to secure “the ability of network and information systems to resist, at a given level of confidence, any action that compromises the availability, authenticity, integrity or confidentiality of stored or transmitted or processed data or the related services offered by, or accessible via, those network and information systems” (NIS Art. 4(2)) [2].

The terms availability, authenticity, integrity and confidentiality are initially derived from the concept of the “CIA Triad” [[definitions of C,I,A based on [48]], [49]]. Applying the general understanding of these terms individually to the operation of SM,

operators/processors of data (i) are obliged to prevent disclosure of data to unauthorized third parties in this process (confidentiality) and (ii) to secure that the information contained in the data and gathered by SM is not altered in transit from the prosumer to the operator/processor, thus remaining authentic (integrity and authenticity) [2]. (iii) Additionally, according to NIS it is incumbent upon national authorities to establish mechanisms that can protect against e.g. distributed denial of service attacks conflicting i.a. with the principle of availability of data (availability) [2].

It is worthwhile mentioning that NIS creates mechanisms for the identification of operators of essential services (OES), which includes energy operators (NIS Directive, Art. 4(4), Art. 5(2), Annex 2) [2]. By the same token, NIS Art. 1(2)(e) obliges OES to inform a National Competent Authority (NAS) about potential cybersecurity incidents, broadly defined in NIS Art. 4(7) as “any event which has an actual adverse effect on the security of network and information systems” [2]. Establishing accountability for data breaches in SM remains problematic due to the great diversity of actors in the smart grid. Hence, the role of all relevant actors needs to be clearly identified and the list of actors continuously updated by NAS to understand for which actions and at what stages an operator/processor can incur responsibility for potential cybersecurity breaches outlined in Table 8.

SGTF2 suggests the implementation of a Network Code on cybersecurity (c.f. Figure 3). It advocates for a minimum baseline protection [14]. In accordance with ISO/IEC 27001:2013, it would entail duties for operators to continuously adjust the cybersecurity mechanisms to be able to anticipate and identify cybersecurity threats against their infrastructure [14]. For this purpose, SGTF2 additionally recommends operators to utilize the EU cybersecurity certification scheme [14], [46].

5. Conclusions

When developing an application that makes use of NILM or operates at any surface of the AMI, cybersecurity and data protection and privacy needs to be considered, which can be done using the GDPR and following the CIA triad. This paper presents a tool in the form of a table (Table 8) that can be used to identify key sections of the GDPR and the CIA triad in order to prioritize respective activities when developing or implementing technology. A sample workflow is presented in Figure 4 to provide an example for the use of the provided table.

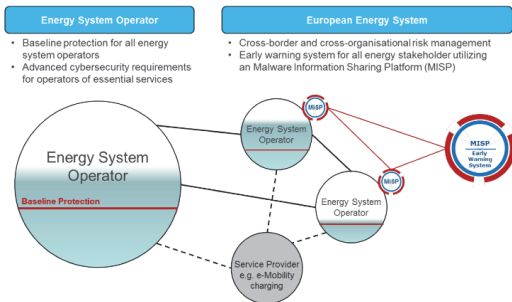


Figure 3. SGTF network code on cybersecurity [14].

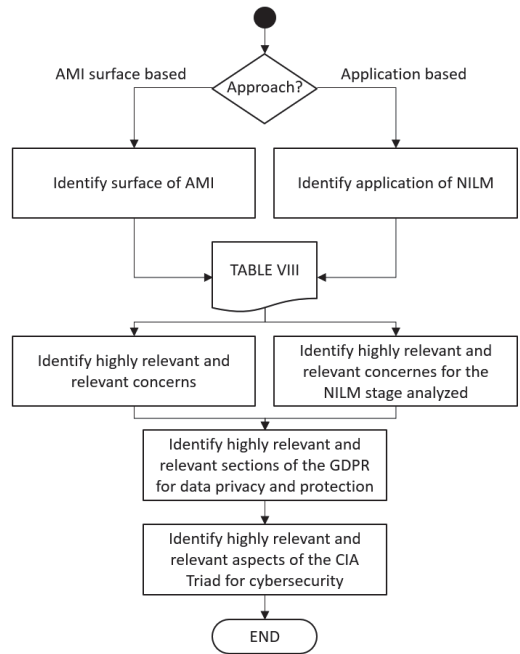


Figure 4. Workflow for using Table 8 to determine to filter more important sections of the GDPR and CIA triad for a specific implementation.

Implementations of ML methods for NILM rarely consider privacy aspects of prosumers. The identified prosumer concerns are relevant for all stages of the NILM process, considering possible implementations on different AMI surfaces, and depend on the proposed application in a HEMS, AAL, recommender systems or fault diagnostics context. Future research activities include the validation of the developed workflow and proposed mapping using real-life use-cases of ML applications in the electric smart grid.

6. Recommendations

Although all surfaces of the AMI are relevant when addressing concerns of residential prosumers, some of them stand out. The HANs and SM are components of the AMI, which are highly relevant for all distinguished privacy and cyber-security concerns of residential prosumers. Utilities and manufacturers are encouraged to emphasize and promote cyber-security and privacy aspects of SM, while end-users are advised to secure their HANs by applying suitable measures and secure technologies. Utility companies are advised to provide insight into their HESs, since it is regarded as a component of the AMI, which is highly relevant in terms of end-user privacy.

Bearing the novelty of SM technology in mind, both the designers of SM and operators of the smart grid system are well advised to ponder how the principle of “data protection by design” underlying the GDPR framework can be fulfilled [45].

A Data Protection Impact Assessment (DPIA), laid down in GDPR Art. 35 [45], provides a suitable tool to address the prosumer concerns mapped in this paper. This mechanism makes it mandatory for operators to assess any data security, privacy or cybersecurity risk which is “likely to result in a high risk to the rights and freedoms of natural persons” [13], [45]. Ideally, this procedure is to be carried out prior to the wide-scale application of a new technology, which makes use of personal data. In general, a DPIA can be described as an accountability mechanism and “a process for building and demonstrating compliance” with GDPR [13]. This mechanism would help operationalize the policymakers’ expectations towards SM for the benefit of the climate and the protection of the rights of the prosumer.

Additionally, the DPIA could be guided by the seven key requirements of the High-Level Expert Group on AI [50], which

were reaffirmed in the EU Commission White Paper on AI [51]. While these requirements chime with the IEEE Global Initiative on Ethics of Autonomous and Intelligent Systems [52], the authors recommend further research towards the operationalization of the seven key requirements, proposed by the High-Level Expert Group on AI, in electric smart grids.

ACKNOWLEDGMENTS

This work was supported by the European Commission through the H2020 project Finest Twins (grant No. 856602). Additionally, funding was provided by ASTRA “TTÜ arenguprogramm aastateks 2016-2022” (Doctoral School in Economics and Innovation Project code: 2014-2020.4.01.16-0032) as part of the European Regional Development Funding Scheme (EU programming period of 2014-2020).

Table 8. Mapping of ML angles via prosumer concerns based on relevance: Technical and legal views

		Prosumer Concerns												
		Price discrimination	Denial of prosumer services	Target to excessive advertisements	Identification of home appliances	Exhibition of user habits and lifestyle	Exhibition of illnesses and	Personification of anonymous data	Disconnection of home appliances	Burglary, arson, vandalism etc.	Attractive target to burglary	Target to kidnapping	Denial of personal mobility	
Technical	Surfaces of AMI	Home Area Network	0	0	++	++	++	++	++	++	++	++	++	++
		Smart Meter	+	0	+	++	++	++	++	+	++	++	++	++
		Smart Meter Data Collector	0	0	++	+	+	+	+	+	+	+	+	+
		AMI Networks	0	0	+	+	+	+	+	+	+	+	+	+
		AMI Protocols	0	0	+	+	+	+	+	+	+	+	+	+
	Head-End Management System	++	++	++	++	++	++	++	++	+	+	+	+	
Applications of NILM	Home Energy Management System	α	α, ε	α, ε	γ	ε	0	α, ε	$\alpha, \beta,$	δ, ε	γ, δ	δ, ε	$\alpha, \beta,$	
	Ambient Assisted Living	0			0		ε		$\gamma, \delta, \varepsilon$		γ, δ	δ, ε	$\gamma, \delta, \varepsilon$	
	Recommender System	α			γ		0							
	Fault Diagnostics	0			0		0							
Legal	Data Protection and Privacy (I)	GDPR Art. 5(1)(a)	++	++	++	++	++	++	++	+	+	+	+	
		GDPR Art. 5(1)(b)	++	++	++	++	++	++	++	+	+	+	+	
		GDPR Art. 5(1)(c)	++	++	++	++	++	++	++	+	+	+	+	
		GDPR Art. 5(1)(d)	+	+	+	+	+	+	+	+	+	+	+	
		GDPR Art. 5(1)(e)	+	+	+	+	+	+	+	+	+	+	+	
		GDPR Art. 5(1)(f)	+	+	+	++	++	++	++	++	++	++	++	
		GDPR Art. 5(1)(g)	++	++	++	++	++	++	++	++	++	++	++	
	Data Protection and Privacy (II)	GDPR Art. 12	++	++	++	++	++	++	++	+	+	+	+	
		GDPR Art. 13, 14, 15	++	++	++	++	++	++	++	+	+	+	+	
		GDPR Art. 16, 17, 18, 19, 20	++	++	++	+	+	+	0	0	0	0	0	
		GDPR Art. 21, 22	++	++	++	++	++	++	++	0	0	0	0	
	Data Protection and Privacy (III)	GDPR Art. 24	++	++	++	++	++	++	++	++	++	++	++	
		GDPR Art. 28	++	++	++	++	++	++	++	+	+	+	+	
		GDPR Art. 32	+	+	+	++	++	++	++	++	++	++	++	
	Cybersecurity: CIA Triad	Confidentiality	0	0	0	0	0	0	0	0	++	++	++	
Integrity/Authenticity		0	0	0	0	0	0	0	++	0	0	0		
Availability		0	0	0	0	0	0	0	0	0	0	++		

++ = highly relevant; + = relevant; 0 = not relevant/applicable; α = Metering NILM stage; β = Event detection NILM stage; γ = Feature extraction NILM stage; δ = Classification NILM stage; ε = Analysis of classification NILM stage

REFERENCES

- [1] Directorate-General for Energy (European Commission), "Clean energy for all Europeans," 26.07.2019 [Online]. Available: <https://op.europa.eu/en/publication-detail/-/publication/b4e46873-7528-11e9-9f05-01aa75cd71a1/language-en/format-PDF/source-126837758>.
- [2] Directive (EU) 2016/1148, OJ L 194, 19.7.2016, p. 1–30.
- [3] T. Häring, A. Rosin, and H. Biechl, "Using common household thermal storages to support the PV- and battery system in nearly zero energy buildings in off-grid mode," *Sustain. Energy Technol. Assessments*, vol. 35, no. May, pp. 12–24, Oct. 2019, doi: 10.1016/j.seta.2019.05.014.
- [4] T. Korotko, A. Rosin, and R. Ahmadiyahangar, "Development of prosumer logical structure and object modeling," Apr. 2019, doi: 10.1109/CPE.2019.8862390.
- [5] R. Ahmadiyahangar, T. Häring, A. Rosin, T. Korotko, and J. Martins, "Residential Load Forecasting for Flexibility Prediction Using Machine Learning-Based Regression Model," in *Proceedings - 2019 IEEE International Conference on Environment and Electrical Engineering and 2019 IEEE Industrial and Commercial Power Systems Europe, IEEEIC/I and CPS Europe 2019*, Jun. 2019, pp. 1–4, doi: 10.1109/IEEEIC.2019.8783634.
- [6] S. Mishra, H. Koduvere, I. Palu, R. Kuhl-Thalfeldt, and A. Rosin, "Assessing demand side flexibility with renewable energy resources," in *2016 IEEE 16th International Conference on Environment and Electrical Engineering (EEEIC)*, Jun. 2016, pp. 1–6, doi: 10.1109/EEEIC.2016.7555546.
- [7] M. R. Asghar, G. Dán, D. Miorandi, and I. Chlmatc, "Smart meter data privacy: A survey," *IEEE Commun. Surv. Tutorials*, vol. 19, no. 4, pp. 2820–2835, Jun. 2017, doi: 10.1109/COMST.2017.2720195.
- [8] H. He and J. Yan, "Cyber-physical attacks and defences in the smart grid: a survey," *IET Cyber-Physical Syst. Theory Appl.*, vol. 1, no. 1, pp. 13–27, Dec. 2016, doi: 10.1049/iet-cps.2016.0019.
- [9] P. Kumar, Y. Lin, G. Bai, A. Paverd, J. S. Dong, and A. Martin, "Smart Grid Metering Networks: A Survey on Security, Privacy and Open Research Issues," *IEEE Commun. Surv. Tutorials*, vol. 21, no. 3, pp. 2886–2927, Jul. 2019, doi: 10.1109/COMST.2019.2899354.
- [10] M. A. Mengistu, A. A. Girmay, C. Camarda, A. Acquaviva, and E. Patti, "A Cloud-Based On-Line Disaggregation Algorithm for Home Appliance Loads," *IEEE Trans. Smart Grid*, vol. 10, no. 3, pp. 3430–3439, May 2019, doi: 10.1109/TSG.2018.2826844.
- [11] S. Hosseini, N. Henaou, S. Kelouwani, K. Agbossou, and A. Cardenas, "A Study on Markovian and Deep Learning Based Architectures for Household Appliance-level Load Modeling and Recognition," in *2019 IEEE 28th International Symposium on Industrial Electronics (ISIE)*, Jun. 2019, vol. 2019-June, pp. 35–40, doi: 10.1109/ISIE.2019.8781186.
- [12] G. Tang, Z. Ling, F. Li, D. Tang, and J. Tang, "Occupancy-aided energy disaggregation," *Comput. Networks*, vol. 117, pp. 42–51, Apr. 2017, doi: 10.1016/j.comnet.2016.11.019.
- [13] Smart Grid Task Force, "Expert Group 2: Regulatory Recommendations for Privacy, Data Protection and Cyber-Security in the Smart Grid Environment – Data Protection Impact Assessment Template for Smart Grid and Smart Metering systems," v.2 of 13 September 2018. [Online]. Available at: https://ec.europa.eu/energy/sites/ener/files/documents/dpia_for_publication_2018.pdf.
- [14] Smart Grid Task Force, "Expert Group 2: Recommendations to the European Commission for the Implementation of Sector-Specific Rules for Cybersecurity Aspects of Cross-Border Electricity Flows, on Common Minimum Requirements, Planning, Monitoring, Reporting and Crisis Management," June 2019. [Online]. Available at: https://ec.europa.eu/energy/sites/ener/files/sgtf_eg2_report_final_report_2019.pdf.
- [15] Directive (EU) 2019/944, OJ L 158, 14.6.2019, p. 125–199.
- [16] F. Al-Turjman and M. Abujubbeh, "IoT-enabled smart grid via SM: An overview," *Futur. Gener. Comput. Syst.*, vol. 96, pp. 579–590, Jul. 2019, doi: 10.1016/j.future.2019.02.012.
- [17] M. Wigan, "User issues for smart meter technology," *IEEE Technol. Soc. Mag.*, vol. 33, no. 1, pp. 49–53, Mar. 2014, doi: 10.1109/MTS.2014.2301856.
- [18] D. L. S. Mendes, R. A. L. Rabelo, A. F. S. Veloso, J. J. P. C. Rodrigues, and J. V. dos Reis Junior, "An adaptive data compression mechanism for smart meters considering a demand side management scenario," *J. Clean. Prod.*, vol. 255, May 2020, doi: 10.1016/j.jclepro.2020.120190.
- [19] J. E. Rubio, C. Alcaraz, and J. Lopez, "Recommender system for privacy-preserving solutions in smart metering," *Pervasive Mob. Comput.*, vol. 41, pp. 205–218, Oct. 2017, doi: 10.1016/j.pmcj.2017.03.008.
- [20] L. Wei, L. P. Rondon, A. Moghadasi, and A. I. Sarwat, "Review of Cyber-Physical Attacks and Counter Defense Mechanisms for Advanced Metering Infrastructure in Smart Grid," *Proc. IEEE Power Eng. Soc. Transm. Distrib. Conf.*, vol. 2018-April, May 2018, Accessed: Apr. 22, 2020. [Online]. Available: <http://arxiv.org/abs/1805.07422>.
- [21] CEN-CENELEC-ETSI, "Functional architecture for communications in smart metering systems," pp. 1–70, 2011, [Online]. Available: ftp://ftp.cen.eu/cen/Sectors/List/Measurement/Smartmeters/CENCLCETSI_TR50572.pdf.
- [22] D. Jacobson and L. Dickerman, "Distributed intelligence: A critical piece of the microgrid puzzle," *Electr. J.*, vol. 32, no. 5, pp. 10–13, Jun. 2019, doi: 10.1016/j.tej.2019.05.001.
- [23] S. Tonyali, K. Akkaya, N. Saputro, A. S. Uluagac, and M. Nojournian, "Privacy-preserving protocols for secure and reliable data aggregation in IoT-enabled Smart Metering systems," *Futur. Gener. Comput. Syst.*, vol. 78, pp. 547–557, Jan. 2018, doi: 10.1016/j.future.2017.04.031.

- [24] J. Foreman and D. Gurugubelli, "Cyber Attack Surface Analysis of Advanced Metering Infrastructure," 2016.
- [25] M. Bae, K. Kim, and H. Kim, "Preserving privacy and efficiency in data communication and aggregation for AMI network," *J. Netw. Comput. Appl.*, vol. 59, pp. 333–344, Jan. 2016, doi: 10.1016/j.jnca.2015.07.005.
- [26] N. Fadhel, F. Lombardi, L. Aniello, A. Margheri, and V. Sassone, "Towards a semantic modelling for threat analysis of IoT applications: A case study on transactive energy," in *IET Conference Publications*, 2019, vol. 2019, no. CP756, doi: 10.1049/cp.2019.0147.
- [27] G. Giaconi, D. Gunduz, and H. V. Poor, "Smart Meter Privacy with Renewable Energy and an Energy Storage Device," in *IEEE Transactions on Information Forensics and Security*, Jan. 2018, vol. 13, no. 1, pp. 129–142, doi: 10.1109/TIFS.2017.2744601.
- [28] M. S. Piscitelli, S. Brandi, and A. Capozzoli, "Recognition and classification of typical load profiles in buildings with non-intrusive learning approach," *Appl. Energy*, vol. 255, p. 113727, Dec. 2019, doi: 10.1016/j.apenergy.2019.113727.
- [29] M. Wigan, "User issues for smart meter technology," *IEEE Technol. Soc. Mag.*, vol. 33, no. 1, pp. 49–53, Mar. 2014, doi: 10.1109/MTS.2014.2301856.
- [30] S. Yussof, M. E. Rusli, Y. Yusoff, R. Ismail, and A. A. Ghapar, "Financial impacts of smart meter security and privacy breach," *Conf. Proc. - 6th Int. Conf. Inf. Technol. Multimed. UNTEN Cultiv. Creat. Enabling Technol. Through Internet Things, ICIMU 2014*, pp. 11–14, 2015, doi: 10.1109/ICIMU.2014.7066595.
- [31] L. Pereira and N. Nunes, "Performance evaluation in non-intrusive load monitoring: Datasets, metrics, and tools—A review," *Wiley Interdiscip. Rev. Data Min. Knowl. Discov.*, vol. 8, no. 6, Nov. 2018, doi: 10.1002/widm.1265.
- [32] A. Miyasawa, Y. Fujimoto, and Y. Hayashi, "Energy disaggregation based on smart metering data via semi-binary nonnegative matrix factorization," *Energy Build.*, vol. 183, pp. 547–558, Jan. 2019, doi: 10.1016/j.enbuild.2018.10.030.
- [33] G. A. Raiker, B. Subba Reddy, L. Umanand, A. Yadav, and M. M. Shaikh, "Approach to Non-Intrusive Load Monitoring using Factorial Hidden Markov Model," in *2018 IEEE 13th International Conference on Industrial and Information Systems (ICIIS)*, Dec. 2018, pp. 381–386, doi: 10.1109/ICIINFS.2018.8721436.
- [34] T. Bernard, M. Verbunt, G. Vom Bogel, and T. Wellmann, "Non-Intrusive Load Monitoring (NILM): Unsupervised Machine Learning and Feature Fusion: Energy Management for Private and Industrial Applications," in *2018 International Conference on Smart Grid and Clean Energy Technologies (ICSGCE)*, May 2018, pp. 174–180, doi: 10.1109/ICSGCE.2018.8556735.
- [35] M. Devlin and B. P. Hayes, "Non-Intrusive Load Monitoring using Electricity Smart Meter Data: A Deep Learning Approach," in *2019 IEEE Power & Energy Society General Meeting (PESGM)*, Aug. 2019, vol. 2019-Augus, pp. 1–5, doi: 10.1109/PESGM40551.2019.8973732.
- [36] M. Aiad and P. H. Lee, "Unsupervised approach for load disaggregation with devices interactions," *Energy Build.*, vol. 116, pp. 96–103, Mar. 2016, doi: 10.1016/j.enbuild.2015.12.043.
- [37] A. Ruano, A. Hernandez, J. Ureña, M. Ruano, and J. Garcia, "NILM techniques for intelligent home energy management and ambient assisted living: A review," *Energies*, vol. 12, no. 11, MDPI AG, Jun. 10, 2019, doi: 10.3390/en12112203.
- [38] J. Cho, Z. Hu, and M. Sartipi, "Non-Intrusive A/C Load Disaggregation Using Deep Learning," in *2018 IEEE/PES Transmission and Distribution Conference and Exposition (T&D)*, Apr. 2018, vol. 2018-April, pp. 1–5, doi: 10.1109/TDC.2018.8440358.
- [39] A. U. Rehman, T. Tjing Lie, B. Valles, and S. R. Tito, "Low Complexity Non-Intrusive Load Disaggregation of Air Conditioning Unit and Electric Vehicle Charging," in *2019 IEEE Innovative Smart Grid Technologies - Asia (ISGT Asia)*, May 2019, pp. 2607–2612, doi: 10.1109/ISGT-Asia.2019.8881113.
- [40] S. Singh and A. Majumdar, "Deep Sparse Coding for Non-Intrusive Load Monitoring," *IEEE Trans. Smart Grid*, vol. 9, no. 5, pp. 4669–4678, Sep. 2018, doi: 10.1109/TSG.2017.2666220.
- [41] T.-T.-H. Le, J. Kim, and H. Kim, "Classification performance using gated recurrent unit recurrent neural network on energy disaggregation," in *2016 International Conference on Machine Learning and Cybernetics (ICMLC)*, Jul. 2016, vol. 1, pp. 105–110, doi: 10.1109/ICMLC.2016.7860885.
- [42] P. A. Schirmer, I. Mporas, and M. Paraskevas, "Evaluation of Regression Algorithms and Features on the Energy Disaggregation Task," in *2019 10th International Conference on Information, Intelligence, Systems and Applications (IISA)*, Jul. 2019, pp. 1–4, doi: 10.1109/IISA.2019.8900695.
- [43] A. Boulemtafes, A. Derhab, and Y. Challal, "A review of privacy-preserving techniques for deep learning," *Neurocomputing*, vol. 384, pp. 21–45, Apr. 2020, doi: 10.1016/j.neucom.2019.11.041.
- [44] R. G. Rajasekaran, S. Manikandaraj, and R. Kamaleshwar, "Implementation of Machine Learning Algorithm for predicting user behavior and smart energy management," in *2017 International Conference on Data Management, Analytics and Innovation (ICDMAI)*, Feb. 2017, pp. 24–30, doi: 10.1109/ICDMAI.2017.8073480.
- [45] Regulation (EU) 2016/679, OJ L 119, 4.5.2016, p. 1–88.
- [46] Regulation (EU) 2019/881, OJ L 151, 7.6.2019, p. 15–69.
- [47] Intersoft Consulting. "Recital 32: Conditions for Consent." *gdpr-info.eu*. <https://gdpr-info.eu/recitals/no-32/> (accessed January 14, 2020).
- [48] A. Agarwal and A. Agarwal, "The Security Risks Associated with Cloud Computing," *INT'L J. Comput. Appl. Eng. SCI*, pp. 257–258, 2011, Accessed: May 06, 2020. [Online]. Available: <http://citeseerx.ist.psu.edu/viewdoc/summary?doi=10.1.1.207.9119>.

- [49] A. Kasper and A. Antonov, "Towards Conceptualizing EU Cybersecurity Law," in ZEI Discussion Paper Series, C 253 (2019), Accessed: May 14, 2020. [Online]. Available: <http://www.zei.uni-bonn.de/aktuelles/2019/zei-discussion-paper-c-253-2019>
- [50] A. Antonov and T. Kerikmäe, "Trustworthy AI as a Future Driver for Competitiveness and Social Change in the EU," in *The EU in the 21st Century*, Springer International Publishing, 2020, pp. 135–154.
- [51] European Commission, "White Paper on Artificial Intelligence: A European approach to excellence and trust," EU, Brussels, Belgium, Rep. COM(2020) 65 final, 19.2.2020. Accessed: 14 May 2020. [Online]. Available: https://ec.europa.eu/info/sites/info/files/commission-white-paper-artificial-intelligence-feb2020_en.pdf.
- [52] D. L. S. Mendes, R. A. L. Rabelo, A. F. S. Veloso, J. J. P. C. Rodrigues, and J. V. dos Reis Junior, "An adaptive data compression mechanism for smart meters considering a demand side management scenario," *J. Clean. Prod.*, vol. 255, May 2020, doi: 10.1016/j.jclepro.2020.120190.

Publication III

T. Häring, R. Ahmadiyahangar, A. Rosin and H. Biechl, "Machine Learning Approach for Flexibility Characterisation of Residential Space Heating," IECON 2021 – 47th Annual Conference of the IEEE Industrial Electronics Society, 2021, pp. 1–6, doi: 10.1109/IECON48115.2021.9589216.

Machine Learning Approach for Flexibility Characterisation of Residential Space Heating

Tobias Häring, Roya Ahmadihangar, Argo Rosin
Smart City Center of Excellence & Department of Electrical Power
Engineering and Mechatronics
Tallinn University of Technology
Tallinn, Estonia
tobias.haring@taltech.ee

Helmuth Biechl
Institute of Electrical Power Systems (IEES)
University of Applied Sciences Kempten
Kempten, Germany
& Department of Electrical Power Engineering and Mechatronics
Tallinn University of Technology
Tallinn, Estonia

Abstract— Due to an increasing share of renewable energy sources the balancing of energy production and consumption is getting a lot of interest considering future smart grids. In this context, many investigations on demand-response programs are being conducted to achieve flexibility from different energy storages and loads. As space heating is an important schedulable load for flexibility simulations, there are different modelling approaches due to its interdisciplinary nature. Models can be built from the civil engineering or electrical engineering point of view, depending on the computational expense and accuracy level. Scheduling optimizations need a lot of simulations, preferably with computationally light models. Thus, this work will use a computationally light neural network load prediction model for space heating which is based on a detailed civil engineering model. Simulations with different scheduling times were conducted to see the long- and short-term effects of the demand response action. Results show, that applying the same demand response action at different times results in different behaviors of the system resp. energy consumption, which requires further studies for developing optimized scheduling methods.

Keywords— Flexibility, Space Heating, Microgrid, nZEB, Smart City, Demand Response

I. INTRODUCTION

Due to several national and international legislations and programs, the share of renewable energy production is increasing constantly. This is great in terms of sustainability and environmentally friendliness, but it leaves challenges to the distribution system operators. Several of these renewable energy sources, like photovoltaic systems [1] or wind turbines [2], are volatile and need to be balanced with the energy demand for grid stability [3]. Adjusting the energy demand with e.g. energy storage systems [4], is called demand side management or energy system flexibility, which is an officially recognized concept in power systems [5], [6].

On the one hand, there is the possibility to add storage systems like batteries [7] or flywheels [8], or combine different systems to hybrid storages [9] for balancing and power quality improvement [10] on the demand side. On the other hand, the

energy consumption can be directly influenced, which reduces the need for such storage systems. Different household devices [11], like freezers [12], ventilation systems [13], water heaters [14] or space heating [15], can be scheduled to change the energy demand temporarily.

The latter, space heating, makes up for a high share of residential loads [16], but it is of an interdisciplinary nature. This means that there are modelling approaches from different directions.

From the electrical engineering point of view, there are usually simplified models with limited or no thermal modelling. An aggregated model for space heating is presented in [17]. The space heating model is based on simple temperature differences. [18] proposes a simplified white-box model for space heating which is based on temperature differences during the timesteps as well. These are both computational light models, which could be used for flexibility analysis and scheduling optimizations, but the accuracy is significantly lower than with accurate civil engineering models.

From the civil engineering point of view, there are detailed thermal models with high computational effort. [19] presents a detailed model of a heat pump but does not include detailed demand response or flexibility investigations. Similarly in [20] the thermal model is very detailed for the control center. This reduces the usability for flexibility scheduling optimizations as the computational effort would be high.

There are several publications considering the scheduling optimization of various devices. Authors of [21] propose a particle swarm optimizations while [22] uses different individual scheduling methods. Both publications show simplified models for the schedulable loads.

Therefore, this work will focus on the use of a machine learning algorithm for load prediction [23] of the space heating model with better accuracy than a simple white box model. With this model the scheduling of space heating flexibility can be analyzed considering short- and long-term effects by applying different scheduling methods and times to create a basis for developing scheduling optimizations in future work.

This research was supported by the Estonian Centre of Excellence in Zero Energy and Resource Efficient Smart Buildings and Districts, ZEBE (grant No. 2014-2020.4.01.15-0016) and by the European Commission through the H2020 project Finest Twins (grant No. 856602).

The paper is organized as follows: The methodology is presented in Section II. Section III shows the results of the simulations. Finally, the results in brief with conclusions are presented in Section IV.

II. METHODOLOGY

The final aim of the work is to investigate the short- and long-term influences of space heating flexibility on energy consumption compared to a fixed set point control. In this case, a computationally light space heating model for a building needs to be used to investigate multiple scenarios, which could be used for optimizations in the scheduling. This will also enable the scaling of this methodology from a single building to microgrid or smart city level with reasonable computational effort. The used methodology is as follows:

- In the first step, an existing model of a building is used to train a simple neural network model to predict the energy consumption of the heating system of this building (c.f. Fig. 1: S I)
- In the second stage (c.f. Fig. 1: S II), the space heating model based is integrated into a microgrid simulation. For simplification, the focus in this work is set on the flexibility from the space heating model, and therefore the other microgrid components are considered to provide no flexibility and work on a fixed schedule. Thus, the schedulable part of the microgrid is solely the space heating model.

The overview of the methodology is given in Fig. 1.

As mentioned above, for the flexibility simulations, an existing building model in IDA-ICE software is used. This building model represents a small single-family house with one floor and a detached roof. It is one of the sample houses used for a residential nZEBs project in Estonia [24]. The building and its model have been developed and used by Simson et al. in several previous studies [25]. Based on simulation data from this model, a simple neural network model is trained in Matlab to predict the space heating energy consumption of the building based on the selected setpoint. The detailed methodology for the neural network model is presented in [26].

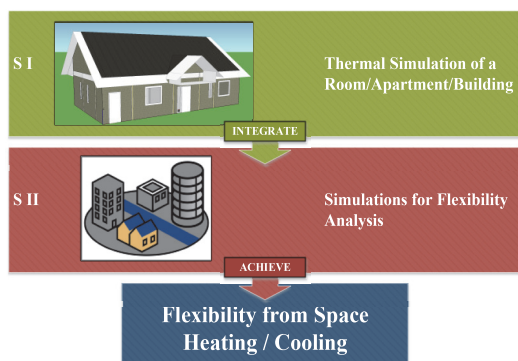


Fig. 1. Methodology Overview

Compared to a simple white box model as shown in [18], the accuracy is improved: The mean power value error is reduced from 8% to 6% and the root mean square error for the power prediction is reduced from 28 W/m² to 17 W/m². The calculation time is the same for the neural network and white box model, which is about 15% of the calculation time for the original detailed building model. Thus, the neural network model is used for flexibility simulations. A flowchart for these flexibility simulations is shown in Fig. 2.

After the input data was imported, one of the 3 types of flexibility simulations were done in Matlab:

- Changing the setpoint for 1 day
- Changing the setpoint for 1 hour
- Changing the setpoint for 15 min

The 1-day setpoint change could be used for rough day-ahead or several days ahead flexibility planning. Changing the setpoint for 1 hour can be suitable for tertiary control purposes or intraday corrections. The 15 min setpoint change is useful for more dynamical flexibility systems. Setpoint changes on less than 15 min basis are not considered in this investigation, as time constants and duty cycles of heating systems are usually high and additional constraints for example minimum run- and pause-times for heat pumps need to be considered in the control additionally.

The setpoints for the rooms have 3 settings and are always controlled simultaneously for all rooms:

- High: 23°C
- Normal: 22°C
- Low: 21°C

Depending on the type of simulation (day, hour, 15min), one simulation for changing the setpoint for one interval (day/hour/15min) to high resp. low setting, while leaving it at normal for the rest of the simulation, is conducted. This is done for each interval through the number of days/hours/quarter hours (c.f. TABLE I) that are simulated. Additionally, one simulation only with the normal setpoint is conducted. This results in a total number of simulations for each room of 2 times the number of intervals plus the additional normal setpoint simulation.

In the post-processing, the obtained temperature and power data are separated into the high, low and normal setpoint results to show the flexibility that can be obtained between the different settings of the thermostat for each interval (day, hour, 15min).

To see the flexibility that can be achieved by changing the setpoints from normal to a high or low setting, two different metrics are shown. One is intra-interval flexibility, which shows the maximum, normal, and minimum energy consumption that can be achieved within one interval. This is especially interesting for the distribution system operators for implementing DSM programs. The second is long-term effect of this flexibility, which shows the total energy consumption over all intervals if the setpoints for one interval were set too high or low. This is of more interest to the consumers as they can see how their total energy consumption will be affected in a long-term perspective.



Fig. 2. Flowchart for flexibility simulations

TABLE I. NUMBER OF INTERVALS FOR EACH FLEXIBILITY SIMULATION TYPE

Type	Number of Intervals	Number of simulations per room
1-day intervals	90 days	181
1-hour intervals	240 hours (=10 days)	481
15-min intervals	960 quarter hours (=10 days)	1921

III. RESULTS

For the 90 day simulation, the simulation intervals are shown in Fig. 3 for the moving low setpoint and Fig. 4 for the moving high setpoint. The number of the simulation interval corresponds to the number of the day on which the setpoint was changed to low resp. high, while the setpoint for the remaining days was set to normal. It can be clearly seen, that the energy consumption is lower for days with a low setpoint and higher for days with a high setpoint. The setpoint change seems to have a minor effect on immediately following days in most cases. For the first few simulation intervals, a larger effect on the following days can be noticed. This shows the complexity of predicting the flexibility of a space heating system.

The previously described intra interval and long-term flexibility metrics will show more exact results on effects:

For the 90 day simulation with 1-day intervals, it can be seen, that the intra-interval flexibility is not the same for every day, as the heating demand varies over time as shown in Fig. 5. In Fig. 6, it is evident, that the long-term flexibility mostly corresponds to the intra-interval and does not have too much influence. Only for day 47, it can be seen that the overall energy consumption for 90 days is even lower with the high setpoint than with a normal one.

Using setpoint changes on an hourly basis in the 240 hour simulations shows, that reducing the temperature setpoint to the low setting often does not reduce the energy consumption by a lot (c.f. Fig. 7). In the contrary, if the setpoint is increased by 1°C to the high setting, the energy consumption can be increased by a larger margin. Looking at the long-term flexibility of the hourly setpoint changes in Fig. 8 shows, that there are some visible effects. Sometimes the total energy consumption for the 10-day period can be higher than with a normal setpoint, even though the low setpoint was chosen (e.g. hour 57). On the other hand, the total energy consumption may be lower when a high setpoint is chosen (e.g. hour 91).

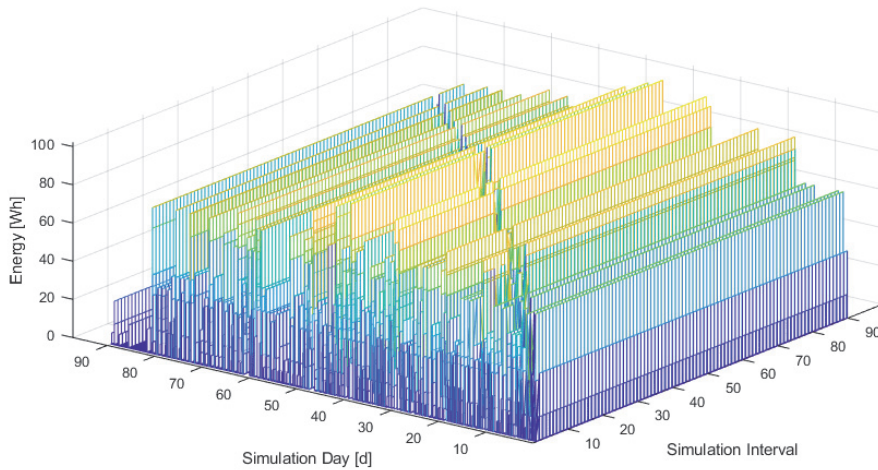


Fig. 3. Energy consumption for different simulation intervals with low setpoint. The number of the simulation interval corresponds to the day with a low setpoint while other days have a normal setpoint; e.g.: For simulation interval 50, only day 50 has a low setpoint.

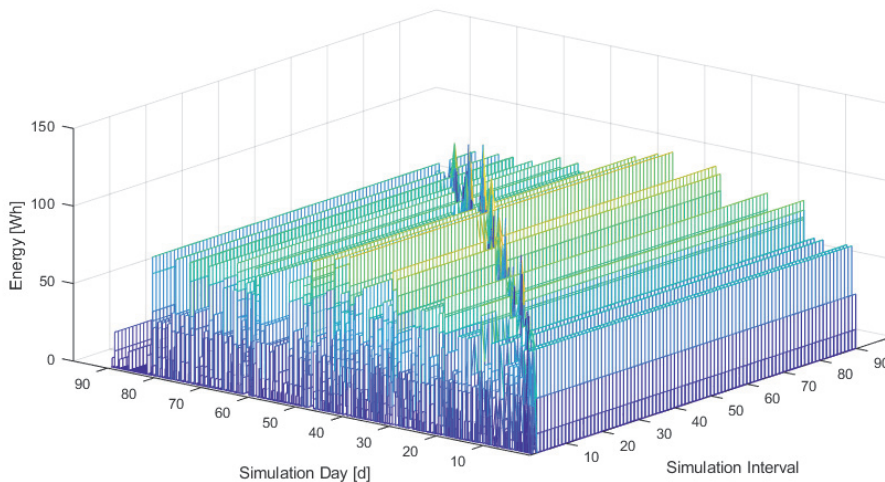


Fig. 4. Energy consumption for different simulation intervals with high setpoint. The number of the simulation interval corresponds to the day with a high setpoint while other days have a normal setpoint; e.g.: For simulation interval 50, only day 50 has a high setpoint.

As 15 minutes is a typical framework for DSM programs, simulations on such a basis are done as well. The intra-interval flexibility shows the same behavior like with a 1-hour basis (c.f. Fig. 9). It is easier to increase the power consumption during an interval than reduce it. The long-term flexibility shown in Fig. 10 is similar to the one of the hourly-interval simulations as well. It is evident, that changing the setpoint to low or high can have

a positive or negative effect on the long-term energy consumption. For example at 200 quarter hours there is a higher long term energy consumption with the low setpoint than the other setpoints and at around 880 quarter hours the high setpoint leads to a lower long term energy consumption than other setpoints.

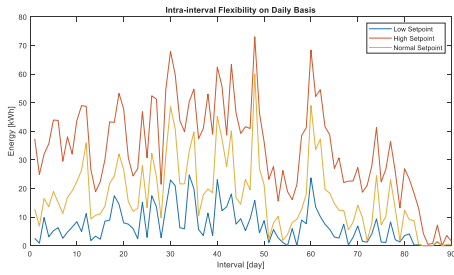


Fig. 5. Intra-interval flexibility for 90 days on a daily basis

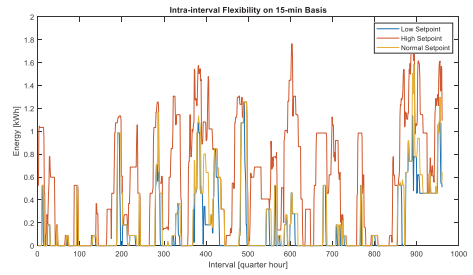


Fig. 9. Intra-interval flexibility for 960 quarter hours on a 15-min basis

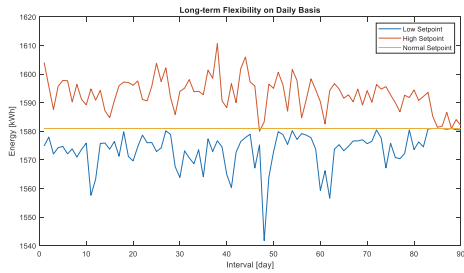


Fig. 6. Long-term flexibility for 90 days on a daily basis

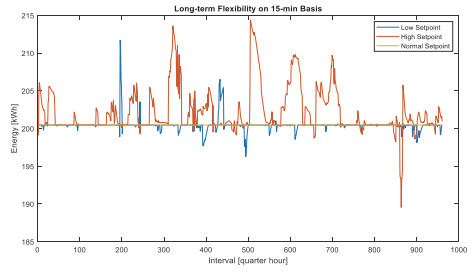


Fig. 10. Long-term flexibility for 960 quarter hours on a 15-min basis

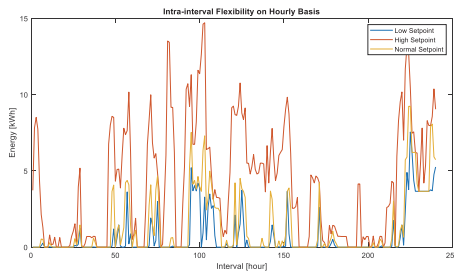


Fig. 7. Intra-interval flexibility for 240 hours on an hourly basis

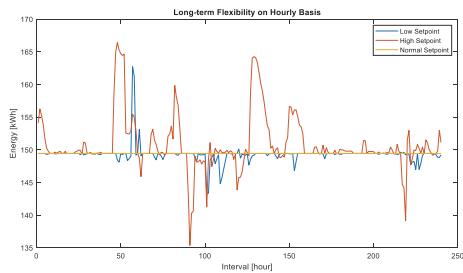


Fig. 8. Long-term flexibility for 240 hours on an hourly basis with optimized neural network model

IV. CONCLUSIONS

To achieve flexibility with a demand-side management control strategy, different devices can be used like space heating. As this is an interdisciplinary research field, complex models of civil engineering and electrical engineering need to be brought together. To investigate different flexibility scenarios, which could be used for scheduling optimizations, a computationally light space heating model is advisable. This will also enable the simulation of larger microgrids and smart cities with reasonable computational effort. The chosen simple neural network model showed around 2% better accuracy compared to a simple white box model, while reducing the computational time by around 85% compared to a detailed civil engineering model, which makes it suitable for the chosen kind of simulation.

The flexibility simulations with the space heating model showed, that it is easier to increase the energy consumption during a certain interval than to reduce it. On a short term view all simulations show that a lower setpoint can but does not have to lead to temporary lower energy consumption. For each day there is a different amount of flexibility available. Especially for space heating applications, this is a crucial part of flexibility prediction, as it cannot be assumed that the flexibility is the same for each day. This is also true for hours and quarter hours. On average, the energy consumption within an interval (day, hour, quarter hour) can be reduced by more than 30% and increased by 100% or more. To plan flexibility such a model can quickly provide better estimations than an aggregated model.

Considering the long-term energy consumption, it should be noted that lowering the setpoint for a certain interval does not necessarily result in lower overall energy consumption. This is also known as the rebound effect because the system will need

additional energy to get back to the regular setpoint. Contrary to that, increasing the setpoint during one interval does not necessarily increase the total long-term energy consumption. With a lower setpoint energy consumption of -4% up to +9% are possible with a tendency to negative values. Energy consumption with a higher setpoint can be between -9% and +12% with a tendency to positive values.

For future work, these simulations should be extended to multiple buildings and include other schedulable loads as well, like water heaters or freezers, to get flexibility predictions for microgrids or smart cities which can be used for scheduling optimizations.

REFERENCES

- [1] S. Pawakul and W. Srirattana-wichaiakul, "Price-based demand response strategy for coordinated PV distributed generation and demand side management in distribution network," in 2020 2nd International Conference on Smart Power and Internet Energy Systems, SPIES 2020, 2020, pp. 492–497, doi: 10.1109/SPIES48661.2020.9243154.
- [2] S. H. Rouhani, R. Ahmadihangar, T. Haring, and A. Rosin, "Improving Dynamic Stability of deregulated power system," in 2020 IEEE 61st Annual International Scientific Conference on Power and Electrical Engineering of Riga Technical University, RTUCON 2020 - Proceedings, 2020, doi: 10.1109/RTUCON51174.2020.9316618.
- [3] Q. Fan et al., "Research and Simulation Analysis on Transient Stability of Wind Power Accessing in Regional Grid," in Proceedings of 2018 2nd IEEE Advanced Information Management, Communicates, Electronic and Automation Control Conference, IMCEC 2018, 2018, pp. 389–393, doi: 10.1109/IMCEC.2018.8469411.
- [4] R. Ahmadihangar et al., "Energy Storage Expansion Planning in Microgrid," in Proceedings - 2020 IEEE 14th International Conference on Compatibility, Power Electronics and Power Engineering, CPE-POWERENG 2020, 2020, pp. 433–437, doi: 10.1109/CPE-POWERENG48600.2020.9161502.
- [5] International Energy Agency, *Harassing Variable Renewables - A Guide to the Balancing Challenge*. OECD/IEA, 2011.
- [6] North American Electric Reliability Corporation, "Accommodating High Levels of Variable Generation," North Am. Electr. Reliab. Corp., no. April, p. 104, 2009.
- [7] R. Ahmadihangar et al., "Flexibility investigation of price-responsive batteries in the microgrids cluster," in Proceedings - 2020 IEEE 14th International Conference on Compatibility, Power Electronics and Power Engineering, CPE-POWERENG 2020, 2020, pp. 456–461, doi: 10.1109/CPE-POWERENG48600.2020.9161667.
- [8] F. Plaum, T. Haring, R. Ahmadihangar, and A. Rosin, "Power Smoothing in Smart Buildings using Flywheel Energy Storage," in Proceedings - 2020 IEEE 14th International Conference on Compatibility, Power Electronics and Power Engineering, CPE-POWERENG 2020, 2020, pp. 473–477, doi: 10.1109/CPE-POWERENG48600.2020.9161458.
- [9] N. Cinay, T. Haring, A. Rosin, T. Korotko, R. Ahmadihangar, and H. Biechl, "Lifetime-Oriented Control Strategies for Hybrid Energy Storage Systems in an Islanded Microgrid," in 2021 22nd IEEE International Conference on Industrial Technology (ICIT), 2021, pp. 1267–1272, doi: 10.1109/ICIT46573.2021.9453617.
- [10] I. B. Yazdi, A. A. Khodadoost Arani, and G. B. Gharehpajian, "Determining optimal capacity of FESS using PSO to enhance stability of microgrid after islanding mode, considering investment costs," in 2016 Smart Grids Conference, SGC 2016, 2017, pp. 19–24, doi: 10.1109/SGC.2016.7882946.
- [11] A. Tiwari and N. M. Pindoriya, "Optimal scheduling of home appliances under automated demand response," in 2020 21st National Power Systems Conference, NPSC 2020, 2020, doi: 10.1109/NPSC49263.2020.9331827.
- [12] T. Haring, R. Ahmadihangar, A. Rosin, H. Biechl, and T. Korotko, "Comparison of the impact of different household occupancies on load matching algorithms," in 2019 Electric Power Quality and Supply Reliability Conference (PQ) & 2019 Symposium on Electrical Engineering and Mechatronics (SEEM), 2019, pp. 1–6, doi: 10.1109/PQ.2019.8818270.
- [13] V. Maask, T. Haring, R. Ahmadihangar, A. Rosin, and T. Korotko, "Analysis of Ventilation Load Flexibility Depending on Indoor Climate Conditions," in 2020 IEEE International Conference on Industrial Technology (ICIT), 2020, pp. 607–612, doi: 10.1109/ICIT45562.2020.9067153.
- [14] T. Haring, R. Ahmadihangar, A. Rosin, and H. Biechl, "Impact of Load Matching Algorithms on the Battery Capacity with different Household Occupancies," in IECON 2019 - 45th Annual Conference of the IEEE Industrial Electronics Society, 2019, pp. 2541–2547, doi: 10.1109/IECON.2019.8927495.
- [15] P. Manner, J. Salmelin, S. Honkapuro, I. Alapera, and S. Annala, "A novel method to utilize direct electrical space heating for explicit demand response purposes -proof of concept," in IEEE PES Innovative Smart Grid Technologies Conference Europe, 2020, vol. 2020-October, pp. 86–90, doi: 10.1109/ISGT-Europe47291.2020.9248893.
- [16] J. P. Alves and J. N. Fidalgo, "Classification of Buildings Energetic Performance Using Artificial Immune Algorithms," in SEST 2019 - 2nd International Conference on Smart Energy Systems and Technologies, 2019, doi: 10.1109/SEST.2019.8849140.
- [17] L. Zhou et al., "Day-ahead and intraday optimization models for demand response of the aggregators of thermostatically controlled loads," in Asia-Pacific Power and Energy Engineering Conference, APPEEC, 2020, vol. 2020-September, doi: 10.1109/APPEEC48164.2020.9220563.
- [18] T. Haring, A. Rosin, and H. Biechl, "Using common household thermal storages to support the PV- and battery system in nearly zero energy buildings in off-grid mode," *Sustain. Energy Technol. Assessments*, vol. 35, no. May, pp. 12–24, Oct. 2019, doi: 10.1016/j.seta.2019.05.014.
- [19] J. Clauß and L. Georges, "Model complexity of heat pump systems to investigate the building energy flexibility and guidelines for model implementation," *Appl. Energy*, vol. 255, p. 113847, Dec. 2019, doi: 10.1016/j.apenergy.2019.113847.
- [20] T. Haring, A. Rosin, T. M. Kull, J. Helguero, and H. Biechl, "Thermal Modelling of a Control Center for Flexibility Analysis in nZEB Nanogrids," in 2020 IEEE 61st Annual International Scientific Conference on Power and Electrical Engineering of Riga Technical University, RTUCON 2020 - Proceedings, 2020, doi: 10.1109/RTUCON51174.2020.9316568.
- [21] S. He, T. Gong, S. Chen, and J. Tang, "Research on optimal scheduling strategy of adjustable load based on particle swarm optimization," in Proceedings - 2020 Management Science Informatization and Economic Innovation Development Conference, MSIEID 2020, 2020, pp. 77–80, doi: 10.1109/MSIEID52046.2020.00022.
- [22] H. O. Alwan, H. Sadeghian, and Z. Wang, "Decentralized Demand Side Management Optimization for Residential and Commercial Load," in IEEE International Conference on Electro Information Technology, 2018, vol. 2018-May, pp. 712–717, doi: 10.1109/EIT.2018.8500213.
- [23] T. Haring, R. Ahmadihangar, A. Rosin, T. Korotko, and H. Biechl, "Accuracy Analysis of Selected Time Series and Machine Learning Methods for Smart Cities based on Estonian Electricity Consumption Forecast," 2020, pp. 425–428, doi: 10.1109/cpe-powereng48600.2020.9161690.
- [24] "Liginullenergia eluhooned. Väikemajad," 2017. .
- [25] R. Simson et al., "The Impact of Infiltration on Heating Systems Dimensioning in Estonian Climate," in E3S Web of Conferences, 12th Nordic Symposium on Building Physics, 2020, p. to be published.
- [26] T. Haring, T. M. Kull, R. Ahmadihangar, A. Rosin, M. Thalfeldt, and H. Biechl, "Microgrid Oriented modeling of space heating system based on neural networks," *J. Build. Eng.*, vol. 43, p. 103150, Nov. 2021, doi: 10.1016/j.jobte.2021.103150.

Publication IV

N. Cinay, T. Häring, A. Rosin, T. Korötko, R. Ahmadiyahangar and H. Biechl, "Lifetime-Oriented Control Strategies for Hybrid Energy Storage Systems in an Islanded Microgrid," 2021 22nd IEEE International Conference on Industrial Technology (ICIT), 2021, pp. 1267-1272, doi: 10.1109/ICIT46573.2021.9453617.

Lifetime-Oriented Control Strategies for Hybrid Energy Storage Systems in an Islanded Microgrid

Nazli Cinay, Tobias Häring, Argo Rosin, Tarmo Korõtko, Roya Ahmadiyahangar
Smart City Center of Excellence (Finest Twins) & Department of Electrical Power Engineering and Mechatronics
Tallinn University of Technology
Tallinn, Estonia
tobias.haring@taltech.ee

Helmuth Biechl
Institute of Electrical Power Systems (IEES)
University of Applied Sciences Kempten
Kempten, Germany
& Department of Electrical Power Engineering and Mechatronics
Tallinn University of Technology
Tallinn, Estonia

Abstract— Alternative energy sources are becoming more important to ensure the supply of adequate and reliable energy. This forecloses environmental damage by outdated power plants and fossil fuel stocks, which are finite and have to be produced laboriously. Thus, energy management strategies for an islanded smart grid with combined energy storage systems, namely flywheel and battery storage, have been investigated in this paper. Mathematical models for these storage systems were developed in Matlab by analysing typical parameters and characteristics and were derived from simplified equations. Other microgrid components, the load profile, and photovoltaic (PV) system, were based on existing measurement data. Various control algorithms based on the battery's state of charge (SOC), load profile, and available PV power were developed in this paper. The simulations were done for a detached house and settlement for different scenarios including control strategies with and without different flywheel control algorithms. Finally, a reduction of the battery cycles and an increase of maximum off-grid mode time was achieved.

Keywords—flywheel, battery storage, energy management system, SOC, microgrid, islanded mode, smart grid

I. INTRODUCTION

Power failures and long-term power failures due to natural disasters are no more uncommon [1]. Stocks of fossil fuels such as oil, coal and gas are finite and increasingly difficult to produce, and more and more environmental damage is being established [2]. Coal and gas-fired power plants for power generation distribute electricity many miles through often outdated infrastructure, which increases the error rate immensely [2]. In this situation, the development of sustainable and distributed energy sources and their integration into the energy grids is essential and will be an important part of the emerging Smart Cities of the future. These Smart Cities will be comprised of multiple Smart Grids respectively microgrids.

An integrated energy system comprising interconnected loads and distributed energy storage (DES), which can operate grid-connected or in islanded mode is defined as a microgrid [3]. A common simple residential microgrid model is based on a load profile, PV and battery storage. Additional flywheel energy storage systems in microgrids can be used for power smoothing of fluctuating loads, as a backup alternative to improve the

reliability in energy supply and to reduce the use of diesel generators to reduce carbon emissions, which has been researched already in [4], [5], [6] and [7]. The study in [8] presents an approach, where battery and vacuum insulated tank is used, to cover both the electricity and heating demand and to increase the renewable energy share for detached house.

Different energy management systems (EMS) for microgrids have been presented in literature [9]. The authors of [10] and [11] for example have shown an energy management solution which facilitates the optimum and economic control of energy flow throughout a microgrid system with different loads. In [12] the optimal power scheduling method for demand response in the home energy management system is developed by combining the real-time pricing (RTP) and inclining block rate (IBR) model. By combining those methods, the power scheduling method, the reduction in electricity cost and power peak-to-average ratio could be improved. The performance and feasibility of thermal storages in households were presented in [13]. The EMS for an off-grid solar-powered system is investigated by [14]. These studies contain mainly the price-based control to maximize the efficiency and utility of different loads.

In [15] an EMS in islanded mode is examined, where thermal storages are used to support the battery energy storage system (BESS) for longer off-grid mode time. However, the lifetime of battery storage is not taken into account. Similarly in [16], a microgrid battery storage management system was investigated to reduce the running costs by optimal scheduling of storage systems. This paper includes the next-day forecasted load, generation profiles, and spot electricity prices without the battery charging cycles. Energy management strategy of islanded microgrid based on power flow control was investigated in [17] to adjust the SOC of battery and control battery storage systems to avoid over-charging and over-discharging and their frequent transition between charge and discharge.

In [18] and [19] the authors present a mathematical model of a battery energy storage system considering all the electrical detail of the system. In [20] the fundamental methods of how to determine the state of charge (SOC) of lithium-ion (Li-Ion) batteries based on two different equivalent circuit diagrams were

shown. Another battery storage model was developed in Matlab Simulink in [21].

The focus in this paper is on the efficient control of energy storage depending on available power generation of the PV system and the different load profiles to reduce the charge cycles and increase the off-grid mode time. To find efficient control strategies, sufficient models of energy storage needs to be set up.

Previous mentioned papers do not consider the reduction of charge cycles and increasing off-grid mode time of the battery for residential microgrid. Therefore, we implemented in this paper, the usage of different control strategies for energy storage in an islanded microgrid on the battery's state of charge, load profile, and available PV power. The control strategies will be done for a management system in a detached house and settlement. Therefore, simplified mathematical models of battery and flywheel storage systems are used. The flywheel energy storage is integrated for short term load leveling to reduce charging cycles for the battery storage for increased battery life as well as to increase off-grid mode time, which leads to the reduction of raw material for the need of battery systems, which is beneficial for the environment.

This paper is organized as follows: Section II describes the modeling of microgrid components and different control strategies. In Section III the simulation results of the modeled system are shown, followed by the conclusion in Section IV.

II. SYSTEM MODELING

For system modeling a common model of a residential microgrid with battery and flywheel as energy storage, load profile, and PV system as the only power source is used. All those models will be described in the following. The models were created in Matlab (m.file) as a function with certain input and output parameters.

A. Mathematical object models

Battery storage:

The following simplified battery storage model was created to be able to follow better their dynamic responses [22]. The battery model was based on the state of charge (SOC) of the battery model due to battery initial state of charge (SOC_{init}), charge / discharge current (I_{batt}), battery capacity (C_{batt}) and efficiency (η) during the time (t). The SOC at a certain time step (dt) could be obtained as follows (1) [22, 23].

$$SOC(t) = SOC_{init} + \int_0^t \eta * \frac{I_{batt}(t)}{C_{batt}} * dt \quad (1)$$

Where I_{batt} was positive for charging the battery and negative for discharging. The maximum charging and discharging currents depend on the battery's capacity, on the temperature as well as on the manufacturer's specifications in the data sheet. For simplification, the battery internal temperature, prediction of the output voltage, estimation of power loss as well as the aging of the battery were neglected. All batteries are affected by self-discharge. The self-discharge rate of Li-Ion battery is about 5 percent within the first 24 hours and up to 2 percent per month afterwards. Under normal circumstances, the self-discharge of the Li-Ion battery is reasonably steady throughout its service life, but full state-of-

charge and elevated temperature can cause an increase. Table 1 displays the change of self-discharge rate per month of Li-ion batteries with rising temperature and state-of-charge [23].

These values are estimated with linear function approximation to be able to include them in the battery model. Due to different SOC, the linear function was expanded with some factors and interpolation. The self-discharge of the battery is calculated as follows:

$$s1 = T_{amb} * m + c \quad (2)$$

$$m = k * SOC \quad (3)$$

$$c = l * SOC \quad (4)$$

where $s1$ – self-discharge proportion depending on the temperature and SOC
 T_{amb} – actual ambient temperature, °C
 m – slope at various SOC, 1/°C
 c – is the y-value in which the line intersects the y-axis
 k – the estimated slope of the linear approximation
 l – estimated factor where the line intersects the y-axis

The total self-discharge rate of the battery model is described as

$$dSOC = -((s1 + (s2 * SOC)) * dt) \quad (5)$$

where $dSOC$ – total self-discharge rate of the Lithium-Ion battery
 $s1$ – self-discharge rate depending on temperature and SOC
 $s2$ – self-discharge rate of Li-Ion battery in the first 24 hours
 dt – time step, h

This is included as a function in Matlab, where the specific self-discharge rate will be chosen depending on the current temperature and SOC value.

With the rising temperature, not only the self-discharge will be affected but also the aging of the maximum storage capacity, which should also be considered in the battery model. Therefore, the maximum available storage capacity is defined as a function in Matlab, where the input is the current ambient temperature and output the maximum available capacity. The current capacity retention will be chosen by the current ambient temperature. The complete Matlab code structure of the simplified battery model is illustrated in a block diagram in Fig. 1.

TABLE I. SELF-DISCHARGE PER MONTH OF LI-ION AT VARIOUS TEMPERATURES AND STATE-OF-CHARGE [20]

State-of-charge	0°C	25°C	60°C
Full charge	6%	20%	35%
40-60% charge	2%	4%	15%

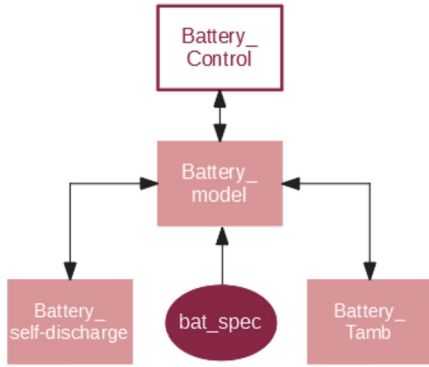


Fig. 1. Matlab code structure of battery model.

Flywheel storage:

Flywheel energy storages are used for power smoothing in smart buildings [4]. Since this work is considering a hybrid energy storage solution, a simplified model of a flywheel was created. The formulas in [4], were transposed for the created flywheel model. The simplified flywheel model is also based on the flywheels SOC value. For that, the current angular velocity (w) depending on the current SOC will be computed as shown in equation (6).

$$w = \sqrt{(SOC_{init} * (w_{max}^2 - w_{min}^2)) + w_{min}^2} \quad (6)$$

Where SOC_{init} – initial value of SOC of flywheel (0...1, where 1= full charged, and 0 = discharged)
 w_{min} – minimum angular velocity (lower limit of the usable speed range), rad/s
 w_{max} – maximum angular velocity (upper limit of the usable speed range), rad/s

The angular velocity of the flywheel (w_f), will be detected with the input parameter Ef , which is defined from the flywheel control model.

$$w_f = \sqrt{\frac{Ef \times eff \times 2}{J}} \quad (7)$$

where Ef – output energy of flywheel, kWh
 eff – flywheel efficiency, %
 J – the inertia of the flywheel, kgm^2

Afterward the new angular velocity (w_{new}) is determined, which is the difference between the current angular velocity based on the current SOC value and the angular velocity of the flywheel (8). If the output energy of the flywheel is negative w_f will be negative ($-w_f$), otherwise positive ($+w_f$).

$$w_{new} = w - w_f \quad (8)$$

where w_{new} - newly determined angular velocity, rad/s
 w – current angular velocity, rad/s

w_f – angular velocity of the flywheel, rad/s

The resulting new SOC of the flywheel will be then calculated as follows:

$$SOC_{new} = \frac{w_{new}^2 - w_{min}^2}{w_{max}^2 - w_{min}^2} \quad (9)$$

where SOC_{new} – new value of flywheel state-of-charge
 w_{new} – newly determining angular velocity, rad/s
 w_{min} – minimum angular velocity (lower limit of the usable speed range), rad/s
 w_{max} – maximum angular velocity (upper limit of the usable speed range), rad/s

Load profile:

The load profiles for the residential microgrid were generated with Load Profile Generator Software, to have load profiles with a suitable timestep and for a suitable object size [24]. Two different load profiles for different residential microgrid applications, a detached house, and settlement, were generated. The load profile of a detached house was generated for a family with two children with an annual power consumption of 3987,97 kWh [24]. The annual power consumption of a settlement was generated for 61 different households like families, couples, singles, shared apartments, and retired couples, which was 197 MWh/year. The simulations of the load profiles can be found in [25].

PV system:

Instead of modeling a whole PV system in Matlab, one-minute measurement data of an existing station in Laastu Talu OÜ, Nõrava in Estonia were used. The Station contained 668 PV panels, which are divided between 6 inverter - 2 with 20 kVA and 4 with 30 kVA. The Station had a combined output power of 177 kWp. For particular applications such as a detached house or settlement, the existing PV plant is either too large or too small. Therefore, the used PV system was scaled and simulated accordingly in [25]. The scaled PV output power is 5.77 kWp for a detached house and 286 kWp for a settlement application.

B. Control and simulation strategies

The goal of this work is to develop simplified control strategies for energy storages in an islanded microgrid to extend operation time and to reduce charging cycles for the battery storage (incl. lifetime). This has the additional benefit of reducing the amount of raw material needed for battery production. The importance of battery management and control systems were described in [25]. The safe and efficient functioning while meeting different requirements of battery storage systems is depending on the proper control of the system.

The battery control is based on the charging and discharging current of the battery. Each battery system has specific conditions and limitations in terms of depth of discharge (DOD), charging speed, charging, and discharging to adverse ambient temperatures [26]. These requirements are similar within the battery family and can be extended to almost all batteries in use. The limitations of the used battery control model are shown in Table 2.

TABLE II. BATTERY CONTROL MODEL LIMITATIONS

<i>State-of-charge</i>	<i>Set new current value [A]</i>
SOC > 0.9 AND I > 0	Inew = 0
SOC <= 0.2 AND I < 0	Inew = 0
Tamb <= 10 AND I > 0	Inew = min(Inew, 0.3 * Imax)
Tamb >= 30 AND I > 0	Inew = min(Inew, 0.5 * Imax)
I < 0	Inew = max(Inew, -Imax)
I > 0	Inew = max(Inew, Imax)

The battery control model is defined to stop charging or discharging if the maximum or minimum SOC is reached. It is better to charge a battery more often than draining it fully. Therefore, the SOC limitations are set to a maximum of 90% and a minimum of 20% [27]. The maximum charging current of the battery at different ambient temperatures was appointed due to given available operating temperatures and specifications in the datasheet.

The flywheel model was controlled in two different ways to be able to compare the results of a moving average (MA) and a custom controlled flywheel.

The power of the MA controlled flywheel is resulting by subtracting the MA value of the historical load profiles from the measured power draw of the load at the current time step (10). The MA value is defined as the sum of the historical load profile values divided by their length. For the moving average control simulation, two different lengths of moving average (30 and 60 P_{load}) were used, which was also used in [4] for comparison.

$$P_f(i) = P_{load}(i) - \frac{\sum_{k=i-N}^i P_{load}(k)}{N} \quad (10)$$

where $P_f(i)$ – power of flywheel at timestep i, W
 $P_{load}(i)$ – power of load at timestep i, W
 N – length of MA

The output energy of the flywheel system results simply by multiplying the output power (P_f) with the time step, which operates then as the input of the flywheel model.

The moving average control of the flywheel is established quite simple, without charging the flywheel or considering the supplied PV power. To be able to control the microgrid more effectively, a custom control strategy was developed. This contains 4 different algorithms, which control the flywheel depending on the current generated PV power and load profile. The 4 algorithms, which were derived are listed in Table 3.

The flywheel model compensates for a small portion of the load demand and then the battery model automatically compensates the rest. Therefore, no additional communication between the two controllers is necessary.

TABLE III. FLYWHEEL CUSTOM CONTROL ALGORITHMS

<i>Algorithm</i>	<i>Method</i>	<i>Description</i>
A	Trendline of PV and load profile	Charging/ Discharging flywheel storage aligns of the trendline, which is the slope of PV and load profile (=mpv and mload) If mpv > mload, then charging If mpv < mload, then discharging
B	Average historical values of PV and load profile	If mpvavg > mloadavg, then charging If mpvavg < mloadavg, then discharging
C	Adjusting flywheel on the current PV and load values	Current load = Ploadnew; Current PV power = Ppvnew; P_temponew=Ploadnew-Ppvnew If P_temponew < 0, then charging If P_temponew > 0, then discharging
D	Controlling flywheel within defined timeframe	If time between 8am - 7pm and Ppvnew > Ploadnew, then charging If time between 8am - 7pm and Ppvnew < Ploadnew, then discharging

C. Case study

Since this work is based on an islanded microgrid the frequency is considered to be kept constant in any case. The nominally mains voltage is at 230 V ± 10% at 50 Hz. For the following case studies, it is assumed that the system includes an inverter, which is controlling the exceeding nominal voltage and keeps it constant. The system voltage is calculated in (11) by dividing the total power by the total ac current of the system. The total power is the summation of the power of all power sources, including the battery while discharging.

$$V_{sys} = \frac{P_{tot}}{I_{tot}} \quad (11)$$

where V_{sys} – system voltage, V
 P_{tot} – total power of all power sources and battery while discharging, W
 I_{tot} – total ac current of the system, A

For the case study three different scenarios were defined, which will be chosen by activating or deactivating a certain flywheel control model with the specific control algorithm. An overview of the simulation scenarios is given in Table 4. The simulation scenarios were conducted for a detached house as well as for a settlement microgrid system. The simulation results of both applications with the different scenarios are described in the next chapter.

The first scenario is including the simulation of a microgrid by considering only the load profile, PV, and battery control system. This is created as a base scenario to be able to compare the battery storage behaviour when using different control systems and the additional energy storage system flywheel.

TABLE IV. SIMULATION SCENARIOS

Scenario Number	Activated appliances	Control models
1	Battery	Only battery control
2	Battery Flywheel	Battery control Flywheel MA control
3	Battery Flywheel	Battery control Flywheel custom control

III. RESULTS

The simulations were done for a detached house as well as for a settlement simulation with all three simulation scenarios. The results are presented in Table 5 with all simulated scenarios and control algorithms. The scenario numbers are listed in the first column. The chosen applications detached house (D) and settlement (S) is in the second column. The best result for the detached house application could be achieved with the scenario 3 algorithm D, with 360 battery charge cycles and off-grid mode time 21h 22min. The maximum off-grid time with 21h 25min could be reached with scenario 3 and algorithm A for the settlement application. The battery charge cycle was 382 cycles. Additionally, the cycle lifetime could be increased up to over 10 years for both applications. The cycle lifetime of the battery is the result of the division of the maximum cycle lifetime of the battery, which was taken from the datasheet and the calculated cycles per year (12).

$$\text{Cycle lifetime [year]} = \frac{\text{Max.cycle lifetime of battery}}{\text{Calculated cycles per year}}$$

These are theoretical values, which are based on given values in the datasheet. For verification, these should be practically tested. Another important aspect that needs to be considered is the financing of the project. The financial analysis is briefly discussed in [25].

TABLE V. OVERVIEW SIMULATION RESULTS

Scenario	Model	Algorithm	Charge cycles/year	Cycle lifetime [year]	Max. off-grid time
1	D	-	542	8.3	10h 22min
	S	-	403	11	20h 58min
2	D	MA 30	496	9	20h 48min
		MA 60	455	9.9	20h 55min
	S	MA 30	403	11	21h 12min
		MA 60	403	11	20h 58min
3	D	A	378	11.9	21h 06min
		D	360	12.5	21h 22min
	S	A	382	11.7	21h 25min
		D	384	11.7	21h 07min

D = detached house; S = Settlement; MA30 /60 = Moving average length 30 or 60; Different Algorithms = A, B, C, D (c.f. Table III).

For comparison the SOC behaviour of the base scenario and scenario 3 is shown in Figure 2. The initial SOC value of battery and flywheel were set to 1 (=full charged). It is assumed that the battery and flywheel is fully charged from the previous day. It can be seen that the battery in scenario 3 is less charged and discharged compared to scenario 2. The maximum off-grid time is defined as the maximum uninterrupted time, where the system voltage is between the maximum and minimum defined voltage limitation. For the base scenario of detached house simulation, an off-grid time of 10h 22min could be achieved. By using scenario 3 with algorithm D for the same application, voltage drops at 10h 23min could be removed and the maximum off-grid time increased up to 21h 22min. The maximum off-grid time applies from midnight. Thus, it is verified that the proposed control method results in better off-grid mode time, charge cycles and battery lifetime. The simulations for the settlement application can be seen in [25].

IV. CONCLUSION

In this paper, control strategies for energy storage in an islanded microgrid were investigated. Therefore, simplified mathematical models of battery and flywheel storage systems were used. The emphasis of the work was to integrate a flywheel model for short term load leveling to reduce charging cycles for the battery storage for increased battery lifetime and off-grid mode time. This could be achieved with the development of control strategies and algorithms for different applications such as detached houses and settlements. The best results could be achieved for both applications with scenario 3, which contains the custom control. By using algorithm D for the detached house and algorithm A for the settlement, the charge cycles of the battery could be reduced up to 360 and 382 cycles. The maximum off-grid time for a detached house and settlement simulation could be increased up to 21h. Finally, it could be achieved a reduction of the battery cycles up to 34% for the detached house and 5.4% for the settlement application. The maximum off-grid mode time of the system could be increased almost the entire day both applications compared to a system with only a battery storage system. In future work, the practical verification of the achieved values should be investigated. Furthermore, the economics should be evaluated with such algorithms.

ACKNOWLEDGMENT

This work was supported by the European Commission through the H2020 project Finest Twins (grant No. 856602), and Estonian Centre of Excellence in Zero Energy and Resource Efficient Smart Buildings and Districts ZEBE, grant 2014-2020.4.01.15-0016 funded by European Regional Development Fund

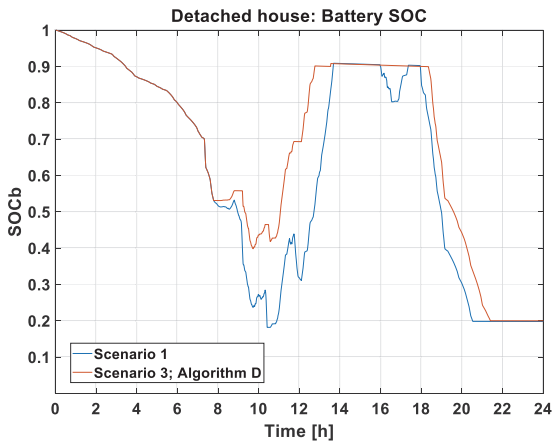


Fig. 2. Detached house SOC behaviour of the battery

REFERENCES

[1] Florian, "gridx," [Online]. Available: <https://gridx.de/2018/02/08/microgrids-und-die-dezentrale-energieverde/>. [Accessed 29 February 2019]

[2] L. Czarnecki, "Photovoltaik: Grundlagen, Systeme und Betrieb," bookboon, 2018.

[3] S. Borlase, Smart Grids: Infrastructure, Technology and Solutions, Boca Raton: Taylor & Francis Group, 2013.

[4] F. Plaum, T. Häring, R. Ahmadihangar, A. Rosin, „Power Smoothing in Smart Grids using Flywheel Energy Storage,” in 14th International Conference on Compatibility, Power Electronics and Power Engineering, Setúbal, Portugal, 2020.

[5] A. M. Aly, A. M. Kassem, K. Sayed, I. Aboelhasan, “Design of Microgrid with Flywheel Energy Storage System Using HOMER Software for Case Study”, in 2019 International Conference on Innovative Trends in Computer Engineering (ITCE), Aswan, 2019.

[6] L. Tziiovani, P. Kolios, L. Hadjidemetriou, and E. Kyriakides, “Grid Friendly Operation of a PV-Storage System with Profit Maximization and Reliability Enhancement,” in SEST 2019 - 2nd International Conference on Smart Energy Systems and Technologies, 2019.

[7] A. Awad, I. Tumar, M. Hussein, W. Ghanem, and J. A. Sa’ed, “PV output power smoothing using flywheel storage system,” in Conference Proceedings - 2017 17th IEEE International Conference on Environment and Electrical Engineering and 2017 1st IEEE Industrial and Commercial Power Systems Europe, IEEEIC / I and CPS Europe 2017, 2017.

[8] J. Kalder, M. Hovi, A. Allik, A. Annuk, “Interseasonal heat storage for residential buildings with renewable energy generation”, in Engineering for Rural Development, Jelgava, 22.-24.05.2019.

[9] D. Serna-Suárez, G. Ordóñez-Plata, G. Carrillo-Caicedo, "Microgrid's Energy Management Systems: A survey," in 2015 12th International Conference on the European Energy Market (EEM), Lisbon, 2015.

[10] S. Ganesan, S. Padmanaban, R. Varadarajan, U. Subramaniam, L. Mihet-Popa, “Study and Analysis of an Intelligent Microgrid Energy

Management Solution with Distributed Energy Sources,” in Energies 2017, 10, 1419.

[11] L. Aleixo, A. Z. Morch, A. Rosin, O. S. Grande, H. Sæle and I. Palu, "Ecogrid EU project — Real time price based load control and economic benefits in a wind production based system," *22nd International Conference and Exhibition on Electricity Distribution (CIRED 2013)*, Stockholm, 2013, pp. 1-4.

[12] Z. Zhao, W. C. Lee, Y. Shin, K. Song, “An Optimal Power Scheduling Method for Demand Response in Home Energy Management System”, in IEEE Transactions on Smart Grid, vol. 4, no. 3, pp. 1391-1400, Sept. 2013.

[13] Rosin, A., Link, S., Lehtla, M., Martins, J., Drovtar, I., Roasto, I. Performance and feasibility analysis of electricity price based control models for thermal storages in households. (2017) *Sustainable Cities and Society*, 32, pp. 366-374.

[14] D. Zelazo, R. Dai, M. Mesbahi, “An energy management system for off-grid power systems,” in *Energy Systems* 3(2), 2012.

[15] T. Häring, R. Ahmadihangar, A. Rosin, H. Biechl, “Impact of Load Matching Algorithms on the Battery Capacity with different Household Occupancies”, in 2019 45th IECON Annual Conference of the IEEE Industrial Electronics Society, Lisbon, 2019.

[16] P. Mahat, J. E. Jiménez, E. R. Moldes, S. I. Haug, I. G. Szczesny, K. E. Pollestad, L. C. Totu, "A micro-grid battery storage management," 2013 IEEE Power & Energy Society General Meeting, Vancouver, BC, 2013, pp. 1-5.

[17] Y. Zhang, H. J. Jia, L. Guo, "Energy management strategy of islanded microgrid based on power flow control," 2012 IEEE PES Innovative Smart Grid Technologies (ISGT), Washington, DC, 2012, pp. 1-8.

[18] A. Rahmoun, A. Armstorfer, H. Biechl, A. Rosin, “Mathematical Modeling of a Battery Energy Storage System in Grid Froming Mode,” in 2017 58th International Scientific Conference on Power and Electrical Engineering of Riga Technical University (RTUCON), Riga, 2017.

[19] A. Rahmoun, A. Armstorfer, J. Helguero, H. Biechl and A. Rosin, "Mathematical modeling and dynamic behavior of a Lithium-Ion battery system for microgrid application," *2016 IEEE International Energy Conference (ENERGYCON)*, Leuven, 2016, pp. 1-6.

[20] A. Rahmoun, H. Biechl, "Modelling of Li-ion batteries using equivalent circuit diagrams," *Electrical, Control and Communication Engineering*, no. 7b, 2012.

[21] I. Baboselac, Ž. Hederic, T. Bencic “MATLAB Simulation Model for Dynamic Mode of the Lithium-Ion Batteries to Power the EV”, in *Technical Journal* 11(1-2), 2017.

[22] Y. Tian, D. Li, J. Tiana, B. Xia, "State of charge estimation of lithium-ion batteries using an optimal adaptive gain nonlinear observer," *Electrochimica Acta*, vol. 225, pp. 225-234, 2017.

[23] Wen-Yeou Chang, "The State of Charge Estimating Methods for Battery: A Review," *ISRN Applied Mathematics*, p. 7, 5 July 2013.

[24] Noah Pflugrad, "Load Profile Generator," 2016. [Online]. Available: <https://www.loadprofilegenerator.de>. [Accessed 21 10 2019].

[25] N. Cinay, “Research and Development of control strategies for energy storages in an islanded microgrid,” Master thesis, School of Engineering, Tallinn University of Technology, Tallinn, 2020.

[26] "Battery University," [Online]. Available: https://batteryuniversity.com/learn/article/how_to_prolong_lithium_based_batteries. [Accessed 16 November 2019].

[27] "Battery University," [Online]. Available: https://batteryuniversity.com/learn/article/how_to_make_batteries_more_reliable_and_longer_lasting_1. [Accessed 13 May 2019].

Publication V

T. Häring, A. Rosin, T. M. Kull, J. Helguero and H. Biechl, “Thermal Modelling of a Control Center for Flexibility Analysis in nZEB Nanogrids,” 2020 IEEE 61th International Scientific Conference on Power and Electrical Engineering of Riga Technical University (RTUCON), 2020, pp. 1–6, doi: 10.1109/RTUCON51174.2020.9316568.

Thermal Modelling of a Control Center for Flexibility Analysis in nZEB Nanogrids

Tobias Häring, Argo Rosin
Smart City Center of Excellence
(Finest Twins) & Department of
Electrical Power Engineering and
Mechatronics
Tallinn University of Technology
Tallinn, Estonia
tobias.haring@taltech.ee

Tuule Mall Kull
Department of Civil Engineering and
Architecture
Tallinn University of Technology
Tallinn, Estonia

Jorge Helguero, Helmuth Biechl
Institute of Electrical Power Systems
(IEES)
University of Applied Sciences
Kempten
Kempten, Germany

Abstract— Due to the increasing share of volatile renewable energy sources, like photovoltaics (PV) and wind energy in nearly Zero Energy Buildings (nZEB), there is an increasing need for demand-side management (DSM) or demand response (DR) programs to balance the production and consumption in the grid. The flexibility that can be obtained for smart grids from such DR methods is not limited to appliances like water heaters or dishwashers but can also be achieved with space heating and air-conditioning. In such an interdisciplinary investigation, often one part is simplified, in this case, typically either the thermal models or the implemented DR strategy are very detailed. In this work, a detailed thermal model of a control center is obtained and calibrated in IDA ICE building-modelling software with measurements from a test site in Germany. Afterward, several price-based load matching algorithms are applied to the model to see the possible flexibility exploitation with the thermal capacity of this small building. Not all investigated algorithms show good performance but some of them show promising results. Thus, this model can be used for DR methods and should be extended to work with more DSM strategies and provide ancillary services.

Keywords— Flexibility, Smart City, nZEB, Thermal Storage, Space Heating, Demand Response, Nanogrid

I. INTRODUCTION

As the share of renewable energy production is increasing worldwide, with some countries already having renewable energy shares of 30% and more, the operational complexity for the electrical power grid increases accordingly. This development creates despite its sustainability and environmental friendliness several challenges for grid operators. The volatility and unpredictability of the renewable energy sources, like photovoltaics (PV) or wind power, which are popular to be installed in nearly Zero Energy Buildings (nZEB), can create imbalances between energy production and consumption. This makes the planning of energy production especially complicated to prevent mismatches and therefore unstable energy supply for the customers. One concept to tackle this problem is to use demand response techniques [1], which aim to adapt the load by scheduling certain household devices. Such demand response (DR) or demand-side

This work was supported by the Estonian Centre of Excellence in Zero Energy and Resource Efficient Smart Buildings and Districts ZEBE, grant 2014-2020.4.01.15-0016 funded by European Regional Development Fund; and supported by the European Commission through the H2020 project Finest Twins (grant No. 856602).

management (DSM) methods, which are an important part of smart grids and smart cities, can be applied on many different devices in a household, for example, freezer, water heater [2], or other appliances like dishwashers [3]. These DR and DSM concepts can increase the flexibility [4] of the system, which is an officially recognized concept in power systems [5], [6], which helps to improve the balance between energy production and consumption. Like this, it is possible to react to unexpected changes and more efficiently plan the energy generation and use.

Additionally, it is not just possible to use various appliances in a household for DR. The thermal capacity of the whole building, meaning the space heating, air conditioning [7], and ventilation systems [8] can be used for DSM.

In this context, several publications present a complex DR control approach but use simplified thermal models to estimate the electrical energy demand of the heating systems for example. In [9] the authors propose a price-based control strategy with a minimalistic model of the space heating, assuming it to be a certain percentage of the energy consumption. The authors of [10] show possible DSM strategies with space heating /cooling with a multi-agent system. They are using a simple aggregated model for their research. [11] presents a DSM approach with a simplified thermal model for houses. From that, the flexibility of the system is assessed and the heat pumps are controlled in a DR scheme. Similarly, in [12] different load matching control algorithms are used to optimize the system in a DSM manner. A simplified thermal model based on temperature differences due to different influences is used to estimate the electrical consumption.

On the other hand, there are publications, which consider a very detailed thermal model but use a simple control strategy. The heat pump model presented in [13] is very detailed. The demand response control strategy presented is comparably simple. The thermal models of buildings presented in [14] are quite detailed but the demand response methods are limited somehow and do not show the anticipated results. Several other publications like [15] show very detailed thermal models but do not consider DR or DSM methods at all.

Therefore, this work aims to create a detailed thermal model of a control center, which is part of a nanogrid with PV-installations and home battery energy storage systems. This thermal model should provide good performance based on comparisons with measurements of the real object. It is then being used with different price-based load matching algorithms to achieve an efficient demand response control of the space heating in the control center. The model is additionally already created in a way that it can be used for more detailed future investigations on the nanogrid with more demand-side management methods and providing ancillary services to the grid.

The paper is organized as follows: The methodology, including the measurements, modeling, calibration, and simulation setup, is presented in Section II. Section III shows the results of the simulations. Finally, the results in brief with conclusions are presented in Section IV.

II. METHODOLOGY

The control center is part of the Energy Campus Wildpoldsried in the city of Wildpoldsried in southern Germany. It is part of University of Applied Sciences Kempten, Germany. The work of this paper is a cooperation between Tallinn University of Technology and University of Applied Sciences Kempten.

A. Control Center Measurements

To obtain the necessary data to model the control center and calibrate the model, measurements were needed. Therefore, four temperature sensors were used, three of which were placed inside the control center and one outside. The temperature sensors on the inside were placed on different heights and different positions in the room (c.f. Fig. 1). The sensor outside was placed in a wind and weather protected place. Several days were measured from the 21st Nov. 2019 until 25th Nov. 2019 with a free-floating control center, where all heat sources were turned off, and from 25th Nov. 2019 until 27th Nov. 2019 with an electric heater inside the control center. The power consumption of the electric heater was measured with a portable power meter.

An additional free-floating measurement with three sensors on the outside and 1 sensor on the inside was conducted to see the influence of the outside sensor placement on the measurements. The used temperature sensors were EL-USB-2 EH / Temp Data Loggers.

Additionally, during the measurements, the data of a nearby weather station was stored. It contained measurements for the outside temperature, global irradiation, air pressure, humidity, dew point, wind speed and wind direction.

Thermal imaging of the electric heater was done as well, to see the heat dissipation of the used device. The electric heater from EUROM was operated at 1300 W during the thermal imaging and during the measurement time (c.f. Fig. 2).

B. Control Center Model and Calibration

The container was modeled in IDA ICE 4.8 building simulation software. The floorplan and 3D model pictures of

the container are shown in Fig. 3. The constructions and window parameters were inputs given by the container producer. The small corridor after the external door was not modeled as the corridor door to the room was kept open during the whole experiment. The climate data from the closest weather station were used as boundary conditions.

To calibrate the model, the parameter values for infiltration, power emitted by the computers, and the furniture area were varied. These values were chosen as no information about these was available. As reliable wind direction data was missing, infiltration was set to constant. Although maximum computer power was known, the computers did not work on nominal power the whole time. As the profile of usage was not measured, the computer power was also assumed to be constant. The furniture is modeled in IDA ICE as a capacity with a heat transfer coefficient of 6 W/(m²K). The area of the furniture is the furniture surface facing the room air where the heat is transferred.

The quality of the model was assessed by the average absolute error between the simulated and measured air temperatures in the room. IDA ICE models the room with ideally mixed air so there is one air temperature in the room. The simulated temperature was compared to the average temperature measured by the sensors.

Parametric analysis was carried out first for the free-floating periods to calibrate the envelope and then for the period with an electrical heater to check the heat-up performance. The results were adapted in the simulation of the whole experiment period. The found values for the varied parameters are 0.05 l/s-m² of infiltration rate per external surfaces, 80 W power of the computers, and 26 m² of furniture area.



Fig. 1. EL-USB-2 EH / Temp Data Logger placed on top of a shelf



Fig. 2. EUROM electric heater placed in the middle of the control center for calibration measurement



Fig. 3. The container model in IDA ICE with floorplan on the left and 3D view on the right. The compass is shown for orientation in both pictures

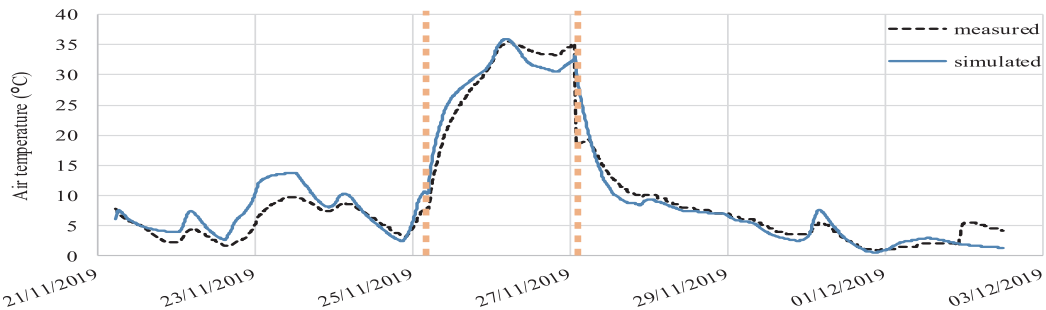


Fig. 4. The behavior of the air temperature in the simulation compared to the average of measurements. The vertical orange lines separate the three different periods – 1st free-floating, electric heating, and 2nd free-floating period

Ideal heater and cooler were set to achieve the initial state of the container. The setpoint value of the cooler was set to 0.1 degrees higher than the heater's and the latter was estimated by minimizing the average absolute error during the first free-heating period. The lowest error was achieved while aiming for a temperature between 3.75 °C and 3.85 °C, although the initial measured temperature was 8.2 °C. This was probably because the pre-simulation conditioning of the model is constant but the actual behavior is dynamic.

The resulting temperature behavior is compared to the average measured temperature in Fig. 4. The average absolute error for the whole period was 1.61 °C, for the three periods the errors were 1.92 °C, 2.08 °C and 1.00 °C. The error in the heating period is mostly caused by a small shift in time and the moment around the time when heating was turned off. The air temperature in the room drops drastically in a very short time. It is not clear whether the door was opened for a longer time or is this an error in the measurement.

The error during the first period shows that either the initial state was not estimated ideally or the heat capacity or heat loss of the container is modeled too low. The calibration during the last period is almost ideal as in reality the temperatures are not ideally mixed and the energetically effective temperature of the measured period is not known. As the general behavior of the container is close to the average measurements, the achieved result is suitable for the following work.

C. Price-based Load Matching Algorithm Control

Different price-based load matching algorithms were implemented in this model to see the responsiveness of the control center to set point based control strategies. Therefore, the electric heaters were controlled with a thermostatic two-step controller. In the first step, a fixed setpoint value of 22°C was selected with a 1°C deadband. This will be the basic benchmark for comparison with the other control strategies.

To have prices with smaller fluctuations than the spot market prices, the hourly day-ahead prices of the Nordpool database [16] for Estonia were obtained for the setpoint control algorithms. The prices without additional fees and taxes from November 22nd until December 2nd, 2019 were used for the setpoint calculation (c.f. Fig. 5). The seven different price-based setpoint calculation algorithms (A-F) were based on [2],

[17] and [18]. The algorithms are shown in TABLE I. Their performance has been positively evaluated under different occupancy- and other considerations for simple models of a freezer, water heater and space heating for a household in an apartment [19] and [20]. The pre-calculated setpoints for each algorithm were created as an input look-up table for the set point of the thermostatic controller in the IDA-ICE simulations. The parameters for the setpoint calculation algorithms and the two-step thermostatic control are shown in TABLE II. The minimum (Pr_{min}), maximum (Pr_{max}) and average (Pr_{avg}) price, and the price deviation (Pr_{dev}) are calculated from the Nordpool prices for each day. Each simulation was done in the timeframe of Nov. 22nd until Dec. 2nd, 2019.

TABLE I. DESCRIPTION OF PRICE-BASED SET POINT CALCULATION ALGORITHMS [2],[17],[18]

Algorithm	Description of set point calculation algorithm
A	$T_{set} = T_{set,max} - (Pr - Pr_{min}) * \frac{T_{set,max} - T_{set,min}}{Pr_{max} - Pr_{min}}$
B	$T_{set} = T_{goal} - (Pr - Pr_{avg}) * \frac{ T_{set,min} - T_{goal} }{Pr_{dev}}$
C	$T_{set} = T_{goal} - (Pr - Pr_{avg}) * \frac{T_{set,min} - T_{goal}}{Pr_{min} - Pr_{avg}}$
D	$T_{set} = T_{goal} - (Pr - Pr_{min}) * \frac{T_{set,min} - T_{goal}}{Pr_{min} - Pr_{avg}}$
E	$T_{set} = T_{goal} - (Pr - Pr_{avg}) * \frac{T_{set,max} - T_{set,min}}{Pr_{max} - Pr_{min}}$
F	$T_{set} = T_{goal} - (Pr - Pr_{min}) * \frac{T_{set,max} - T_{set,min}}{Pr_{max} - Pr_{min}}$
G	$Pr \geq Pr_{avg} \rightarrow T_{set} = T_{set,min};$ $Otherwise \rightarrow T_{set} = T_{set,max};$

TABLE II. PARAMETERS FOR SETPOINT CALCULATION ALGORITHMS

Parameter	Symbol	Value
Maximum Set Point	$T_{set,max}$	24 [°C]
Minimum Set Point	$T_{set,min}$	20 [°C]
Goal Set Point	T_{goal}	22 [°C]
Two-step Controller Deadband	-	1 [°C]

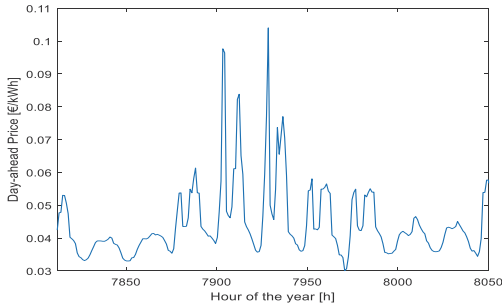


Fig. 5. Nordpool hourly day-ahead prices without additional fees and taxes for November 22nd until December 2nd, 2019

III. RESULTS

The setpoint calculation algorithms show slightly different behavior for the selected price pattern. The results for the indoor air temperature can be seen in Fig. 6. The $\pm 0.5^\circ\text{C}$ deadband is not reached in the shown curves because the data was plotted with a smoothing filter to better compare the behavior of the different algorithms.

Algorithm A, B and C show similar behavior with only slightly different setpoint selection. They vary between the maximum and minimum setpoint. This behavior considers both, user comfort and price orientation.

Algorithm D and F vary between the minimum and goal set point. This means that the setpoint is selected more price-oriented than user comfort-oriented. This was also found in [19].

Algorithm E selected set points between the minimum and the maximum. But it tends to select less extreme set points, which tend to be closer to the goal set point than the ones selected by algorithms A, B and C. This provides both, user comfort and price orientation.

Algorithm G switches between the maximum and minimum setpoint as expected. For the selected set point boundaries this might not be a comfortable temperature behavior for the user as the temperature differences are quite high.

To see which algorithm shows the best price-oriented results, the hourly price multiplied with the consumption due to heating for each hour were cumulated to see the price development over time, which is shown in Fig. 7. The final values for the cumulative costs are additionally shown in TABLE III.

At the end of the simulation time algorithms A, B and C show higher energy consumption costs than the fixed setpoint control. This is an unexpected result. Closer examination shows, that the cumulative costs show strong increases during the price peaks at around hours 7910 and 7920 and this difference only slightly decreases until the end of the simulation. The behavior is similar for algorithm G, which shows final cumulative costs around the costs of the fixed setpoint control. Even though day-ahead prices with typically

smaller fluctuations than spot prices were used for the simulations, the selected algorithms seem to show undesirable behavior for price peaks with this more detailed space heating model.

Algorithm D and F show the best price-oriented performance as expected. The cumulative energy consumption costs are the lowest. The two price peaks do not seem to have a big impact on these algorithms either.

The cumulative costs for algorithm E are lower than for a fixed set point control but higher than with algorithm D or F. The price peaks do not affect this algorithm much. Thus, this algorithm shows the best performance in total, considering user comfort and price orientation.

The user comfort and cost reductions for each algorithm are shown in TABLE III. As can be seen, the algorithms show different results with the simple space heating model from [19] compared to this model. Algorithms A, B and C provide cost reductions with the simple model, whereas the cumulative costs are higher with the IDA-ICE-model. As mentioned before, this is caused by the price peaks of the used price pattern, which are for a different time period than the ones of the simple model. Nevertheless, such an algorithm should work with all different possible price-patterns similarly good and always provide cost reductions or at least price parity with a fixed setpoint control.

IV. CONCLUSIONS

The modeled control center in IDA ICE software was suitable for the use with nanogrid simulations after the initial calibrations. The model showed the expected behavior in comparison to the measurements and could therefore be used for the setpoint algorithm control simulations.

Different load matching control algorithms were implemented to investigate the behavior of space heating as a thermal storage with such a model. To generate set points for the two-step thermostatic control, prices from the Nordpool database could be used.

Not all algorithms showed preferable behavior. Algorithms A; B and C even increased the consumption costs than a fixed set point control while providing average user comfort. Algorithm G provided a lower user comfort while achieving about the same cumulative costs like a fixed set point control. Thus, these implementations provide no benefits while adding

TABLE III. USER COMFORT COMPARED TO A FIXED SETPOINT (FSP) CONTROL AND COST REDUCTION COMPARISON BETWEEN THIS MODEL AND THE SIMPLE MODEL FROM [19]

Algorithm	User Comfort	Cumulative Costs [€]	Cost Reduction	Cost Reduction in [19]
A	0	8.65	--	+
B	0	8.56	-	+
C	0	8.59	-	+
D	--	7.76	++	++
E	0	8.27	+	+
F	--	7.80	++	++
G	-	8.53	0	0
FSP	0	8.54	0	0

++ highest; + high; 0 none; - lower; -- lowest;

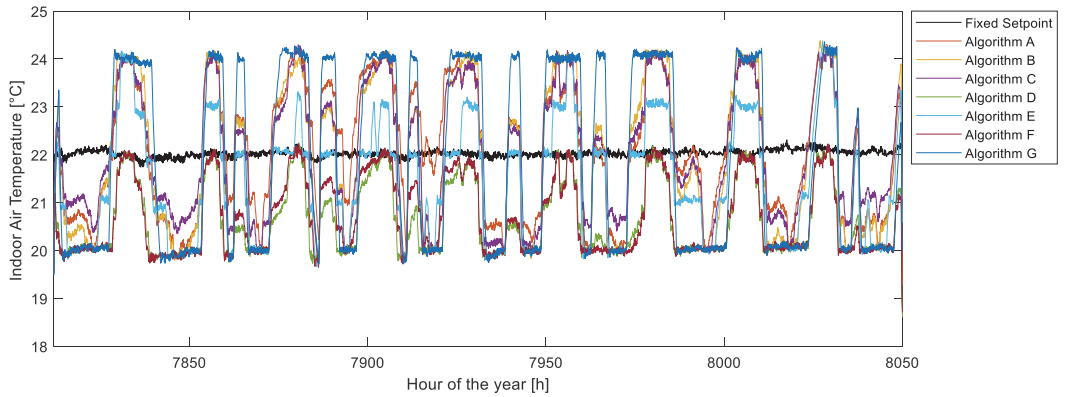


Fig. 6. Indoor air temperature results for set point calculation algorithms A-G and a fixed set point

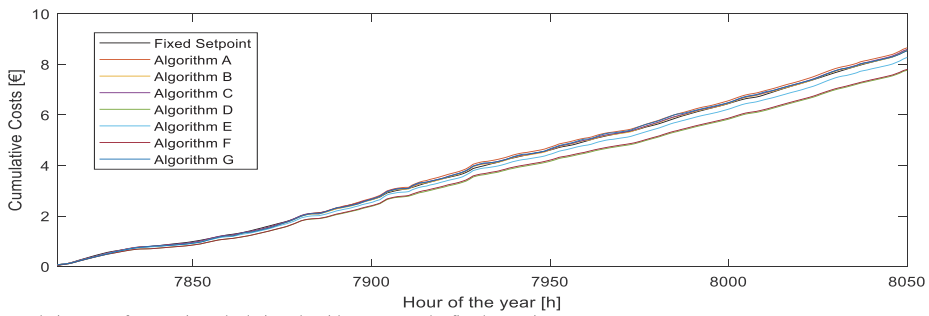


Fig. 7. Cumulative costs for setpoint calculation algorithms A-G and a fixed set point

complexity in this application case. Algorithms D and F reduce consumption costs at the cost of lower user comfort. For some users, this might be the preferred control method to achieve maximum cost reductions. Overall, algorithm E shows the best compromise of the two considerations. The consumption costs can be reduced while maintaining user comfort. Therefore, this is the preferred control strategy to control space heating based on market prices.

The results of the simulations show that such a thermal model can be used for research and development of flexibility-oriented control strategies, as the models show similar results like simple thermal models that have been used before. However, the more complex models also reveal problems of some of these algorithms to work efficiently with space heating, which were not noticed with the simple model before. Therefore, more complex models need to be taken into account for further research.

In future work, this model needs to be extended to more common heating devices such as heat pumps, and control strategies for islanded nanogrids or ancillary services should be taken into account. Using a thermal model of a complete apartment block could be useful for aggregated simulations as well.

REFERENCES

- [1] I. Palu, O. S. Grande, H. Saele, A. Rosin, A. Z. Morch, and L. Aleixo, "Ecogrid EU project - real time price based load control and economic benefits in a wind production based system," in 22nd International Conference and Exhibition on Electricity Distribution (CIRED 2013), 2013, pp. 1474–1474, doi: 10.1049/cp.2013.1253.
- [2] A. Rosin, S. Link, M. Lehtla, J. Martins, I. Drovtnar, and I. Roasto, "Performance and feasibility analysis of electricity price based control models for thermal storages in households," *Sustain. Cities Soc.*, vol. 32, pp. 366–374, Jul. 2017, doi: 10.1016/j.scs.2017.04.008.
- [3] S. Mishra, H. Koduvere, I. Palu, R. Kuhi-Thalfeldt, and A. Rosin, "Assessing demand side flexibility with renewable energy resources," in *EEEIC 2016 - International Conference on Environment and Electrical Engineering*, 2016, doi: 10.1109/EEEIC.2016.7555546.
- [4] R. Ahmadihangar, T. Häring, A. Rosin, T. Korötko, and J. Martins, "Residential Load Forecasting for Flexibility Prediction Using Machine Learning-Based Regression Model," in *Proceedings - 2019 IEEE International Conference on Environment and Electrical Engineering and 2019 IEEE Industrial and Commercial Power Systems Europe, EEEIC/I and CPS Europe 2019*, 2019, pp. 1–4, doi: 10.1109/EEEIC.2019.8783634.
- [5] International Energy Agency, *Harnessing Variable Renewables - A Guide to the Balancing Challenge*. OECD/IEA, 2011.
- [6] North American Electric Reliability Corporation, "Accommodating High Levels of Variable Generation," *North Am. Electr. Reliab. Corp.*, no. April, p. 104, 2009.

- [7] T. Häring, A. Rosin, and H. Biechl, "Using common household thermal storages to support the PV- and battery system in nearly zero energy buildings in off-grid mode," *Sustain. Energy Technol. Assessments*, vol. 35, no. May, pp. 12–24, Oct. 2019, doi: 10.1016/j.seta.2019.05.014.
- [8] V. Maask, T. Haring, R. Ahmadiyahangar, A. Rosin, and T. Korotko, "Analysis of Ventilation Load Flexibility Depending on Indoor Climate Conditions," in *2020 IEEE International Conference on Industrial Technology (ICIT)*, 2020, pp. 607–612, doi: 10.1109/ICIT45562.2020.9067153.
- [9] O. Kilkki, A. Alahäivälä, and I. Seilonen, "Optimized control of price-based demand response with electric storage space heating," *IEEE Trans. Ind. Informatics*, vol. 11, no. 1, pp. 281–288, Feb. 2015, doi: 10.1109/TII.2014.2342032.
- [10] B. Feron and A. Monti, "Integration of space heating demand flexibility in a home energy management system using a market-based multi agent system," in *IEEE Power and Energy Society General Meeting*, 2018, vol. 2018-Janua, pp. 1–5, doi: 10.1109/PESGM.2017.8273810.
- [11] M. Pau, J. L. Cremer, F. Ponci, and A. Monti, "Impact of customers flexibility in heat pumps scheduling for demand side management," in *Conference Proceedings - 2017 17th IEEE International Conference on Environment and Electrical Engineering and 2017 1st IEEE Industrial and Commercial Power Systems Europe, EEEIC / I and CPS Europe 2017*, 2017, doi: 10.1109/EEEIC.2017.7977681.
- [12] T. Haring, R. Ahmadiyahangar, A. Rosin, and H. Biechl, "Impact of Load Matching Algorithms on the Battery Capacity with different Household Occupancies," in *IECON 2019 - 45th Annual Conference of the IEEE Industrial Electronics Society*, 2019, pp. 2541–2547, doi: 10.1109/IECON.2019.8927495.
- [13] J. Clauß and L. Georges, "Model complexity of heat pump systems to investigate the building energy flexibility and guidelines for model implementation," *Appl. Energy*, vol. 255, p. 113847, Dec. 2019, doi: 10.1016/j.apenergy.2019.113847.
- [14] R. E. Hedegaard, M. H. Kristensen, T. H. Pedersen, A. Brun, and S. Petersen, "Bottom-up modelling methodology for urban-scale analysis of residential space heating demand response," *Appl. Energy*, vol. 242, pp. 181–204, May 2019, doi: 10.1016/j.apenergy.2019.03.063.
- [15] L. Georges, M. Thalfeldt, Ø. Skreiberg, and W. Fornari, "Validation of a transient zonal model to predict the detailed indoor thermal environment: Case of electric radiators and wood stoves," *Build. Environ.*, vol. 149, pp. 169–181, Feb. 2019, doi: 10.1016/j.buildenv.2018.12.020.
- [16] "Market data | Nord Pool." [Online]. Available: <https://www.nordpoolgroup.com/Market-data/Dayahead/Area-Prices/EE/Hourly/?view=table>. [Accessed: 20-Feb-2020].
- [17] H. D.J et al., "Pacific Northwest GridWise™ Testbed Demonstration Projects, Volume I: The Olympic Peninsula Project." 2007.
- [18] C. H. K. Goh and J. Apt, "Consumer Strategies for Controlling Electric Water Heaters under Dynamic Pricing," *Carnegie Mellon Electr. Ind. Cent. Work. Pap.*, pp. 1–8, 2005.
- [19] T. Haring, R. Ahmadiyahangar, A. Rosin, H. Biechl, and T. Korotko, "Comparison of the impact of different household occupancies on load matching algorithms," in *2019 Electric Power Quality and Supply Reliability Conference (PQ) & 2019 Symposium on Electrical Engineering and Mechatronics (SEEM)*, 2019, pp. 1–6, doi: 10.1109/PQ.2019.8818270.
- [20] T. Häring, "Research And Development Of Thermal Storage Control Models," M.Sc.Eng thesis, Tallinn University of Technology, 2018.

Tobias Häring received the B.Eng. in Industrial Engineering from Kempten University of Applied Sciences, Germany in 2016, M.Eng. in Electrical Engineering from Kempten University of Applied Sciences, Germany in 2018 and M.Sc.Eng. in Electrical Drives and Power Electronics from Tallinn University of Technology, Estonia in 2018. He is currently working as a Doctoral Student / Early Stage Researcher at Tallinn University of Technology, Estonia. His main research interests are microgrids, distributed/renewable generation, demand side management, storage technologies and machine learning.

Publication VI

F. Plaum, T. Häring, R. Ahmadiyahangar and A. Rosin, "Power Smoothing in Smart Buildings using Flywheel Energy Storage," 2020 IEEE 14th International Conference on Compatibility, Power Electronics and Power Engineering (CPE-POWERENG), 2020, pp. 473–477, doi: 10.1109/CPE-POWERENG48600.2020.9161458.

Power Smoothing in Smart Buildings using Flywheel Energy Storage

Freddy Plaum, Tobias Häring, Roya Ahmadihangar, Argo Rosin
Smart City Center of Excellence (Finest Twins) & Department of Electrical Power Engineering and Mechatronics
Tallinn University of Technology
Tallinn, Estonia
freddy.plaum@taltech.ee

Abstract—Emergence of concepts such as smart grids and smart cities has led to a more closely monitored and managed power systems. As such, the power production is shifting towards more distributed generation consisting of renewable energy sources whose fluctuating nature complicates the balancing of supply and demand. Demand response methods have been employed to smooth the power needs by shifting loads to when there is a surplus of production. In this paper, power smoothing of fluctuating loads using a flywheel storage system is investigated for a small grid connected microgrid. A model of a low speed flywheel system is developed with a current control of the grid-side converter and field-oriented control of the motor-side converter. A moving average filter is used for power smoothing in a small microgrid. The performance of power smoothing could be adjusted by varying the length of the time window of moving average filter. An 81.9 % reduction in RMSE of grid power fluctuations was accomplished showing that flywheel storage can be successfully used to smoothen microgrid power.

Keywords—flywheel energy storage system, power smoothing, microgrid, smart grid, smart city, model

I. INTRODUCTION

Due to the rising concerns over the global environmental issues, a change in the paradigm of how the electrical energy is being produced and transported to the consumers has been seen. The power production is moving from the employment of few large-scale power plants to a more distributed generation (DG) closer to the consumers [1]. Smart cities have been discussed as prospective future urban areas, where production and consumption are closely monitored resources and managed efficiently [2]. Because of this, a rapid increase in the usage of renewable energy sources (RES) has been seen. The increase of renewables however aggravates the problem of energy production and consumption balancing due to the inherently fluctuating nature of renewable sources, such as solar and wind power. Additionally, different demand response (DR) methods have been developed that work based on market prices [3] or for example PV-power measurements [4]. Nevertheless, these scheduling methods are often not enough to balance the production sufficiently, in fact, they might result in a simultaneous turn on of devices thus causing sharp peaks in the power draw. These imbalances can cause disturbances in the electrical grids that manifest as deviations from the nominal grid frequency. To alleviate this, power smoothing techniques could be employed by the utilization of energy storage systems (ESS), such as battery energy storage systems (BESS) [5] or flywheel energy storage systems (FESS). Power smoothing for frequency regulation is performed for high frequency changes in power flow by charging the ESS when there is an excess of power and discharging when there is a deficit of power. This can be applied in islanded mode as well as in grid-connected mode like other balancing techniques, e.g. demand response with thermal storages [6], [7].

Power smoothing methods can be divided into methods that rely on ESS and methods that don't. Often battery, flywheel or supercapacitor based storage systems are utilized for power smoothing due to their fast reaction speed. ESS based power smoothing methods can be used to reduce fluctuation of grid consisting of many various producers and consumers with different profiles. On the other hand, power smoothing methods that don't use ESS are usually specific for the producer at hand. For example, wind power output can be smoothed by methods of increasing the rotor inertia, pitch angle control or DC-link voltage control [8].

Flywheel systems are electromechanical energy storage systems that store energy in a rotating mass. This energy can be transferred by either accelerating or decelerating the flywheel. Flywheel systems can operate over the course of millions of charge cycles, compared to BESS that are limited to around 1000 to 5000 charge cycles. However, the weakness of flywheel systems is that their self-discharge is much higher compared to BESS, 5-15 %/h compared to 0.1-0.2 %/day [9]. From these characteristics it could be concluded that the optimal applications of flywheel systems are high power, cyclic applications that require constant power exchange with the grid, such as power smoothing. Supercapacitors on the other hand are preferable for high-power short-term energy storage, but they do not provide high enough storage capacity for microgrid applications and are more expensive than other mentioned storage systems [10].

The application of a FESS for power smoothing has been researched previously. The authors of [11] investigate a PV and flywheel hybrid system in a non-residential building that is controlled to minimize the electricity price and to reduce peak power exchange with the grid through load leveling daily consumption. Continuous power smoothing in a PV and flywheel hybrid system using a moving average control is explored by [12]. The authors of [13] propose a hybrid energy storage system with a flywheel, a lead acid battery storage and a PV system, where the self-sufficiency of the system was increased from 36.8 % to 51.9 % with the addition of a FESS. Voltage and frequency regulation using a FESS was investigated by [14] in the case of sudden loss of generation. Power output smoothing of wind turbines using a FESS has also been proposed by [15], who employed a second order adaptive notch filter. Similarly, the authors of [16] used a flywheel storage for frequency regulation of wind turbine generator (WTG) using a fuzzy PI control.

In this paper, the usage of FESS for power smoothing in a small microgrid with fluctuating loads is investigated using Matlab/Simulink simulations. The paper is organized as follows: Section II shows the methodology. The scenarios and results of simulations are presented in Section III. Finally, the results in brief with conclusions are presented in Section IV.

II. MODEL DESCRIPTION

A. Object Model of the FESS

The flywheel system was modeled using Matlab/Simulink software. The object model of the FESS was constructed using premade components from the Simscape Electrical library. The modeled flywheel consisted of an asynchronous machine, bidirectional AC/DC converters, DC-link capacitor and a LC filter at the front end. The flywheel system was modeled based on a 15 kVA FESS located in Tallinn University of Technology. The model parameters are presented Table I.

B. Control of the FESS

Flywheel systems compose of two back-to-back bidirectional AC/DC converters. To facilitate a smooth energy flow between the flywheel and the grid, both of these converters need to be operated, however the objective of controlling them is different. The working principle of the modeled FESS is presented in Fig. 1. The Grid-Side Converter (GSC) is used to exchange energy between the DC-link and the grid. In this work, the GSC was controlled to output the commanded power from the FESS using the Current Control. As the energy is being transferred to or from the DC-link, its voltage starts to either increase or decrease. From this, the objective of controlling the Motor-Side Converter is to maintain the DC-link voltage within acceptable levels by supplying energy to or from the flywheel. The DC-link Voltage Control is used to generate the torque T_{ref} and flux $\Psi_{s,ref}$ references for the Field Oriented Control (FOC). While the Power Smoothing Control is used to generate active P_{ref} and reactive Q_{ref} power references for the Current Control based on the power smoothing algorithm employed.

C. Current Control of Grid-Side Converter

Current control method is used in this work to control the power output of the GSC. This method entails a Park transformation of three-phase grid voltages u_{abc} and currents i_{abc} from their natural abc reference frame into synchronously rotating dq reference frame forms u_{dq} and i_{dq} . The instantaneous active and reactive power in dq reference frame can be expressed with (1) and (2) [17].

$$P = \frac{3}{2}(u_d i_d + u_q i_q) \quad (1)$$

$$Q = \frac{3}{2}(u_q i_d - u_d i_q) \quad (2)$$

These power equations can be simplified by aligning the grid voltage with the rotating reference frame reducing the voltage $u_q = 0$, turning the power equations to (3) and (4). From this it can be seen that by regulating the currents i_d and i_q the active and reactive power output of the GSC can be controlled independently from each other.

$$P = \frac{3}{2}u_d i_d \quad (3)$$

$$Q = -\frac{3}{2}u_d i_q \quad (4)$$

The current control model used in this work is shown in Fig. 2. Based on the active and reactive power reference values P_{ref} , Q_{ref} and measured grid voltage u_d the output current references $i_{d,ref}$, $i_{q,ref}$ can be calculated.

TABLE I. FESS OBJECT MODEL PARAMETERS [18] [19]

FESS Parameters	Symbol	Value
Power	P_n	15 kVA
Energy Capacity	E_{fw}	300 kW
Speed Range	N_{fw}	500 – 6000 rpm
DC-link Capacitance	C_{DC}	500 μ F
DC-link Voltage	U_{DC}	700 V
Inverter Switching Frequency	f_{sw}	16 kHz
LC Filter Parameters	Symbol	Value
Filter Inductance	L_f	6.2 mH
Filter Capacitance	C_f	3 μ F

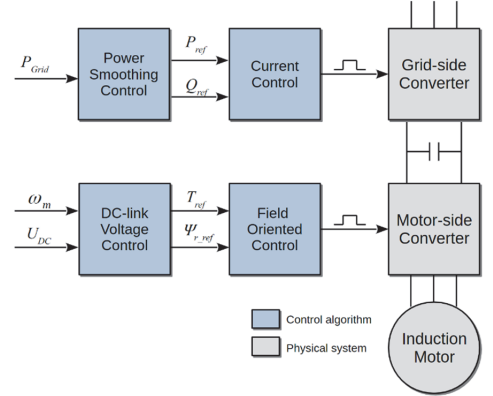


Fig. 1. Working principle of control of the modeled FESS.

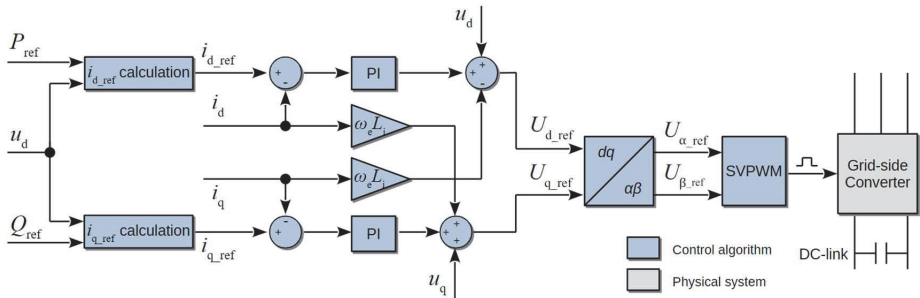


Fig. 2. Current Control model of grid-side converter [19].

The difference between measured current output i_d, i_q and calculated reference values is fed into a PI controller that tries to minimize them by outputting a voltage difference from the measured grid voltages u_d, u_q needed to facilitate that current flow. The $i_d \omega_e L_i$ and $i_q \omega_e L_i$ are decoupling components, where ω_e is grid frequency in rad/s and L_i is inductance of LC filter inductor. The final voltages $U_{d.ref}, U_{q.ref}$ are transformed to $\alpha\beta$ stationary reference frame for the Space Vector Pulse Width Modulation (SVPWM) that generates the switching for the GSC.

D. DC-link Voltage Control

The DC-link Voltage Control aims to regulate the DC-link voltage by managing the energy flow between the flywheel and the DC-link capacitor. This involves regulating the rotational speed of the flywheel. DC-link voltage can be raised by decelerating the flywheel and increased by accelerating it. The model for DC-link Voltage Control is presented in Fig. 3. The inputs of this control are the measured DC-link voltage and rotational speed of the flywheel. A PI controller is used to minimize the difference between measured voltage $U_{DC.meas}$ and the nominal DC-link voltage of $U_{DC.ref} = 700$ by outputting a new reference speed ω_{ref} . Another PI controller minimizes the speed error between the measured speed ω_{fw} and reference speed by outputting a torque reference T_{ref} needed to change the rotational speed.

An induction machine was used in this work as a motor/generator unit. For operations above the nominal speed, a flux weakening has to be employed. Based on the measured rotational speed a flux reference Ψ_{ref} was calculated using (5) [20], where Ψ_{nom} is nominal flux, ω_{nom} is nominal rotational speed and ω_{meas} measured rotational speed of the induction machine. The generated torque and flux references of DC-link Voltage Control are forwarded for the FOC that is used to generate switching of the MSC transistors.

$$\Psi_{ref} = \frac{\omega_{nom}}{|\omega_{meas}|} \Psi_{nom} \quad (5)$$

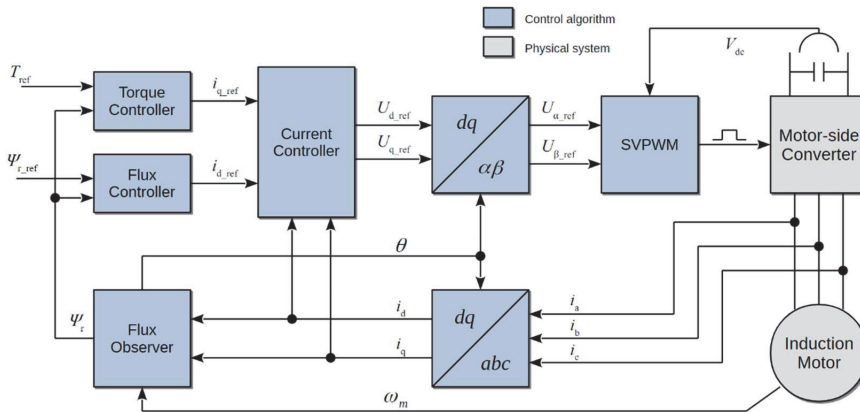


Fig. 4. Field-Oriented Control model of motor-side converter.

E. Field-Oriented Control of Motor-Side Converter

Energy exchange between the flywheel and the DC-link capacitor is handled by MSC. Field-Oriented Control (FOC) is used in this work for that purpose, its model is shown in Fig. 4. This type of FOC is specifically called Indirect Field-Oriented Control (IFOC), because the rotor flux Ψ_r is not measured directly; it is estimated through the measurement of stator current i_{ds} and by knowing the parameters of the induction motor. Rotor flux can be derived by solving the first order differential equation shown in (6) [20].

$$\frac{d}{dt} \Psi_r = -\left(\frac{R_r}{L_r}\right) \Psi_r + \left(\frac{L_m R_r}{L_r}\right) i_{ds} \quad (6)$$

With FOC, the control of induction machine torque and flux can be decoupled by regulating the torque forming current i_{qs} and the flux forming current i_{ds} independently. The flux forming stator current reference $i_{ds.ref}$ can be evaluated using a PI controller by minimizing the error between the reference flux $\Psi_{r.ref}$ and the estimated flux. The torque forming current $i_{qs.ref}$ can be calculated using (7) [20].

$$i_{q.ref} = \frac{2}{3} \frac{1}{n_p} \frac{L_r T_{ref}}{L_m \Psi_r} \quad (7)$$

The stator voltage $U_{d.ref}, U_{q.ref}$ references are evaluated by the Current Controller block by minimizing the error between measured and reference stator currents using PI controllers. SVPWM is used again to generate the switching for MSC.

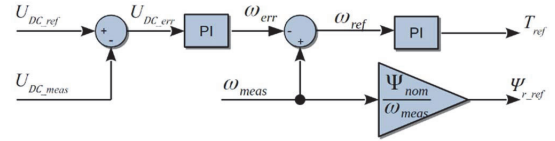


Fig. 3. Model of DC-link Voltage Control.

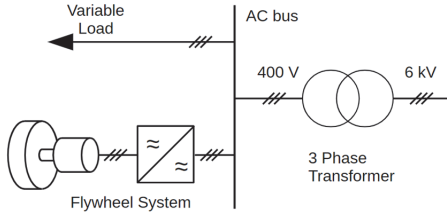


Fig. 5. Simulated microgrid topology.

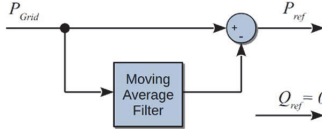


Fig. 6. Working principle of Power Smoothing Control.

III. CASE STUDY – POWER SMOOTHING SIMULATION

A. Microgrid Description

The microgrid topology used in the simulation of this work is presented in Fig. 5. It consists of a 15 kVA FESS, a variable load and a step-down transformer to connect to a 6 kV medium voltage grid. The power profile for the variable load was constructed from one second power measurement of the NRG building in Tallinn University of Technology and can be seen in Fig. 7(a) as grid power without power smoothing. Two simulations are performed: with and without FESS. Without FESS, the outside grid supplies the power for the load. The objective of employing a FESS in this paper is to use it for smoothing out the high frequency changes in power draw.

B. Power Smoothing Control Model

The working principle of power smoothing is presented in Fig. 6. A moving average filter was used to smooth out high frequency changes in the power flow. The difference in the measured active power P_{Grid} and moving average filter output was used as a reference setpoint P_{ref} for the active power output of the FESS. This way, high frequency changes in power draw were compensated by the FESS and low frequency changes by the grid. Reactive power reference was set as 0.

C. Results

At the beginning of the simulation the flywheel was precharged by accelerating it to a speed of about 4400 rpm. At simulation time $t = 30$ s, variable load was connected to the grid. Simulation results are presented in Fig. 7, where (a) shows grid power draw with and without power smoothing, (b) shows the supplied power by the flywheel and (c) the rotational speed of the flywheel. It can be seen that when power smoothing is performed with the FESS the grid power draw fluctuations are much smaller, they are compensated by the flywheel, as seen by the sharp drops in the rotational speed at times $t = 50$ s and $t = 110$ s when sharp peaks in the load are witnessed. Root Mean Squared Value (RMSE) was used to assess the effectiveness of power smoothing. Without power smoothing the RMSE value was 1030 W. Power smoothing was tested with two different time windows for the moving average. For a 30 second time window a RMSE value of 312 W, a 69.7 % drop was seen, and for a time window of 60 seconds a RMSE value of 186 W, a 81.9 % drop was observed.

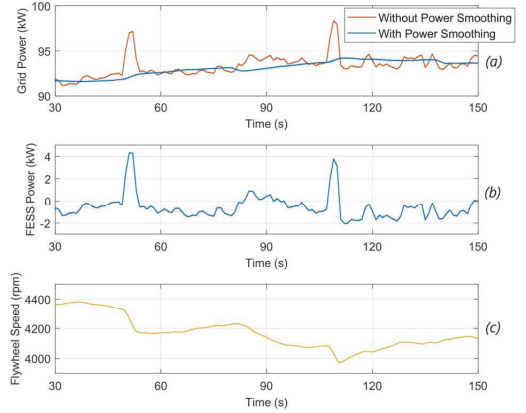


Fig. 7. Power smoothing simulation results: grid power with and without power smoothing (a), flywheel power (b) and flywheel rotational speed (c).

IV. CONCLUSIONS

In this work, power smoothing of variable load of a microgrid using a FESS was investigated. Power smoothing can be employed for fluctuating loads and producers with stochastic nature such as PV-systems or wind farms. Power smoothing with FESS helps to ensure stable grid operation by reducing variations in grid power draw. This as a result can help to improve the stability of grid frequency, especially in microgrids, as they tend to have smaller inertia. A 15 kVA flywheel system with a capacitance of 300 kW was modeled. One second measurements of the NRG building in Tallinn University of Technology were used as a load profile. Power smoothing was simulated in a small microgrid with FESS, variable load and a grid connection. The models presented in this work can also be used for power smoothing of fluctuating producers. The aim of the simulation was to use FESS to compensate higher frequency changes in load and to allow grid to supply low frequency power. In this work, a moving average filter was used for the power smoothing control. Depending on the length of the time window the performance of power smoothing could be adjusted. Root Mean Squared Value (RMSE) was used to assess the effectiveness of power smoothing. Without power smoothing the RMSE value of the load profile was 1030 W. A RMSE value of 312W, 69.5 % drop was observed with a 30 second time window and a RMSE value of 186 W, 81.9 % drop was seen with a 60 second time window. Larger time windows improve the performance of the power smoothing, however it increased the power flow between the FESS.

In the future work, adjustment of power smoothing performance based on the state of charge should be investigated.

ACKNOWLEDGMENT

This work was supported by the Estonian Centre of Excellence in Zero Energy and Resource Efficient Smart Buildings and Districts ZEBE, grant 2014- 2020.4.01.15-0016 funded by European Regional Development Fund; and supported by the European Commission through the H2020 project Finest Twins (grant No. 856602).

REFERENCES

- [1] T. Morstyn, B. Hredzak, and V. G. Agelidis, "Control Strategies for Microgrids with Distributed Energy Storage Systems: An Overview," *IEEE Trans. Smart Grid*, vol. 9, no. 4, pp. 3652–3666, Jul. 2018.
- [2] M. Masera, E. F. Bompard, F. Profumo, and N. Hadjsaid, "Smart (Electricity) Grids for Smart Cities: Assessing Roles and Societal Impacts," *Proceedings of the IEEE*, vol. 106, no. 4. Institute of Electrical and Electronics Engineers Inc., pp. 613–625, 01-Apr-2018.
- [3] A. Rosin, S. Link, M. Lehtla, J. Martins, I. Drovutar, and I. Roasto, "Performance and feasibility analysis of electricity price based control models for thermal storages in households," *Sustain. Cities Soc.*, vol. 32, pp. 366–374, Jul. 2017.
- [4] T. Häring, A. Rosin, and H. Biechl, "Using common household thermal storages to support the PV- and battery system in nearly zero energy buildings in off-grid mode," *Sustain. Energy Technol. Assessments*, vol. 35, pp. 12–24, Oct. 2019.
- [5] A. Rahmoun, A. Armstorfer, J. Helguero, H. Biechl, and A. Rosin, "Mathematical modeling and dynamic behavior of a Lithium-Ion battery system for microgrid application," in 2016 IEEE International Energy Conference, ENERGYCON 2016, 2016.
- [6] T. Haring, R. Ahmadihangar, A. Rosin, H. Biechl, and T. Korotko, "Comparison of the impact of different household occupancies on load matching algorithms," in 2019 Electric Power Quality and Supply Reliability Conference and 2019 Symposium on Electrical Engineering and Mechatronics, PQ and SEEM 2019, 2019.
- [7] T. Haring, R. Ahmadihangar, A. Rosin, and H. Biechl, "Impact of Load Matching Algorithms on the Battery Capacity with different Household Occupancies," in IECON 2019 - 45th Annual Conference of the IEEE Industrial Electronics Society, 2019, pp. 2541–2547.
- [8] A. M. Howlader, N. Urasaki, A. Yona, T. Senjyu, and A. Y. Saber, "A review of output power smoothing methods for wind energy conversion systems," *Renewable and Sustainable Energy Reviews*, vol. 26, pp. 135–146, 2013.
- [9] A. Rahmoun, "Mathematical Modeling and Analysis of a Battery Energy Storage System for Microgrids," Ph.D. dissertation, Department of Electrical Power Engineering and Mechatronics, Tallinn University of Technology, Tallinn, 2017.
- [10] I. Roasto, T. Lehtla, T. Moller, and A. Rosin, "Control of Ultracapacitors Energy Exchange," 2009, pp. 1401–1406.
- [11] L. Tziouvani, P. Kolios, L. Hadjidemetriou, and E. Kyriakides, "Grid Friendly Operation of a PV-Storage System with Profit Maximization and Reliability Enhancement," in SEST 2019 - 2nd International Conference on Smart Energy Systems and Technologies, 2019.
- [12] A. Awad, I. Tumar, M. Hussein, W. Ghanem, and J. A. Sa'ed, "PV output power smoothing using flywheel storage system," in Conference Proceedings - 2017 17th IEEE International Conference on Environment and Electrical Engineering and 2017 1st IEEE Industrial and Commercial Power Systems Europe, EEEIC / I and CPS Europe 2017, 2017.
- [13] X. Li, N. Erd, and A. Binder, "Evaluation of flywheel energy storage systems for residential photovoltaic installations," in 2016 International Symposium on Power Electronics, Electrical Drives, Automation and Motion, SPEEDAM 2016, 2016, pp. 255–260.
- [14] A. A. Roya, F. Ghardashi, D. Kabiri, A. Sheykholeslami, and H. Haeri, "Voltage and frequency control in smart distribution systems in presence of DER using flywheel energy storage system," *IET Conf. Publ.*, vol. 2013, no. 615 CP, pp. 10–13, 2013.
- [15] A. A. A. El-Naga, M. I. Marei, and H. S. K. El-Goharey, "Second order adaptive notch filter based wind power smoothing using flywheel energy storage system," in 2017 19th International Middle-East Power Systems Conference, MEPCON 2017 - Proceedings, 2018, vol. 2018-February, pp. 314–319.
- [16] D. Achour, M. Kesraoui, and A. Chaib, "A novel frequency control for a wind turbine generator associated with a flywheel," in 2017 8th International Renewable Energy Congress, IREC 2017, 2017.
- [17] H. Akagi, E. H. Watanabe, and M. Aredes, *Instantaneous power theory and applications to power conditioning*. Wiley, 2007.
- [18] Rossetta Technik GmbH, "Flywheel storage system T3-15." Technical documentation.
- [19] F. Plaum, "Development of Power Conditioning Control Strategies for Flywheel Storage in Microgrid," M.S thesis, Department of Electrical Power Engineering and Mechatronics, Tallinn University of Technology, Tallinn, 2019.
- [20] N. P. Quang and J.-A. Dittrich, *Vector control of three-phase AC machines : system development in the practice*. Springer-Verlag Berlin Heidelberg, 2015.

Publication VII

T. Häring, R. Ahmadiyahangar, A. Rosin and H. Biechl, "Impact of Load Matching Algorithms on the Battery Capacity with different Household Occupancies," IECON 2019 – 45th Annual Conference of the IEEE Industrial Electronics Society, 2019, pp. 2541–2547, doi: 10.1109/IECON.2019.8927495.

Impact of Load Matching Algorithms on the Battery Capacity with different Household Occupancies

Tobias Häring, Roya Ahmadihangar, Argo Rosin
Department of Electrical Power Engineering and Mechatronics
Tallinn University of Technology
Tallinn, Estonia
tobias.haring@taltech.ee

Helmut Biechl
Institute of Electrical Power Systems (IEES)
University of Applied Sciences Kempten
Kempten, Germany

Abstract— Due to an increasing use of renewable energy sources in the power grid, it is of high importance to balance supply and demand for grid utilities and microgrid operators. If there are mismatches in the balancing, microgrids with islanded operation capabilities would be preferable. In islanded mode, nearly zero energy buildings commonly use a stand-alone photovoltaics power supply with a battery storage. A battery storage is expensive and the capacity in case of off-grid operation depends on the electricity consumption of the dwelling's occupants. Using thermostatically controlled appliances like a freezer, water heater and space heating as additional storage systems can reduce the capacity of the battery storage system or increase the operation time in islanded mode for a fixed battery size. This paper analyzes the battery capacity dependency both on the control algorithms for the thermal storages and on the occupancy of the dwelling. Possible battery reductions for different selected occupancies are presented in this work by comparing the simulation results of different load matching algorithms to each other and between the different occupancies. The analysis of those results enables recommendations on the most suitable algorithm for most occupancy scenarios of an existing dwelling with respect to a minimized battery capacity. This can be particularly useful, for example, for dwelling and apartment owners who are renting out dwellings.

Keywords— *thermal storage, thermostatically controlled load, islanded mode, demand response, microgrid, occupant behavior*

I. INTRODUCTION

Growing population and higher living standards create a need for higher demand for electric energy all around the world. In this high electricity demand, the share of renewable energy sources is in constant increase. The provided volatile electric power of those renewable energy sources needs increasing attention [1]. Some studies even consider scenarios with a 100% renewable energy generation market [2]. This development forces grid utilities and microgrid operators to keep the frequency and power levels stable and within their limits, which can be established with a sufficient control of supply and demand.

Grid utilities can control the power system energy supply by changing the output generation of power plants. For the demand side, customers can be offered lucrative proposals by grid utilities to engage in the demand side management (DSM) programs.

Dwellings provide different typical loads to be scheduled in a demand side management manner [3]. Some of the schedulable devices available in most households can be used as thermal storages for DSM, like a freezer, water heater or space heating/cooling. As these appliances can compose 50% of electrical energy consumption in buildings [4], they are the main focus of this paper.

The scheduling of loads, including a water heater as a thermostatically controlled load, is reported in [5]. This general approach gains cost reductions with a real time price based control. Performance and feasibility of different price based load shaping algorithms for thermal storages are shown in [6]. Possible power resp. cost reductions are presented and compared for different algorithms. The user comfort is taken into account. The studies in [7] propose a simple scheduling algorithm for a water heater. The off-grid building system also includes a PV-system and a battery storage. One of the results in this paper demonstrates changes in the battery capacity according to the annual energy consumption of households. The proposed simple shifting algorithm for the water heater battery storage enables reductions of about 15-25%.

The study in [8] uses thermal- and battery storages to improve grid friendliness. The power/voltage quality is shown to be influenced by the battery storage size. But all scenarios presented in this article are conducted for a grid connected system. In another article [9], energy and cost savings in an isolated grid were achieved with a demand response approach. Renewable energy sources are included in the model as well. However, the authors focus on washing-, drying machines and dishwashers for scheduling instead of thermal storages. Changes of battery storage system capacity are neglected. Therefore, energy storing possibilities in the proposed system are not analyzed.

The studies above cover mainly technical problems resp. influences on the components. Another aspect that needs to be discussed is the user impact on those systems. In [10] the authors show that the occupant behavior influences the comfort level and energy consumption of users. A smart zoning approach is shown to reduce the energy consumption. Other articles on occupant behavior, for instance [11], overlook the influence of price based control algorithms. Focus is on occupant behavior and on the evaluation of its effect on the energy performance of a building. Several devices are accounted for in the study. The influence of occupant behavior on the energy consumption of a

building in general is proven. Nevertheless, influences on load matching control strategies are not investigated.

The studies reviewed above suggest that the thermal storages can be scheduled in a DSM-manner with typical cost savings of about 5-30%. According to other studies shown, the power quality can be improved using such devices. Similar to [12], combining those two aspects and scheduling the loads with a sophisticated algorithm in an islanded system can help reduce the battery capacity necessary to ensure stable operation even more than a simple load shifting presented in [7]. In the paper, the focus is on an islanded system and the corresponding battery reduction possibilities.

However, the aim of this study is not merely to reduce this battery storage capacity but rather analyzing the influence of different dwelling occupancies on the possible battery capacity reductions based on different control algorithms. This enables finding control strategies for different household occupancies that work with the lowest battery storage system capacity. This does not only provide the possibility to operate in islanded mode for longer periods but can also help dwelling owners to estimate the performance of such a system for different occupancies of existing dwellings. Additionally, it can help in the next step to optimize the control of not just one household, but expand the investigation to apartment building level and give recommendations for improving the power/voltage quality and battery storage investment costs for all tenants of a building. Later such a system can be expanded to microgrid level with aggregated loads.

This paper is organized as follows: Section II describes the modeling of the different objects and components, and the methodology of the simulation and control strategies in detail, followed by the simulation results in Section III. Conclusions and recommendations are presented in Section IV.

II. SYSTEM MODELING

To recommend suitable control strategies and estimate possible battery reductions, a model of a suitable system is necessary. There are three common household thermal storage systems: a freezer, a water heater and space heating. The mathematical object models of these three systems are described in this section. For islanded operation, simple PV-power source and battery storage system models are needed as well. All these models are based on datasheets of typical devices. Specific control strategies, including PV-power and SOC based load matching algorithms, are presented. The different occupancies of an existing dwelling and other inputs that are needed for the simulation are described.

A. Mathematical object models

The freezer model is based on the temperature changes due to food exchange (T_{food}), ambient losses ($T_{amb,loss}$) and freezing (T_{freeze}) during the time step. The cabinet temperature at the end of the time step (T_{next}) could be obtained from the temperature at the beginning of the time step (T_i) as follows (1) [6], [12]:

$$T_{next} = T_i - T_{freeze} - T_{food} - T_{amb,loss} \quad (1)$$

The model for the water heater is similar. The temperature of the water inside the boiler at the end of the time step (T_{next})

was obtained from the temperature at the beginning of the time step (T_i) and the temperature changes during the time step due to heating ($T_{heating}$), water exchange (T_{cw}) and ambient losses ($T_{amb,loss}$) (2) [6], [12]:

$$T_{next} = T_i + T_{heating} - T_{cw} - T_{amb,loss} \quad (2)$$

The space heating/cooling model is based on the temperature changes during the time step due to heating/cooling (T_{hc}) with the heat pump resp. electrical heater, the ambient air exchange (T_{air}), ambient losses through outside walls and windows ($T_{amb,loss}$), people in the room (T_p), and sun irradiation through the windows (T_{sun}). The temperature at the end of the time step (T_{next}) was obtained from the temperature at the beginning of the time step (T_i) as follows [6], [12] (3):

$$T_{next} = T_i + T_{hc} - T_{air} - T_{amb,loss} + T_p + T_{sun} \quad (3)$$

Unlike the very accurate battery model shown in [13], it was sufficient in this work for both the battery storage and the PV-system model to be reduced to their basic working principles. As a result, comparisons of two systems with exactly the same conditions, except for a different control strategy for the thermal storages, were obtained. Thus, small errors occurring due to the simplified models had a minor influence on the results as they occurred in both systems and therefore could be omitted. For the PV-model, datasheet values and maximum power point calculations were used. The ambient conditions for the model were similar to those described in [14]. The resulting irradiation (E_{res}) on the photovoltaics panels was calculated from the direct (E_b), diffuse (E_d) and reflective (E_r) irradiation values (4). Those irradiation values were calculated according to [15] based on typical irradiation data for Tallinn, Estonia [16]:

$$E_{res} = E_b + E_d + E_r \quad (4)$$

The short circuit current (I_{SC}) depending on the irradiation can be derived from the datasheet (5) [17]:

$$I_{SC} = \frac{I_{SC1000}}{1000} * E_{res} \quad (5)$$

The current (I_{mpp}) in the maximum power point (MPP) is approximately at 85% (mppappr) of the short circuit current value (6) [17]:

$$I_{mpp} = mppappr * I_{SC} \quad (6)$$

The respective voltage (V_{mpp}) in the MPP is provided by the datasheet (7) [17]:

$$V_{mpp} = \frac{offsetmpp}{m_{mpp} - I_{mpp}} \quad (7)$$

The maximum available power (P_{mpp}) for a given irradiance is the product of the voltage and current in the MPP (8):

$$P_{mpp} = I_{mpp} * V_{mpp} \quad (8)$$

The battery storage model is represented by a capacity and a state of charge (SOC) value. The charging efficiency (η_c) for a Lithium-Ion battery is approximately 98% [18]. The discharging efficiency (η_d) for the model was obtained from datasheet values according to the battery's capacity (C_{bat}) with a numerical value equation (9) [18]:

$$\eta_d = -\frac{0.7}{2} * \left(-\frac{I}{C_{bat}}\right) + 1.055 \quad (9)$$

The current (I) can be calculated according to the magnitude of the charging / discharging power (Pi) and the charging (Vcharge) and discharging (Vbat) voltage (10):

$$\text{if } P_i > 0: I = \frac{P_i}{V_{charge}}; \text{ if } P_i < 0: I = \frac{P_i}{V_{bat}} \quad (10)$$

The new SOC of the battery (SOCnew) after the time step with a step width of Δt is calculated depending on the charging/discharging mode and the SOC at the beginning of the time step (SOCold) (11):

$$\begin{aligned} \text{if } P_i > 0: SOC_{new} &= \frac{(SOC_{old} * C_{bat} * V_{bat}) + (I * V_{charge}) * \Delta t * \eta_c}{C_{bat} * V_{bat}}; \\ \text{if } P_i < 0: SOC_{new} &= \frac{(SOC_{old} * C_{bat} * V_{bat}) + (I * V_{bat}) * \Delta t * \eta_d}{C_{bat} * V_{bat}} \end{aligned} \quad (11)$$

The ambient conditions are fixed similar to [14]. It is assumed that the battery is placed in a controlled environment, including a constant ambient temperature. The modeling is shown in more detail in [12].

To achieve a simple and clear structure, the models of the thermal storages (1)-(3), PV-system (4)-(8) and battery storage (9)-(11) were embedded in a system model in this paper. This model includes a simplified PV-inverter and a battery controller. The connections between the components were assumed to have neither losses nor parasitic elements. The ambient conditions were fixed for all the devices and simulations and the thermal storages did not influence each other. Sizing and dimensions for the freezer, water heater and space heating were the same for every simulation, which enabled comparisons and the representation of an existing dwelling. The control model and input data for these object models are shown in the next section.

B. Control and simulation strategies

In the islanded mode, the frequency was considered to be kept constant in any case. The voltage was limited. If the energy production exceeded the consumption, the average PV-power would be reduced. If the consumption exceeded the energy production, the voltage would show a drop. The battery controller automatically charged resp. discharged the battery storage, depending on the available PV-power and the energy consumption of the household. If the voltage drop exceeds the defined limits, a real system will shut down as a protection precaution. To model this, the simulation was aborted in this case. The PV-system and battery storage were assumed to be independent systems that are not controlled by the set point calculation algorithms for the thermal storages.

Depending on the energy consumption and supply, it was determined whether the system was operating stable or shutting down for protection. The smallest battery capacity that enables stable system operation for the duration of one week was considered as the minimum battery capacity.

The chosen thermal storages are typically controlled by a thermostatic 2-step control with a fixed set point. A 2-step control where the set point was calculated with different algorithms was used for all other simulations. Those algorithms were based on the available PV-power or the battery's SOC. This enabled comparisons between the fixed set point control

and the PV-power and SOC based control algorithms to obtain a battery capacity reduction in percent.

Seven different PV-power based set point calculation algorithms (A-G) [6], [19], [20] described in detail in [12] were applied. Both linear and nonlinear algorithms were used. They were modified price based set point calculation algorithms, which can be used in the islanded mode to work with the PV-power instead of the electricity price by inverting them. For example, for a water heater, the set point should be high when the price is low; on the other hand, it should be low when the PV-production is low and vice versa. The algorithms are shown in TABLE I and visualized in Fig. 1. The user comfort (Cuser) for all simulations was set to 1.

TABLE I. PV-POWER BASED SET POINT CALCULATION ALGORITHMS (AL) [6], [19], [20]; COOLING = FREEZER AND SPACE COOLING; HEATING = WATER HEATER AND SPACE HEATING

AL	Description of set point calculation algorithm
A	Cooling: $T_{set} = T_{set,max} - C_{user} * (Pwr - Pwr_{min}) * \frac{T_{set,max} - T_{set,min}}{Pwr_{max} - Pwr_{min}}$ Heating: $T_{set} = T_{set,min} + C_{user} * (Pwr - Pwr_{min}) * \frac{T_{set,max} - T_{set,min}}{Pwr_{max} - Pwr_{min}}$
B	Cooling: $T_{set} = T_{goal} - C_{user} * (Pwr - Pwr_{mavg}) * \frac{T_{set,min} - T_{goal}}{Pwr_{avg} - Pwr_{mavg}}$ Heating: $T_{set} = T_{goal} + C_{user} * (Pwr - Pwr_{mavg}) * \frac{T_{set,max} - T_{goal}}{Pwr_{avg} - Pwr_{mavg}}$
C	Cooling: $T_{set} = T_{goal} - C_{user} * (Pwr - Pwr_{mavg}) * \frac{T_{set,min} - T_{goal}}{Pwr_{min} - Pwr_{mavg}}$ Heating: $T_{set} = T_{goal} + C_{user} * (Pwr - Pwr_{mavg}) * \frac{T_{set,max} - T_{goal}}{Pwr_{max} - Pwr_{mavg}}$
D	Cooling: $T_{set} = T_{goal} - C_{user} * (Pwr - Pwr_{min}) * \frac{T_{set,min} - T_{goal}}{Pwr_{min} - Pwr_{mavg}}$ Heating: $T_{set} = T_{goal} + C_{user} * (Pwr - Pwr_{min}) * \frac{T_{set,max} - T_{goal}}{Pwr_{max} - Pwr_{mavg}}$
E	Cooling: $T_{set} = T_{goal} - C_{user} * (Pwr - Pwr_{mavg}) * \frac{T_{set,max} - T_{set,min}}{Pwr_{max} - Pwr_{min}}$ Heating: $T_{set} = T_{goal} + C_{user} * (Pwr - Pwr_{mavg}) * \frac{T_{set,max} - T_{set,min}}{Pwr_{max} - Pwr_{min}}$
F	Cooling: $T_{set} = T_{goal} - C_{user} * (Pwr - Pwr_{min}) * \frac{T_{set,max} - T_{set,min}}{Pwr_{max} - Pwr_{min}}$ Heating: $T_{set} = T_{goal} + C_{user} * (Pwr - Pwr_{min}) * \frac{T_{set,max} - T_{set,min}}{Pwr_{max} - Pwr_{min}}$
G	Cooling: $Pwr \geq Pwr_{mavg} \rightarrow T_{set} = T_{set,min}; \text{ Otherwise } \rightarrow T_{set} = T_{set,max};$ Heating: $Pwr \geq Pwr_{mavg} \rightarrow T_{set} = T_{set,max}; \text{ Otherwise } \rightarrow T_{set} = T_{set,min};$

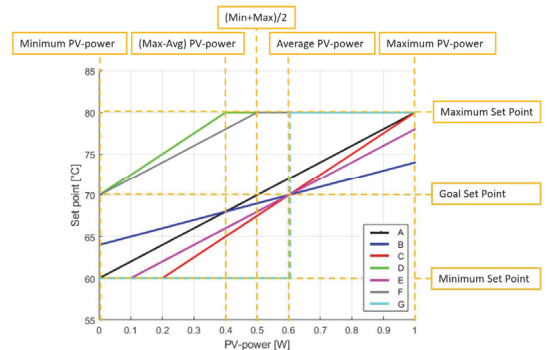


Fig. 1. Set point calculation for a water heater with algorithms A-G for an example PV-power range of 0-1 W with an assumed average PV-power of 0.6 W.

Algorithm H was solely voltage based. This means that it switched the thermal storages to minimum consumption set point if the system voltage dropped to the minimum acceptable voltage level to prevent a system shutdown. Otherwise it operated at the fixed set point resp. goal set point level. Algorithms I-K are based on the SOC of the battery storage system. They are linear and nonlinear. Algorithms H-K are presented in TABLE II and visualized in Fig. 2. The user comfort (C_{user}) for all simulations was set to 1.

C. Case study

For all simulations, a system with a freezer, water heater and space heating/cooling was considered. These devices were controlled in each household. The time frame for each simulation was one week in summer, starting at Monday 00:00 a.m. with a time step of 5 min. The patterns for the apartment electricity, food and warm water consumption and patterns of people in the room were used for one week.

Different predefined household occupancies implemented in LoadProfileGenerator [21] were selected and categorized to eight groups to represent some typical occupancy scenarios for dwellings.

To select representative household occupancies, statistics of the Federal Statistical Office of Germany have been analyzed. TABLE III shows selection criteria, their share and the corresponding household, which they are represented by in this work. Descriptions of the chosen household occupancies of this work are shown in TABLE IV.

The average dwelling size is 92.3 m² in Germany [22] and 66.7 m² in Estonia [23]. Family houses are included in those numbers. To find a more suitable dwelling size for an average apartment building the average dwelling size per person can be considered. Those are 44.8 m² in Germany [22] and 30.5 m² in Estonia [24]. Considering that the majority of people in Estonia and Germany, about 40% [25], are living alone, a dwelling with a size of 67.4 m² was selected to represent a typical dwelling.

Their electricity, water and food consumption per day were different. With the LoadProfileGenerator software, the electricity consumption patterns were created with the corresponding room occupancy and hot water consumption patterns. Thus, these patterns were artificial profiles based on a behavioral model. According to [26], the artificially created load profiles show adequate similarity to measured load profiles. Additionally, the simulations in this work were validated with measured profiles for a similar occupancy of a similar dwelling. The results agreed well to those of a corresponding artificial profile.

The daily electricity consumption of the chosen household occupancies and their descriptions are shown in TABLE IV. The values are presented without the thermal storages. The 5-min power consumption patterns of the different households for one week are presented in Fig. 3. As seen from the table and the figure, each kind of occupancy of the dwelling is featured by a different electricity consumption. For households with working or studying occupants, electricity consumption on workdays is lower as they spend less time at home than on the weekend.

TABLE II. VOLTAGE AND SOC BASED SET POINT CALCULATION ALGORITHMS (AL); COOLING = FREEZER AND SPACE COOLING; HEATING = WATER HEATER AND SPACE HEATING

AL	Description of set point calculation algorithm
H	Cooling: $T_{set} = T_{goal}$ Heating: $T_{set} = T_{goal}$
I	Cooling: $SOC \geq SOC_{min} + 0.2 \rightarrow T_{set} = T_{goal}, \text{Otherwise} \rightarrow T_{set} = T_{set,max}$; Heating: $SOC \geq SOC_{min} + 0.2 \rightarrow T_{set} = T_{goal}, \text{Otherwise} \rightarrow T_{set} = T_{set,min}$;
J	Cooling: $T_{set} = T_{set,max} - C_{user} * (SOC - SOC_{min}) * \frac{T_{set,max} - T_{set,min}}{DOD_{max}}$ Heating: $T_{set} = T_{set,min} + C_{user} * (SOC - SOC_{min}) * \frac{T_{set,max} - T_{set,min}}{DOD_{max}}$
K	Cooling: $SOC \geq (1 + SOC_{min})/2 \rightarrow T_{set} = T_{set,max}$; $\text{Otherwise} \rightarrow T_{set} = T_{set,min}$; Heating: $SOC \geq (1 + SOC_{min})/2 \rightarrow T_{set} = T_{set,min}$; $\text{Otherwise} \rightarrow T_{set} = T_{set,max}$;

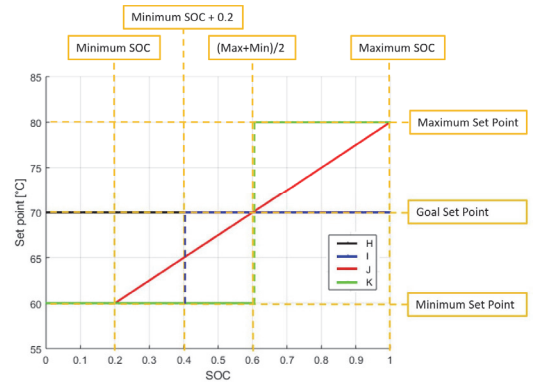


Fig. 2. Set point calculation for a water heater with algorithms H-K based on the SOC.

TABLE III: SELECTION CRITERIA, THEIR SHARE AND THEIR REPRESENTATION IN THE SELECTED HOUSEHOLDS

Number of people per dwelling		
Number of people	Share	Represented in household
1	42%	ii, iii, v
2	33%	i, vii
3	12%	vii
4	9%	iv, vi
Number of children per dwelling		
Number of children	Share	Represented in household
0	72%	i, ii, iii, v, vii, viii
1 or 2	25%	iv, vi
Number of people working per dwelling		
Number of people	Share	Represented in household
0	34%	iii, iv, v, vii, viii
1	36%	ii, vi
2	26%	i
Employment status of the person with the main income per dwelling		
Employment status	Share	Represented in household
Retired	36%	v, viii
Employed	48%	i, ii, vi
Other	16%	iii, iv, vii

TABLE IV. OCCUPANCY DESCRIPTION FOR THE DIFFERENT HOUSEHOLDS AND THEIR AVERAGE ELECTRICITY CONSUMPTION PER DAY

Household	i	ii	iii	iv	v	vi	vii	viii
Working	2	1	-	-	-	1	-	-
Studying	-	-	1	-	-	-	3	-
Unemployed	-	-	-	2	-	1	-	-
Retired	-	-	-	-	1	-	-	2
Children	-	-	-	2	-	2	-	-
Σ	2	1	1	4	1	4	3	2
El. Consumption [kWh/d]	9.82	4.18	2.15	14.63	2.58	13.10	9.22	5.85

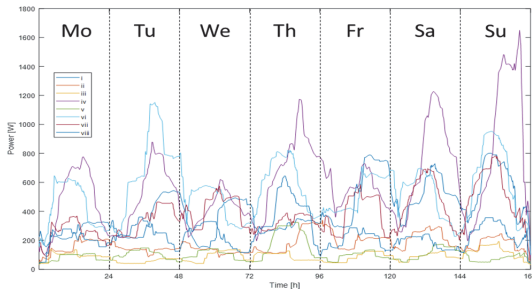


Fig. 3. 5-min power consumption data for households i-viii for one week.

The energy consumption of household vi is very high at the beginning of the week because the working family member stayed at home due to illness. The peaks for household iv are especially high on weekends. The reason is that most family members spend much time at home and only one child goes to school. Different sleeping habits of the people in the different households lead to slightly varying minimum electricity consumptions at night. Other variables in the simulations, like size of the water heater or area and orientation of the apartment, were not changed for different occupancy profiles to have a solid base for comparison. Energy consumption, water and food consumption patterns were different for each of these households to compare and analyze the performance of the chosen algorithms in different environments. This enables recommending a good control strategy for different occupancy situations. The PV-system size was chosen to be 7.65 kWp. It was the same size for all household occupancies to simulate an existing dwelling with already installed PV-system. Thus, it was chosen oversized for the lower energy consumption households.

The simulations worked as follows: A simulation started with the battery capacity of 10Ah and a SOC of 100%. If the voltage during the simulation was below 85% of the reference voltage for more than two time steps, all parameters were reset and the simulation restarted with a larger battery capacity. These voltage boundaries are based on the EN 50160:2010 grid norm to ensure stable operation. Before completion, the simulation inspected the end-SOC. If it was lower than the start-SOC, the simulation would restart with that end-SOC as the new start-SOC value. This ensured that the islanded system was able to maintain stable operation for more than one week. It was based on the assumption that the household profiles used in the simulations represented a typical or in the best case, a profile slightly higher than average. The lowest battery capacity that passed the simulation and could provide a constant SOC was considered the minimum possible capacity.

The example below explains the procedure that was used to obtain the results. It was necessary to obtain two simulation results to receive the battery capacity reductions for household ii with algorithm K. First, a simulation with household ii and the thermal storages with a fixed set point control was conducted to obtain a value for the minimum battery capacity. A second simulation was done with the same thermal storages, the same household profile and the same size PV-system. In this simulation, the thermal storages were controlled by algorithm K. A second value for the minimum battery capacity was obtained and could be compared to the first value to calculate a percent value for the reduction of the battery capacity. The procedure had to be repeated for each household and each algorithm to receive all the results. It was required to do the fixed set point simulation once for each household. Since the absolute battery capacities resp. electricity costs were compared for the same household profile and the reductions are relative values, it was possible to compare these reductions in percent not just between the different algorithms but also between the different households.

A total of 96 simulations were conducted for the 8-occupancy patterns, each with 11 set point calculation algorithms and fixed set point control. The results of those simulations are presented in the next section.

III. RESULTS

The minimum battery capacity results with a fixed set point control for the households are shown in TABLE V.

The results presented in Fig. 4 suggest that reductions in battery capacity do not appear in any conditions. For the PV-power based algorithms, high reductions in battery capacity occur in low electricity consumption households like iii or v.

In high electricity consumption households there is mainly an increase in the necessary battery capacity. The reason might be that the PV-system was of the same size for all tested households. During the day there are phases when both the PV-production and the consumption are high. When additional consumption from shifting the thermal storages is added to that period without considering the battery's SOC, then as a result, energy consumption is higher than production. This leads to a shutdown and a larger battery is needed. Contrary with low consumption households like ii and v, the highest battery reduction of all algorithms is achieved. In general, an observation is that algorithm A usually shows the best results whereas the performance of algorithms D and F is the lowest.

The voltage based algorithm H is a simple algorithm; its advantage is that only a voltage measurement in the system is necessary. This means that there is no need to interface the controller with the battery storage or PV-system. The results for this algorithm (cf. Fig. 5) show that it works best with low consumption households. But more importantly, it always shows battery capacity reduction or at least the same battery capacity like with a fixed set point. It only interferes when the system tends to become unstable instead of permanently changing the set point. It does not show the best results, neither does it show bad results. Reducing the battery capacity by up to 27% is a good result for this simple algorithm.

The SOC based algorithms I-K (cf. Fig. 5) show better performance with low electricity consumption households due to more available PV-power. Reductions can be up to 73% in household iii. This value is extremely high probably because of an unfortunate timing coincidence between the fixed set point control and the battery state of charge. Because most algorithms manage to surpass this problem, the battery reduction percentage is higher here. The reductions for the other households between 1% and 39% are more likely to be achieved during regular operation. The reduction in battery capacity with SOC based algorithms might not always be the highest possible, like seen for household ii or v, but it did not lead to an increase in necessary battery capacity in these simulations. Possible reductions are usually higher with SOC based algorithms. Algorithm K usually shows the best performance except for household v. Algorithm I performs better than J for higher consumption households while J performs better with lower consumption households.

Example results for the battery's state of charge and the temperature change for the water heater with a fixed set point and algorithm K for household ii are shown in Fig. 6. It can be seen that for values of the SOC higher than 0.6, the temperature set point of the water heater is set to the maximum value. If the SOC is below 0.6, then the minimum consumption set point is chosen. Even though the temperature in the water heater is often higher than with a fixed set point control, the battery storage capacity can be reduced by more than 1/3 (cf. Fig. 5). The state of charge of the smaller battery does not differ significantly from the SOC of the larger battery storage needed for a fixed set point control. As can be seen, for the set point algorithm control, there is a ripple in the SOC and temperature curves for the transition phase at a SOC of 0.6. Because the battery is charging while the water heater is on the minimum consumption set point, the algorithm will switch to maximum consumption set point when reaching the SOC of 0.6. This causes the battery to discharge if the available power from the PV-system is not sufficient. The battery discharges until its SOC reaches 0.6 and the algorithm switches to minimum consumption set point for the water heater. Now the available PV-power is sufficient for charging the battery and the SOC will increase again. This circle is repeated, causing these ripples in the SOC and temperature curves. This behavior is undesirable and needs to be optimized for future work.

Battery reduction results in [12] show values in the range of 15-25% for a simple water heater shifting algorithm depending on the household's overall energy consumption. These simulations show possible battery reductions for the system with multiple thermal storages and SOC or voltage based algorithms of up to 39%, excluding the special case of household iii. This is in the same range of possible battery reduction. Results for the PV-power based algorithms are in a wide range between high increase and high reduction of battery capacity. In the case of battery capacity reduction, the results are similar to those in the paper mentioned above.

TABLE V. MINIMUM BATTERY STORAGE CAPACITIES FOR THE DIFFERENT HOUSEHOLDS WITH A FIXED SET POINT CONTROL

Household	i	ii	iii	iv	v	vi	vii	viii
Battery Capacity [kWh]	5.7	1.3	0.6	9.6	0.8	16.8	13.8	11.4

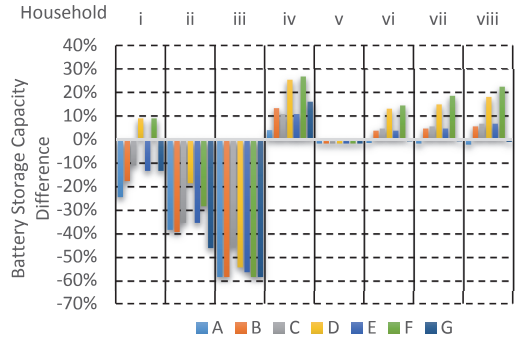


Fig. 4. Battery capacity differences for algorithms A-G in households i-viii in percent compared to a fixed set point.

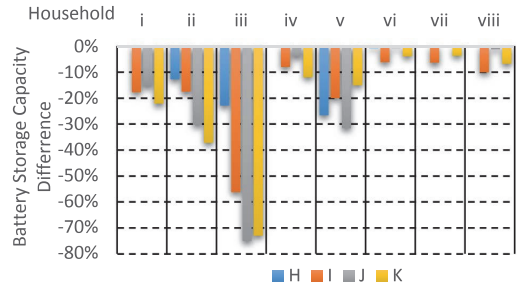


Fig. 5. Battery capacity differences for algorithms H-K in households i-viii in percent compared to a fixed set point.

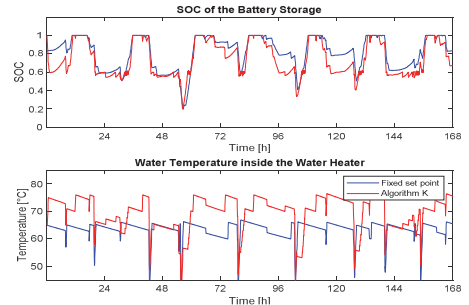


Fig. 6. SOC of the battery storage and temperature of the water heater for household ii with a fixed set point and algorithm K for 1 week.

In general, the results of the simulations are presented as battery capacity reductions. If the necessary battery capacity for permanent stable operation is smaller, then the operation time for a fixed battery storage capacity is longer. The same is valid for other seasons. If there is less PV-power available during winter time, the building or microgrid can operate longer in islanded mode. All algorithms that achieve smaller necessary battery capacities in the simulations enable longer islanded operation time with fixed battery- and PV-system sizes. Thus, recommendations based on the results also apply to the case of prolonging the off-grid operation with a fixed battery storage capacity or during other seasons.

IV. CONCLUSIONS

Thermal storages like a freezer, water heater and space heating/cooling can be scheduled in a DSM-manner to improve the power quality. Sophisticated set point algorithms applied to those thermal storages in an islanded system can help reduce the battery capacity necessary to ensure stable operation. Different load matching control algorithms for thermal storages were investigated to analyze the influence of different dwelling occupancies on the possible battery storage capacity. The set point calculation algorithms were based on photovoltaic power, voltage and the battery's state of charge. Artificially generated load profiles for different dwelling occupancy scenarios were used. The PV-power based algorithms did not show preferable behavior. Results for these algorithms ranged between high increase and high reduction of battery capacity. High increase applies especially if the PV-system is small compared to the household electricity consumption. The voltage based algorithm showed constant good results of up to 27% reduction while being simpler to implement than other proposed control strategies. It is suitable especially for lower consumption households. With the SOC based algorithms, higher battery reductions of up to 39% could be achieved, while also never increasing the necessary battery capacity.

Therefore, the preferred control strategy for off-grid operation would be voltage or SOC based set point control. Best performance for all different dwelling occupancies was shown by algorithm K. PV-power based control can achieve better results but only in a system with an oversized PV-system.

In the future work, it is required to focus on the effect of aggregation, for example, in an apartment building with multiple households or even in a complete microgrid.

ACKNOWLEDGMENT

This work was supported by the Estonian Research Council grant PUT1680), and Estonian Centre of Excellence in Zero Energy and Resource Efficient Smart Buildings and Districts ZEBE, grant 2014- 2020.4.01.15-0016 funded by European Regional Development Fund.

REFERENCES

- [1] Mertens K., Photovoltaik - Lehrbuch zu Grundlagen, Technologie und Praxis, 3rd ed., Carl Hanser Verlag, 2015, pp. 23-29.
- [2] Zapata S., Castaneda M., Jimenez M., Aristizabal A. J., Franco C. J. & Dyrner I., "Long-term effects of 100% renewable generation on the Colombian power market," *Sustainable Energy Technologies and Assessments*, vol. 30, pp. 183-191, 2018.
- [3] Rahate N.D. & Kinhekar N., "Demand side management for household equipment's," in *International Conference on Information, Communication, Instrumentation and Control (ICICIC)*, Indore, India, 2017.
- [4] Rosin A., Moller T., Lehtla M. & Hoimoja H., "Analysis of Household Electricity Consumption Patterns and Economy of Water Heating Shifting and Saving Bulbs," *Scientific Journal of Riga Technical University*, vol. 27, pp. 15-20, 2010.
- [5] Aleixo L., Rosin A., Saele H., Morch A.Z., Grande O.S. & Palu I., "Ecogrid EU project - real time price based load control and economic benefits in a wind production based system," in *22nd International Conference and Exhibition on Electricity Distribution (CIRED 2013)*, Stockholm, Sweden, 2013.
- [6] Rosin A., Link S., Lehtla M., Marins J., Drovitar I. & Roasto I., "Performance and feasibility analysis of electricity price based control models for thermal storages in households," *Sustainable Cities and Societies*, 2017.
- [7] Goldsworthy M.J. & Sethuvenkatraman S., "The off-grid PV-battery powered home revisited; the effects of high efficiency air-conditioning and load shifting," *Solar Energy*, vol. 172, pp. 69-77, 2018.
- [8] Medici V., Salani M., Nespoli L., Giusti A., Derboni M., Vermes N., Rizzoli A. E. & Rivola D., "Evaluation Of The Potential Of Electric Storage Using Decentralized Demand Side Management Algorithms," *Energy Procedia*, vol. 135, pp. 203-209, 2017.
- [9] Neves D., Pina A. & Silva C. A., "Comparison of different demand response optimization goals on an isolated microgrid," *Sustainable Energy Technologies and Assessments*, vol. 30, pp. 209-215, 2018.
- [10] Baldi S., Korkas C. D., Lv M. & Kosmatopoulos E. B., "Automating occupant-building interaction via smart zoning of thermostatic loads: A switched self-tuning approach," *Applied Energy*, vol. 231, pp. 1246-1258, 2018.
- [11] Gucyeter B., "Evaluating diverse patterns of occupant behavior regarding control-based activities in energy performance simulation," *Frontiers of Architectural Research*, vol. 7, pp. 167-179, 2018.
- [12] Häring T., "Research and development of thermal storage control models," M.Sc.Eng thesis, Tallinn University of Technology, Tallinn, 15 01 2018. [Online]. Available: <https://digi.lib.tu.ee/i/?11177>. [Accessed 29 01 2019].
- [13] Rahmoun A., Armstorfer A., Helguero J., Biechl H. & Rosin A., "Mathematical modeling and dynamic behavior of a Lithium-Ion battery system for microgrid application," in *2016 IEEE International Energy Conference (ENERGYCON)*, Leuven, Belgium, 2016.
- [14] Palacios-Garcia E. J., Moreno-Muñoz A., Santiago I., Moreno-Garcia I. M. & Milanés-Montero M. I., "PV Hosting Capacity Analysis and Enhancement Using High Resolution Stochastic Modeling," *Energies*, vol. 10, no. 10, 2017.
- [15] American Society of Heating, Refrigerating and Air-Conditioning Engineers, Inc., *ASHRAE Handbook - Fundamentals*, 2009.
- [16] American Society of Heating, Refrigerating and Air-Conditioning Engineers, Inc., *ASHRAE Handbook - Fundamentals*, 2013.
- [17] Papaioannou I.T., Alexiadis M.C., Demoulias C.S., Labridis D.P. & Dokopoulos P.S., "Modeling and Field Measurements of Photovoltaic," *IEEE Transactions on Power Delivery Units Connected to LV Grid. Study of Penetration Scenarios*, vol. 26, no. 2, pp. 979-987, 2011.
- [18] Victron Energy, "www.victronenergy.com," [Online]. Available: <https://www.victronenergy.com/blog/2015/03/30/batteries-lithium-ion-vs-agm/>. [Accessed 25 07 2017].
- [19] Goh C. H. K. & Apt J., "Consumer strategies for controlling electric water heaters under dynamic pricing," 2004.
- [20] Hammerstrom D. J., Ambrosio R., Carlton T. A., DeSteele J. G., Horst G. R., Kajfasz R., Kiesling L., Michie P., Pratt R. G., Yao M., Brous J., Chassin D. P., Guttromson R. T., Järvregren O. M., Katipamula S., Le N. T., Oliver T. V., & Thompson S. E., "Pacific Northwest GridWise TM Testbed Demonstration Projects. Part I. Olympic Peninsula Project," 2007.
- [21] P. N., "LoadProfileGenerator," [Online]. Available: <https://www.loadprofilegenerator.de>. [Accessed 25 01 2019].
- [22] Statistisches Bundesamt (Destatis), "Bevölkerung und Erwerbstätigkeit - Haushalte und Familien - Ergebnisse des Mikrozensus," 2017.
- [23] Eurostat, "Eurostat," 2012. [Online]. Available: http://appsso.eurostat.ec.europa.eu/nui/show.do?dataset=ilc_hcmh02&lang=en. [Accessed 16 04 2019].
- [24] Statistikaamet, "Eesti Statistika," 19 03 2013. [Online]. Available: https://www.stat.ee/65359?parent_id=32784. [Accessed 16 04 2019].
- [25] Statistisches Bundesamt (Destatis), "Datenreport 2018," 2018.
- [26] Pflugradt N., Teuscher J., Platzer B. & Schufft W., "Analysing low-voltage grids using a behaviour based load profile generator," in *International Conference on Renewable Energies and Power Quality*, Bilbao, Spain, 2013.

Publication VIII

T. Häring, R. Ahmadiyahangar, A. Rosin, H. Biechl and T. Korötko, "Comparison of the Impact of Different Household Occupancies on Load Matching Algorithms," 2019 Electric Power Quality and Supply Reliability Conference (PQ) & 2019 Symposium on Electrical Engineering and Mechatronics (SEEM), 2019, pp. 1–6, doi: 10.1109/PQ.2019.8818270.

Comparison of the Impact of Different Household Occupancies on Load Matching Algorithms

Tobias Häring
Department of Electrical Power
Engineering and Mechatronics
Tallinn University of Technology
Tallinn, Estonia
tobias.haring@taltech.ee

Roya Ahmadihangar
Department of Electrical Power
Engineering and Mechatronics
Tallinn University of Technology
Tallinn, Estonia
roya.ahmadi@taltech.ee

Argo Rosin
Department of Electrical Power
Engineering and Mechatronics
Tallinn University of Technology
Tallinn, Estonia
argo.rosin@taltech.ee

Helmuth Biechl
Faculty of Electrical Engineering
University of Applied Sciences Kempten
Kempten, Germany
biechl@hs-kempten.de

Tarmo Korõtko
Department of Electrical Power
Engineering and Mechatronics
Tallinn University of Technology
Tallinn, Estonia
tarmo.korotko@taltech.ee

Abstract—Necessary balancing of supply and demand due to an increasing amount of renewable energy sources in the grid can be achieved with demand side management (DSM) resp. scheduling loads like a freezer, a water heater or space heating. Engaging in DSM with such controlled thermal storages can be lucrative for customers to reduce their electricity costs with small impact on their comfort. This paper proves that the height of those savings depends not just on the control algorithms but also on the occupancy of the dwelling. Simulations with object models of the scheduled appliances show the performance of different price based set point calculation algorithms. Estimation of possible savings for the different selected occupancies is achieved in this work by comparison of the simulation results of different load matching algorithms to each other and between the different occupancies. This enables recommendations on the selection of the algorithm depending on the occupancy of an existing dwelling with respect to maximum possible electricity cost savings. This can come in handy for example for dwelling and apartment owners who are renting out dwellings.

Keywords—thermal storage, thermostatically controlled load, price based control, demand response, microgrid, object model, occupant behavior

I. INTRODUCTION

More and more renewable energy sources in the grid force distribution system and also micro grid operators to establish a sufficient control of supply and demand to keep frequency and power levels stable and within their limits. For the demand side grid utilities can to provide lucrative offers for customers to engage in the demand side management (DSM). There are different loads in a typical dwelling that can be scheduled [1]. Some of these schedulable devices, can be used as thermal storages for DSM, like freezer, water heater or space heating/cooling. Unlike ultracapacitors [2] or batteries [3] for example, those energy storages are already commonly available in households. Thus, this paper focuses on such appliances as they can compose 50% of the electrical energy consumption in buildings [4], can be used as an energy storage and do not interfere with the user comfort too much.

Several papers present scheduling models/algorithms, like [5]. The performance and feasibility of the algorithm for a water heater is not shown in detail since the whole system is considered in this project and not separate appliances.

This work was supported by the Estonian Research Council grant PUT (PUT1680), and Estonian Centre of Excellence in Zero Energy and Resource Efficient Smart Buildings and Districts ZEBE, grant 2014- 2020.4.01.15-0016 funded by European Regional Development Fund.

Other articles focus on the performance and feasibility for a single appliance. In [6] the implementation of a load shaping algorithm on the example of a water heater is shown. A payback period based on the algorithms performance is estimated to show the feasibility of such a control strategy. In [7] the authors present a model predictive scheduling method for freezers based on the day ahead market prices. The model is compared to measurements and shows good similarity. Applying the proposed algorithm shows cost reductions.

But all those papers, including [6], [8], [9], are focused on price based control for one appliance, like a water heater or a freezer. The authors of [8] show a general approach on scheduling loads based on real time prices. They include a water heater as such a schedulable load and present possible cost reductions. The performance of different price based load shaping algorithms is shown in [9]. A freezer and a water heater are controlled with and without pre-freezing / -heating. Possible power resp. cost reduction are presented and compared for the different algorithms. The appliances are investigated separately.

To have a better view on the total possible cost saving multiple devices should be taken into account. Papers which consider multiple thermostatically controlled devices usually focus on one control algorithm. An aggregated control for multiple thermostatically controlled devices is shown in [10]. Using a market price based control the electricity costs could be reduced compared to a fixed set point control. The authors of [11] use the definition of “equivalent storage capacity” to describe the thermostatically controlled loads. Space heating / cooling, water heater and refrigerating appliances are taken into account and an aggregator is used. A comparison to a battery storage for scheduling consumption is made considering investment costs.

In [12] it is shown that the occupant behavior has an influence on the energy consumption and comfort level of users. A smart zoning approach is used to reduce the energy consumption. Other articles investigate the occupant behavior but do not consider the influence on price based control algorithms. In [13] the authors attempt to evaluate the effect of occupant behavior on the energy performance of a building. Different devices are taken into account for this study. It is shown that the occupant behavior influences the energy consumption of a building in general. But possible influences on price based control are not shown.

This work takes into account thermal storage control strategies for multiple devices in one household in grid connected operation to reduce electricity costs. Comparing different set point calculation algorithms provides a base for recommendations on improving control strategies for different household consumption patterns resp. different dwelling occupancies. Thus, in an existing dwelling it should be possible to estimate the possible cost savings on electricity prices based on its occupancy. This can also help in a next step to optimize the control of not just one household, but expand the investigation to apartment building level and give recommendations on improving the electricity costs for all tenants of the building. Later such a system can be expanded to microgrid level with aggregated loads.

The paper is organized as follows: The mathematical object models, methodology and control strategies are presented in the Section II. Section III shows the results of the different simulations. Finally, the results in brief with conclusions and recommendations are presented in Section IV.

II. SYSTEM MODELING

To give recommendations on suitable control strategies and possible cost savings it is necessary to model a suitable system. Commonly, there are three household thermal storage systems: a freezer, a water heater and space heating. This section describes mathematical object models of these three systems. These models are based on datasheets of typical devices. Specific control strategies, including price based load matching algorithms, are presented. Other parameters and input data for the simulations, which include the different occupancies of an existing dwelling, are described.

A. Mathematical Object Models

First, The freezer model is based on the temperature changes due to food exchange (T_{food}), ambient losses ($T_{amb,loss}$) and freezing (T_{freeze}) during the time step. The cabinet temperature at the end of the time step (T_{next}) could be obtained from the temperature at the beginning of the time step (T_i) as follows (1) [9], [14] :

$$T_{next} = T_i - T_{freeze} - T_{food} - T_{amb,loss} \quad (1)$$

The model for the water heater was similar. The temperature of the water inside the boiler at the end of the time step (T_{next}), was obtained from the temperature at the beginning of the time step (T_i) and the temperature changes during the time step due to heating ($T_{heating}$), water exchange (T_{cw}) and ambient losses ($T_{amb,loss}$) (2) [9], [14]:

$$T_{next} = T_i + T_{heating} - T_{cw} - T_{amb,loss} \quad (2)$$

The space heating/cooling model is based on the temperature changes during the time step due to heating/cooling (T_{hc}) with the heat pump resp. electrical heater, the ambient air exchange (T_{air}), ambient losses through outside walls and windows ($T_{amb,loss}$), people in the room (T_p) and sun irradiation through the windows (T_{sun}). The temperature at the end of the time step (T_{next}) was obtained from the temperature at the beginning of the time step (T_i) like follows [9], [10] (3):

$$T_{next} = T_i + T_{hc} - T_{air} - T_{amb,loss} + T_p + T_{sun} \quad (3)$$

In this paper to achieve a simple and clear structure, models (1)–(3) were combined to one system model. For all the connections between the components there were neither losses nor parasitic elements taken into account. The ambient

conditions for the devices were fixed for all simulations and the thermal storages did not influence each other. Freezer, water heater and space heating had the same sizing and dimensions for every simulation to represent an existing dwelling and make comparisons possible. These object models needed a control model and input data which is shown in the next section.

B. Control Strategies

For all simulations in this work, a system with a freezer, water heater and space heating/cooling was considered. All these devices were controlled in each household. Thermostatic 2-step control with a fixed set point is the typical way to control the thermal storages. Such a 2-step control was used for all other simulations as well. But for those the set point was calculated with different algorithms according to the price signal. According to the price ($P_{(i)}$) and electrical energy consumption ($E_{(i)}$) during each time step, an average electricity price per day ($P_{avg,d}$) can be calculated (4):

$$P_{avg,d} = \frac{1}{7} \sum_{i=1}^{2016} P_{(i)} * E_{(i)} \quad (4)$$

To determine the performance of different set point calculation algorithms, the average price per day was compared to a fixed set point control. The result of this comparison is an electricity cost difference in percent.

Seven different price based set point calculation algorithms (A–G) [5], [6], [9] were implemented which are shown in more detail in [14]. Both linear and nonlinear algorithms were used. All algorithms are shown for the example of a water heater in Fig. 1. The algorithms in detail are shown in Table I. The user comfort (C_{user}) is set to 1 for all simulations.

C. Case Study

Each simulation was for one week, starting at Monday 00:00 a.m. with a time step of 5 min. Apartment electricity, food and warm water consumption patterns as well as the pattern of people in the room represented one week.

The thermal storages operated according to their set point and the price was calculated according to day-ahead market price hourly data from the Nord Pool Elspot database for Estonia [15].

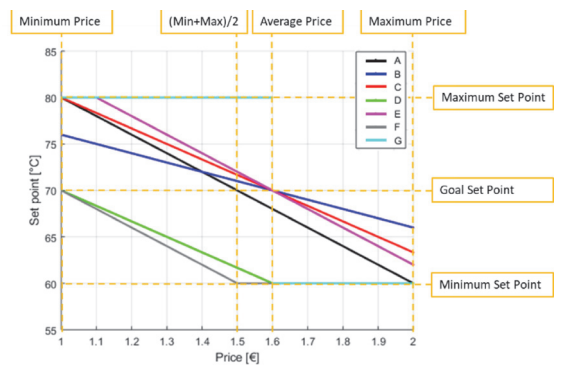


Fig. 1. Set point calculation for a water heater with algorithms A–G for an example price range of 1–2 € with an assumed average price of 1.6 €.

TABLE I. PRICE BASED CONTROL ALGORITHMS [5], [6], [9]; COOLING = FREEZER AND SPACE COOLING; HEATING = WATER HEATER AND SPACE HEATING

Algorithm	Description of set point calculation algorithm
A	Cooling: $T_{set} = T_{set,min} + C_{user} * (Pr - Pr_{min}) * \frac{T_{set,max} - T_{set,min}}{Pr_{max} - Pr_{min}}$
	Heating: $T_{set} = T_{set,max} - C_{user} * (Pr - Pr_{min}) * \frac{T_{set,max} - T_{set,min}}{Pr_{max} - Pr_{min}}$
B	Cooling: $T_{set} = T_{goal} + C_{user} * (Pr - Pr_{mavg}) * \frac{ T_{set,max} - T_{goal} }{Pr_{dev}}$
	Heating: $T_{set} = T_{goal} - C_{user} * (Pr - Pr_{mavg}) * \frac{ T_{set,min} - T_{goal} }{Pr_{dev}}$
C	Cooling: $T_{set} = T_{goal} + C_{user} * (Pr - Pr_{mavg}) * \frac{T_{set,max} - T_{goal}}{Pr_{max} - Pr_{mavg}}$
	Heating: $T_{set} = T_{goal} - C_{user} * (Pr - Pr_{mavg}) * \frac{T_{set,min} - T_{goal}}{Pr_{min} - Pr_{mavg}}$
D	Cooling: $T_{set} = T_{goal} + C_{user} * (Pr - Pr_{min}) * \frac{T_{set,max} - T_{goal}}{Pr_{max} - Pr_{mavg}}$
	Heating: $T_{set} = T_{goal} - C_{user} * (Pr - Pr_{min}) * \frac{T_{set,min} - T_{goal}}{Pr_{min} - Pr_{mavg}}$
E	Cooling: $T_{set} = T_{goal} + C_{user} * (Pr - Pr_{mavg}) * \frac{T_{set,max} - T_{set,min}}{Pr_{max} - Pr_{min}}$
	Heating: $T_{set} = T_{goal} - C_{user} * (Pr - Pr_{mavg}) * \frac{T_{set,max} - T_{set,min}}{Pr_{max} - Pr_{min}}$
F	Cooling: $T_{set} = T_{goal} + C_{user} * (Pr - Pr_{min}) * \frac{T_{set,max} - T_{set,min}}{Pr_{max} - Pr_{min}}$
	Heating: $T_{set} = T_{goal} - C_{user} * (Pr - Pr_{min}) * \frac{T_{set,max} - T_{set,min}}{Pr_{max} - Pr_{min}}$
G	Cooling: $Pr \geq Pr_{mavg} \rightarrow T_{set} = T_{set,max} ; \textit{Otherwise} \rightarrow T_{set} = T_{set,min} ;$
	Heating: $Pr \geq Pr_{mavg} \rightarrow T_{set} = T_{set,min} ; \textit{Otherwise} \rightarrow T_{set} = T_{set,max} ;$

Different household occupancies were selected from the predefined ones implemented in LoadProfileGenerator [16] and categorized to 8 groups. They represent some typical occupancy scenarios for dwellings. Their electricity consumption per day as well as water and food consumption were different. The electricity consumption patterns with the corresponding room occupancy and hot water consumption patterns were created with the LoadProfileGenerator software. This means that they were artificial profiles based on a behavioral model. In [17] it is reported that the load profiles show good similarity to the measured load profiles.

Additionally, the simulations were validated with measured profiles for a similar occupancy of a similar dwelling and similar results compared to the corresponding artificial profile could be obtained. To show the influence of different seasons, patterns and ambient conditions were available for summer and winter time. This included the occupancy, electricity consumption, day-ahead prices and for example the ambient temperatures.

The chosen household occupancies with their daily electricity consumption without the thermal storages for the summer conditions are shown in Table II and the 5 min power consumption patterns for 1 week for summer conditions are presented in Fig. 2.

As seen from the table and the figure, the electricity consumption is different for each kind of occupancy of the dwelling. For the households where the occupants are working or studying, the electricity consumption for the weekends is higher as they spend more time at home. Household vi has a very high energy consumption at the beginning of the week as the working family member is sick and stays at home. There are very high peaks for household iv which are even higher at

the weekend. This is due to the fact that only one child is going to school and the other family members spend a lot of time at home. Depending on the different sleeping habits for the people of the different households the time of the minimum electricity consumption at night varies slightly. To have a solid base for comparison, other variables in the simulations, like size of the freezer or volume of the apartment, were not changed for different occupancy profiles.

The energy consumption patterns as well as the water and food consumption were different for each of these households. Thus, the performance of the chosen algorithms in different environments could be compared and analyzed. This enables recommendations concerning a good control strategy for different occupancy situations. A total of 128 simulations were conducted for the 8 occupancy patterns, each with 7 price based algorithms and fixed set point control and at summer/winter conditions.

TABLE II. OCCUPANCY DESCRIPTION FOR THE DIFFERENT HOUSEHOLDS (HH) WITH THEIR RESPECTIVE AVERAGE ELECTRICITY CONSUMPTION PER DAY (EL. CONSUMPTION)

HH	Description	El. Consumption
i	Couple; both working	9.82 kWh/d
ii	Single; working	4.18 kWh/d
iii	Student; studying	2.15 kWh/d
iv	Family; 2 children; both unemployed	14.63 kWh/d
v	Single; retired	2.58 kWh/d
vi	Family; 2 children; 1 working and 1 unemployed	13.10 kWh/d
vii	Flat sharing Students; 3 studying	9.22 kWh/d
viii	Couple; both retired	5.85 kWh/d

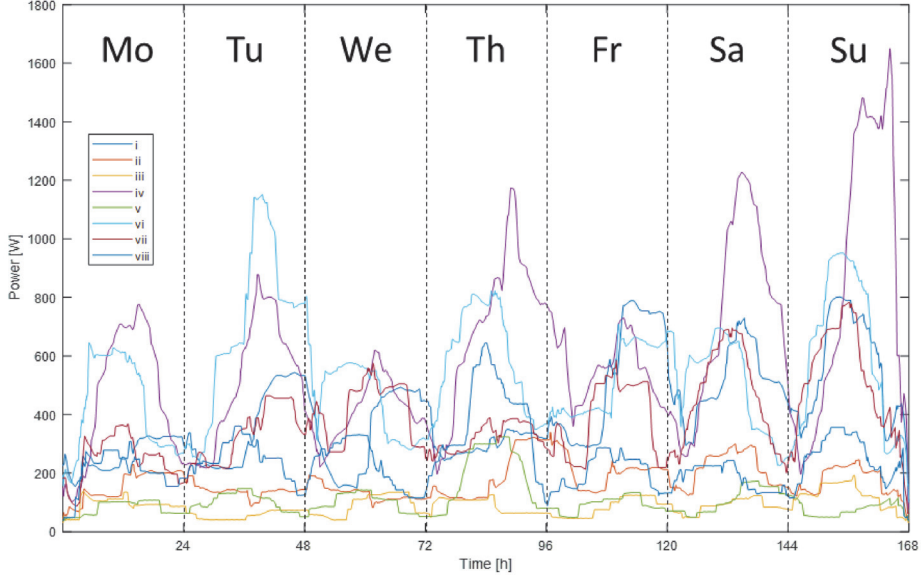


Fig. 2. 5 min power consumption data for households i-viii for the duration of 1 week in summer conditions.

III. SIMULATION RESULTS

All simulations were developed and conducted in Matlab R2018b. For these grid connected simulations the price based control strategies show the following results for the different household occupancy profiles. These results are also shown in Table III and Table IV. Additionally, an overview of the different algorithms is presented in Table V.

In general, it can be noted that algorithms D and F achieve the best results compared to the other price based algorithms. This seems to be due to the operating range of these algorithms. The set point mostly changes between the goal set point and the minimum consumption set point, which represents the lowest user comfort. Other algorithms use the whole range between the minimum and maximum consumption set point. The higher energy consumption during low price periods due to the higher consumption set point cannot be stored long enough with other algorithms to reduce energy costs in high price periods sufficiently. The result is a higher overall average electricity price per day. Therefore, Algorithms A, B, C and E usually have a lower performance. Nevertheless, compared to a fixed set point control they always provide cost saving opportunities.

The worst performance is shown by algorithm G which sometimes even increases the electricity costs. The reason for this behavior is the simple 2 step implementation of this algorithm. If the price is higher than the average price, the minimum consumption set point is chosen and otherwise the maximum consumption set point. Like explained previously, the higher energy consumption during low price periods cannot be stored long enough to reduce costs during high price periods sufficiently. Since there are only two states for the set point in this algorithm, the influence of this effect is even higher because the maximum consumption set point is chosen for longer time and is not decreasing for slightly higher prices.

In contrast the algorithm will also stay at the minimum consumption set point at high price periods for longer time than with other algorithms. Depending on the use of the thermal storage (e.g. food exchange or water exchange), which is different for each of the household occupancies, this can lead to a higher electricity price.

For example: The price is slightly below the average price. This means the thermal storage is with algorithm G at the maximum consumption set point whereas the fixed set point control is at the goal set point. If somebody in the dwelling is taking a shower now, heating up the exchanged water will take more energy because the water heater is at the maximum set point compared to the goal set point with a fixed set point control. On the other hand, it is vice versa if the electricity price is slightly higher than the average price and a lot of energy and electricity costs can be saved. If this negative example is more likely than the positive one for a certain household occupation, then the electricity costs can be even higher than with a fixed set point control. Additionally, the thermal storage will be at maximum consumption set point for a longer time where the ambient losses are highest. This cannot be compensated with the extended periods at the minimum consumption set point where these losses are lower as ambient losses are not changing in a linear way with the temperature difference. All of that can lead higher electricity costs compared to a fixed set point control, like shown in Table III and Table IV. Household i for example shows cost reductions of up to 21% compared to a fixed set point control. This is achieved by algorithms D and F in winter conditions. The worst result is presented by algorithm G in summer settings which increases the costs by 1%. The other algorithms are showing reductions around 3–5%. Similar patterns can be observed for all other households as well.

TABLE III. COST DIFFERENCES FOR ALGORITHMS A-G IN HOUSEHOLDS I-VIII IN PERCENT FOR SUMMER CONDITIONS

Household \ Algorithm	A	B	C	D	E	F	G
i	-1%	-3%	-3%	-16%	-4%	-16%	1%
ii	-5%	-6%	-8%	-20%	-8%	-20%	0%
iii	-1%	-3%	-5%	-17%	-5%	-18%	6%
iv	-4%	-7%	-8%	-18%	-8%	-17%	-5%
v	-1%	-2%	-4%	-16%	-4%	-18%	4%
vi	-2%	-4%	-5%	-14%	-5%	-13%	-2%
vii	-2%	-3%	-4%	-14%	-5%	-13%	-2%
viii	-2%	-3%	-4%	-13%	-5%	-13%	-2%

TABLE IV. COST DIFFERENCES FOR ALGORITHMS A-G IN HOUSEHOLDS I-VIII IN PERCENT FOR WINTER CONDITIONS

Household \ Algorithm	A	B	C	D	E	F	G
i	-5%	-4%	-5%	-21%	-5%	-21%	-3%
ii	-5%	-3%	-5%	-22%	-5%	-23%	2%
iii	-4%	-2%	-3%	-22%	-5%	-22%	3%
iv	-4%	-3%	-3%	-17%	-3%	-17%	-5%
v	-3%	0%	-3%	-21%	-3%	-23%	4%
vi	-3%	-1%	-2%	-16%	-2%	-16%	-3%
vii	-3%	-1%	-2%	-16%	-2%	-16%	-3%
viii	-2%	-2%	-2%	-16%	-2%	-16%	-3%

TABLE V. CLASSIFICATION OF ALGORITHMS A-G

Algorithm	Goal Set Point Operation	Algorithm Scaling and Shifting	Cost Savings	User Comfort
A	(Max. Price + Min. Price)/2	Max. and Min. Price scaling	+	0
B	Average Price	Price deviation scaling; Avg. Price shifting	+	0
C	Average Price	Min. and Avg. Price scaling	+	0
D	Minimum Price	Min. and Avg. Price scaling	++	-
E	Average Price	Max. and Min. Price scaling; Avg. Price shifting	+	0
F	Minimum Price	Min. Price and (Max. Price + Min. Price)/2 scaling	++	-
G	Never	2 point (min/max); Avg. Price shifting	0	0

++ highest; + high, 0 medium; - low

Algorithm G always shows the worst results which mark the minimum values. Increase of electricity costs of up to 6% can be observed. D and F always present the maximum reduction values. The other algorithms are usually in a range of 1%-8% of cost reductions. Another observation that can be made is that with higher household occupancy the cost savings tend to be a smaller percentage of the whole energy costs. This is due to the fact that there are more people living in the household which raises the electricity consumption and also water and food consumption. This creates less flexibility for the algorithms to optimize the electricity consumption according to the price pattern. More people means more disturbances for the thermal storages, like water exchange. The thermal storages need to restore the temperature set point and during that time there is less possibility for scheduling. There is no significant difference between summer and winter conditions. As a validation it can be mentioned that previous research [6], [9] typically presents cost savings for single appliances like freezer or water heater between 5%-30% range. The different appliances show different performances with the algorithms, so the combined cost reduction is smaller than with a single appliance.

IV. CONCLUSIONS

Different price based set point calculation algorithms have been presented to reduce the electricity costs in grid connected operation. To analyze the performance of these algorithms for different household occupancies, a system with a freezer,

water heater and space heating/cooling was used. The load profiles for the different occupancies were generated on a behavioral model.

From the presented algorithms it can be concluded that algorithm D and F show the highest cost savings. This is due to longer operation times at low consumption set points than the other algorithms or a fixed set point control. This behavior can be observed for all selected household occupancies. It is a trade-off with the user comfort, but the algorithms keep the set point within the user defined minimum and maximum acceptable values.

In general, the cost savings tend to be higher the smaller the energy consumption and number of occupants is due to higher flexibility for the algorithms. For low energy consumption households that savings can be up to 23% and for higher energy consumption households cost reductions up to 13% and more are shown. Therefore, the recommended load matching set point algorithms for such a thermal storage control system are D or F for all dwelling occupancies with expected savings of 13%-23% depending on the occupancy of the dwelling.

Recommendation for future works is to reduce the number of simplifications of the object models to improve the accuracy. Further, the effect of aggregation for example in an apartment building with multiple households or even a complete microgrid needs to be investigated.

REFERENCES

- [1] N. D. Rahate and N. Kinhekar, "Demand side management for household equipments," in International Conference on Information, Communication, Instrumentation and Control (ICICIC), Indore, India, 2017.
- [2] I. Roasto, T. Lehtla, T. Moller, and A. Rosin, "Control of ultracapacitors energy exchange," in 12th International Power Electronics and Motion Control Conference, Portoroz, Slovenia, 2006.
- [3] A. Rahmoun, A. Armstorfer, J. Helguero, H. Biechl, and A. Rosin, "Mathematical modeling and dynamic behavior of a Lithium-Ion battery system for microgrid application," in 2016 IEEE International Energy Conference (ENERGYCON), Leuven, Belgium, 2016.
- [4] A. Rosin, T. Moller, M. Lehtla, and H. Hoimoja, "Analysis of household electricity consumption patterns and economy of water heating shifting and saving bulbs," Scientific Journal of Riga Technical University, vol. 27, pp. 15–20, 2010.
- [5] D. J. Hammerstrom, R. Ambrosio, T. A. Carlon, J. G. DeSteele, G. R. Horst, R. Kajfasz, L. Kiesling, P. Michie, R. G. Pratt, M. Yao, J. Brous, D. P. Chassin, R. T. Guttromson, O. M. Järvegren, S. Katipamula, N. T. Le, T. V. Oliver, and S. E. Thompson, "Pacific Northwest GridWise TM Testbed Demonstration Projects. Part I. Olympic Peninsula Project," 2007.
- [6] C. H. K. Goh and J. Apt, "Consumer strategies for controlling electric water heaters under dynamic pricing," 2004.
- [7] R. Bálint, A. Fodor, K. M. Hangos, and A. Magyar, "Cost-optimal model predictive scheduling of freezers," Control Engineering Practice, vol. 80, pp. 61–69, 2018.
- [8] L. Aleixo, A. Rosin, H. Saele, A. Z. Morch, O. S. Grande, and I. Palu, "Ecogrid EU project – real time price based load control and economic benefits in a wind production based system," in 22nd International Conference and Exhibition on Electricity Distribution (CIRED 2013), Stockholm, Sweden, 2013.
- [9] A. Rosin, S. Link, M. Lehtla, J. Marins, I. Drovtar, and I. Roasto, "Performance and feasibility analysis of electricity price based control models for thermal storages in households," Sustainable Cities and Societies, 2017.
- [10] Y. Zhou, C. Wang, J. Wu, J. Wang, M. Cheng, and G. Li, "Optimal scheduling of aggregated thermostatically controlled loads with renewable generation in the intraday electricity market," Applied Energy, vol. 188, pp. 456–465, 2017.
- [11] F. Sossan, "Equivalent electricity storage capacity of domestic thermostatically controlled loads," Energy, vol. 122, pp. 767–778, 2017.
- [12] S. Baldi, C. D. Korkas, M. Lv, and E. B. Kosmatopoulos, "Automating occupant-building interaction via smart zoning of thermostatic loads: A switched self-tuning approach," Applied Energy, vol. 231, pp. 1246–1258, 2018.
- [13] B. Gucyeter, "Evaluating diverse patterns of occupant behavior regarding control-based activities in energy performance simulation," Frontiers of Architectural Research, vol. 7, pp. 167–179, 2018.
- [14] T. Häring, "Research and development of thermal storage control models," M.Sc.Eng thesis, Tallinn University of Technology, Tallinn, 15 01 2018. [Online]. Available: <https://digi.lib.ttu.ee/i/?11177>. [Accessed 29 01 2019].
- [15] Nord Pool AS, "nordpoolgroup.com," 2017. [Online]. Available: <https://www.nordpoolgroup.com/Market-data/Dayahead/Area-Prices/EE/Hourly/?view=table>. [Accessed 25 02 2019].
- [16] N. Pflugrath, "LoadProfileGenerator," [Online]. Available: <https://www.loadprofilegenerator.de>. [Accessed 25 01 2019].
- [17] N. Pflugrath, J. Teuscher, B. Platzer, and W. Schufft, "Analysing low-voltage grids using a behaviour based load profile generator," in International Conference on Renewable Energies and Power Quality, Bilbao, Spain, 2013.

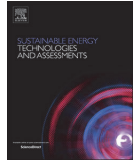
Publication IX

T. Häring, A. Rosin, and H. Biechl, "Using common household thermal storages to support the PV- and battery system in nearly zero energy buildings in off-grid mode," *Sustainable Energy Technologies and Assessments*, vol. 35, pp. 12–24, Oct. 2019, doi: 10.1016/j.seta.2019.05.014.



Contents lists available at ScienceDirect

Sustainable Energy Technologies and Assessments

journal homepage: www.elsevier.com/locate/seta

Using common household thermal storages to support the PV- and battery system in nearly zero energy buildings in off-grid mode

Tobias Häring^{a,*}, Argo Rosin^a, Helmuth Biechl^b^a Department of Electrical Power Engineering and Mechatronics, School of Engineering, Tallinn University of Technology, Ehitajate Tee 5, 19086 Tallinn, Estonia^b Institute of Electrical Power Systems (IEES), University of Applied Sciences Kempten, Bahnhofstraße 61, 87435 Kempten (Allgäu), Germany

ARTICLE INFO

Keywords:

Thermal storage
Demand side management
Off-grid
Renewable energy
nZEB

ABSTRACT

This paper investigates the use of common thermal storage systems for demand side management in off-grid situations for nearly zero energy buildings. Typical parameters and characteristics were analyzed to develop mathematical models for freezers, water heaters and space heating/cooling. The models used in this work are based on simplified equations derived from differential equations. Simplified models of a battery storage and a PV-system have been added. Models for the thermal storages, PV-system and battery storage were merged to one system model. All models and simulations were designed and conducted with Matlab. Various pre-defined price based set point calculation algorithms were modified to work with the off-grid system based on the system's voltage and available PV-power. Voltage and battery's state of charge based algorithms are developed in this work. In a system with a freezer, water heater and space heating/cooling that is powered by a PV-system only, a possible battery storage capacity reduction of up to 50% with PV-power based and up to 36% with SOC based algorithms compared to the same system with fixed set point thermostatic control could be achieved. Additionally, the capacity could even be reduced by up to 18% by solely reacting to voltage drops.

Introduction

The world's need for electric energy is constantly increasing. This is a result of growing population and higher living standards all around the world. To serve this high demand on electric power, it is necessary to focus more and more on renewable energy sources, providing volatile electric power. [1] Some studies even consider scenarios with a 100% renewable energy generation market [2].

This forces the grid utilities and also micro grid operators to establish a sufficient control of supply and demand to keep frequency and power levels stable and within their limits.

Grid utilities can influence the energy supply side by taking part in control power and energy market with their power stations. The power generation of these power plants will be changed according to the energy demand to balance the grid.

For the demand side, it is possible for grid utilities to provide lucrative offers for customers to engage in so-called demand side management (DSM). There are different loads in a typical dwelling that can be scheduled [3]. Often this scheduling reduces the user comfort [4], depending on the devices. Some of these schedulable devices, that are available in most households, can be used as thermal storages for DSM, like freezer, water heater or space heating/cooling. Additional energy

storage capacity can be utilized this way without investing into other additional storage systems like ultracapacitors [5] or batteries [6]. This paper focuses on such appliances as they can compose 50% of the electrical energy consumption in buildings [7].

There are several papers that present scheduling models/algorithms, like [8], and some also focus on their performance and feasibility [9]. In [10] the authors present a model predictive scheduling method for freezers based on the day ahead market prices. The authors of [11] schedule loads, including a water heater, based on real time prices. This approach enables cost reductions. But most of these papers do not take into account a user comfort level, which also influences the performance of such algorithms like presented in [4].

In [12] the performance and feasibility aspects are studied and the user comfort is considered. The authors of [13] consider those aspects in their investigation as well. Still all those papers are focused on price based control, thus improving cost savings in a power grid connected system. Only few papers can be found on using thermal storages or scheduling other loads to increase the power quality in off-grid mode [14]. Grid backup or diesel generators are often used in such investigations [15]. In [16] the authors include a simple scheduling algorithm for a water heater and one result shows changes in the necessary battery capacity according to the annual energy consumption of

* Corresponding author.

E-mail addresses: tobias.haring@taltech.ee (T. Häring), argo.rosin@taltech.ee (A. Rosin), biechl@hs-kempten.de (H. Biechl).

Nomenclature	
A_x	(Surface) Area of Object \times [m ²]
α	Coefficient: $U_x \cdot A_x$ [W/K]
β	Coefficient: $1/(V_x \cdot c_{px})$ [K/J]
COP	Coefficient of Performance
c_{px}	Specific Heat Capacity of \times [J kg ⁻¹ K ⁻¹]
C_{user}	User Comfort/Scaling for Algorithm
DOD _{max}	Maximum desired Depth of Discharge of the Battery System
DSM	Demand Side (Energy) Management
Δt	Time Step Width [h]
η_x	Efficiency of Appliance x [%]
k_i	Number of People in the Room during Time Step i
m_i	Mass of exchanged Food during Time Step i [kg]
nZEB	Nearly Zero Energy Building
P_c	Rated Electrical Power for Cooling of the Heat Pump [W]
$P_{el,f}$	Steady State Electrical Power of Freezer [W]
P_h	Rated Electrical Power for Heating of the Heat Pump [W]
P_{max}	Maximum Rated Power of Freezer/Heater [W]
P_{person}	Heat Dissipation of an Adult during 1 Hour [W]
PV	Photovoltaics
P_{wr}	Available Electrical Power during Time Step [W]
$P_{wr,dev}$	Electrical Power Deviation within Calculation Window [W]
$P_{wr,mavg}$	Average Electrical Power within Calculation Window [W]
$P_{wr,max}$	Maximum Electrical Power within Calculation Window [W]
$P_{wr,min}$	Minimum Electrical Power within Calculation Window [W]
RMS	Root-mean-square
S_i	Effect of Solar Irradiation on Windows: off/on {0,1}
SOC	State of Charge
SOC _{min}	Minimum desired State of Charge of the Battery System
T_{amb}	Ambient Temperature [°C]
$T_{amb,loss}$	Temperature Change due to Ambient Losses [K]
T_{cw}	Temperature Change due to Water Fluctuation [K]
T_f	Temperature of exchanged Food [°C]
T_{fc}	Corrected Temperature of exchanged Food [°C]
T_{food}	Temperature Change due to Food Exchange [K]
T_{freeze}	Temperature Change due to Freezing Power [K]
T_{goal}	Goal Temperature for Algorithm (User defined) [°C]
T_{hc}	Temperature Change due to Heating/Cooling [K]
$T_{heating}$	Temperature Change due to Heating Element [K]
T_i	Temperature of Appliance/Room at Beginning of Time Step i [°C]
T_{next}	Temperature of Appliance at End of Time Step i [°C]
T_{people}	Temperature Change due to People in the Room [K]
T_{set}	Set Point Temperature for next Time Step [°C]
$T_{set,max}$	Maximum Set Point Temperature (User defined) [°C]
$T_{set,min}$	Minimum Set Point Temperature (User defined) [°C]
$T_{sun,rad}$	Temperature Change due to Solar Radiation [°C]
T_{window}	Temperature Change due to Opened Windows [K]
U_x	U-value of Object \times [W m ⁻² K ⁻¹]
V_i	Volume of Air/Water Fluctuation during Time Step i [m ³]
V_{max}	Volume of Air in the Apartment/House [m ³]
V_n	Nominal Voltage [V]
V_{wood}	Volume of Wood (Furniture) in the Apartment/House
V_x	Maximum Volume of Appliance \times [m ³]
$V_{fr,max}$	Freezing Volume in kg per 24 h [l/kg]
y_i	Status of the Appliance: off/on {0,1}
z_i	Status of the Heat Pump: Cooling/Heating {0,1}

a household. They used a PV-powered off grid building in Australia with a battery storage system. Even with this simple shifting algorithm they present battery storage reductions of about 15–25%.

The authors of [12] focus on a single appliance under investigation only, like a water heater or a freezer. For a price based control approach this is suitable as the cost savings can be added up. In an off-grid system this is not possible as the total energy consumption of the household has to be taken into account.

In [17] the authors investigate a power quality control strategy for water heaters. There is a maximum peak load for the water heaters implemented to increase the power quality but all considerations are done for a grid-connected system and other components or an off-grid system are not taken into account.

The authors of [18] present a model for residential buildings with space heating/cooling but they do not take into account an off-grid system or scheduling algorithms. In [19] a similar modelling approach is shown with additional PV-system and battery storage system. Such systems are important for off-grid investigations. Increasing the self-consumption of the households and investigations on battery storage and PV-system size are presented. However, that paper focuses on the battery control strategy and does not take an off-grid situation into account. A peak shaving scheduling model for air conditioning is shown in [20]. Since the focus is on reducing peak loads, the thermal model of the building for the air conditioning as well as the rest of the micro grid infrastructure is not taken into account in this model. In [21] different control strategies for heating, ventilation and cooling systems are investigated considering the reduction of load peaks. The focus is put on the energy consumption of the space heating/cooling systems and other components of a micro grid are not taken into account. One of the strategies presented in [22] shows a load scheduling by using the thermal inertia of a building. The load peak of the heat pump could be shifted with a set point regulation method. The investigation is in the

context of industrial micro grids though and does not consider other devices or off grid situations. The authors of [23] present a stochastic model based control to increase the power reliability with the HVAC system. The control selects on of two different set points for each operation mode of the HVAC system according to the temperature and battery status.

Using a battery for power quality purposes is shown in [24]. Control methods for a battery storage system to reduce peak loads in the grid with positive results are presented. Load scheduling and the use in a small micro grid is not addressed in this article.

In [25] an approach to use thermal- and battery storages to improve grid friendliness is presented. The possible influence on the power quality is shown to depend on the battery storage size. But for all scenarios the system is connected to the grid.

A micro grid with PV-system and battery storage is investigated in [26]. But the focus of interest is put on the battery storage system design regarding its sizing in such a system and does not take into account a scheduling algorithm for thermal storages. In [27] a technology free modelling approach is shown for a micro grid. The authors include many technologies and also consider load shifting for different appliances in the model. But it is a grid connected simulation, thus battery reductions due to scheduling algorithms are not considered. The authors of [28] investigate energy and cost savings in an isolated grid including renewable energy sources with a demand response approach. However, they only consider washing-, drying machines and dish-washers for scheduling and no thermal storages. The impact on battery storage systems is not taken into account as well.

The optimization of sizing various components in a micro grid are shown in [29]. This includes wind turbines, PV-system and battery storage. But the authors do not take into account the influence of scheduling loads on the sizing of the components.

The previously mentioned papers suggest that the thermal storages

can be scheduled in a DSM-manner. Cost savings of about 5–8% [10] resp. up to 30% [12] are presented. Other presented papers show the possibility of power quality improvements with such devices. So it should as well be possible with suitable control strategies to optimize the power quality of an islanded system, which is powered by a PV-system only for example. Other publications suggest simple scheduling algorithms to improve the power reliability in islanded operation. Scheduling the loads with a sophisticated algorithm can help reduce the battery capacity that is needed to ensure stable operation even more than a simple load shifting like presented in [16]. This will result in potential cost reductions, as battery storage is still expensive [30].

Thus, this paper does not focus on price based control of thermal energy storages, but takes into account an off-grid system and the corresponding voltage based control model including the influence of a user comfort level for the majority of algorithms under investigation. Set point calculation algorithms for off-grid operation are developed in this work. These algorithms control different thermal storages that influence the whole islanded system rather than just the energy consumption of one appliance itself. Thus, the results are based on the whole system evaluation instead of a single device’s energy consumption. The off-grid system used in this work is powered by a PV-system only and has a mandatory battery storage which is a common configuration for nearly zero energy buildings (nZEBs). It simulates a micro grid that is in off grid mode for example during a fault ride through situation.

The previously mentioned thermal storages under investigation are relevant in typical Estonian and German dwellings because of their high share of energy consumption [7] and long lifetime of 10–20 years [31]. This is convenient for the user, as the devices do not have to be switched out that often. This makes these appliances interesting objects of investigation. As this paper aims to get a first insight into the scale of possible battery capacity resp. investment cost reductions, the models used here are simplified to keep the computational calculation time and power low.

This paper is organized as follows. Section “System Modeling” describes the models and simulations scenarios. Section “Simulation Results” presents and discusses the results of the simulations and finally, conclusions are presented in “Conclusions”.

System modeling

The object models are based on simplified equations. The correct function of the models is verified subsequently to avoid mistakes in the modeling. All the models have been developed using Matlab. Specific parameters for the different models are taken from datasheets of typical household devices (c.f. Table 1).

Mathematical object models

Several simplifications in the modeling make the following pre-conditions necessary for the thermal storage object models:

For the freezer:

- The freezer is always completely full. Food is replaced immediately. This has an effect on the total thermal capacitance, especially if the freezer is opened often. It is a sufficient simplification as most people keep their freezers full and open them rarely.
- The thermal capacitance of the freezer itself is neglected. Since the thermal capacitance of the food is much higher, a small error in the total thermal capacitance is introduced.
- The food is assumed to behave like water resp. ice. Most groceries have a high water content and the error in the specific heat capacity is small.
- The food is uniform. The overall food temperature will increase if food is replaced.
- Door opening losses are very small with a chest-type freezer and

therefore they are not considered.

For the water heater:

- The water heater is always completely full. Water is replaced immediately. As a result the mean water temperature of the whole water heater will decrease.
- The thermal capacitance of the water heater itself is neglected. The thermal capacitance of the water is much higher, thus the error introduced in the total thermal capacitance is small.
- The water is uniform. The overall water temperature in the water heater will decrease if hot water is used.

For space heating/cooling:

- Space heating/cooling is performed with a heat pump. Space heating can be switched to an electric heater. This is necessary because the efficiency of the heat pump can be low in winter time.
- The thermal capacitance of the walls is neglected. This introduces an error to the total thermal capacitance.
- People in the room are modeled as heat sources. The thermal energy is distributed uniformly in the whole apartment.
- Furniture is considered to be wood and uniform. The temperature of the whole furniture is changing and differences of the thermal capacitance of different furniture materials is neglected. This introduces an error to the total thermal capacitance.
- Solar heat gain through windows is based on typical irradiation data of the region.

Freezer model

The freezer model is based on [12]. The U-value of the freezer (U_f) is calculated using datasheet values. If the replacement food temperature is higher than 0 °C, the specific heat coefficient of water has to be considered. To be able to use the specific heat coefficient of ice for the whole temperature spectrum, it is required to calculate a corrected food temperature for the food warmer than 0 °C (1) [12]:

$$T_{fc} = T_i - \frac{(m_i * c_{pi} * T_i) + (m_i * c_{pw} * (-T_f))}{m_i * c_{pi}} \tag{1}$$

Otherwise, T_{fc} is equal to T_p .

The coefficients α (3) and β (4) enable calculation of the coefficient of performance (COP) of the freezer (2) [12]:

$$COP_f = \frac{\left(\frac{V_{fr,max}}{V_f}\right) * (-18\text{Å}^\circ\text{C} - T_{fc,25}) + \beta * 24h * \alpha * (-18\text{Å}^\circ\text{C} - 20\text{Å}^\circ\text{C})}{\beta * 24h * P_{el,f} * (-1)} \tag{2}$$

$$\alpha = U_f * A_f \tag{3}$$

$$\beta = \frac{1}{V_f * c_{pi}} \tag{4}$$

$V_{fr,max}$ is the amount of food with a temperature of 25 °C that can be

Table 1
Datasheet values for household appliance models.

Freezer [32]		Water heater [33]	
Surface Area	5.86 m ²	Surface Area	2.493 m ²
Average Annual Power Consumption	174 kWh	Rated Power	4.5 kW
Rated Power	120 W	Volume	150 l
Freezing Volume	286 l		
Freezing Capacity	22 kg/24 h		
Temperature Rise Time	25 h		

frozen within 24 h to a temperature of $-18\text{ }^\circ\text{C}$, without a change in the cabinet temperature. The ambient temperature is considered $20\text{ }^\circ\text{C}$.

$T_{fc,25}$ is the corrected food temperature for $T_f = 25\text{ }^\circ\text{C}$ and $T_i = -18\text{ }^\circ\text{C}$.

$P_{el,f}$ is the electrical power of the freezer.

Now it is possible to calculate all the temperature changes during the time step (5)–(7) [12]:

$$T_{freeze} = \beta * \Delta t * P_{el,f} * COP_f * \gamma_i \quad (5)$$

$$T_{food} = \left(\frac{m_i}{V_f} \right) * (T_i - T_{fc}) \quad (6)$$

$$T_{amb,loss} = \beta * \Delta t * \alpha * (T_i - T_{amb}) \quad (7)$$

With these temperature changes, the cabinet temperature at the end of the time step (T_{next}) can be obtained as follows (8) [12]:

$$T_{next} = T_i - T_{freeze} - T_{food} - T_{amb,loss} \quad (8)$$

Water heater model

The mathematical model of the water heater is similar to that proposed in [12].

α (9) and β (10) were calculated as follows [12]:

$$\alpha = U_{wh} * A_{wh} \quad (9)$$

$$\beta = \frac{1}{V_{wh} * c_{pw}} \quad (10)$$

U_{wh} is the U-value of the water heater. A pre-calculated value of $0.4\text{ Wm}^{-2}\text{K}^{-1}$ was used. A_{wh} is the surface area of the tank.

The temperature changes during the time step can be calculated as follows (11)–(13) [12]:

$$T_{heating} = \beta * \Delta t * P_{max} * \eta_{wh} * \gamma_i \quad (11)$$

$$T_{cw} = \left(\frac{V_i}{V_{wh}} \right) * (T_i - T_{cw}) \quad (12)$$

$$T_{amb,loss} = \beta * \Delta t * \alpha * (T_i - T_{amb}) \quad (13)$$

P_{max} is the rated heating power and η_{wh} is the heating efficiency given in the datasheet.

The output variable T_{next} representing the temperature of the water inside the boiler at the end of the time step, is obtained with the temperature changes (14) [12]:

$$T_{next} = T_i + T_{heating} - T_{cw} - T_{amb,loss} \quad (14)$$

Space heating/cooling model

The model for space heating/cooling was developed similar to the water heater and freezer models. With some additions, it is possible to create a mathematical model that can show the behavior of space heating/cooling in the same fashion as in the other thermal storage models.

The heat dissipation of an adult during 1 h (P_{person}) was set according to [34]. Maximum air and wood volumes (V_{max} , V_{wood}) were calculated with areas of floor and roof and the height of the room. The maximum air fluctuation during one time step was set to the maximum air volume. To obtain a more exact U-value of the outside walls, the λ -values or insulating capacities of bricks and insulation with their thicknesses t were used. A ventilation model is omitted for simplification. Instead a volume of air is assumed to be replaced through an open window. Values for these parameters are presented in Table 2

The variables α (15) and β (16) were obtained as follows:

$$\alpha = U_{wall} * (A_{wall} - \sum A_{window}) + U_{window} * \sum A_{window} \quad (15)$$

$$\beta = \frac{1}{V_{max} * \rho_{air} * c_{p,air} + V_{wood} * \rho_{wood} * c_{p,wood}} \quad (16)$$

using the densities (ρ_x) and c_p values of air and wood.

In the case of space heating, α does not only depend on one material, but on walls and windows, so it is necessary to take both into account. The variable β only takes air and furniture in the room into account. Furniture is assumed to be made of wood. The thermal capacitance of the walls is not taken into account although it has considerable influence on the temperature in long-term durations. But for time steps of 5 min, the influence is much smaller than the temperature change due to opened windows.

The solar irradiation power due to the windows depends on the window areas and the resulting irradiation values. Direct beam, diffuse and reflective irradiation were taken into account. The calculation includes longitude and latitude values together with clear sky average irradiation data at noon [35]. In addition, a normal distribution model is applied to match the clear sky irradiation data to measured values in [36].

Typical values for a heat pump are $COP = 1.0$ at $-18\text{ }^\circ\text{C}$ and $COP = 3.5$ at $10\text{ }^\circ\text{C}$. With these values, it is possible to make a linear approximation and limit the COP to a maximum of 4.5 and a minimum of 0.5. Because the COP is also affected by the difference of T_c and T_h , it is necessary to include a lift effect as described in [37]. In [38] a second order polynomial as an approximation for measured data was shown to be sufficient. If there is a low for COP for the heat pump in winter settings, it is possible to use electric heaters in the model instead.

The temperature changes during time step i can be calculated as (17)–(21) [12,34]:

$$T_{people} = k_i * P_{person} * \Delta t * \beta \quad (17)$$

$$T_{window} = \left(\frac{V_i}{V_{max}} \right) * (T_i - T_{amb}) \quad (18)$$

$$T_{amb,loss} = \beta * \Delta t * \alpha * (T_i - T_{amb}) \quad (19)$$

$$T_{sun,rad} = P_{solar} * \Delta t * \beta * s_i \quad (20)$$

$$T_{hc} = \beta * \Delta t * (z_i * P_h + ((z_i - 1) * (-1)) * P_c) * COP_{sp} * \gamma_i \quad (21)$$

The temperature changes due to the number of people (T_{people}), the air fluctuation of opened windows or ventilation system (T_{window}), ambient losses through the walls and windows ($T_{amb,loss}$), the solar irradiation through the windows ($T_{sun,rad}$) and the heating/cooling with the heat pump (T_{hc}).

The temperature at the end of the time step (T_{next}) can be calculated as shown in (22):

$$T_{next} = T_i + T_{hc} - T_{window} - T_{amb,loss} + T_{people} + T_{sun,rad} \quad (22)$$

Simplified electrical models

Both the battery storage and the PV-system model were reduced to their basic working principles. These simplifications are sufficient, as those electrical components do not represent the central elements of this investigation. All results are represented as a comparison between

Table 2
Parameters of space heating/cooling model.

Parameter	Value
P_{person}	140 W [34]
V_{max}	168.5 m ³
V_{wood}	5%
U_{window}	0.6 W/(m ² K)
λ_{brick}	0.037 (m K)/W
$\lambda_{insulation}$	0.18 (m K)/W
t_{brick}	0.25 m
$t_{insulation}$	0.1 m

two systems with exactly the same conditions except a different control strategy for thermal storages. Thus, small errors occurring due to the simplified models have a minor influence on the results as they occur in both systems and therefore can be omitted.

In summary, the following conditions apply to the electrical models:

- The solar irradiation is based on typical irradiation data for the region obtained from [35]. It considers direct, diffuse and reflective

irradiation based on calculations presented in [34]. The irradiation is then adjusted with a correction factor to fit measured values.

- The PV-model itself uses datasheet values to obtain the maximum PV-power at the maximum power point according to the irradiation similar to [39].
- Ambient conditions are fixed for the PV-model like described in [39].
- The battery storage model is represented by a capacity and a state of

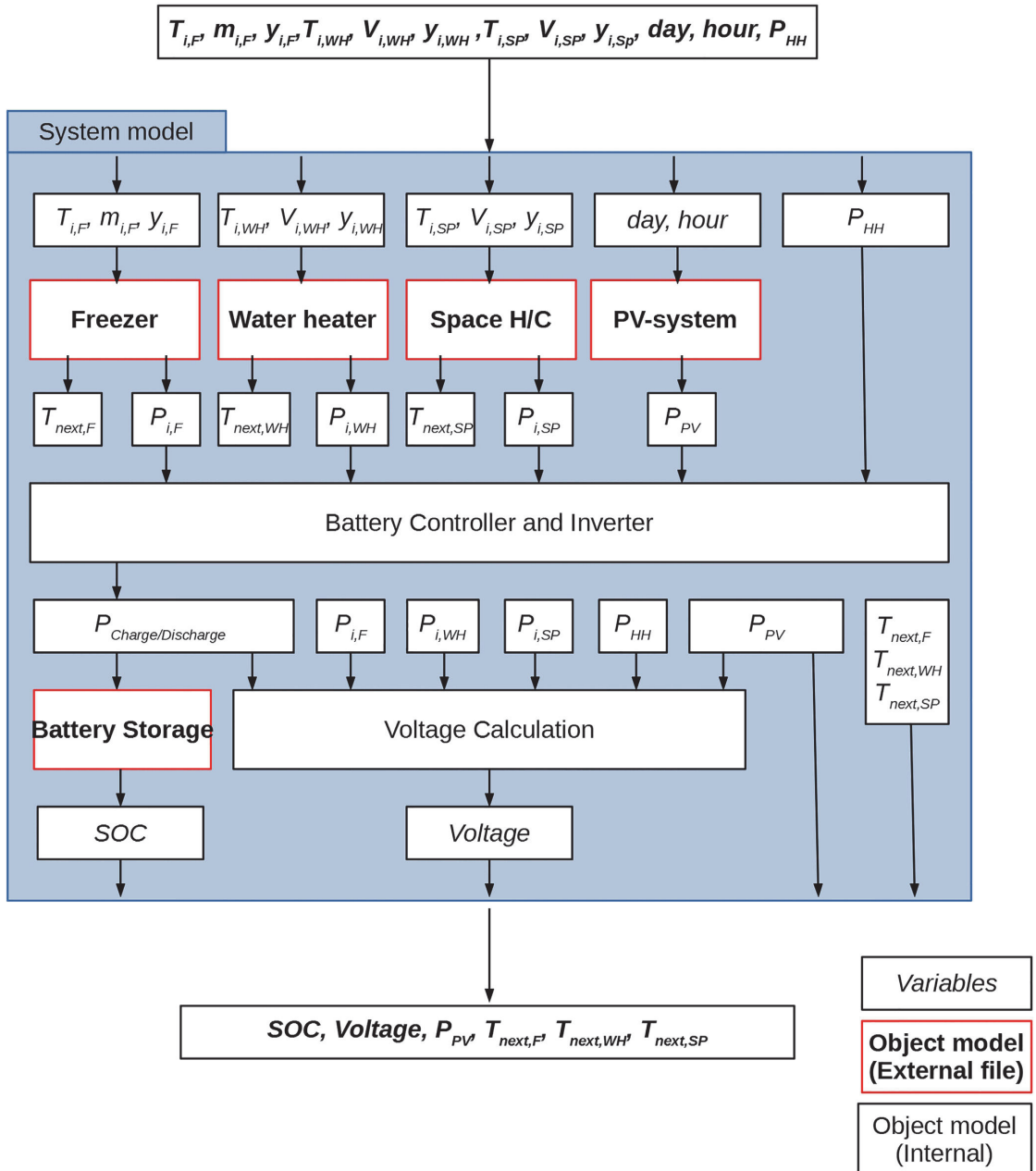


Fig. 1. Simplified system model schematic.

charge (SOC) value with charging and discharging efficiencies based on datasheet values [40] from Lithium-Ion (Li-Ion) batteries. This simple modelling is sufficient as the main interest lies in the possible reduction of battery capacity in a system with the same conditions except a different thermal storage control. Thus, lifetime, remaining capacity, temperature changes etc. are not necessary to consider in the model.

- Ambient conditions are fixed for the battery storage model.
- Inverter and battery controller are modeled within the complete system model.

The overall PV-system model has a similar approach like presented in [19]. Like described in [41] there are many influences on the actual PV-power generation, so a simple model will be sufficient as the results of the simulations are only going to be compared to each other. The battery storage system has the same simple approach like [19] suggests and a more accurate model is for not needed for this work and would only increase computation time.

Model verification

The correct behavior of each previously described model was verified with different simulations. Each test simulation showed the behavior of one influencing parameter, like ambient losses, people in the room or solar irradiation.

Additionally, the models were verified against measured data. This shows the error that is introduced to the simulations by each model.

For the freezer model, a simulations according to the requirements of the European Union commission delegated regulation (EU) No 1060/2010 with varied initial conditions was conducted. The average energy consumption in the simulations was 162 kWh/a. The EU energy label states a measured value of 172 kWh/a. This results in an error of 5.8%.

The power consumption of a water heater and the corresponding water consumption was measured for 1 week with a time step of 5 min. The same water consumption pattern was applied to the water heater simulation model. Comparing the average power consumption of the measured water heater with the simulation showed an error of 5.9%.

The space heating/cooling model was verified against an accurate simulation model, which was created with IDA Indoor Climate and Energy (IDA ICE). The documentation of IDA ICE [42] shows an overall error of less than 5% for the software according to CEN standards EN 15255-2007 and EN 15265-2007. The error of the average energy consumption of the space heating/cooling model compared to the IDA ICE model was 8.3%. This results in an overall error of the space heating/cooling model of less than 13.3%.

The battery storage model was verified against measured data from a Li-Ion battery. The charging current error was 11.6% and the discharging current error was 6.4%.

It is not necessary to quantify the error for the supplied power of the PV-system model. This is due to the volatile power supply of the system, which depends on many unpredictable effects, like clouds, that have a higher influence on the resulting power supply than a modeling error. Additionally, the model is, like mentioned in the previous section, based on historical data, which deliver a sufficient estimation of the irradiation magnitude depending on the season. Lastly, the exact magnitude of the delivered PV-power has no influence on the set point calculation algorithms, as they are scaled between the maximum and minimum delivered PV-power.

Complete system model

To achieve a simpler and clearer structure, all previously described models were combined to one system model. This model also includes a simplified PV-inverter and battery controller. For all the connections between the components there are neither losses nor parasitic elements taken into account.

In the off-grid mode, the PV-inverter works as follows. The frequency is considered to be kept constant in any case. The voltage is

limited to the nominal root-mean-square (RMS) voltage of 230 V (V_N). It cannot be exceeded. If the battery is charged and the PV-system produces more energy than the household consumes, the average PV-power during the time step will be reduced. As this is a very simplified model, it is not specified in the simulation how the PV-power is reduced. The battery storage automatically charges resp. discharges, depending on available PV-power and energy consumption of the household. Thus, if the battery is discharged and the PV-system does not provide enough power, the modeled system shows a voltage drop. If this voltage drop exceeds the defined limits, the simulation will be aborted, because the real system would shut down completely as a protection precaution.

A specific DC-AC converter between the battery/PV-system and the other components was omitted for simplification. It is not needed for such an energy simulation and the error added to the results will be sufficiently small.

For this complete system model, it is also assumed that the PV-system and battery storage are independent systems, which are not controlled by the algorithms developed in this work. These algorithms only deal with the control of the thermal storages. A schematic of the complete system model is shown in Fig. 1.

In summary, the following pre-conditions apply to the complete system for all simulations:

- The ambient conditions of the freezer model are fixed during the simulation. The freezer is assumed to be placed inside the building, where the temperature is kept constant.
- The ambient conditions of the water heater model are fixed during the simulation. The water heater is assumed to be placed inside the building, where the temperature is kept constant.
- The ambient conditions of the space heating/cooling model are fixed during the simulation except the ambient temperature, including the solar irradiation. It depends on the winter/summer settings. There is no shading from trees or other houses due to different sun angles or window shades/curtains that are closed.
- The thermal storage models do not influence each other thermally as they are assumed to be placed in separate locations.
- The ambient conditions of the PV-system and battery storage are fixed during the simulation. The battery is assumed to be in a controlled environment with constant temperature and there is no shading from other houses or trees on the PV-panels.
- Connections between the components are considered ideal which is applicable for such an energy simulation.
- The off-grid system only has the PV-system and battery storage as a power source. This is a common configuration in nZEBs.
- The number of PV-modules is fixed.
- The frequency of the off-grid system is fixed in any case. This is the assumed working principle of the inverter.
- The voltage of the off-grid system is limited. If there is more energy production than consumption, the average PV-power is reduced. If there is more consumption than energy production, the voltage is considered to show a drop.
- Safety margins for the battery capacity calculations are neglected. As the results are a comparison of two values, the safety margin would be added in both cases resulting in the same ratio.

Simulation and control strategies

For off-grid situation, the following scenarios apply:

- Freezer
- Water heater
- Space heating/cooling
- All previous appliances

All these scenarios are conducted without grid connection. To do

comparisons, each one is completed once at summer and once at winter settings for:

- Fixed set point thermostatic control
- Voltage and PV-power based algorithms 0–6 resp. 0–7
- Voltage (and SOC) based algorithms 8–11

The simulation can be conducted with winter settings or with summer settings. This affects some parameters, like the ambient temperature or the number of PV-modules. A simulation is one week with winter or summer settings. As a time step $\Delta t = 1/12$ [h] (= 5 min) was chosen. Apartment electricity (cf. Fig. 2), food (cf. Fig. 3) and warm water consumption patterns (cf. Fig. 4) represent one week.

People are in the apartment from 0:00–9:00 and 17:00–24:00 on workdays and the whole day on weekends (cf. Fig. 5).

The windows are opened for 10 min twice a day (cf. Fig. 6).

The off-grid simulations work the following way:

- A simulation starts with the smallest battery capacity of 10Ah and a SOC of 100%.
- If the voltage during the simulation is below the reference voltage minus 15% for more than two time steps, all parameters are reset and the simulation restarts with a 10Ah larger battery capacity. The voltage boundaries are based on the EN 50160:2010 grid norm to ensure stable operation.
- Before completion, the simulation checks if the SOC at the end is lower than the SOC at the beginning. If it is lower, the simulation restarts with that SOC value again. This ensures that the off-grid system is able to maintain stable operation for more than one week. It is based on the assumption that the household profile used in the simulation represents a typical or in best case, a profile slightly higher than average.
- If the simulation runs 4 times with decreasing SOC, it will also pass as a stable configuration.
- The lowest battery capacity that passes the simulation and can provide a constant SOC represents the minimum possible capacity. Then the control switches to a more accurate step width of 1Ah steps

to receive values that are more exact.

Thermostatic control with a fixed set point

The thermostatic control with a fixed set point is the easiest way to operate a freezer, water heater and space heating/cooling. This kind of control is also typical for the components and therefore will be used to create reference values for the comparison with the voltage based control.

The freezer has a fixed set point of 18 °C, the water heater of 60 °C and for space heating/cooling it is set to 20 °C. It is a two-step control or bang-bang control. Fig. 7 shows this control for cooling applications like the freezer or space cooling resp. for heating applications like the water heater and space heating. This control was used for all simulations. For the voltage based control the set point was recalculated according to the algorithm.

Voltage based control for off-grid system

Twelve off-grid algorithms were implemented to calculate set points for the thermostatic control. These algorithms are based on power, voltage and state of charge values that are available from the other system components. The results were then compared to the fixed set point thermostatic control. The initial values of the voltage based control simulations were the same as in the thermostatic control scenarios with a fixed set point. The block scheme of the control model, which will be explained in this chapter is also shown in Fig. 8 for the freezer.

All the off-grid algorithms had the following nonlinear condition implemented: If the grid-voltage in the off-grid system is dropping below the limit of 85% of the nominal voltage (V_N), the minimum energy consumption set point was chosen. Otherwise the set point was calculated according to the available PV-power (Algorithm 0–7) or SOC (Algorithm 9–11). The voltage drop reaction itself can be visualized like shown in Fig. 9. In the marked area, the set point is calculated according to PV-power or SOC based algorithms. It can be near the maximum or near the minimum set point.

The first eight algorithms (Algorithm 0–7) are modified price based control algorithms as proposed in [8,9,12]. Instead of the price, the

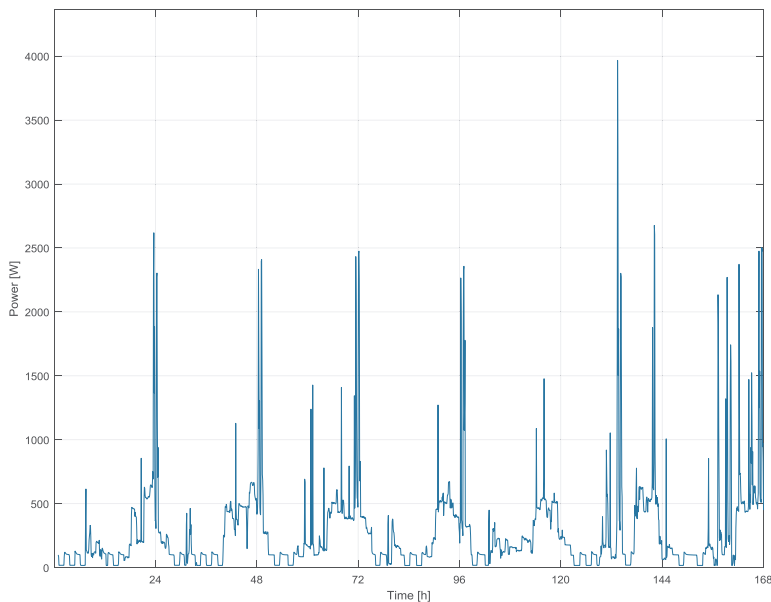


Fig. 2. Power consumption of the example household without the thermal storages for winter and summer simulations.

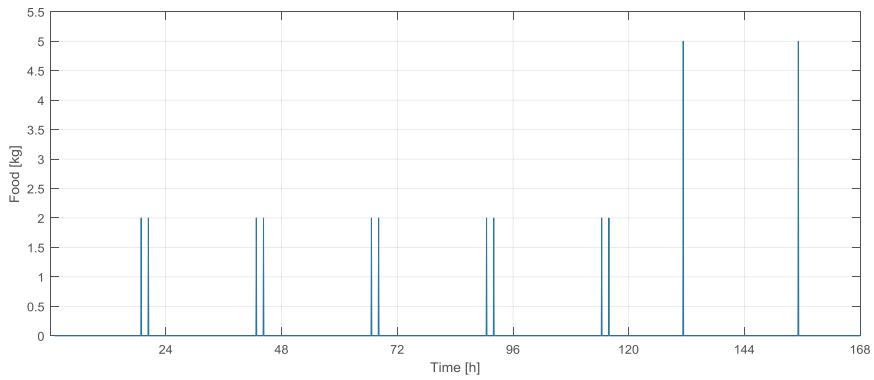


Fig. 3. Food consumption for winter and summer simulations.

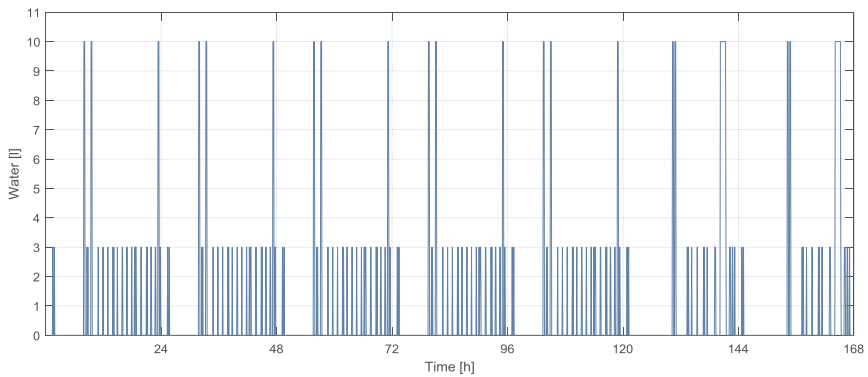


Fig. 4. Warm water consumption for winter and summer simulations.

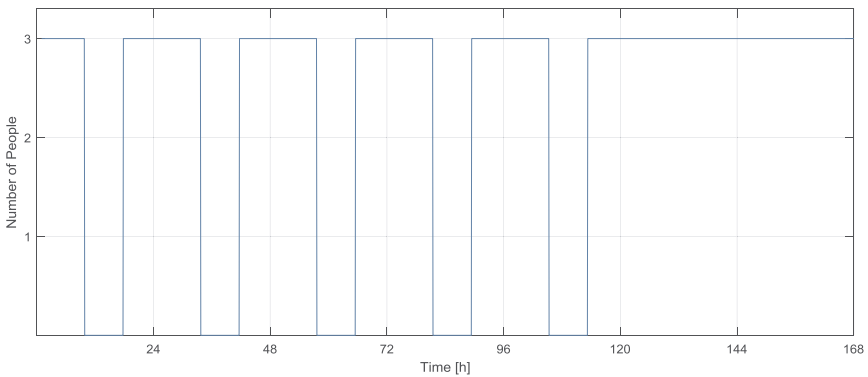


Fig. 5. Number of people in the apartment for winter and summer simulations.

basis for calculation was the estimated maximum power the PV-system could provide. To make the algorithms work properly, they have to be adapted because their behavior has to be exactly the opposite. If the available power is high, the consumed power should be high whilst in the price based control, a low price leads to high consumption. Algorithm 7 represents a mixed approach with the best algorithms 0–6 for each appliance in a system with all three of them activated.

Algorithm 8 is a simple voltage drop reaction. If the voltage is stable, it operates at the fixed or goal set point, otherwise at the minimum or maximum in the case of cooling (cf. Fig. 9).

Algorithm 9 is a SOC limit-based control algorithm. If the battery's state of charge drops below a certain value, it switches from the fixed or goal to the minimum (heating) resp. maximum (cooling) set point. Algorithm 10 changes the set point according to the SOC of the battery

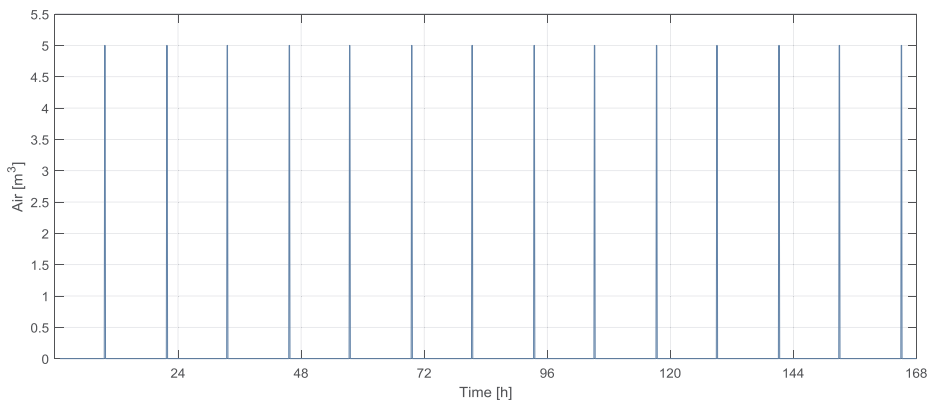


Fig. 6. Air exchange in the apartment for winter and summer simulations.

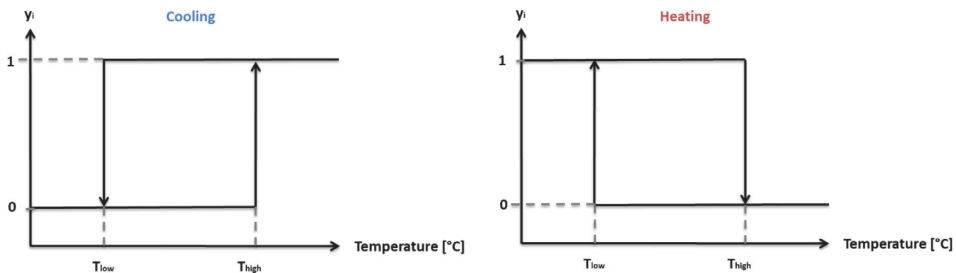


Fig. 7. 2-step control for cooling resp. heating applications.

in a linear way. A similar approach like in algorithm 0. Algorithm 11 switches between the minimum and the maximum set point according to the battery's state of charge, comparable to algorithm 6.

Most of these algorithms take into account a user comfort level variable C_{user} that modifies the behavior of the algorithm slightly to fit the users' needs. ($C_{\text{user}} = 0$: highest comfort; $C_{\text{user}} > 0$: lower comfort)

These algorithms are shown in Tables 3 and 4.

Simulation results

Algorithms 3 and 5 show poor results, whereas algorithm 0, 1 and 6 perform best. Algorithm 7, as a combination of the best algorithms for each thermal storage alone, shows the best results here. In off-grid mode and for an on-grid system with weak electrical installations, to prevent simultaneous turn-ons, it might be better to use different algorithms for different thermal storages to increase the power quality. This also applies for the control of a whole nZEB instead of just one apartment.

The SOC based algorithms also show good results. With number 9, 10 and 11, it is possible to reduce battery storage by 27–36%. This is around 1/3. In summer settings, algorithm 10 even shows the best overall results. This is an important finding, as the value for the maximum available PV-power might not be obtainable, whereas the SOC-state always is. Further, these algorithms do not depend on the energy source of the microgrid.

Another important conclusion can be drawn from the results of algorithm 8. Just by switching to the minimum set point if the voltage starts dropping, it is possible to reduce the battery capacity by up to 18%. That is a very good result, as this algorithm only relies on the voltage measurement and needs no additional measurements in a real

system. It is totally independent of the system configuration whether there is a PV-system, wind turbines, a battery storage, a flywheel or any other component.

The results for the freezer show low reductions for the battery storage of less than 5%. This applies to all algorithms. The energy consumption of the freezer is fairly low, compared to the remaining household's energy consumption and therefore, the scheduling of the device has a small impact on the necessary battery capacity.

For the freezer and the water heater the results for winter and summer settings are very similar. The different algorithms show mostly the same behavior which leads to similar battery reduction values. For space heating/cooling there are huge differences between summer and winter settings and simultaneously small differences between most of the different algorithms. Space heating shows much less battery capacity reduction potential than space cooling. This depends on the geographical selection of the ambient conditions. In Estonia there is a small need for space cooling since it is a northern country. Vice versa the winters are cold and the need for space heating is high. Thus, there is more flexibility in scheduling the space cooling compared to space heating. Space cooling is scheduled more efficiently by the algorithms, yielding higher battery reductions for summer time.

Results of a system with a water heater show a similar behavior to the system with all three thermal storages. The best algorithms for the water heater are usually the best algorithms for the system with all three appliances. The water heater's share of the total energy consumption is the most significant, leading to a high influence on the battery storage capacity reduction.

For space heating/cooling it can be observed, that algorithm 10 shows the best results for SOC based algorithms whereas algorithm 9 and 11 seem to show the worst results of all algorithms. The result for

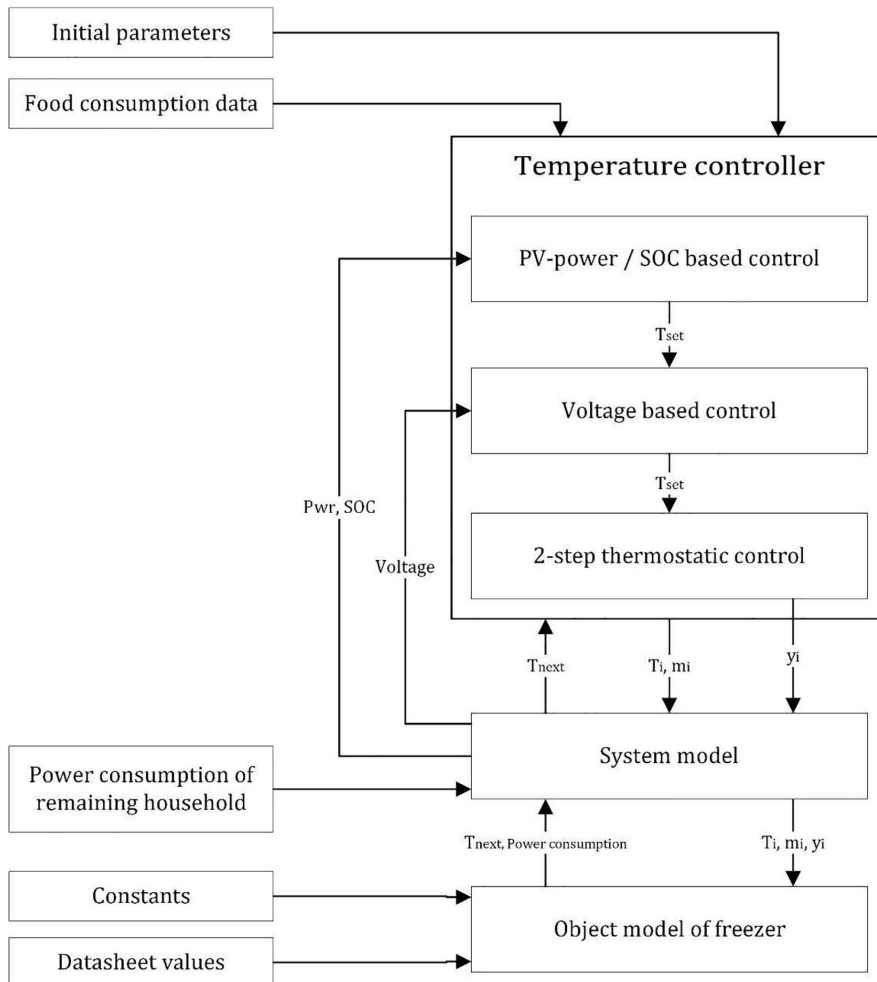


Fig. 8. Simplified control scheme (freezer example).

space cooling with algorithm 11 in summer settings is unusual. Due to a coincidence between the algorithm set point calculation, the power consumption and the SOC of the battery system, the minimum capacity increased. Such coincidences can happen any time, also with fixed set point control. For that reason, safety margins are typically added to the minimum battery capacity. The same effect can be seen for space heating in the opposite direction with algorithm 10 in winter settings.

Further, it can be observed that large savings in systems with one thermal storage each do not necessarily lead to large savings in a system with all three of them and vice versa.

Simulations for the off-grid algorithms determine the results shown in Tables 5 and 6 for a user comfort level of 1.0. The values in the tables show the percentage of the reduction of the battery storage for the complete household compared to the fixed set point thermostatic control.

During the simulations, the voltage level can go very low within 5 min and a real system would have shut down in that state already, while the simulation passed successfully. For future work, it is required to select a smaller time step for the voltage calculation. Then it can represent a real system more accurately.

There are only few scientific papers that deal with thermal storages in off-grid situations and even less concerning battery reductions. Battery reduction results presented in [16] show values in the range of 15–25% for a simple water heater shifting algorithm depending on the households overall energy consumption. These simulations show possible battery reductions for a system with a water heater only of 10–38%, excluding the solely voltage based algorithm 8, which is basically a fixed set point control. Since there is a lack of other results presented in literature concerning battery storage capacity reductions with thermal storages in off-grid mode, the quality of the results has to be estimated in other ways. Performing price based simulations with the same initial conditions and the models yield cost savings in the range of 5–28%. Other scientific articles like [9] and [12] typically present savings between 5 and 30%, which is in the same range. Since the investigation of battery storage reduction and cost reductions is similar in many ways, the performance of the algorithms can also be roughly compared. The PV-power based algorithms show reductions between 3 and 50% whilst the price based algorithms they were derived from show 5–28% cost savings resp. 5–30% in other literature. This is a wider range of values for the off-grid simulations due to dependencies

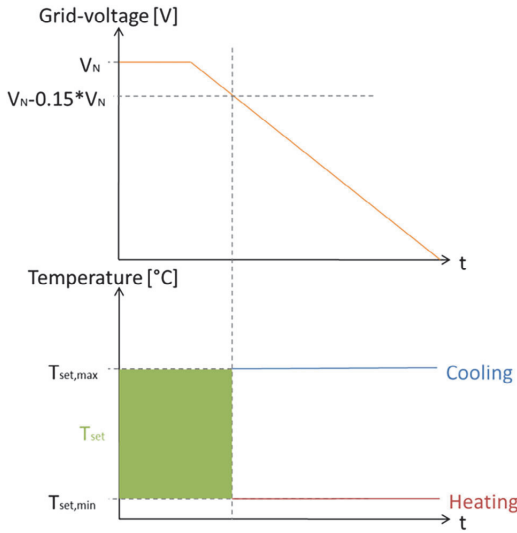


Fig. 9. Voltage drop reaction visualization for heating and cooling appliances.

Table 3
Voltage and PV-power based control algorithms [8,9,12]; Cooling = Freezer and space cooling (summer); Heating = Water heater and space heating (winter).

Number	Description of set point calculation algorithm
0	Cooling: $T_{set} = T_{set,max} - C_{user} * (Pwr - Pwr_{fmin}) * \frac{T_{set,max} - T_{set,min}}{Pwr_{fmax} - Pwr_{fmin}}$ Heating: $T_{set} = T_{set,min} + C_{user} * (Pwr - Pwr_{fmin}) * \frac{T_{set,max} - T_{set,min}}{Pwr_{fmax} - Pwr_{fmin}}$
1	Cooling: $T_{set} = T_{goal} - C_{user} * (Pwr - Pwr_{fmavg}) * \frac{T_{set,min} - T_{goal}}{Pwr_{fdev}}$ Heating: $T_{set} = T_{goal} + C_{user} * (Pwr - Pwr_{fmavg}) * \frac{T_{set,max} - T_{goal}}{Pwr_{fdev}}$
2	Cooling: $T_{set} = T_{goal} - C_{user} * (Pwr - Pwr_{fmavg}) * \frac{T_{set,min} - T_{goal}}{Pwr_{fmin} - Pwr_{fmavg}}$ Heating: $T_{set} = T_{goal} + C_{user} * (Pwr - Pwr_{fmavg}) * \frac{T_{set,max} - T_{goal}}{Pwr_{fmax} - Pwr_{fmavg}}$
3	Cooling: $T_{set} = T_{goal} - C_{user} * (Pwr - Pwr_{fmin}) * \frac{T_{set,min} - T_{goal}}{Pwr_{fmin} - Pwr_{fmavg}}$ Heating: $T_{set} = T_{goal} + C_{user} * (Pwr - Pwr_{fmin}) * \frac{T_{set,max} - T_{goal}}{Pwr_{fmax} - Pwr_{fmavg}}$
4	Cooling: $T_{set} = T_{goal} - C_{user} * (Pwr - Pwr_{fmavg}) * \frac{T_{set,max} - T_{set,min}}{Pwr_{fmax} - Pwr_{fmin}}$ Heating: $T_{set} = T_{goal} + C_{user} * (Pwr - Pwr_{fmavg}) * \frac{T_{set,max} - T_{set,min}}{Pwr_{fmax} - Pwr_{fmin}}$
5	Cooling: $T_{set} = T_{goal} - C_{user} * (Pwr - Pwr_{fmin}) * \frac{T_{set,max} - T_{set,min}}{Pwr_{fmax} - Pwr_{fmin}}$ Heating: $T_{set} = T_{goal} + C_{user} * (Pwr - Pwr_{fmin}) * \frac{T_{set,max} - T_{set,min}}{Pwr_{fmax} - Pwr_{fmin}}$
6	Cooling: $Pwr \geq Pwr_{fmavg} \rightarrow T_{set} = T_{set,min}; \text{Otherwise} \rightarrow T_{set} = T_{set,max};$ Heating: $Pwr \geq Pwr_{fmavg} \rightarrow T_{set} = T_{set,max}; \text{Otherwise} \rightarrow T_{set} = T_{set,min};$
7	Determines a predefined combination of algorithms for scenario with freezer, water heater and space heating/cooling combined.

on more variables, but they are still on the same level, suggesting legitimate results for the simulations.

Additionally the results showed that less comfort for the user ($C_{user} > 0$) results in a higher possible battery capacity reduction. A comfort value of 0.5 performs about 5–25% worse than a value of 1.0 but still shows better results than a fixed set point control. $C_{user} = 2.0$ can perform up to 20% better than $C_{user} = 1.0$. A user comfort level of 0 is equivalent to a fixed set point control.

Comparing this to the values in [12] shows similar results. The values presented suggest worse performance at a level of 0.5 of about

Table 4

Voltage and SOC based control algorithms; Cooling = Freezer and space cooling (summer); Heating = Water heater and space heating (winter).

Number	Description of set point calculation algorithm
8	Cooling: $T_{set} = T_{goal}$ Heating: $T_{set} = T_{goal}$
9	Cooling: $SOC \geq SOC_{min} + 0.2 \rightarrow T_{set} = T_{goal}; \text{Otherwise} \rightarrow T_{set} = T_{set,max};$ Heating: $SOC \geq SOC_{min} + 0.2 \rightarrow T_{set} = T_{goal}; \text{Otherwise} \rightarrow T_{set} = T_{set,min};$
10	Cooling: $T_{set} = T_{set,max} - C_{user} * (SOC - SOC_{min}) * \frac{T_{set,max} - T_{set,min}}{DOD_{max}}$ Heating: $T_{set} = T_{set,min} + C_{user} * (SOC - SOC_{min}) * \frac{T_{set,max} - T_{set,min}}{DOD_{max}}$
11	Cooling: $SOC \geq (1 + SOC_{min})/2 \rightarrow T_{set} = T_{set,max}; \text{Otherwise} \rightarrow T_{set} = T_{set,min};$ Heating: $SOC \geq (1 + SOC_{min})/2 \rightarrow T_{set} = T_{set,min}; \text{Otherwise} \rightarrow T_{set} = T_{set,max};$

0–15% compared to 1.0. A user comfort value of 2.0 also performs up to 20% better. Running price based simulations with the models in this work shows worse performance of up to 20% ($C_{user} = 0.5$) resp. better performance up to 10% ($C_{user} = 2.0$). Those are similar results. Concerning the comparison between price based algorithms and off-grid algorithms, there are small differences, but the results are still in a similar range of values. This suggests that the obtained values from the simulations are valid.

Conclusions

For a typical household in an nZEB, a freezer, a water heater and space heating resp. cooling can be used as thermal storages for demand side management.

A fixed set point thermostatic control simulation for every scenario is necessary to obtain a basis for comparison with other control strategies. The scenarios include off-grid situations for a system with each thermal storage alone in a household, and a system using all three of them. Different price based algorithms proposed in literature were used as a basis to develop off-grid algorithms, depending on different input parameters. Results for the off-grid control are as follows.

Using algorithms based on power, voltage and SOC measurements shows useful results for off-grid systems. Since the freezer has low power consumption, the difference to the fixed set point control is negligible. For the other appliances, the SOC based algorithms show good performance similar to those based on PV-power. However, SOC values are usually available whereas the PV-power does not necessarily have to be, so a SOC based control is preferable. Further, a simple voltage drop based algorithm, which is switching to minimum energy consumption set points, can already reduce the size of the battery storage.

The results also show that there is a higher potential in battery capacity reduction for space cooling in summer than it is for space heating in winter for a northern country with mild summers and cold winters. The influence of the water heater is very high due to its large share of the total energy consumption of the dwelling. Therefore, it is the most important appliance to consider when scheduling thermal storages in off-grid operation.

Coincidences between the algorithm set point calculation, the power consumption and the SOC of the battery system can happen for any scenario, which might lead to an increase in the necessary battery capacity. For that reason, safety margins are typically added to the minimum battery capacity.

The recommendation for off-grid systems is the use of SOC based algorithms, or just a voltage based one. Battery capacity reductions by around 1/3 could be achieved. The impact of the user comfort level can be up to 25% of battery storage reduction, which is a significant value.

Table 5

Battery capacity reductions with different PV-power based algorithms in comparison with thermostatic control with a fixed set point

Algorithm	Summer settings				Winter settings			
	Freezer	Water Heater	Space H/C	All	Freezer	Water Heater	Space H/C	All
0	-4%	-32%	-34%	-46%	-3%	-34%	-6%	-29%
1	0%	-34%	-34%	-48%	-3%	-32%	-6%	-29%
2	0%	-16%	-34%	-39%	-3%	-17%	-6%	-17%
3	-4%	-12%	-29%	-17%	-3%	-15%	-6%	-7%
4	-4%	-23%	-34%	-40%	-3%	-26%	-6%	-14%
5	-4%	-10%	-26%	-17%	-3%	-15%	-6%	-9%
6	0%	-38%	-34%	-50%	-3%	-34%	-6%	-31%
7	(0)	(6)	(1)	-50%	(0)	(6)	(1)	-34%

Table 6

Battery capacity reductions with different SOC based algorithms in comparison with thermostatic control with a fixed set point.

Algorithm	Summer settings				Winter settings			
	Freezer	Water Heater	Space H/C	All	Freezer	Water Heater	Space H/C	All
8	0%	-1%	0%	-12%	0%	-15%	0%	-18%
9	0%	-21%	0%	-30%	-3%	-30%	0%	-27%
10	0%	-25%	-24%	-35%	-3%	-31%	-30%	-35%
11	0%	-21%	3%	-36%	0%	-36%	-4%	-30%

In addition, the user comfort influences the possible battery capacity reduction significantly and should therefore be taken into account.

During this work, many simplifications had to be made. As future work, tests to verify the results of this work are planned, object models will be optimized and the time step width of the simulation has to be reduced to obtain results that are more accurate.

Acknowledgements

This work was supported by the Estonian Research Council grant PUT (PUT1680), and Estonian Centre of Excellence in Zero Energy and Resource Efficient Smart Buildings and Districts ZEBE, grant 2014-2020.4.01.15-0016 funded by European Regional Development Fund

References

- Mertens K. Photovoltaik - Lehrbuch zu Grundlagen, Technologie und Praxis. 3rd ed. Carl Hanser Verlag; 2015. p. 23–9.
- Zapata S, Castaneda M, Jimenez M, Aristizabal AJ, Franco CJ, Dyer I. Long-term effects of 100% renewable generation on the Colombian power market. *Sustain Energy Technol Assess* 2018;30:183–91.
- Rahate ND, Kinhekar N. Demand side management for household equipment's Indore, India International conference on information, communication, instrumentation and control (ICICIC). 2017.
- Good N, Ellis KA, Mancarella P. Review and classification of barriers and enablers of demand response in the smart grid. *Renew Sustain Energy Rev* 2017;72:57–72.
- Roasto I, Lehtla T, Moller T, Rosin A. Control of ultracapacitors energy exchange. 12th international power electronics and motion control conference. 2006. Portoroz, Slovenia.
- Rahmoun A, Armstorfer A, Helguero J, Biechl H, Rosin A. Mathematical modeling and dynamic behavior of a Lithium-Ion battery system for microgrid application. 2016 IEEE International Energy Conference (ENERGYCON). 2016. Belgium, Leuven.
- Rosin A, Moller T, Lehtla M, Hoimoja H. Analysis of household electricity consumption patterns and economy of water heating shifting and Saving Bulbs. *Sci J Riga Tech Univ* 2010;27:15–20.
- Hammerstrom DJ, Ambrosio R, Carlon TA, DeSteele JG, Horst GR, Kajfasz R et al. "Pacific Northwest GridWise TM Testbed Demonstration Projects. Part I. Olympic Peninsula Project"; 2007.
- Goh CHK, Apt J. "Consumer strategies for controlling electric water heaters under dynamic pricing," 2004.
- Bálint R, Fodor A, Hangos KM, Magyar A. Cost-optimal model predictive scheduling of freezers. *Control Eng Pract* 2018;80:61–9.
- Aleixo L, Rosin A, Saele H, Morch AZ, Grande OS, Palu I. Ecogrid EU project - real time price based load control and economic benefits in a wind production based system. 22nd international conference and exhibition on electricity distribution (CIRED 2013). 2013. Stockholm, Sweden.
- Rosin A, Link S, Lehtla M, Marins J, Drovitar I, Roasto I. Performance and feasibility analysis of electricity price based control models for thermal storages in households. *Sustain Cities Sci* 2017.
- Kapsalis V, Safouri G, Hadellis L. Cost/comfort-oriented optimization algorithm for operation scheduling of electric water heaters under dynamic pricing. *J Cleaner Prod* 2018;198:1053–65.
- Masaba K, Ntakirutimana A, Ustun TS. Design and implementation of a load scheduling embedded system for off grid solar power systems. IEEE PES innovative smart grid technologies conference Europe (ISGT-Europe). 2016. Ljubljana, Slovenia.
- Aldaouab I, Daniels M. Microgrid battery and thermal storage for improved renewable penetration and curtailment. International energy and sustainability conference (IESC). 2017. Farmingdale, NY, USA.
- Goldsworthy MJ, Sethuvenkatraman S. The off-grid PV-battery powered home revisited; the effects of high efficiency air-conditioning and load shifting. *Sol Energy* 2018;172:69–77.
- Roux M, Apperley M, Booysen MJ. Comfort, peak load and energy: centralised control of water heaters for demand-driven prioritisation. *Energy Sustain Dev* 2018;44:78–86.
- Palacios-Garcia EJ, Moreno-Munoz A, Santiago I, Flores-Arias JM, Bellido-Outeirino FJ, Moreno-Garcia IM. A stochastic modelling and simulation approach to heating and cooling electricity consumption in the residential sector. *Energy* 2018;144:1080–91.
- Palacios-Garcia EJ, Moreno-Munoz A, Santiago I, Moreno-Garcia IM, Milanés-Montero MI. PV hosting capacity analysis and enhancement using high resolution stochastic modeling. *Energies* 2017;10(10).
- Lizondo D, Rodriguez S, Will A, Jimenez V, Gotay J. An artificial immune network for distributed demand-side management in smart grids. *Inf Sci* 2018;438:32–45.
- Adhikari R, Pipattanasomporn M, Rahman S. An algorithm for optimal management of aggregated HVAC power demand using smart thermostats. *Appl Energy* 2018;217:166–77.

- [22] Carducci F, Giovannelli A, Renzi M, Comodi G. Improving flexibility of industrial microgrids through thermal storage and HVAC management strategies. *Energy Procedia* 2017;142:2728–33.
- [23] Hu H, Augenbroe G. A stochastic model based energy management system for off-grid solar houses. *Build Environ* 2012;50:90–103.
- [24] Agamah SU, Ekonomou L. Energy storage system scheduling for peak demand reduction using evolutionary combinatorial optimisation. *Sustain Energy Technol Assess* 2017;23:73–82.
- [25] Medici V, Salani M, Nespoli L, Giusti A, Derboni M, Vermes N, et al. Evaluation of the potential of electric storage using decentralized demand side management algorithms. *Energy Procedia* 2017;135:203–9.
- [26] Mehra V, Amaty R, Ram RJ. Estimating the value of demand-side management in low-cost, solar. *Energy* 2018;163:74–87.
- [27] Gonzalez de Durana J, Barambones O. Technology-free microgrid modeling with application to demand side. *Appl Energy* 2018;219:165–78.
- [28] Neves D, Pina A, Silva CA. Comparison of different demand response optimization goals on an isolated microgrid. *Sustain Energy Technol Assess* 2018;30:209–15.
- [29] Olatomiwa L, Blanchard R, Mekhilef S, Akinyele D. Hybrid renewable energy supply for rural healthcare facilities: an approach to quality healthcare delivery. *Sustain Energy Technol Assess* 2018;30:121–38.
- [30] Energy US. Information administration (EIA). Washington D.C.: U.S. Battery Storage Market Trends; 2018.
- [31] ATD Home Inspection, " [Online]. Available: <https://www.atdhomeinspection.com/advice/average-product-life/>. [Accessed 02 10 2018].
- [32] Bosch, Datasheet: GSN51AW41.
- [33] AO Smith, "aosmithatlowes.com," [Online]. Available: <https://www.aosmithatlowes.com/products/electric-water-heaters/e6-40r45dv/>. [Accessed 23 05 2017].
- [34] American Society of Heating, Refrigerating and Air-Conditioning Engineers, Inc., ASHRAE Handbook - Fundamentals, 2009.
- [35] American Society of Heating, Refrigerating and Air-Conditioning Engineers, Inc., ASHRAE Handbook - Fundamentals, 2013.
- [36] Rosin A, Rosin K, Auväärt A, Strzelecki R. Dimensioning of household electricity storage for PV-systems and load scheduling based on Nord Pool Spot prices. *PRZEGLĄD ELEKTROTECHNICZNY* 2012;88(4b):294–9.
- [37] CANMET Energy Technology Centre - Varennes, CANETA Research and TECHNOSIM Consulting Group, "Commercial Earth Energy Systems: A Buyer's Guide," Natural Resources Canada; 2002.
- [38] Akmal M, Fox B. Modelling and simulation of underfloor heating system supplied from heat pump. UKSim-AMSS 18th international conference on computer modeling and simulation. 2016.
- [39] Papaioannou IT, Alexiadis MC, Demoulias CS, Labridis DP, Kokopoulos PS. Modeling and field measurements of photovoltaic. *IEEE transactions on power delivery units connected to LV grid study of penetration scenarios*. 2011. p. 979–87.
- [40] Victron Energy, "www.victronenergy.com," [Online]. Available: <https://www.victronenergy.com/blog/2015/03/30/batteries-lithium-ion-vs-agm/>. [Accessed 25 07 2017].
- [41] Richardson I, Thomson M. Integrated simulation of photovoltaic micro-generation and domestic electricity demand: a one-minute resolution open-source model. *Proc Inst Mech Eng, Part A: J Power Energy* 2013;227(1):73–81.
- [42] EquaSimulation Finland Oy, "Equa Online," 11 2010. [Online]. Available: http://www.equasonline.com/iceuser/validation/CEN_VALIDATION_EN_15255_AND_15265.pdf. [Accessed 22 04 2019].

Curriculum vitae

Personal data

Name: Tobias Häring
Date of birth: 08.06.1994
Place of birth: Kempten (Allgäu), Germany
Citizenship: Germany

Contact data

E-mail: tobias.haring@taltech.ee

Education

2018 – 2022 Tallinn University of Technology, Ph.D.
2017 – 2018 Tallinn University of Technology, M.Sc.Eng.
2016 – 2018 University of Applied Sciences Kempten, M.Eng.
2012 – 2016 University of Applied Sciences Kempten, B.Eng.
2004 – 2012 Allgäu Gymnasium Kempten, Secondary Education

Language competence

German Mother tongue
English Proficient
Estonian Intermediate
Spanish Intermediate

Professional employment

2018 – 2022 Tallinn University of Technology, Early Stage Researcher
2015 – 2016 Vereinigte Wertach-Elektrizitätswerke, Bachelor's degree candidate
2014 – 2015 Vereinigte Wertach-Elektrizitätswerke, Intern

Research projects

2022 – Training: "Machine learning and its applications to increase resource and energy efficiency in industry" (Tallinn University of Technology, EDIH-AIRE)
2022 – Expertise for Enefit (Tallinn University of Technology, Eesti Energia AS)
2021 – AI4Cities (Tallinn University of Technology, Fusebox OÜ)
Since 2020 – FINEST Twins (Tallinn University of Technology)
2020 – Campulse Project (Tallinn University of Technology)
2020 – Expertise for GridIO (Tallinn University of Technology, GridIO OÜ)
2019 – PENTAMET project (Tallinn University of Technology, Pentamet LLC)
2017 – Scientific Project (Kempten University of Applied Sciences)

Elulookirjeldus

Isikuandmed

Nimi: Tobias Häring
Sünniaeg: 08.06.1994
Sünnikoht: Kempten (Allgäu), Saksamaa
Kodakondsus: Saksamaa

Kontaktandmed

E-post: tobias.haring@taltech.ee

Hariduskäik

2018 – 2022 Tallinna Tehnikaülikool, Ph.D.
2017 – 2018 Tallinna Tehnikaülikool, M.Sc.Eng.
2016 – 2018 Kempteni Kõrgkool, M.Eng.
2012 – 2016 Kempteni Kõrgkool, B.Eng.
2004 – 2012 Allgäu Gymnasium Kempten, Keskkharidus

Keelteoskus

Saksa keel Emakeel
Inglise keel Kõrgtase
Eesti keel Kesktase
Hispaania keel Kesktase

Teenistuskäik

2018 – 2022 Tallinna Tehnikaülikool, Nooremteadur
2015 – 2016 Vereinigte Wertach-Elektrizitätswerke, Bakalaureuse kraadi kandidaat
2014 – 2015 Vereinigte Wertach-Elektrizitätswerke, Praktikant

Projektid

2022 – Koolitus: “Masinõpe ja selle rakendused tööstusele ressursi- ja energiatõhususe tõstmiseks” (Tallinn University of Technology, EDIH-AIRE)
2022 – Expertise for Enefit (Tallinna Tehnikaülikool, Eesti Energia AS)
2021 – AI4Cities (Tallinna Tehnikaülikool, Fusebox OÜ)
2020 – FINEST Twins (Tallinna Tehnikaülikool)
2020 – Campulse Project (Tallinna Tehnikaülikool)
2020 – Expertise for GridIO (Tallinna Tehnikaülikool, GridIO OÜ)
2019 – PENTAMET project (Tallinna Tehnikaülikool, Pentamet LLC)
2017 – Scientific Project (Kempteni Kõrgkool)

ISSN 2585-6901 (PDF)
ISBN 978-9949-83-828-8 (PDF)